



Development And Characterisation Of Monolithic Silica  
Stationary Phases For Ion Chromatography

By

**Edel Sugrue,  
BSc. (Hons), AMRSC, GradICI**

**A thesis submitted to Dublin City University in part fulfilment for the degree of**

**DOCTOR OF PHILOSOPHY**

Supervisor: Dr. Brett Paull,  
School of Chemical Sciences.  
Dublin City University.

January 2006

*I hereby certify that this material, which I now submit for assessment on the programme of study leading to the award of Ph.D in Analytical Chemistry is entirely my own work and has not been taken from the work of others save and to the extent that such work has been cited and acknowledged within the text of my work.*

Signed: Kelal Sugana (Candidate) ID No.: 97045039

Date: 9 May, 2006

## Acknowledgements

Firstly I would like to express my appreciation to my supervisor *Dr. Brett Paull* for his advice, guidance and patience throughout my time in his research group. In addition, I would like to thank *Prof Pavel Nesterenko*, for the modification of the silica monoliths used in this research project.

To all the *technical staff* in the School of Chemical Sciences, in particular *Maurice Burke* for all his time and assistance throughout this work.

I would especially like to thank all the *members of my research group*, both past and present, for all your help and support, and more importantly, for all the good times and laughs that you have provided!!!

In the words of John Lennon, "I get by with a little help from my friends", and there are three very important people, without whose unstinting friendship and support, I don't think I would have survived the last three years. *Eadaoin*, you made the bad times good and the good times even better, and it was a privilege to work and party with you over the last few years. To the smartest postgraduate in the world ever, *Jonathan*, you were always there to listen (and listen!!!) and always willing to lend a hand in times of trouble. I will always value your friendships and wish you both all the success in the world. Finally, to my best friend in the whole, wide world, *Colmán*, your support and love has been my guiding light throughout the last three years. To quote Henry Ford, "My best friend is the one that brings out the best in me", and without a doubt, this applies to you. Thank you for always believing in me and being there for me, even if I didn't always make it easy!!! Hopefully *Colmán* all our troubles will be little ones, and the little ones be no trouble at all.

Finally, and most importantly, I want to thank my family: my wonderful parents; *Mary and Tommy*, my amazing sister *Kerry* and my adorable brother *Enda*, for all your love, support and encouragement throughout my life and especially since I began my academic journey all those years ago. I would also like to thank my *extended family and friend* for all your support and best wishes, which is most appreciated.

Thank you all.

## Table of Contents

<b>Abstract</b>	i
<b>Publications and Presentations</b>	ii
<b>List of Abbreviations</b>	iv
<b>List of Symbols</b>	v
<b>List of Figures</b>	vi
<b>List of Tables</b>	xxi

### **Chapter 1: Introduction to monolithic silica stationary phases and their application to ion chromatography**

<b><i>1.1: The development and applications of monolithic HPLC columns</i></b>	<b>2</b>
1.1.1: The need for faster HPLC separations	2
1.1.2: Development of HPLC silica stationary phases	3
1.1.3: Hydrodynamics of chromatography	4
1.1.3.1: Flow irregularities	5
1.1.3.2: Transverse and longitudinal diffusion	7
1.1.3.3: Mass transfer	7
1.1.4: Limits of particle-packed HPLC columns	8
1.1.5: Advances in rapid, high throughput analysis	9
1.1.6: Monolithic columns for fast HPLC separations	14
1.1.6.1: Milestones in the development of monolithic columns	15
1.1.6.2: Types of monolithic columns	16
1.1.7: Polymer monoliths	17
1.1.7.1: Structural properties	18
1.1.8: Monolithic silica columns	18
1.1.8.1: Structural properties	20
1.1.8.2: Preparation of silica monoliths	20
1.1.8.3: Comparison of silica monolithic and particle-packed HPLC columns	20
1.1.9: Advantages of monolithic columns	23

1.1.10: Limitations of monolithic columns	24
1.1.11: Applications of silica monoliths in high-speed chromatographic separations	25
1.1.11.1: Drug and pharmaceutical analysis	26
1.1.11.2: Bio analytical separations	31
1.1.11.3: Rapid ion chromatography using monolithic silica stationary phases	32

## ***1.2: Ion Chromatography***

1.2.1: Ion-exchange chromatography	39
1.2.1.1: Ion-exchange stationary phases	39
1.2.1.2: Ion-exchange separation mechanism	40
1.2.1.3: Factors affecting selectivity in ion-exchange	41
1.2.1.4: The influence of eluent properties in ion-exchange	42
1.2.2: Ion-interaction chromatography	43
1.2.2.1: Retention mechanism in ion-interaction chromatography	44
1.2.2.2: Factors affecting selectivity	45
1.2.3: Chelation-exchange chromatography	46
1.2.3.1: Principles of complexation	47
1.2.3.1.1: Stability of metal chelates	47
1.2.3.2: Chelation stationary phases	48
1.2.3.3: The effect of eluent parameters on analyte retention in chelation ion chromatography (CIC)	49
1.2.3.4: The determination of metals in complex matrices using chelation ion chromatography (CIC)	51
1.2.4: Complexation ion chromatography	54
1.2.4.1: Metal determination using complex ion chromatographic methods	55
1.2.5: Zwitterionic ion chromatography	57
1.2.5.1: Types of zwitterionic ion-exchanger	57
1.2.5.2: Coated zwitterionic stationary phases	58
1.2.5.3: Proposed separation mechanisms in ZIC	59
1.2.5.4: Mechanism of separation in ZIC using electrolytic eluents	60

<b>1.3: Detection methods in ion chromatography</b>	
1.3.1: Introduction	62
1.3.2: Conductivity detection	63
1.3.2.1: Definitions and equations	63
1.3.2.2: Effect of analyte concentration	64
1.3.2.3: Influence of temperature	65
1.3.3: Suppressed conductivity detection	65
1.3.3.1: Types of suppressors	66
1.3.3.2: Operating principles of membrane suppressors	67
1.3.4: Spectrophotometric detection	69
1.3.4.1: Direct spectrophotometric detection and the Beer-Lambert's Law	69
1.3.4.2: Indirect spectrophotometric detection	70
1.3.4.3: Indirect spectrophotometric detection of anions and cations	71
1.3.5: Detection by post-column reaction	72
1.3.5.1: Post-column detection of inorganic cations	74
<b>References</b>	77

**Chapter 2: Alkali and alkaline earth metal ion selectivity on an IDA functionalised silica monolith**

<b>2.1: Introduction</b>	86
2.1.1: Objective	89
<b>2.2: Experimental</b>	
2.2.1: Modification of a silica monolith with iminodiacetic acid	90
2.2.2: Instrumentation	90
2.2.3: Reagents	91
<b>2.3: Results and Discussion</b>	
2.3.1: Physical analysis of the functionalised monolith	92
2.3.2: Ion-exchange chromatography on a chelation stationary phase	93
2.3.2.1: Separation of alkali metals on an IDA functionalised silica monolith	94
2.3.2.2: Ion-exchange properties of a bare silica monolith	95

2.3.2.3: Separation of alkaline earth metals on an IDA silica monolith using low-ionic strength acidic eluents	97
2.3.2.4: The effect of complexing agents on alkaline earth metal selectivity	99
2.3.2.5: Fast separations of alkaline earth metals using low ionic strength acidic eluents with suppressed conductivity detection	103
2.3.3: Separation of alkaline earth metal ions by chelation ion-exchange	104
2.3.3.1: Effect of eluent ionic strength	104
2.3.3.2: Comparison of alkaline earth selectivity for an IDA silica gel packed column and IDA functionalised silica monolithic column.	106
2.3.3.3: The effect of eluent pH on alkaline earth metal ion selectivity	107
2.3.3.4: The effect of eluent pH on the retention of alkaline earth metal ions on a bare silica monolithic column	109
<b>2.4: Conclusion</b>	112
<b>References</b>	113
<b>Chapter 3: Determination of alkaline earth metal cations in complex matrices</b>	
<b>3.1: Introduction</b>	116
3.1.1: Objective	117
<b>3.2: Experimental</b>	
3.2.1: Modification of a silica monolith	117
3.2.2: Instrumentation	117
3.2.3: Reagents	117
<b>3.3: Results and Discussion</b>	118
3.3.1: Application of the IDA silica monolith to the determination of Sr (II) in excess calcium matrices	118
3.3.2: Determination of Mg (II) and Ca (II) in high ionic strength samples	119
3.3.2.1: Selection of a suitable eluent	120

3.3.2.2: Investigation of sample matrix effects using a commercial IDA silica gel column	121
3.3.2.3: Matrix Effects On Separation Efficiency	122
3.3.2.4: Comparison of efficiency studies performed on a 10 cm IDA silica monolithic column and a 3 cm particle-packed IDA silica column	124
3.3.2.5: A sub-minute separation of Mg (II) and Ca (II) in 1 M and 2 M KCl brines	127
3.3.2.6: Analytical Performance Data	129
3.3.2.7: Quantitative determination of Mg (II) and Ca (II) impurities of laboratory grade KCl and NaCl salts	131
<b>3.4: Conclusion</b>	134
<b>References</b>	135
<b>Chapter 4: Chelation ion chromatography of transition and heavy metal ions on an IDA functionalised silica monolith</b>	
<b>4.1: Introduction</b>	137
4.1.1: Objective	137
<b>4.2: Experimental</b>	
4.2.1: Modification of a silica monolith with iminodiacetic acid	138
4.2.2: Instrumentation	138
4.2.3: Reagents	138
<b>4.3: Results and Discussion</b>	
4.3.1: Separation of heavy and transition metal ions using a non-complexing eluent	138
4.3.2: Simultaneous separation of alkaline earth and transition metals ions	141
4.3.3: Optimisation of Mn (II), Cd (II), Co (II) Zn (II) and Pb (II) separation	142
4.3.3.1: Comparison of IDA silica monolithic and IDA silica gel columns	146
4.3.3.2: Investigation into the formation of chloro-complexes by Cd (II) and Pb (II)	148

4.3.3.3: The effect of different inorganic eluents on Cd (II) and Pb (II) efficiency	149
4.3.3.4: Fast separations of Mn (II), Cd (II), Zn (II) and Pb (II)	150
<b>4.4 Conclusion</b>	154
<b>References</b>	155
<b>Chapter 5: Cation and anion selectivity on a L-lysine functionalised silica monolith</b>	
<b>5.1: Introduction</b>	157
5.1.1: Objective	159
<b>5.2: Experimental</b>	
5.2.1: Modification of a silica monolith with iminodiacetic acid	160
5.2.2: Instrumentation	160
5.2.3: Reagents	161
<b>5.3: Results and Discussion</b>	
5.3.1: Cation selectivity	162
5.3.1.1: Separation of alkali and alkaline earth metal ions on the L-lysine silica monolith	162
5.3.1.2: Transition and heavy metal cation selectivity	164
5.3.1.3: Cation-exchange capacity	166
5.3.2: Anion selectivity	168
5.3.2.1: Anion retention on an L-lysine silica monolith	168
5.3.2.2: Rapid separations and speciation studies	170
5.3.2.3: Effect of pH on anion selectivity and anion-exchange capacity	173
5.3.2.4: Effect of eluent concentration on anion retention	180
5.3.3: Optimising rapid anion separations	182
5.3.3.1: The use of a pH gradient	182
5.3.3.2: The use of elevated flow rates	183
5.3.3.3: The effect of eluent concentration on peak efficiency	185
5.3.3.4: Application of flow gradients to separation of nitrite, bromate, bromide, nitrate, iodide and thiocyanate	188
5.3.3.5: Analytical performance	193

<b>5.4: Conclusion</b>	195
<b>References</b>	196

## **Chapter 6: Ligand exchange chromatography of amino acids using a copper (II) modified lysine functionalised silica monolith**

### **6.1: Introduction**

6.1.1: Properties of amino acids	198
6.1.2: Separations of amino acids	199
6.1.3: Detection of amino acids	201
6.1.4: Objective	203

### **6.2: Experimental**

6.2.1: Column modification	203
6.2.2: Instrumentation	204
6.2.3: Reagents	204

### **6.3: Results and Discussion**

6.3.1: The effect of eluent concentration on amino acid retention	206
6.3.2: The effect of eluent pH on amino acid retention	208
6.3.3: Fluorescence detection of amino acids	212
6.3.3.1: Alternative nucleophilic agents	213
6.3.4: Amino acid selectivity study	217
6.3.5: Rapid amino acid separations	219
6.3.6: Chiral ligand-exchange chromatography	223

### **6.4: Conclusion**

<b>References</b>	226
-------------------	-----

## **Chapter 7: Solvent enhanced ion chromatography of transition and alkaline earth metal ions on a bare silica monolith**

### **7.1: Introduction**

7.1.1: Objective	233
------------------	-----

### **7.2: Experimental**

7.2.1: Instrumentation	233
7.2.2: Reagents	234

### **7.3: Results and Discussion**

7.3.1: Alkaline earth metal ion selectivity on a bare silica monolith	235
---	-----

7.3.1.1: The effect of organic solvent concentration on cation retention	235
7.3.1.2: The effect of buffer concentration cation retention	236
7.3.1.3: The effect of buffer pH on cation retention	239
7.3.1.4: Flow rate study	241
7.3.1.5: The use of an alternative acetate buffer	244
7.3.2: Transition and heavy metal ion selectivity on a bare silica monolith	246
7.3.2.1: The effect of organic solvent concentration on cation retention	246
7.3.2.2: The effect of buffer concentration on cation retention	248
7.3.2.3: The combined effect of varying % acetonitrile and buffer concentration	250
7.3.2.4: The effect of buffer pH on cation retention	251
7.3.2.5: Flow rate study	252
7.3.2.6: The use of an alternative acetate buffer	255
7.3.3: The effect of solvent polarity on cation retention and selectivity	256
7.3.3.1: The effect of methanol concentration on transition and heavy metal selectivity	258
<b>7.4: Conclusion</b>	261
<b>References</b>	262
<b>Overall Summary and Future Work</b>	263
<b>Appendix I</b>	269
<b>Appendix II</b>	272
<b>Appendix III</b>	277

## Abstract

Silica based monolithic HPLC columns have received much attention in recent years, particularly those modified for reversed-phase separations. However, for ion-exchange, silica based monolithic columns have received only limited attention. Therefore, the aim of this work was the development and characterisation of novel monolithic stationary phases for the rapid separation of inorganic and organic ions.

A 10 cm bare silica monolith has been modified on-column with iminodiacetic acid (IDA) groups and characterised for its selectivity toward alkali, alkaline earth and selected transition metal cations. The applicability of this IDA silica monolithic column for the rapid determination of alkaline earth metals in complex matrices was demonstrated. A second 10 cm bare silica monolith was functionalised with lysine (2,6-diaminohexanoic acid) groups, and both the cation- and anion-exchange properties of the lysine functionalised monolith were evaluated, with a separation of 6 UV absorbing anions achieved in less than 100 seconds. By dynamically modifying the surface of the lysine functionalised silica monolith with copper (II) ions, it was possible to separate L-amino acids via ligand-exchange chromatography, using flow rates up to 7 mL/min. Finally, the ion-exchange properties of a bare silica monolith were evaluated. The separation of alkaline and transition metal ions on a 10 cm bare silica monolith was possible using acetonitrile or methanol based ammonium and sodium acetate buffered eluents. The effects of eluent ionic strength, organic content and pH on cation retention were evaluated, and in addition, the effect of solvent polarity on cation selectivity was also investigated.

## Publications and Presentations

Iminodiacetic acid functionalised monolithic silica chelating ion-exchanger for rapid determination of alkaline earth metal ions in high ionic strength samples.

Edel Sugrue, Pavel N. Nesterenko and Brett Paull, *Analyst*, **128** (2003) 417.

Ion-exchange properties of monolithic and particle type iminodiacetic acid modified silica.

Edel Sugrue, Pavel N. Nesterenko and Brett Paull, *J. Sep. Sci.*, **27** 10-11 (2004) 921.

Fast ion chromatography of inorganic anions and cations on a lysine bonded porous silica monolith.

Edel Sugrue, Pavel N. Nesterenko and Brett Paull, *J. Chromatogr. A*, **1075** (2005) 167.

Solvent enhanced ion chromatography of alkaline earth and transition metal ions on a bare silica monolith.

Edel Sugrue, Pavel N. Nesterenko and Brett Paull, *Anal. Chim. Acta.*, **553** (2005) 27.

## Oral Presentations

*'Ion exchange properties of monolithic and particle type iminodiacetic acid modified silica stationary phases for the analysis of alkaline earth, transition and heavy metal ions'*, 3<sup>rd</sup> biennial Conference on Analytical Sciences in Ireland, University College Cork, 9-10 September, 2004

*'Ion chromatography of alkaline earth, transition and heavy metal ions on an iminodiacetic acid functionalised silica monolith'*, 17<sup>th</sup> International Ion Chromatography Symposium, University of Trier, Germany, 20-23 September, 2004

*'Retention of cations, anions and amino acids on a lysine functionalised silica monolithic column'*, 18<sup>th</sup> International Ion Chromatography Symposium, Montreal, Canada, 18-21 September 2005

## Poster Presentations

*'The use of an iminodiacetic acid modified monolithic silica column for the rapid determination of alkaline earth metals in brines',*

Edel Sugrue, Pavel N. Nesterenko and Brett Paull. Royal Society of Chemistry Analytical Research Forum, University of Sunderland, UK, 21-23 July 2003.

*'Ion chromatography of alkaline earth, transition and heavy metal ions on an iminodiacetic acid functionalised silica monolith',*

Edel Sugrue, Pavel N. Nesterenko and Brett Paull. Royal Society of Chemistry Analytical Research Forum, University of Central Lancashire, UK, 19-21 July 2004.

*'Ion chromatography of alkaline earth, transition and heavy metal ions on an iminodiacetic acid functionalised silica monolith',*

Edel Sugrue, Pavel N. Nesterenko and Brett Paull. The 7<sup>th</sup> Asian Conference on Analytical Sciences, Hong Kong Baptist University, Kwoloon, Hong Kong, 28-31 July 2004.

*'Solvent enhanced ion chromatography of alkaline earth and transition metal ions on a 10 cm bare silica monolithic column',*

Edel Sugrue, Pavel N. Nesterenko and Brett Paull. Royal Society of Chemistry Analytical Research Forum, University of Plymouth, UK, 18-20 July 2005.

## List of Abbreviations

Ala: alanine  
Arg: arginine  
Asn: asparagine  
Asp: aspartate  
CEC: capillary electrochromatography  
CIC: chelation ion chromatography  
CLEC: chiral ligand-exchange chromatography  
CPC: cetylryridinium chloride  
*o*-CPC: *o*-cresolphthalein complexone  
CTAB: cetyltrimethylammonium bromide  
DDAB: didodecyldimethylammonium bromide  
DIW: deionised water  
DOSS: dicotylsulphosuccinate  
DPA: pyridine-2,6-dicarboxylic acid  
EDTA: ethylenediaminetetraacetic acid  
EOF: electroosmotic flow  
GC: gas chromatography  
Gln: glutamine  
Glu: glutamate  
Gly: glycine  
HETP: height equivalent to theoretical plate  
HPLC: high performance liquid chromatography  
IC: ion chromatography  
i.d.: internal diameter  
IIR: ion-interaction reagent  
Ile: isoleucine  
IDA: iminodiacetic ac  
LEC: ligand-exchange chromatography  
Leu: leucine  
Li-DS: lithium dodecylsulfate  
Lys: lysine

MeCN: acetonitrile  
MeOH: methanol  
Meth: methionine  
NAC: N-acetyl-L-cysteine  
OPA: *o*-phthalaldehyde  
OTC: open tubular column  
PAR: 4-(2-pyridylazo) resorcinol  
PCR: post-column reagent  
PEEK: polyetheretherketone  
Phe: phenylalanine  
POE: polyoxyethylene  
RP: reversed-phase  
RSD: relative standard deviation  
SEIC: solvent enhanced ion chromatography  
Ser: serine  
Thr: threonine  
Tph: tryptophan  
Tyr: tyrosine  
UHPLC: ultra-high pressure liquid chromatography  
UV-Vis: ultraviolet-visible  
Val: valine  
ZIC: zwitterionic ion chromatography

### **List of Symbols**

$E^+$ : eluent cation in cation-exchange chromatography  
 $E^-$ : eluent anion in anion-exchange chromatography  
 $k$ : retention factor, which is the ratio of the relative retention time ( $t'_r$ ) and the column hold-up time ( $t_m$ )  
 $N$ : peak efficiency  
 $R_s$ : resolution

## List of Figures

**Figure 1.1:** The individual contributions of the terms in the van Deemter equation are shown graphically.

**Figure 1.2:** Schematic showing the process of eddy diffusion.

**Figure 1.3:** Schematic showing longitudinal diffusion.

**Figure 1.4:** Schematic of the process of mass transfer.

**Figure 1.5:** Schematic showing the contrast between the hydrodynamic and electroosmotic flow profiles.

**Figure 1.6:** Structure of (a) macropores and (b) mesopores found in monolithic columns.

**Figure 1.7:** Scanning electron microscopy pictures of different types of porous chromatographic materials (a) irregularly shaped silica particles, (b) spherical silica particles, (c) organic polymer monolith (UNO S), (d) organic polymer monolith B (CIM Disk) and (e) silica-based monolith (Chromolith).

**Figure 1.8:** (a) shows the total number of papers published on monolithic columns for HPLC during the time period 1989-2003 and (b) monolithic silica rods (before and after cladding) compared to particulate type silica used in conventional HPLC silica columns.

**Figure 1.9:** Column backpressure  $\Delta P$  as a function of the flow rate  $F$  on three monolithic and a microparticulate column. (■) Pressure drop due to equipment without a column, (♦) rod 216 ( ) rod 225, (●) Purospher RP 18e column.

**Figure 1.10:** A van Deemter plot of the HETP versus linear flow velocity for a Chromolith™ Performance column and equivalent particle-packed HPLC silica columns.

**Figure 1.11:** Chromatograms of the separation of the isoflavones of a soy extract on (a) a LiChrospher RP-18 (250 mm x 4 mm) and on (b) two linked Chromolith Performance RP-18 (100 mm x 4.6 mm) columns.

**Figure 1.12:** Effect of increasing flow rate on the separation of Suprofen using a 60 cm long t-BuCQN modified monolithic silica column. Flow rate 1 to 4 mL/min.

**Figure 1.13:** The 30-second separation of 7 common anions on a 5 cm monolithic column.

**Figure 1.14:** A separation of  $H^+$ , Mg (II), Ca (II) using a Li-DS modified reversed-phase silica monolith.

**Figure 1.15:** Simultaneous separations of anions and cations on two modified  $C_{18}$  monolithic silica columns connected in parallel.

**Figure 1.16:** The dual gradient separation of inorganic anions achieved on a 1cm carboxybetaine modified  $C_{18}$  monolithic column.

**Figure 1.17:** The retention of anions by anion-exchange chromatography.

**Figure 1.18:** Structures of chelating ligands (a)  $\beta$ -diketones, (b) 8-hydroxyquinoline and (c) iminodiacetic acid.

**Figure 1.19:** Schematic showing zwitterionic ion-exchangers with (a) localisation of oppositely charged groups on the surface and (b) localisation of oppositely charged groups in one molecule attached to the surface.

**Figure 1.20:** The structure of 3-(N,N-dimethylmyristylammonio)propanesulfonate (Zwittergent-3-14).

**Figure 1.21:** A schematic showing the proposed mechanism using a  $\text{NaClO}_4$  and a  $\text{CeCl}_3$  eluent.

**Figure 1.22:** Diagram of experimental set-up for suppressed conductivity detection.

**Figure 1.23:** Schematic of the mechanism of suppression for a Dionex anion self-regenerating suppressor.

**Figure 1.24:** Schematic representing indirect UV-Visible detection: (a) shows the background detector response which results from the light absorbing eluent ions and (b) demonstrates the decrease in background signal due to the presence of the transparent analytes passing through the flow cell.

**Figure 1.25:** Schematic of the post-column reaction system experimental set-up for solution post-column reaction detection.

**Figure 1.26:** The chemical structure of (a) *o*-CPC, (b) arsenazo III and (c) PAR.

**Figure 2.1:** Structure of iminodiacetic acid (IDA).

**Figure 2.2:** The effect of  $\text{LiCl}$  eluent concentration on the retention of alkali metal ions on a 10 cm bare silica monolith.

**Figure 2.3:** The analysis of  $\text{Mg (II)}$ ,  $\text{Ca (II)}$ ,  $\text{Sr (II)}$  and  $\text{Ba (II)}$  in the presence of excess  $\text{K}^+$  on a 10 cm IDA functionalised silica monolith. Eluent conditions: 2 mM methansulfonic acid at flow rates of 1 mL/min (blue trace) and 2 mL/min (pink trace) monitored using suppressed conductivity detection.

**Figure 2.4:** Structures of complexing ligands used in ion chromatography, (a) iminodiacetic acid (IDA), (b) dipicolinic acid (DPA), (c) citric and (d) tartaric acid.

**Figure 2.5:** A plot showing the correlation between basicity and stability of Co (II) complexes. IDA= iminodiacetic acid, DPA= dipicolinic acid, TA= tartaric acid and CA= citric acid.

**Figure 2.6:** The selectivity obtained for a mixture of 10 ppm Mg (II), Ca (II), Sr (II) and Ba (II) on a 10 cm IDA functionalised silica monolithic column. Eluent conditions: a mixture of 0.5 mM dipicolinic acid and 2.5 mM methansulfonic acid, flow rate 1 mL/min, and analysis was monitored using suppressed conductivity detection.

**Figure 2.7:** Effect of increasing the KNO<sub>3</sub> eluent concentration (pH 4.85) on the alkaline earth metal ion retention factors ( $k$ ), retained on a 10 cm IDA functionalised silica monolith, flow rate 1 mL/min. Detection conditions: 0.4 mM *o*-CPC in 0.25 M boric acid, pH 10.5, was employed as the post-column reagent and the resultant *o*-CPC- metal complexes were monitored at 570 nm.

**Figure 2.8:** Chromatograms showing the separation of 1-Mg (II), 2-Sr (II), 3-Ba (II) and 4-Ca (II), using an eluent (a) 0.3 M KNO<sub>3</sub>, adjusted to pH 4.2 for the silica gel column and pH 4.85 for the monolithic column, and (b) 0.5 M KNO<sub>3</sub>, adjusted to pH 4.2 for the silica gel column and pH 4.85 for the monolithic column. Flow rate 1 mL/min. Detection conditions: 0.4 mM *o*-CPC in 0.25 M boric acid, pH 10.5, was employed as the post-column reagent and the resultant *o*-CPC- metal complexes were monitored at 570 nm.

**Figure 2.9:** Effect of increasing the eluent pH (0.5 M KNO<sub>3</sub>) on the alkaline earth metal ion retention factors ( $k$ ), retained on a 10 cm IDA functionalised silica monolith. Flow rate 1 mL/min.

**Figure 2.10:** A separation of Mg (II), Ba (II), Sr (II) and Ca (II) on a 10 cm IDA functionalised silica monolith. Eluent Conditions: 0.4 M KCl, pH adjusted to 6.7, flow rate 2 mL/min. Detection conditions: 0.4 mM *o*-CPC in 0.25 M boric acid, pH 10.5, was employed as the post-column reagent and the resultant *o*-CPC- metal complexes were monitored at 570 nm.

**Figure 2.11:** The effect of eluent pH on the retention of alkaline earth metal cations a 10 cm bare silica monolith. Eluent conditions: 5 mM KCl (prepared in 10 mM sodium acetate buffer), pH 6.0, flow rate 1 mL/min.

**Figure 2.12:** The separation of alkaline earth metal cations a 10 cm bare silica monolith. Eluent conditions: 5 mM KCl (prepared in 10 mM sodium acetate buffer), pH 6.0, flow rate 1 mL/min. Detection conditions: 0.4 mM *o*-CPC in 0.25 M boric acid, pH 10.5, was employed as the post-column reagent and the resultant *o*-CPC-metal complexes were monitored at 570 nm.

**Figure 3.1:** A separation of Mg (II), Ba (II), Sr (II) and Ca (II) on a 10 cm IDA functionalised silica monolith. Eluent conditions: 0.4 M KCl, eluent adjusted to pH 6.7, flow rate 2 mL/min. Detection conditions: 0.4 mM *o*-CPC in 0.25 M boric acid, pH 10.5, was employed as the post-column reagent and the resultant *o*-CPC-metal complexes were monitored at 570 nm.

**Figure 3.2:** The separation of a 5ppm Mg (II) and Ca (II) mixture prepared in the following matrices; DIW (navy trace), 1M KCl (pink trace) and 1M NaCl (green trace) on a 10 cm IDA silica monolith. Eluent conditions: 1M KNO<sub>3</sub>, pH 4.85, flow rate 1 mL/min. Detection conditions: 0.4 mM *o*-CPC in 0.25 M boric acid, pH 10.5, was employed as the post-column reagent and the resultant *o*-CPC-metal complexes were monitored at 570 nm.

**Figure 3.3:** Separation of 10 ppm Mg (II) and Ca (II) mixture prepared in DIW (navy trace), 1 M KCl (pink trace), 1M NaCl (green trace) and 1M CsCl (blue trace), on a 25 cm IDA silica gel column. Eluent conditions: 1 M KCl eluent, pH 4.85, flow rate 1 mL/min. Detection conditions: 0.4 mM *o*-CPC in 0.25 M boric acid, pH 10.5, was employed as the post-column reagent and the resultant *o*-CPC-metal complexes were monitored at 570 nm.

**Figure 3.4:** Separation of 10 ppm Mg (II) and Ca (II) in 1M KCl matrix on a 10 cm IDA functionalised monolith. Eluent conditions: 1 M KNO<sub>3</sub> eluent, pH 4.85, flow rate 1 to 4 mL/min. Detection conditions: 0.4 mM *o*-CPC in 0.25 M boric acid, pH 10.5,

was employed as the post-column reagent and the resultant *o*-CPC- metal complexes were monitored at 570 nm.

**Figure 3.5:** Overlay of (a) the Mg (II) van Deemter curves and (b) the Ca (II) van Deemter curves obtained on a 10 cm IDA silica monolith and a 3 cm packed IDA silica gel column.

**Figure 3.6:** The separation of a 10 ppm mixture of Mg (II) and Ca (II) prepared in a 1M KCl matrix. Eluent conditions: 1 M KNO<sub>3</sub> eluent adjusted to pH 4.30 (blue trace) and pH 4.85 (pink trace), flow rate 4 mL/min. Detection conditions: 0.4 mM *o*-CPC in 0.25 M boric acid, pH 10.5, was employed as the post-column reagent and the resultant *o*-CPC- metal complexes were monitored at 570 nm.

**Figure 3.7:** Separations of a 10 ppm Mg (II) and Ca (II) mixture prepared in 1 M KCl matrix (blue trace) and 2 M KCl matrix (pink trace) on a 10 cm IDA functionalised silica monolith. Eluent conditions: 1M KCl eluent, pH 4.85, flow rate 5 mL/min. Detection conditions: 0.4 mM *o*-CPC in 0.25 M boric acid, pH 10.5, was employed as the post-column reagent and the resultant *o*-CPC- metal complexes were monitored at 570 nm.

**Figure 3.8:** a) Overlay of unspiked 1 M NaCl and 1 M NaCl samples spiked with 0.5, 1.0 and 3.0 ppm Mg (II) and Ca (II), b) Standard addition calibration curves for Mg (II) and Ca (II) in a 1M laboratory grade NaCl sample. Eluent conditions: 1M NaNO<sub>3</sub> eluent, pH 5.30, flow rate 2.5 mL/min.

**Figure 3.9:** a) Overlay of unspiked 1 M KCl and 1 M KCl samples spiked with 0.5, 1.0 and 3.0 ppm Mg (II) and Ca (II), b) Standard addition calibration curves for Mg (II) and Ca (II) in a 1M laboratory grade KCl sample. Eluent used 1M NaNO<sub>3</sub>, pH 5.30, flow rate 2.5 mL/min.

**Figure 4.1:** The separation of (a) Mn (II), Co (II), Cd (II) and Zn (II) on a 10 cm IDA functionalised silica monolith and (b) Mn (II), Co (II) and Cd (II) mixture spiked with 20ppm and 40 ppm Co (II) standard Eluent conditions: 0.035 M KCl and 0.065 M

KNO<sub>3</sub>, pH 2.5, flow rate 1 mL/min. Detection conditions: post-column reaction with 0.1 mM PAR, 100 mM NaHCO<sub>3</sub>, 50 mM Na<sub>2</sub>CO<sub>3</sub>, pH 9.8, monitored at 495 nm.

**Figure 4.2:** The separation of Mg (II), Ca (II) and Mn (II) on a 10 cm IDA functionalised silica monolith. Eluent conditions: 0.08 M KNO<sub>3</sub>, pH 4.0, flow rate 1 mL/min. Detection conditions: post-column reaction with 0.1 mM PAR, 100 mM NaHCO<sub>3</sub>, 50 mM Na<sub>2</sub>CO<sub>3</sub>, pH 9.8, monitored at 495 nm.

**Figure 4.3:** (a) The separation of Cd (II), Zn (II) and Pb (II) on a 10 cm IDA silica monolith. Eluent conditions: 0.4 M KCl eluent, adjusted to pH 2.05, flow rate 1 mL/min. Detection conditions: post-column reaction with 0.1 mM PAR, 100 mM NaHCO<sub>3</sub>, 50 mM Na<sub>2</sub>CO<sub>3</sub>, pH 9.8, monitored at 495 nm and (b) van Deemter plot for Cd (II), Zn (II) and Pb (II) obtained on the 10 cm IDA silica monolith.

**Figure 4.4:** The separation of Mn (II), Cd (II), Co (II), Zn (II) and Pb (II) on a 10 cm IDA functionalised silica monolith. Eluent conditions: 0.2 M KCl eluent, adjusted to pH 2.5, flow rate 1 mL/min. Detection conditions: post-column reaction with 0.1 mM PAR, 100 mM NaHCO<sub>3</sub>, 50 mM Na<sub>2</sub>CO<sub>3</sub>, pH 9.8, monitored at 495 nm.

**Figure 4.5:** Overlays of the separation of selected transition and heavy metal cation on a 10 cm IDA functionalised silica monolith (blue trace) and a 25 cm IDA functionalised silica gel column (pink trace). Eluent conditions: 0.2 M KCl eluent, pH 2.02, flow rate 1 mL/min. Detection conditions: post-column reaction with 0.1 mM PAR, 100 mM NaHCO<sub>3</sub>, 50 mM Na<sub>2</sub>CO<sub>3</sub>, pH 9.8, monitored at 495 nm.

**Figure 4.6:** Overlays of the separation of selected transition and heavy metal cation on a 10 cm IDA functionalised silica monolith (blue trace) and a 25 cm IDA functionalised silica gel column (pink trace). Eluent conditions: 0.2 M KCl eluent, pH 2.50, flow rate 1 mL/min. Detection conditions: post-column reaction with 0.1 mM PAR, 100 mM NaHCO<sub>3</sub>, 50 mM Na<sub>2</sub>CO<sub>3</sub>, pH 9.8, monitored at 495 nm.

**Figure 4.7:** Overlays of the separation of 2ppm Mn (II), 5ppm Cd (II), 10 ppm Zn (II) and 20ppm Pb (II) on a 10 cm IDA functionalised silica monolith, using 0.2 M KCl (blue trace), KNO<sub>3</sub> (pink trace) and NaNO<sub>3</sub> (green trace) eluents, adjusted to pH 2.5,

flow rate = 1 mL/min. Detection conditions: post-column reaction with 0.1 mM PAR, 100 mM NaHCO<sub>3</sub>, 50 mM Na<sub>2</sub>CO<sub>3</sub>, pH 9.8, monitored at 495 nm.

**Figure 4.8:** van Deemter plots for Cd (II) and Pb (II) obtained with the 10 cm IDA silica monolithic column using 0.2 M KCl and KNO<sub>3</sub> eluents, pH 2.5.

**Figure 4.9:** (a) The separation of Mn, (II), Cd (II), Zn (II) and Pb (II) on a 10 cm IDA functionalised silica monolith. Eluent conditions: 0.2 M KCl eluent, pH 2.5, flow rate 3 mL/min, and (b) Van Deemter plots for Mn, (II), Cd (II), Zn (II) and Pb (II).

**Figure 4.10:** Overlays of separations of 2ppm Mn (II), 2ppm Cd (II), 10 ppm Zn (II) and 20 ppm Pb (II) on a 10 cm IDA functionalised silica monolithic column, using a 0.2 M KCl eluent (pink trace) and a 0.2 M KNO<sub>3</sub> eluent (blue trace) at 4 mL/min. Detection conditions: post-column reaction with 0.1 mM PAR, 100 mM NaHCO<sub>3</sub>, 50 mM Na<sub>2</sub>CO<sub>3</sub>, pH 9.8, monitored at 495 nm.

**Figure 5.1:** Structure of L-lysine amino acid.

**Figure 5.2:** Overlay of alkali metal standards on a 10 cm L-lysine functionalised silica monolith. Eluent conditions: 3 mM HNO<sub>3</sub>, flow rate 1mL/min. Detection method employed: suppressed conductivity detection.

**Figure 5.3:** Overlay of alkaline earth metal standards on a 10 cm L-lysine functionalised silica monolith. Eluent conditions: 3 mM HNO<sub>3</sub>, flow rate 1mL/min. Detection method employed: suppressed conductivity detection.

**Figure 5.4:** Overlay of Mn (II), Co (II), Cd (II) and Zn (II) standards retained on a 10 cm L-lysine functionalised silica monolith. Eluent conditions: 5 mM KCl eluent, pH 4.51, flow rate 2 mL/min. Detection conditions: post-column reaction with 0.4 mM PAR, 0.5 M ammonia, pH 10.5, monitored at 510 nm.

**Figure 5.5:** Overlays of cation-exchange capacity studies performed on both a 10 cm lysine silica monolith and a 10 cm bare silica monolith using (a) 1 mM CdCl<sub>2</sub> and (b) 1 mM ZnCl<sub>2</sub> at a flow rate of 1 mL/min.

**Figure 5.6:** Separations of nitrite, nitrate, iodide and thiocyanate on a 10 cm L-lysine monolith at flow rates of 3 mL/min (blue trace), 4 mL/min (pink trace) and 4.9 mL/min (green trace). Eluent conditions: 3 mM KCl, pH 6.0 and the analytes were monitored using direct UV at 225 nm.

**Figure 5.7:** Separation of bromate and bromide on a 10 cm L-lysine silica monolith at 2 mL/min (green trace), 3 mL/min (pink trace) and 4 mL/min (blue trace). Eluent conditions: 3 mM KCl eluent, pH 6.0. Analytes were detected by direct UV detection at 214 nm.

**Figure 5.8:** Separation of iodate and iodide on a 10 cm L-lysine functionalised silica monolith at 3 mL/min (blue trace), 4 mL/min (pink trace) and 4.9 mL/min (green trace). Eluent conditions: 3 mM KCl eluent, pH 6.0. Analytes were detected using direct UV detection at 214 nm.

**Figure 5.9:** van Deemter curves showing the effect of eluent flow rate on anion peak efficiency using a 10 cm L-lysine functionalised silica monolith.

**Figure 5.10:** The effect of phosphate buffer eluent pH on anion retention factor, on a 10 cm L-lysine monolithic silica column.

**Figure 5.11:** Effect of phosphate buffer eluent pH on anion selectivity using a 10 cm L-lysine silica monolith, flow rate 2 mL/min. Elution order: 1-nitrite, 2-bromate, 3-bromide, 4-nitrate, 5-iodide and 6-thiocyanate.

**Figure 5.12:** Nitrite van Deemter curve showing the effect of eluent flow rate on nitrite efficiency, over the eluent pH range 3.0 – 6.11.

**Figure 5.13:** Nitrate van Deemter curve showing the effect of eluent flow rate on nitrate efficiency, over the eluent pH range 3.0 – 6.11.

**Figure 5.14:** Iodide van Deemter curve showing the effect of eluent flow rate on iodide efficiency, over the eluent pH range 3.0 – 6.11.

**Figure 5.15:** Thiocyanate van Deemter curve showing the effect of eluent flow rate on thiocyanate efficiency, over the eluent pH range 3.0 – 6.11.

**Figure 5.16:** Overlays of anion-exchange capacity studies performed on a 10 cm lysine silica monolith using 1 mM KI, at (a) pH 6 and (b) pH 3, at a flow rate of 1 mL/min.

**Figure 5.17:** Overlays of the separations of nitrite, bromate, bromide, nitrate, iodide and thiocyanate on a 10 cm L-lysine functionalised silica monolith. Eluent conditions: 2 – 10 mM phosphate buffer eluent, pH 3.0, flow rate 4.9 mL/min, monitored at 214 nm.

**Figure 5.18:** Plot of  $\log k$  versus  $\log [E^-]$  showing the dependence of anion retention on the eluent ionic strength.

**Figure 5.19:** Overlays of the separation of the 6 test anions on the 10 cm L-lysine functionalised monolith analysed by 1) an isocratic separation using 10mM phosphate eluent, pH 3.0, flow rate 5 mL/min (pink trace) and 2) the separation achieved when a pH gradient was applied to increase the pH from pH 3.0 to pH 6.0 at  $t_1 = 3$  minutes and  $t_2 = 5$  minutes (blue trace). Analytes were monitored by direct UV detection at 214 nm.

**Figure 5.20:** Separation of the 6-test anions mixture on a 10cm L-lysine functionalised silica monolithic column. Eluent conditions: 20 mM phosphate buffer eluent, pH 3.0, at flow rates of 5 mL/min (blue trace) and 6 mL/min (pink trace). Analytes were monitored by direct UV detection at 214 nm.

**Figure 5.21:** van Deemter curves showing the effect of elevated flow rates on anion peak efficiency on the 10 cm L-lysine functionalised silica monolith.

**Figure 5.22:** Overlays of the separation of 1-nitrite, 2-bromate, 3-bromide, 4-nitrate, 5-iodide and 6-thiocyanate using 10 mM (blue trace), 20 mM (pink trace), 30 mM

(green trace) and 50 mM (orange trace) phosphate buffer eluent, pH 3.0, flow rate 4.9 mL/min. Analytes were monitored by direct UV detection at 214 nm.

**Figure 5.23:** The effect of phosphate buffer eluent concentration (pH 3.0) on anion peak efficiencies analysed on the 10 cm L-lysine functionalised silica monolithic column, using flow rates of (a) of 1 mL/min and (b) 4.9 mL/min.

**Figure 5.24:** Overlays of 1-nitrite, 2-bromate, 3-bromide, 4-nitrate, 5-iodide and 6-thiocyanate separations on a 10 cm L-lysine functionalised silica monolith using a flow gradient, i.e., the eluent flow rate was increased from 2 - 4.9 mL/min over 5 minutes (blue trace), 4 minutes (pink trace) and 3 minutes (green trace). Eluent conditions: 20 mM phosphate buffer eluent (pH 3.0).

**Figure 5.25:** Overlays of 1-nitrite, 2-bromate, 3-bromide, 4-nitrate, 5-iodide and 6-thiocyanate separations on a 10 cm L-lysine functionalised silica monolith using a flow gradient, i.e., the eluent flow rate was increased from 2 - 4.9 mL/min over 5 minutes (blue trace), 4 minutes (pink trace), 3 minutes (green trace) and 2 minutes (orange trace). Eluent conditions: 30 mM phosphate buffer eluent (pH 3.0).

**Figure 5.26:** van Deemter curve obtained on the 10 cm L-lysine functionalised silica monolith. Eluent conditions: 50 mM phosphate buffer eluent, pH 3.0.

**Figure 5.27:** Overlays of 1-nitrite, 2-bromate, 3-bromide, 4-nitrate, 5-iodide and 6-thiocyanate separation on a 10 cm L-lysine functionalised silica monolith using a flow rate of 1 mL/min (blue trace) and the following flow gradients, i.e., the eluent flow rate was increased from 1 - 4.9 mL/min over 4 minutes (pink trace) and 2 minutes (green trace). Eluent conditions: 50 mM phosphate buffer eluent (pH 3.0).

**Figure 5.28:** Overlays of 1-nitrite, 2-bromate, 3-bromide, 4-nitrate, 5-iodide and 6-thiocyanate separations on a 10 cm L-lysine functionalised silica monolith at 2 mL/min (blue trace) and using a flow gradient, i.e., the eluent flow rate was increased from 2 - 4.9 mL/min over 4 minutes (pink trace), 2 minutes (green trace) Eluent conditions: 50 mM phosphate buffer eluent (pH 3.0).

**Figure 5.29:** Overlays of injection number 1, 5, and 10 of the nitrite, bromate, bromide, nitrate, iodide and thiocyanate mixture on the 10 cm L-lysine functionalised silica monolithic column at flow rate (a) 2 mL/min and (b) 4 mL/min Eluent conditions: 50 mM phosphate buffer eluent, pH 3.0. Analytes were monitored using direct UV detection at 214 nm.

**Figure 6.1:** (a) The basic amino acid structure and (b) the zwitterion structure.

**Figure 6.2:** The reaction of primary and secondary amino acids with Ninhydrin.

**Figure 6.3:** The reaction mechanism for the reaction of *o*-phthaldialdehyde with amino acids, where R is the amino acid residue, HX is the nucleophilic agent.

**Figure 6.4:** Schematic showing the structure of a Cu (II) modified L-lysine functionalised silica monolithic column.

**Figure 6.5:** A plot of amino acid retention factor as a function of sodium acetate/acetic acid buffer concentration (mM), pH 4.7, flow rate 1 mL/min.

**Figure 6.6:** A plot of amino acid retention factor as a function of the Cu (II) acetate concentration present in the mobile phase (30 mM sodium acetate/acetic acid buffer, pH 4.7), flow rate 1 mL/min.

**Figure 6.7:** A plot of amino acid retention factor as a function of mobile phase pH (30 mM sodium acetate/acetic acid and 0.05 mM Cu (II) acetate), flow rate 1 mL/min.

**Figure 6.8:** The separation of mixtures of amino acids on the 10 cm Cu (II)-L-lysine silica monolith, using a 30 mM sodium acetate/acetic acid buffer eluent containing 0.05 mM Cu (II) acetate, with the eluent pH adjusted to 5.0 and 5.2. Flow rate 1 mL/min and detection by UV detection @ 254 nm.

**Figure 6.9:** The separation of amino acid mixtures using (a) isofluentic conditions and a flow gradient and (b) an elevated flow rate of 4.9 mL/min using a 30 mM sodium acetate/ acetic acid buffer (pH 5.2) eluent containing 0.05 mM Cu (II) acetate.

**Figure 6.10:** The separation of mixtures of amino acids on the 10 cm Cu (II)-L-lysine silica monolith, using a 30 mM sodium acetate/ acetic acid buffer eluent containing 0.05 mM Cu (II) acetate, eluent pH 5.7. Flow rate 2 mL/min and detection by UV detection @ 254 nm.

**Figure 6.11:** The detection of 50 ppm amino acids standards using PCR detection using a OPA/ Na<sub>2</sub>SO<sub>3</sub> reagent, heated 90 °C, and fluorescence detection at 328/400 nm.

**Figure 6.12:** The structure of the thiol used in the OPA/thiol post column reagent for the fluorescent detection of amino acids.

**Figure 6.13:** Absorption and fluorescence spectra for the amino acid-OPA/NAC reaction (a) reaction time = 0 minutes and (b) 30 minutes reaction at room temperature.

**Figure 6.14:** The separation of amino acids on the 10 cm Cu (II)-L-lysine functionalised silica monolith using a 30 mM sodium acetate/acetic acid buffer, pH 5.73, 0.05 mM Cu (II) acetate, at flow rates of (a) 2 mL/min and (b) 7 mL/min.

**Figure 6.15:** The two stereoisomers of the amino acid valine.

**Figure 6.16:** Overlays of L- and D-amino acid standards on the 10 cm Cu (II)-lysine monolith using a 30 mM sodium acetate buffer (pH 5.7) and 0.05 mM Cu (II) acetate eluent, flow rate 2 mL/min.

**Figure 7.1:** The types of silanols groups present on the surface of silica.

**Figure 7.2:** Overlays of 20 ppm Mg (II), 20 ppm Ca (II), 40 ppm Sr (II) and 60 ppm Ba (II) standards on a 10 cm bare silica monolith. Eluent conditions: 70 % acetonitrile and 31.3 mM ammonium acetate buffer, pH 4.6, flow rate 1 mL/min. Detection conditions: post-column reaction with *o*-CPC monitored at 570 nm.

**Figure 7.3:** Overlays of 20 ppm Mg and 30 ppm Ca injections on a 10 cm bare silica monolith. Eluent conditions: 80 % acetonitrile and ammonium acetate buffer, pH 4.6, flow rate 1 mL/min. Detection conditions: post-column reaction with PAR monitored at 510 nm.

**Figure 7.4:** Overlays of the separations obtained for the following mixtures: 20 ppm Ca (II), 40 ppm Sr (II) and 60 ppm Ba (II) and 20 ppm Mg (II), 40 ppm Sr (II) and 60 ppm Ba (II). Eluent conditions: 70 % acetonitrile and ammonium acetate buffer (23.4 mM, pH 5.55) eluent, flow rate 2 mL/min. Detection by post-column reaction with *o*-CPC monitored at 570 nm.

**Figure 7.5:** Overlays of 20 ppm Mg (II) and 30 ppm Ca (II) standards on a bare silica monolith. Eluent conditions: 80 % acetonitrile and 41.2 mM ammonium acetate/acetic acid buffer with pH increased from 4.9 –5.9. Flow rate 1 mL/min and detection by post-column reaction detection using PAR monitored at 510 nm.

**Figure 7.6:** Separations of mixtures of 20 ppm Ca (II), 40 ppm Sr (II) and 60 ppm Ba (II) and 40 ppm Mg (II), 40 ppm Sr (II) and 60 ppm Ba (II). Eluent conditions: 70 % acetonitrile and ammonium acetate/acetic acid buffer (23.4 mM, pH 4.6), flow rate 4 mL/min. Detection by post-column reaction with *o*-CPC monitored at 570 nm.

**Figure 7.7:** van Deemter plot for alkaline earth metal cations, obtained using 70 % acetonitrile and ammonium acetate/acetic acid buffer, (23.4 mM, pH 4.6), on a 10 cm bare silica monolith.

**Figure 7.8:** van Deemter Plot for alkaline earth metal cations obtained using 70 % acetonitrile and ammonium acetate/acetic acid buffer (23.4 mM, pH 5.5), on a 10 cm bare silica monolith.

**Figure 7.9:** Ca (II) and Sr (II) standards on the 10 cm bare silica monolith using an eluent composed of 70 % MeCN containing 31.25 mM sodium acetate/acetic acid buffer (pH 4.6), flow rate 1 mL/min.

**Figure 7.10:** Sr (II) standards on the 10 cm bare silica monolith using a mobile phase composed of 70 % MeCN containing 62.5 mM sodium acetate/acetic acid buffer (pH 4.6), flow rate 1 mL/min.

**Figure 7.11:** The effect of mobile phase buffer concentration on cation peak shape using 80 % acetonitrile and (a) 5.2 mM and (b) 20.6 mM ammonium acetate buffer, (pH 4.6).

**Figure 7.12:** Plots for Cu (II), Cd (II), Ni (II), Co (II) and Mn (II) showing the variation of cation retention factors as the % acetonitrile and ammonium acetate/acetic acid buffer concentration (pH 4.6) in the mobile phase increased.

**Figure 7.13:** Baseline separation of selected transition and heavy metal cations on a bare silica monolith. Eluent conditions: 80 % acetonitrile and 10.3 mM ammonium acetate buffer, pH 4.6, flow rate 1 mL/min.

**Figure 7.14:** Separation of a mixture of the transition metal cations on a bare silica monolith using an eluent composed of 80 % acetonitrile and 10.3 mM ammonium acetate buffer (pH 4.62), at flow rates 1, 3 and 5 mL/min.

**Figure 7.15:** van Deemter plots for Cu (II), Cd (II) and Mn (II) on the 10 cm bare silica monolith.

**Figure 7.16:** Separation of transition metal cations on a 10 cm bare silica monolith using an eluent composed of 80 % acetonitrile and 41.2 mM sodium acetate/acetic acid buffer (pH 4.6), flow rate of 1 mL/min.

**Figure 7.17:** The effect of increasing (a) % acetonitrile and (b) % methanol on the retention of Cu (II), Cd (II) and Mn (II). Eluent conditions: organic solvent and 50 mM ammonium acetate/acetic acid buffer (undiluted concentration), pH 4.6. Flow rate: 1 mL/min.

**Figure 7.18:** Overlays of selected transition and heavy metal ion standard injections using (a) 60% methanol containing 21.1 mM ammonium acetate buffer and (b) 80% methanol containing 10.3 mM ammonium acetate buffer (pH 4.6), flow rate 1 mL/min.

## List of Tables

**Table 1.1:** List of current commercial monolithic stationary phases for HPLC separations.

**Table 1.2:** The effect on column backpressure and efficiency when 100 x 4.6 mm Chromolith<sup>TM</sup> Performance PR-18e monolithic columns are linked in series.

**Table 1.3:** Comparison of analytical accuracy for a real sample between the monolithic HPLC method and a traditional GC method.

**Table 1.4:** A comparison of analytical performance reported by Xu *et al.* [91].

**Table 1.5:** A comparison of analytical performance reported by Xu *et al.* [93].

**Table 1.6:** A summary of the different functional groups found on common anion- and cation-exchangers.

**Table 1.7:** Limiting equivalent conductances in aqueous solution at 25°C, units S.cm<sup>2</sup>equiv<sup>-1</sup>.

**Table 1.8:** A summary of the reagents for the post-column detection of inorganic cations.

**Table 2.1:** Summary of the ion chromatographic separations achieved on modified reversed-phase silica monolithic columns.

**Table 2.2:** Elemental and surface analysis of the 10 cm IDA functionalised silica monolith.

**Table 2.3:** The effect of HNO<sub>3</sub> eluent concentration on the retention of alkali and alkaline earth metal ions on a 10 cm, IDA functionalised silica monolithic column. Eluent flow rate 1 mL/min.

**Table 2.4:** The selectivity exhibited for alkali metal ions on a 25 cm IDA functionalised silica gel column and a 10 cm IDA functionalised silica monolithic column.

**Table 2.5:** The selectivity exhibited for alkali metal ions on a 10 cm bare silica monolith and a 10 cm IDA functionalised silica monolithic column.

**Table 2.6:** The effect of methansulfonic acid (MSA) eluent concentration on the retention of alkali and alkaline earth metal ions on a 10 cm, IDA functionalised silica monolithic column. Eluent flow rate 1 mL/min.

**Table 2.7:** The selectivity exhibited for alkali cation on a 25 cm IDA functionalised silica gel column and a 10 cm IDA functionalised silica monolithic column.

**Table 2.8:** The effect of eluent concentration on the retention and resolution of Mg (II), Ca (II) and Ba (II) on the IDA silica monolith.

**Table 2.9:** The effect of KNO<sub>3</sub> eluent (pH 4.85) concentration on of the alkaline earth metal ion retention, flow rate 1 mL/min.

**Table 3.1:** The resolution values obtained for the 10 ppm Mg (II), Ca (II) mixture prepared in both 1 and 2 M KCl brines, separated using 1 M KNO<sub>3</sub> eluent, with a flow rate of 4 mL/min.

**Table 3.2:** Summary of analytical performance data for the 10 cm IDA silica monolith.

**Table 4.1:** The effect of KCl eluent concentration (pH 2.0) on the retention times of Co (II), Cd (II), Zn (II) and Pb (II) on a 10 cm IDA functionalised silica monolith, flow rate 1 mL/min.

**Table 4.2:** The effect of KCl eluent concentration (pH 2.5) on the retention times of Mn (II), Co (II), Cd (II), Zn (II) and Pb (II) on a 10 cm IDA functionalised silica monolith, flow rate 1 mL/min.

**Table 4.3:** The effect of different inorganic eluents on the retention factor of transition metals on the 10 cm IDA silica monolith, flow rate 1 mL/min.

**Table 4.4:** Precision data for 10 repeat injections of a mixture of 2 ppm Mn (II), 2 pm Cd (II), 10 ppm Zn (II) and 20 ppm Pb (II) on the 10 cm IDA silica monolith, using a 0.2 M KCl eluent, pH 2.5, flow rate 3 mL/min.

**Table 4.5:** The resolution data for Mn (II) and Cd (II) on the 10 cm IDA silica monolith using 0.2 M KCl and 0.2 M KNO<sub>3</sub> eluents, (pH 2.5), flow rate 1-4 mL/min.

**Table 5.1:** The effect of KCl eluent pH on the retention factors of selected transition and heavy metal cations retained on a 10 cm L-lysine functionalised silica monolith, flow rate 2 mL/min.

**Table 5.2:** Slope and R<sup>2</sup> values calculated from the plot of log *k* versus log [KCl].

**Table 5.3:** The effect of phthalate eluent concentration (pH 6.5) on anion retention using a 10 cm L-lysine silica monolith, flow rate 1 mL/min.

**Table 5.4:** Summary of results obtained for the anion capacity studies performed on a 10 cm lysine functionalised silica monolith.

**Table 5.5:** The retention data obtained for a selection of UV absorbing anions analysed on the 10 cm L-lysine functionalised silica monolithic column. Eluent conditions: 10 mM phosphate buffer, pH 3.0, flow rate 2 mL/min.

**Table 5.6:** The values of both the slope and  $R^2$  values calculated for each of the anions shown in Fig. 5.18.

**Table 5.7:** Summary of the results obtained for the precision study performed using a 10 cm L-lysine functionalised silica monolith. Eluent conditions: 50 mM phosphate buffer eluent (pH 3.0), flow rates 2 and 4 mL/min. A detection wavelength of 214 nm was employed.

**Table 6.1:** Amino acid selectivity on the 10 cm Cu (II)-L-Lysine functionalised monolith. Eluent: 30 mM sodium acetate/ acetic acid buffer (pH 5.7), 0.05 mM Cu (II) acetate; flow rate 2 mL/min. Fluorescence detection at 340/450 nm using PCR detection with OPA/NAC reagent.

**Table 6.2:** Precision data for the analysis of amino acids on a 10 cm Cu (II) coated – lysine functionalised monolith, using an eluent composed of 30 mM sodium acetate/acetic acid buffer and 0.05 mM Cu (II) acetate, pH 5.73, at a flow rate of 7 mL/min.

**Table 7.1:** Effect of increasing % acetonitrile on the retention of Mg (II), Ca (II), Sr (II) and Ba (II) on a 10 cm bare silica monolithic column. Eluent conditions: acetonitrile and 30 mM ammonium acetate/acetic acid buffer, pH 4.6, flow rate 1 mL/min.

**Table 7.2:** Slope and linear correlation coefficient data determined from plots of  $\log k$  versus  $\log [E^+]$  for each alkaline earth metal cation, flow rate 1 mL/min.

**Table 7.3:** The effect of ammonium acetate buffer pH on the retention of alkaline earth metal cations on a 10 cm bare silica monolith using an eluent composed of 70 % acetonitrile and 23.4 mM ammonium acetate/acetic acid buffer, flow rate 1 mL/min.

**Table 7.4:** The retention factors of transition metal cations on a bare silica monolith using eluents composed of acetonitrile and 20 mM ammonium acetate/acetic acid buffer, pH 4.6, eluent flow rate of 1 mL/min.

**Table 7.5:** Slope and linear correlation coefficient data determined from plots of log k versus log [E<sup>+</sup>] constructed for each transition metal cation.

**Table 7.6:** Retention data showing the effect of varying the ammonium acetate buffer pH on the retention of transition and heavy metal ions on a 10 cm bare silica monolith. Eluent conditions: 80 % acetonitrile and 10 mM acetate buffer, flow rate 1 mL/min.

**Table 7.7:** The effect of increasing acetonitrile content on cation retention on a bare silica monolith, using a mobile phase composed of acetonitrile containing 16 mM sodium acetate buffer/ acetic acid, pH 4.6, 1 mL/min.

**Table 7.8:** Dielectric constant data for acetonitrile and methanol.

# **Chapter 1**

## ***Introduction to monolithic silica stationary phases and their application to ion chromatography***

## **Section 1.1: The development and applications of monolithic silica HPLC columns**

### **1.1.1: The need for faster HPLC separations**

In recent years, the demand on laboratories to improve productivity has necessitated the development of faster, higher through-put analytical procedures [1]. HPLC is routinely used for diverse applications such as product quality control, analysing compound libraries synthesised by combinatorial chemistry methods and environmental monitoring. Pharmaceutical companies have recently developed the idea of combinatorial chemistry in their search for more effective drugs. In such an approach, chemists need to synthesize a large array of compounds and have them analysed quickly. In many cases, this results in thousands of new compounds being produced each month. As a consequence of this, the standard 15 or 20 minute HPLC separation is too time consuming for high through-put analysis. In addition, the HPLC columns themselves must be very robust as the trend is for laboratories to operate 24 hours a day to complete the required volume of analyses [2].

A second motivation for the development of fast HPLC methods is the need for real or near-time monitoring. Real time monitoring requires continuous or extremely rapid analytical measurements, and as such, has been restricted to those analytical techniques/instruments that have fast response times, predominantly spectroscopic or sensor based techniques. The prospect of performing real time measurements with chromatography is a very attractive one, but again, the impediment to realising this goal is the long run times associated with traditional HPLC separations. These run times are too slow for continuous monitoring of many processes, which may have run times of the order of a few minutes. Therefore, for HPLC to be useful in real or near-time monitoring, it is necessary to significantly reduce the time it takes to perform the separation of target solutes [3].

In the past, chromatographic technology has placed certain limitations on the level of laboratory productivity. Not least of these limitations was the available HPLC column technology. The heart of each HPLC method is the column, which enables the

resolution of compounds based upon the selectivity and column performance. Generally HPLC columns consist of a tube (made of stainless steel, glass or synthetic polymers) filled with porous silica particles or in some cases polymer or carbon based particles.

### **1.1.2: Development of HPLC silica stationary phases**

Columns packed with silica particles have been the mainstay of HPLC for the past 30 years. They were developed in stages:

- Irregular particles were the first generation.
- Spherical particles were the second generation.
- High-purity spherical silica particles were the third generation.

At the beginning of the 1970s, companies such as Merck KGaA started producing and marketing the first generation of porous, irregular silica gels with particle size from 5 to 10  $\mu\text{m}$ . Development then proceeded rapidly, and researchers in universities and industry began to produce spherical porous materials. It was assumed that spherical particles would enable HPLC columns to be packed more densely and hence produce better quality separations. The production of a series of surface-modified spherical materials became the challenge for many chromatography companies over the years 1980 to 1990. The third generation of HPLC silica stationary phases was initiated by the ever-increasing demands of chromatographers faced with the task of separating ever more complex mixtures of substances, especially basic pharmaceutical substances. Since 1995, work has been concentrated on refining chromatography materials; developing spherical, porous materials of particle size extending to 3  $\mu\text{m}$  and smaller with optimised surface modifications [4]. Therefore, since the introduction of HPLC more than 30 years ago, column-packing materials have changed dramatically from irregular shaped to spherical, and from large particles to small [5]. To understand this trend and the benefits of using smaller sized particles on the column performance, the theory of the hydrodynamics of chromatography needs to be explained.

### 1.1.3: Hydrodynamics of Chromatography

An important characteristic of a chromatographic system is its efficiency expressed as a dimensionless quantity called the effective plate number. It reflects the number of times the solute partitions between the eluent (mobile phase) and stationary phase during its passage through the column. After 50 or more partitions between the phases, the resultant profile of a solute band closely approaches that given by a Gaussian distribution curve. The effective plate number ( $N_{\text{eff}}$ ) can be defined from the chromatogram of a single band as [6]:

$$N_{\text{eff}} = L/H = (t_r'/\sigma)^2 \quad (\text{Eqn 1.1})$$

Where,  $L$  is the length of column, usually expressed in cm and  $H$  is defined as the height equivalent to a theoretical plate. The width of a Gaussian curve is described by the standard deviation ( $\sigma$ ) and the variance ( $\sigma^2$ ). The relative retention time,  $t_r'$ , is equal to  $t_r - t_m$ , where  $t_r$  is the solute retention time and  $t_m$  is the column void time. Assuming an ideal Gaussian distribution, the width at the base of the peak,  $W_b$ , is equal to four standard deviations:

$$N = 16 (t_r'/W_b)^2 \quad (\text{Eqn 1.2})$$

This width is an impediment to resolution. Resolution can be defined as the degree of separation between two adjacent solute peaks. It is therefore important to understand the parameters that influence peak width. The plate height (HETP) expresses in simple terms the extent of band broadening and the factors that affect broadening. The van Deemter equation describes the dependence of the HETP on the eluent linear velocity. It assumes that the HETP is composed of three different, independent contributions [7]:

$$H = A + B/\mu + C_{\text{stat}}\mu + C_{\text{mobile}}\mu \quad (\text{Eqn 1.3})$$

In the above van Deemter equation the velocity independent  $A$  term is affected by the size and distribution of the interparticle channels and non-uniformities in the packed bed. As Fig. 1.1. demonstrates, the  $B$  term is inversely proportional to the eluent linear velocity ( $\mu$ ), and the  $C$  terms are directly proportional to the linear velocity. Ideally a linear velocity corresponding to the minimum plate height should be employed, however, a loss in efficiency may be traded for shortened analysis time when linear velocities higher than  $\mu_{\text{opt}}$  are used.

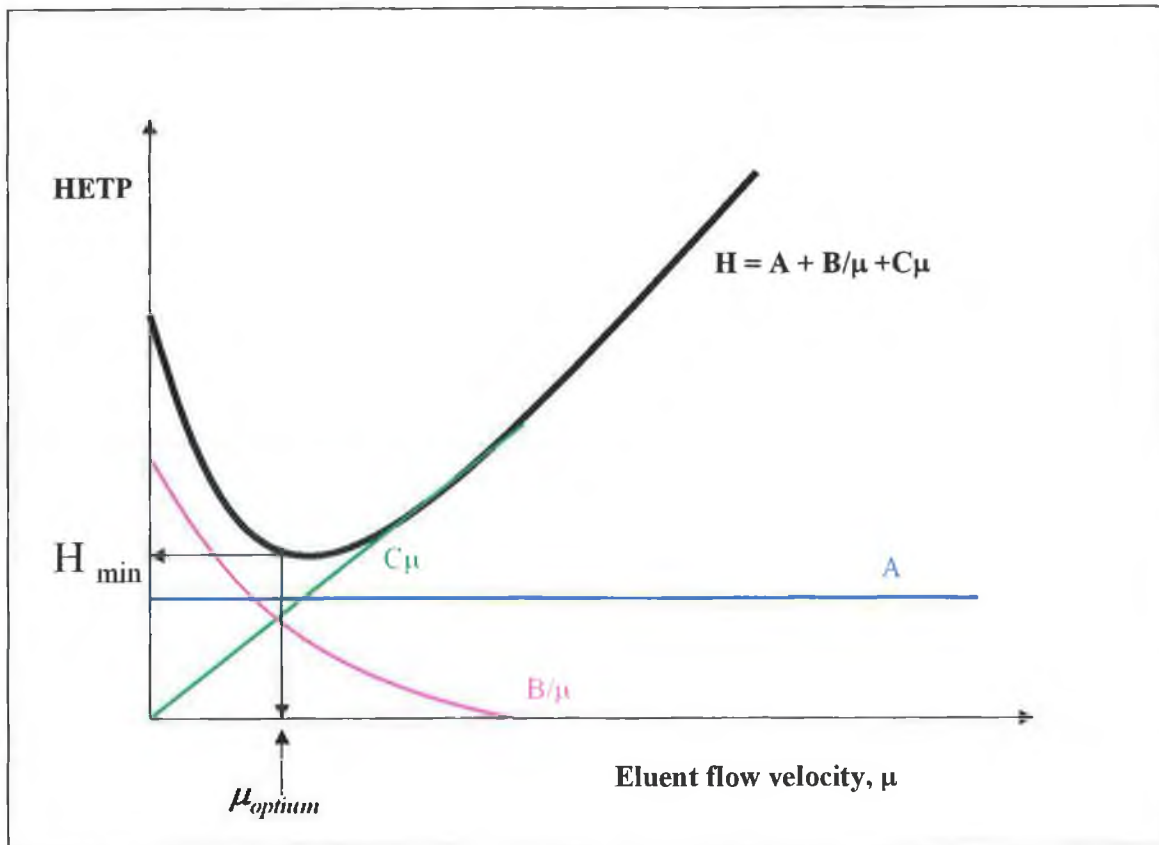


Figure 1.1: The individual contributions of the terms in the van Deemter equation are shown graphically.

### 1.1.3.1: Flow irregularities

Eddy diffusion results from the in-homogeneity of flow velocities and path lengths around packing particles. In the van Deemter equation, the A term is defined as  $A = \lambda d_p$ , where  $d_p$  is the particle diameter and  $\lambda$  is a function of the packing uniformity and the column geometry. Flow paths of unequal length will exist through all packed beds. Some solute molecules of a single species may find themselves swept through the column close to the column wall where the density of packing is comparatively low, especially in small diameter columns. Other solute molecules pass through the more tightly packed centre of the column at the correspondingly lower velocity, see Fig. 1.2. Molecules that follow a shorter path elute before those following a series of erratic (and longer) paths. This results in broadening of elution bands for each solute. To minimise the A term, the mean diameter of the particle in a column packing should be as small as possible and packed as uniformly as possible.

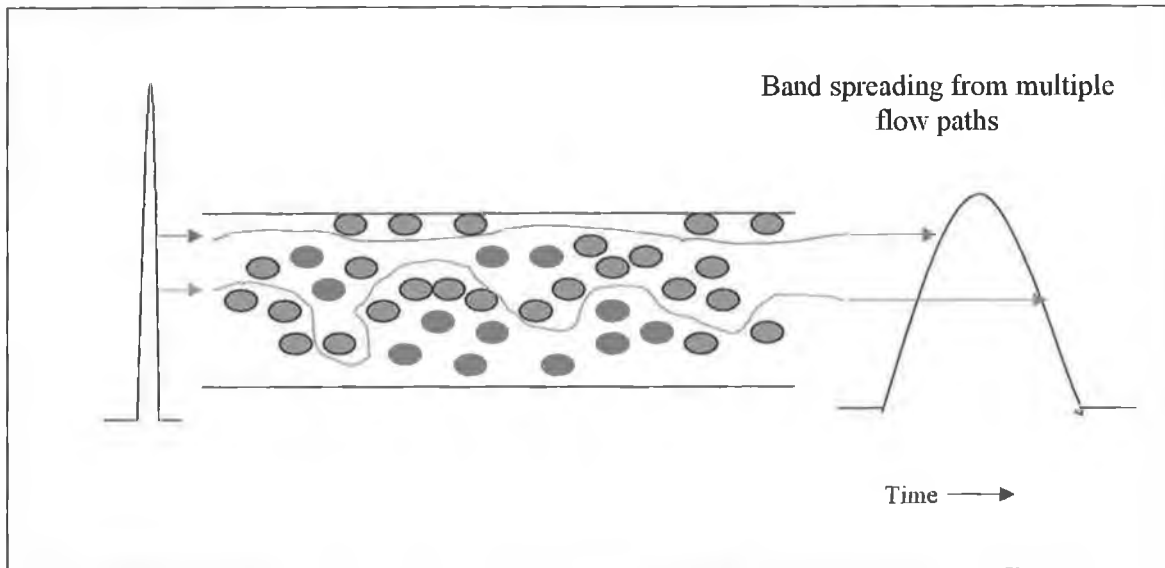


Figure 1.2: Schematic showing the process of eddy diffusion [8].

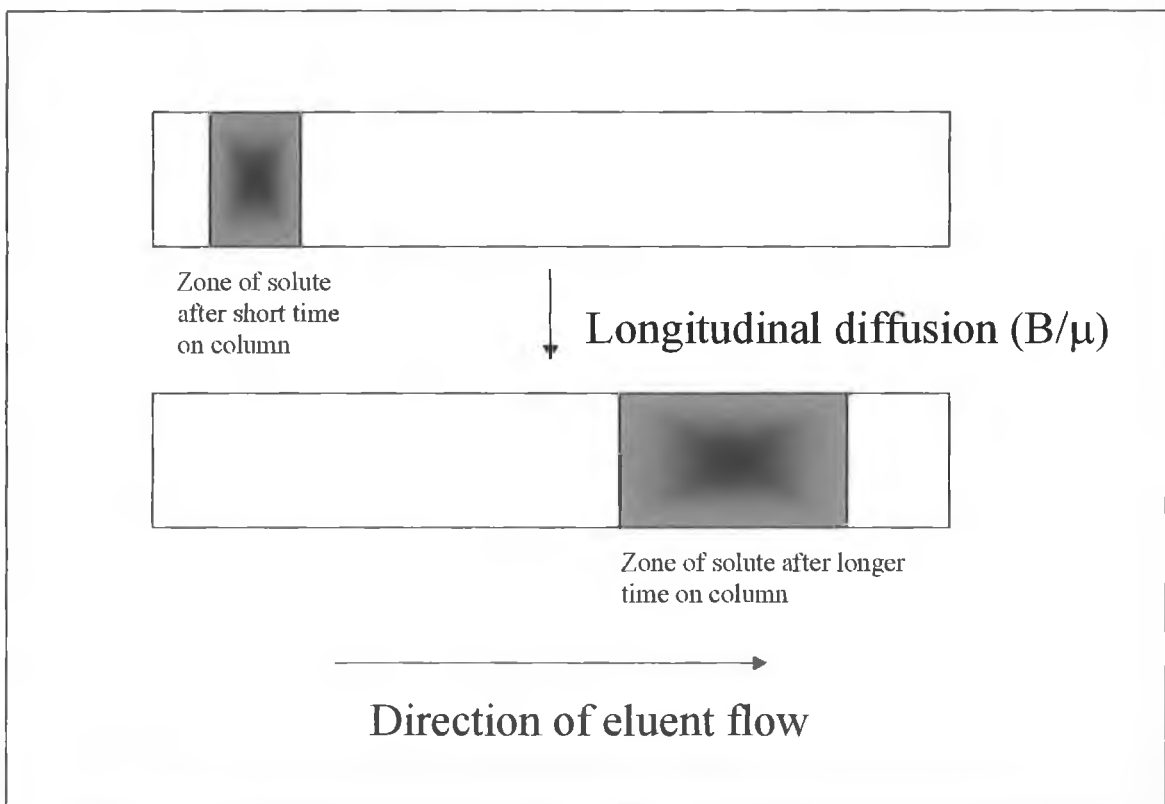


Figure 1.3: Schematic showing longitudinal diffusion [8].

### ***1.1.3.2: Transverse and longitudinal diffusion***

The B term in the van Deemter equation defines the effects of longitudinal, or axial diffusion, that is, random molecular motion within the eluent.  $B = 2\gamma D_m$ , where  $\gamma$  is an obstruction factor, which recognises the fact that longitudinal diffusion is hindered by the packing or bed structure, and  $D_m$  is the solute diffusion coefficient in the eluent. The contribution of longitudinal diffusion to plate height becomes significant only at low eluent flow rates. Molecular diffusion takes place when the eluent is flowing through the packed bed. If the eluent is flowing very slowly, the analyte will remain in the column for a longer period of time. Therefore, band-spreading results from the high diffusion rates of a solute in the eluent, which causes the solute molecules to disperse axially while slowly migrating through the column, see Fig. 1.3. If this happens, peak broadening occurs, but the use of elevated flow rates will minimise these effects.

### ***1.1.3.3: Mass transfer***

In HPLC the solute needs to be transported from the moving eluent to the surface of the stationary phase particle, through the stagnant eluent in the pores of the stationary phase, to the internal surface of the stationary phase where the interaction between the solute and the stationary phase take place (e.g. the adsorption and desorption process), after which the solute is transported back into the moving eluent. In principal, two major contributions to the resistance to mass transfer can be distinguished: mass transfer in the eluent and mass transfer in the stationary phase. The  $C_{\text{stat}}$  term results from resistance to mass transfer of the solutes at the stationary phase interface. Slow molecular movement within the stationary phases means a longer time spent in this phase by a solute molecule, while the other molecules are moving forward with the eluent. The faster the eluent moves through the column and the slower the rate of mass transfer, the broader the solute band that eventually elutes from the column, see Fig. 1.4. The  $C_{\text{mobile}}$  term represents radial mass transfer resistance between adjacent streamlines of eluent. It is proportional to the square of the particle diameter of the packing material,  $d_p^2$ . In the case of mass transfer, band broadening increases with eluent flow velocity, as the sample molecules remaining in the moving eluent become

further removed from stagnant molecules the faster the solvent flux. However, this effect is much less pronounced with smaller particles (1.5-3  $\mu\text{m}$ ) than with larger particles (5-10  $\mu\text{m}$ ) because smaller particles are much less resistant to mass transfer and yield flatter van Deemter curves, allowing for the use of high flow rates.

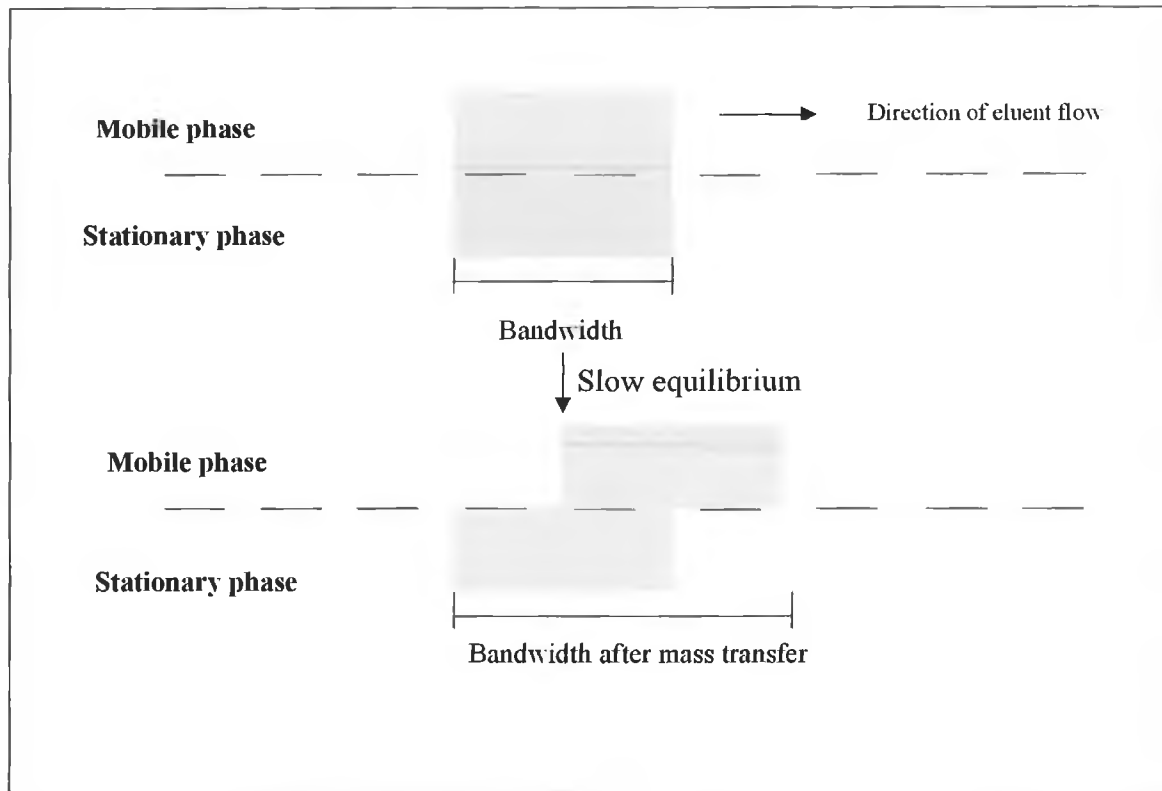


Figure 1.4: Schematic of the process of mass transfer [8].

#### **1.1.4: Limits of particle-packed HPLC columns**

The very nature of stationary phase particles, when packed tightly into a HPLC column, creates a significant obstacle to flow of eluent/sample matrix. The end result is that high column backpressures have to be overcome to produce an acceptable flow rate. Another disadvantage of particle-packed columns is the inevitable shifting and settling of the packed bed, which eventually results in peak tailing and splitting [9].

Equations that define the properties of packing materials and columns include [5]:

$$K = \mu\eta L / \Delta P, \mu = L / t_m \quad (\text{Eqn 1.4})$$

In Equation 1.4, K is the column permeability,  $\mu$  is the linear velocity of the eluent, which is equal to column length (L)/the column void time ( $t_m$ ),  $\eta$  is the solvent viscosity and  $\Delta P$  is the column backpressure. The separation impedance (E) is given by:

$$E = \Delta P t_m / \eta N^2 = (\Delta P / N)(t_m / N)(1 / \eta) = H^2 / K \quad (\text{Eqn 1.5})$$

Reducing  $d_p$  can lead to better column efficiency (larger N) or smaller H due to a smaller A-term and the shorter diffusion path length inside the particle, i.e. smaller C-term in Equation 1.3. The latter is especially true at high eluent linear velocities. The interparticle mass transport is affected by rapid convection in particulate columns, while mass transfer within particles takes place entirely based on molecular diffusion, which is very slow relative to convection, especially for macromolecules. The difference in the time required for a solute to travel through the intra- and interparticle spaces becomes progressively greater as the eluent linear velocity increases, therefore, it is necessary to make the particle smaller to shorten the time required to diffuse within a particle [10].

In the case of a particulate-packed HPLC column, H is roughly proportional to  $d_p$ , whereas  $\Delta P$  is inversely proportional to  $d_p^2$ , and the limitation in the performance of particulate-packed HPLC columns is well recognised to be based on the pressure limit of the solvent delivery system, leading to the current compromise at  $\sim 3\text{-}5 \mu\text{m}$  particle size between column efficiency and pressure drop [11]. Therefore, an increase in column efficiency from using small particles is accompanied by a large increase in  $\Delta P$ . Thus, increasing the flow rate to speed up the separation process sets a limitation as a result of the high backpressure, and working under these conditions usually results in a decrease in the column lifetime and will negatively affect the HPLC equipment [11].

### **1.1.5: Advances in rapid, high through-put separations**

The equations described in Section 1.1.4 demonstrate that operation at high speed is not compatible with high efficiency in the case of columns with larger sized particles

(5-10  $\mu\text{m}$ ), due to a sharp increase in theoretical plate height, and it is not possible with smaller sized particles ( $< 3 \mu\text{m}$ ) either, due to high column backpressure. However, recent improvements in separation speed have been realised by simultaneously decreasing the column length and the particle size so that analysis time is reduced while maintaining efficiency [12]. Short HPLC columns packed with 1.5-3  $\mu\text{m}$  silica particles exhibit excellent mass transfer characteristics previously discussed for smaller particles, whilst the short columns themselves generate only moderate backpressure and can still be used with conventional flow rates.

Previously, fast HPLC has generally been confined to reversed-phase separations of pharmaceuticals [13,14], peptides and proteins [15,16,17,18] and other biological macromolecules [19,20], due to the large range of 1.5-3  $\mu\text{m}$  reversed-phase silica particles commercially available. For example, the separation of 6 peptides, in less than 1 minute, was reported by Moriyama *et al.* [15]. Using a 50 mm x 4.6 mm TSKgel Super- reversed-phase silica column, (2  $\mu\text{m}$  silica particle diameter), the 1 minute separation of oxytocin,  $\alpha$ -endorphin, bombesin, leu-enkephalin,  $\gamma$ -endorphin and somatostatin was achieved using an eluent composed of 13 mM  $\text{HClO}_4$ -acetonitrile, with a 2 minute linear gradient of acetonitrile from 23-56 %, at a flow rate of 2 mL/min. A mixture of nine proteins was separated in under two minutes on a 75 mm x 2.1 mm Poroshell 300 SB reversed-phase silica column (5  $\mu\text{m}$  silica particle diameter) by Kirkland *et al.* [19]. The synthetic mixture of nine proteins was separated in less than 2 minutes at a flow rate of 2 mL/min, column temperature 35  $^\circ\text{C}$ , with excellent peak shapes and resolution exceeding 1.5 for all peaks. Kirkland *et al.* increased the eluent flow rate to 4 mL/min and column temperature to 80  $^\circ\text{C}$ , and the separation of the protein mixture was achieved in 20 seconds, with column backpressure of  $\sim 270$  bar. Further advances in fast HPLC have been demonstrated by Heinig and Henion [13], i.e. five benzodiazepines (previously extracted from urine samples) were separated in under 15 seconds on a 15 mm x 2.1 mm, reversed-phase silica column (3  $\mu\text{m}$  silica particle diameter), using an eluent composed of 3 mM ammonium acetate pH 3.3 and 35 % acetonitrile, at a flow rate of 1.35 mL/min. According to Heinig and Henion the analysis of 240 samples per hour, using LC-MS-MS, could be practical in the future.

In contrast to the reversed-phase separations mentioned, the lack of commercially available ion-exchange resins with the desired properties for rapid chromatographic separations has resulted in rapid separations of small inorganic and organic ions receiving little attention. However this problem can be overcome by carrying out ion-interaction chromatography using reversed-phase materials. Connolly and Paull [21] employed this approach to achieve a sub-minute separation of iodate, bromate, nitrite, bromide and nitrate on a 30 mm x 4.6 mm reversed-phase column (3  $\mu\text{m}$  silica particle size) using an eluent composed of 20 mM tetrabutylammonium chloride (TBA-Cl, the ion-interaction reagent) and 20 % methanol, at a flow rate of 2 mL/min. A rapid separation of nine common anions in less than 180 seconds, flow rate 2 mL/min, was also demonstrated by Connolly and Paull [22], using the 30 mm x 4.6 mm reversed-phase column (3  $\mu\text{m}$  silica particle size) permanently coated with didoeyldimethylammonium bromide (DDAB), and a phthalate eluent for indirect UV detection. However, there still exists a point where the pressure maximum of the chromatographic system (usually  $\sim 200$  bar) is reached and, once again, further increases in separation speed are no longer possible.

Clearly, significant reductions in run time are possible if the pressure necessary for a given linear velocity could be reduced, that is, the column permeability is increased so that higher eluent linear velocities can be applied. Some approaches investigated to overcome the high pressure drop associated with a column having a tightly particle-packed bed include the use of open tubular columns [23], and operating the column at high temperature [24,25], which can increase efficiency or shorten run times by increasing permeability or by facilitating solute diffusion.

- An open tubular column (OTC) is a narrow, hollow capillary with the stationary phase coated on the inside wall. To obtain high performance from an open tubular column, the radius of the column must be small and the stationary phase coating must be as thin as possible to ensure rapid exchange of solute between the eluent and the stationary phase. As discussed previously, because particles packed in a column resist the flow of eluent, the linear flow rate can't be greatly increased. However, for the same length and applied pressure, the linear flow rate in an open tubular column is much higher than that of a packed column. Therefore, an open

tubular column can be made up to 100 times longer than a packed column, to give a similar pressure drop and linear flow rate. A further advantage of open tubular column is that the plate height is reduced because multiple flow paths don't contribute to band broadening [26,27,28].

- High temperature HPLC has been employed as a means of improving column performance because, at increased temperature, the viscosity of the eluent is decreased, which improves mass transfer. If the eluent or the sample is viscous it may be necessary to work under higher temperatures because less pressure is needed to pump the eluent through the column or to inject the sample. However, there are also some disadvantages associated with the use of high temperature; the solubility of silica is greatly increased in all eluents as the temperature is increased, all chemical equilibria are temperature dependent, especially ion equilibria in aqueous solutions, and so, changes in temperature could lead to problems with reproducibility, sample components could decompose at elevated temperatures and there is also a risk of bubble formation leading to uneven baselines and ghost peaks [29, 30].
- Another approach that has been applied to achieve higher efficiency (N) values and shorter separation times in HPLC is to use ultra-high pressure liquid chromatography (UHPLC) [31], where the maximum attainable number of theoretical plates and speed of analysis are functions of the available pressure. For example, fused silica capillaries (66 cm) were packed with 1.5  $\mu\text{m}$ , non-porous reversed-phase silica particles and the optimum linear flow velocity (0.15 cm/s) was achieved at 1380 bar [32,33].
- Capillary electrochromatography (CEC) is a separation technique in which transport through a capillary packed with stationary phase particles is achieved by electroosmotic flow (EOF). The EOF allows the use of much smaller stationary phase particles and longer columns than possible with HPLC because of the absence of backpressure, see Fig. 1.5. Therefore, the possibility of using sub- $\mu\text{m}$  particles in CEC should minimise two sources of band broadening; eddy diffusion and mass transfer [34].

Although capillary electrochromatography (CEC) is known to provide high column efficiency in short analysis time, CEC has not been widely used in routine applications due to the practical difficulties of frit failure or bubble formation [35]. The function of frits in CEC is to retain the capillary packing and they must possess a porous structure so as to allow uniform mobile phase flow through the whole cross-section. It is difficult to reproducibly prepare a highly permeable and mechanically strong end-frit by sintering. Heat generated in sintering process partially destroys the stationary phase. End frits reduce the column separation efficiency and are often responsible for bubble formation during analysis. The presence of bubbles causes a drop in current resulting in interruption of the sample run.

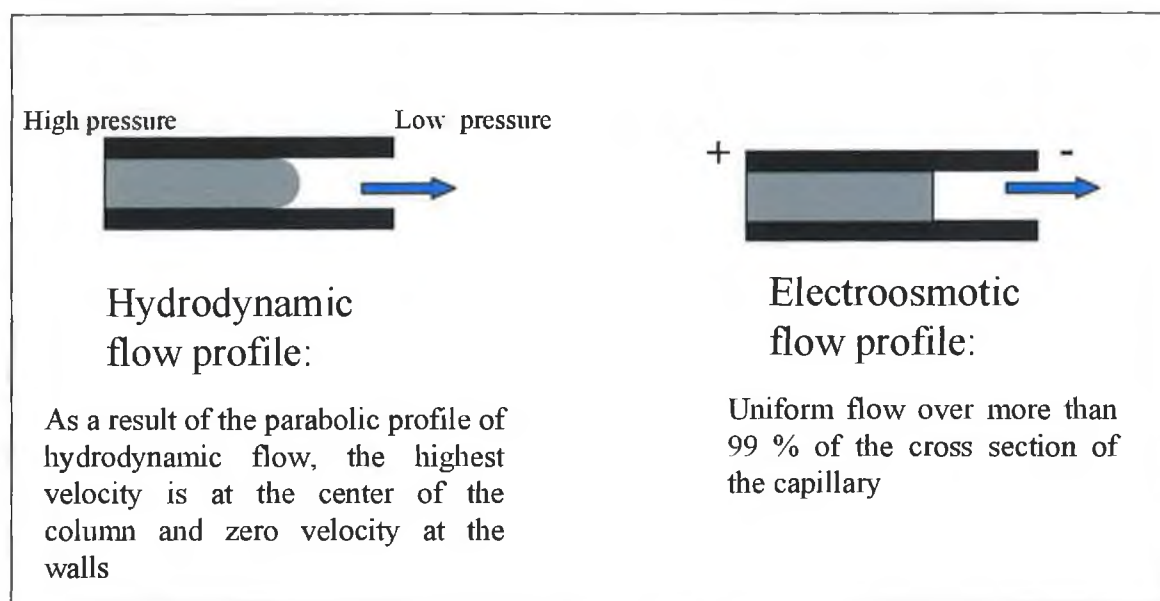


Figure 1.5: Schematic showing the contrast between the hydrodynamic and electroosmotic flow profiles.

However, none of these approaches has been widely accepted as routine yet because of instrumental or operational difficulties. Another approach to overcome the limitation of the high column backpressure drop, associated with particle-packed HPLC columns, is the use of a column made of a single piece of porous solid. In recent years, monolithic structures have been increasingly used as separation media for HPLC [36].

### 1.1.6: Monolithic columns for fast HPLC separations

For the purposes of chromatography, Miyabe and Guiochon [37] describe a monolith as a block of continuous material that is porous and permeable, and hence can be percolated by a solution and has a sufficiently large surface area for numerous solutes to exhibit significant retention. Encapsulated in a tube that prevents the eluent from by-passing the porous medium, this block constitutes a monolithic column. Alternatively, a monolith can be described as a single large “particle” without interparticular voids [2]. Over thirty years ago, the preparation of rigid foam inside a column was undertaken. It was envisioned that communicating pores would provide a network through which the eluent would flow. The motivation came from the realisation that monolithic materials with large throughpores or channels would result in higher permeabilities. A hydrodynamic flow would result in faster separations, while the creation of mesopores on the surface of the monolithic skeletons would provide the surface area required for chromatographic adsorption and desorption process. In recent years this novel type of stationary phase, the monolithic stationary phase, has attracted increasing attention in HPLC [38, 39].

The “single piece”, rod-shaped monolithic column possesses interconnected skeletons, which provide flow paths (throughpores) through the column. The monolithic column can have small sized skeletons and large throughpores, reducing the diffusion path length and flow resistance [5]. Each macropore, shown in Fig. 1.6 (a), is, on average, 2  $\mu\text{m}$  in diameter. The mesopores, 13 nm in diameter, form the further fine porous structure of the monolithic column interior, see Fig. 1.6 (b), and create a large surface area on which adsorption of the target compounds can occur [40, 41]. The size of throughpores in monolithic columns can be similar or much larger than the size of skeletons, resulting in a (throughpore size)/(skeleton size) ratio as large as 3-5 in the case of silica monoliths. In the case of a particle-packed HPLC column, the ratio of the size of interstitial voids to particle size is in the range of 0.25 to 0.4 [42]. It is the difference in these ratios that results in the higher permeability and shorter diffusion path length associated with monolithic columns, which facilitates the use of elevated flow rates without a significant loss in efficiency or problems with high column backpressures.

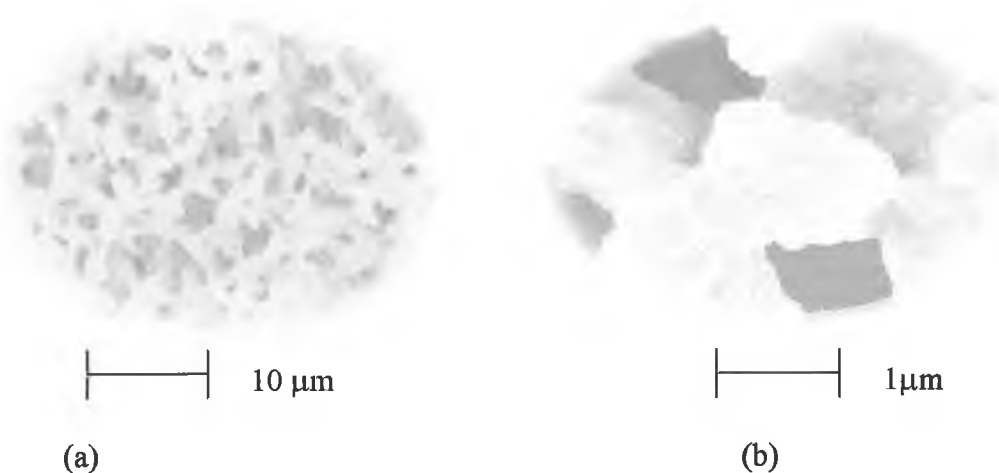


Figure 1.6: Structure of (a) macropores and (b) mesopores found in monolithic columns [40].

#### ***1.1.6.1: Milestones in the development of monolithic columns***

The pioneering development of this type of “single-piece” separation medium can be dated back to the late 1960s and the early 1970s. A swollen poly (2-hydroxyethyl methacrylate) polymer for size exclusion chromatography, to separate proteins under low pressure, was developed in 1967 [43], but permeability was too low to be used in practice. Subsequently, another monolithic open-pore polyurethane foam for both HPLC and GC was developed [44]. Despite excellent permeability, they were found to suffer from excessive swelling and softening in some solvents, which prevented their further use. Other approaches towards continuous media emerged in the late 1980s, including stacked membranes [45], rolled cellulose sheets [46] and rolled woven matrices [47], compressed soft poly(acrylamide) gels [48], and macroporous disks [49].

- The compressed soft gels, called continuous beds developed by Hjerten *et al.* [48] in 1989 mark the point where continuous media were first successfully used in chromatographic separations.
- In the early 1990’s, F. Svec and J.M.J Frechet [50] introduced an entirely new class of continuous media based on rigid macroporous polymer monoliths produced by a very simple “moulding” process.

- Inorganic silica-based monoliths were later reported by several groups [51, 52] in 1996.

### 1.1.6.2: Types of Monolithic Columns

Although monolithic columns are a relatively recent stationary phase format for HPLC and much remains to be done, Guiochon [53] claimed “*the invention and development of monolithic column is a major technological change in column technology*”. Both silica and polymer based monoliths have been extensively studied, and some of the stationary phases that have been commercialised are shown in Table 1.1.

Table 1.1: List of current commercial monolithic stationary phases for HPLC separations [41].

Product	Shape	Producer	Chemistry	Separation Modes
CIM disc	Disc	BIA Separations	Modified polymethacrylate or polystyrene copolymers	Ion-exchange, hydrophobic interaction, reversed-phase, bioaffinity
CB silica plate	Disc	Conchrom	Modified silica	Reversed-phase, normal phase
SepraSorb	Disc	Sepragen	Modified cellulose	Ion-exchange
CIM tube	Tube	BIA Separations	Modified polymethacrylate	Ion-exchange
UNO	Cylinder	BioRad	Polyacrylamide-based copolymers	Ion-exchange
SWIFT	Cylinder	ISCO	Modified polymethacrylate or polystyrene copolymers	Ion-exchange, reversed- phase
Chromolith	Cylinder	Merck	Modified silica	Reversed-phase
Monoliths	Cylinder	LC Packings	Polystyrene copolymer	Reversed- phase

The silica-based monoliths were developed by Tanaka and co-workers [54] in Japan, and introduced by Cabera and co-workers at the HPLC '98 in St. Louis, Missouri, and recently commercialised by Merck (Darmstadt, Germany) as its SilicaRod™ column. The polymeric monolithic columns have also made their mark on separation science. These columns consist of a continuous cross-linked, porous monolithic polymer usually polymethacrylates or methacrylate copolymerisates. They can be fabricated into discs and tubes in convenient housing for easy connection to a HPLC system. Some examples of commercial products are the UNO from BioRad Laboratories (CA, U.S.A), the CIM copolymers from BIA separations (Ljublijana, Solvenia) and swift polystyrene-divinyl benzene monoliths from ISCO (Nebraska, U.S.A.).

### **1.1.7: Polymer monoliths**

In the early 1990's, a new category of macroporous polymer monolithic columns formed by a simple moulding process was introduced [55]. These monoliths are polymerised in-situ within a tube such as a chromatographic column or capillary, in which they remain after the preparation is completed. Typically the mould is filled with a mixture of monomers (one of which must be a cross linker), a free radical initiator and porogenic solvent, then sealed and polymerisation is performed under carefully controlled thermal conditions. The seals are then replaced with fittings and the column attached to a pump. Using a suitable solvent, such as methanol or tetrahydrofuran, the porogens and other unreacted components are removed from the pores and the column is ready for chromatographic operation [41, 56]. Polymer monoliths prepared from styrene, methacrylate, acrylate, acrylamide or cyclic monomers have been reported [57].

#### ***1.1.7.1: Structural properties***

The total porosity of polymer monoliths can often be predicted on the basis of the starting compositions of the polymerisation system. For example, polymer monoliths prepared from a feed containing 40 % monomer commonly posses 60-70 % porosity, most of which is accounted for by “external porosity”: a ratio of voids outside the skeletons, to the column volume. In comparison, the external porosity of a particle-packed column is ~ 40 %. The polymer monolith consists of micrometer-sized

skeletons and flow throughpores. The skeletons can be meso- or microporous with double-pore structure. In the polymer monoliths, the macro- and mesopores form as a void of globular aggregates (see Fig. 1.7 (c), (d)), which differs from the spongy or network structure seen with silica monoliths (Fig. 1.7 (e)) [5, 50, 58].

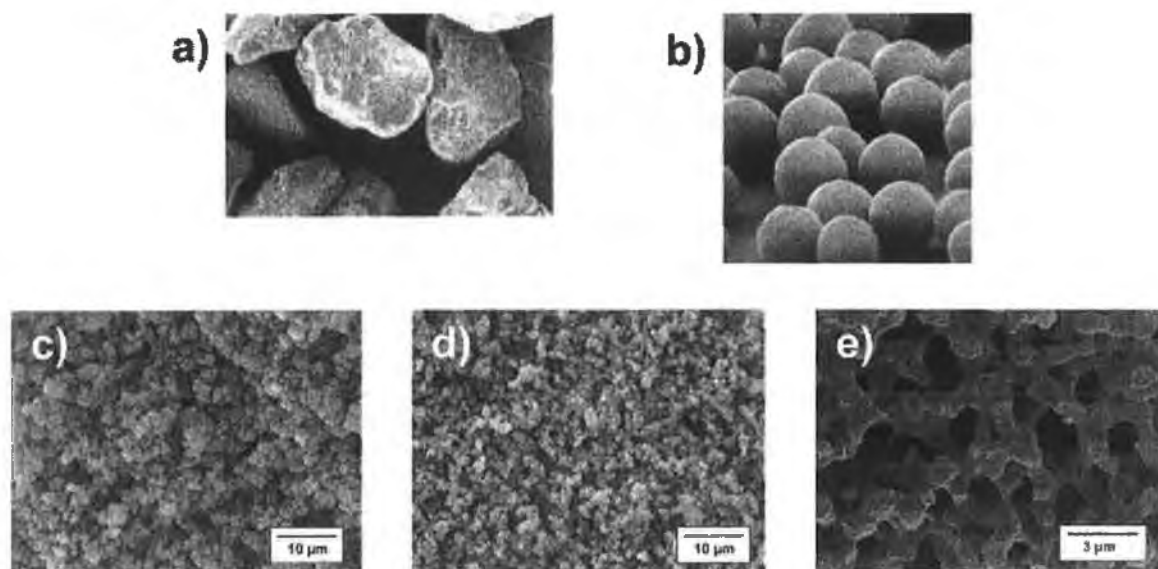


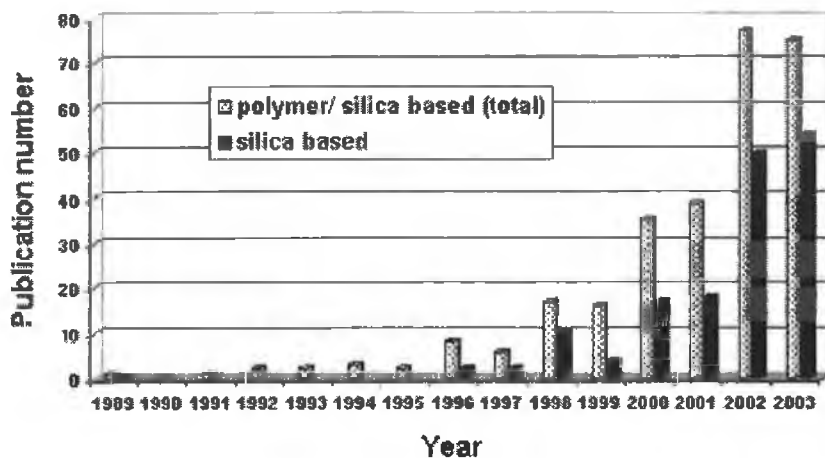
Figure 1.7: Scanning electron microscopy pictures of different types of porous chromatographic materials (a) irregularly shaped silica particles, (b) spherical silica particles, (c) organic polymer monolith (UNO S), (d) organic polymer monolith (CIM Disk) and (e) silica-based monolith (Chromolith) [59].

### **1.1.8: Monolithic Silica Columns**

In a recent review by Cabrera [60], the impressive increase in the number of publications based on silica-based monoliths was highlighted; see Fig. 1.8 (a). The first paper describing the application of porous silica monolithic columns for HPLC was published by Tanaka *et al.* [54]. The bimodal pore structure of the silica monolithic column was prepared using a new sol-gel process developed by Nakanishi and Saga [61] in 1991. By combining a sol-gel reaction with phase separation and a subsequent solvent exchange treatment, double pore silica gel (macropores and mesopores) monoliths were constructed [39]. In contrast to columns made of organic polymers, the silica based monolithic columns cannot be prepared in-situ due to shrinkage problems, and thus the porous silica rod is prepared first, then removed

from the mould, encased in a PEEK tube and modified to produce the chromatographic column, see Fig. 1.8 (b). The Merck KgaA company have developed a proprietary technology for the cladding of 4.6 mm i.d. silica rods with a resistant PEEK polymer, leading to monolithic columns, which are encased in a solvent and pressure resistant material [60].

(a)



(b)



Figure 1.8: (a) shows the total number of papers published on monolithic columns for HPLC during the time period 1989-2003 [60] and (b) monolithic silica rods (before and after cladding) compared to particulate type silica used in conventional HPLC silica columns [62].

### ***1.1.8.1: Structural properties***

Silica based monoliths are designed to possess a rather discrete bimodal pore size distribution and a high correlation of interconnectivity between the two sets of pores. The larger macropores form a flow through channel network outside the monolithic skeleton that rapidly transports solute molecules by convection down the column and to the smaller mesopores inside the silica matrix [63]. The macroporous structure of silica monoliths differs from that of organic polymers. As discussed in Section 1.1.7.1, the morphology of organic polymers consists of clusters of little, organised micro-globules with large pores located among them. However as described above, the structure of the silica rods features a well ordered array of equally sized throughpores and skeletons [2]. In the silica monoliths, the porous skeleton provides a relatively large surface area compared to the interskeleton space, but at the same time, needs only very short diffusion lengths and does not contain micropores to any significant amount.

### ***1.1.8.2: Preparation***

Silica monoliths with a double pore structure are prepared by a sol-gel method from alkoxy silanes in the presence of water-soluble organic polymers [60]. In this system, spinodal decomposition occurs concurrently with gelation due to hydrolytic polymerisation of alkoxy silanes, resulting in the formation of bicontinuous silica-rich and solvent rich phases. After drying and thermal treatment of the wet gel, the silica rich phase becomes the mesopores in the silica skeletons and the solvent rich phase becomes the throughpores. In this double pore silica gel, the throughpore size and the silica skeletons size can be controlled independently by changing the composition of the starting material [10, 63, 64, 65, 66, 67, 68].

### ***1.1.8.3: Comparing silica monolithic and particle-packed HPLC columns***

According to Leinweber and Tallarek [59] “*monolithic chromatographic support structures offer, as compared to conventional particulate materials, a unique combination of high bed permeability, optimised solute transport to and from the active surface sites and a high loading capacity by the introduction of hierarchical*

order in the interconnected pore network and the possibility to independently manipulate the contributing sets of pores.”

According to Merck [69], the surface area of the Chromolith™ columns is  $\sim 300 \text{ m}^2/\text{g}$ , made available by the mesopores. Since the overall porosity of the monolithic silica matrix is greater than 80 %, the user is able to perform chromatography with a significantly lower backpressure than with conventional particle-packed silica HPLC columns, which exhibit total porosity of just 65 %. By optimising the ratio of throughpores to the total porosity and the silica gel skeleton thickness, i.e. increasing column porosity, separations become possible at higher flow rates with very low backpressures. Studies by Bidlingmaier *et al.* [70] have shown that particle-packed, reversed-phase columns exhibit significantly lower total column porosity than the equivalent, reversed-phase monolithic columns. At a flow rate of 1 mL/min, the column pressure drop,  $\Delta P$ , was about 5 times smaller on the monolithic columns than the Purospher RP 18e column, see Fig. 1.9. The Purospher RP 18e column reaches a maximum backpressure of  $\sim 350 \text{ bar}$  at 3 mL/min, whereas monolithic rod columns can be operated at 6 mL/min with a backpressure of 150 bar.

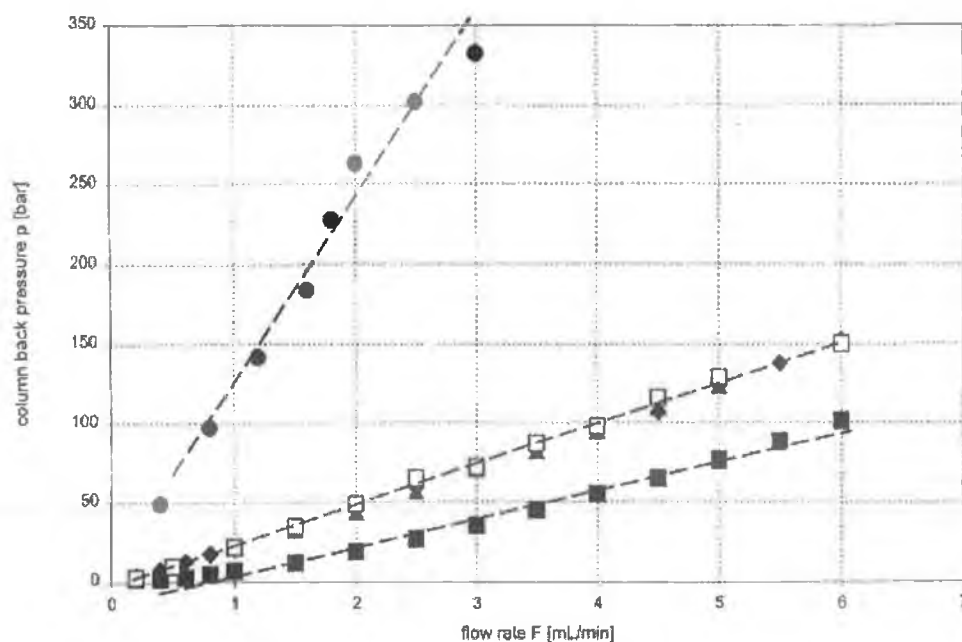


Figure 1.9: Column backpressure  $\Delta P$  as a function of the flow rate  $F$  on three monolithic and a microparticulate column. (■) Pressure drop due to equipment without a column, (◆) rod 216, (□) rod 225, (●) Purospher RP 18e column [70].

In terms of selectivity, a comparative study between a reversed-phase, particle-packed silica HPLC columns and monolithic silica columns, e.g. Chromolith™ and SilicaROD™ monoliths, demonstrated that the selectivity of the two columns is equivalent [11, 69]. As the review of rapid HPLC separations using monolithic silica columns in Section 1.1.11 will demonstrate, this equivalent selectivity allows for easy transfer of existing methods from particle-packed silica HPLC columns to monolithic silica columns. However, the use of monolithic silica columns at elevated flow rates resulted in faster separations.

Another feature of monoliths is the high column efficiency, even at high linear flow velocities. Fig. 1.10 shows that the van Deemter curve for a monolith silica column in comparison to the van Deemter curves obtained for conventional particle-packed HPLC silica columns. The column packed with 3.5  $\mu\text{m}$  silica particles cannot be operated at higher velocities because the high flow resistance leads to high column backpressure. Although the separation efficiency of the silica monolith does decrease as the linear flow velocity increases, Fig. 1.10 clearly demonstrates that the loss in efficiency is not as significant as in the case of the HPLC column packed with 5  $\mu\text{m}$  silica particles. It is therefore possible to operate monolithic columns at high flow rates with minimal loss of peak resolution. The minimum of the van Deemter plot ( $H_{\text{min}}$ ) of the monolithic silica column represents a theoretical plate height ( $H$ ) of 8  $\mu\text{m}$ , which corresponds to 125,000 plates/m and this efficiency corresponds to the value of  $H_{\text{min}}$  for a HPLC column packed with 3.5  $\mu\text{m}$  silica particles.

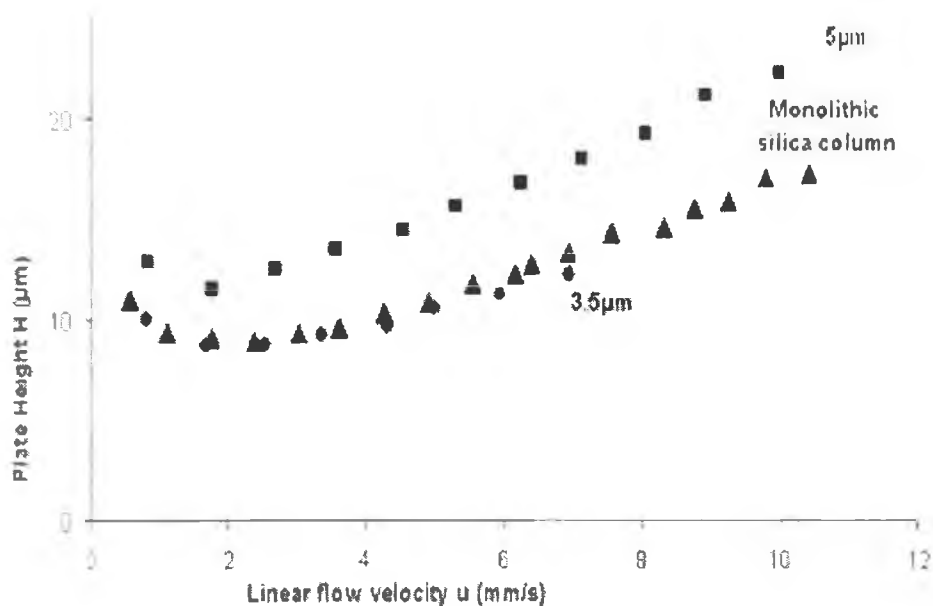


Figure 1.10: A van Deemter plot of the HETP versus linear flow velocity for a Chromolith™ Performance column and equivalent particle-packed HPLC silica columns [69].

### 1.1.9: Advantages of monolithic columns

As the previous sections have demonstrated, the unique properties of monolithic columns include:

- The high separation efficiency exhibited even at high linear flow velocities, which results in an increase in sample throughput [11, 62, 69].
- The nature of monolithic columns eliminates inlet bed settling or bed splitting under high pressure, and as a result, column reliability, reproducibility and long life are ensured.
- Monolithic columns can be linked in series, producing a column with a theoretical plate count that is significantly higher than a conventional column packed with silica particles between 1.5–3 µm in diameter, while producing pressures well below the HPLC system limit, see Table 1.2.

Table 1.2: The effect on column backpressure and efficiency when 100 mm x 4.6 mm Chromolith™ Performance PR-18e monolithic columns are linked in series [69].

Number of Chromolith Performance Columns	Length (mm)	Backpressure (bar)	Total plate number
Chromolith Performance x 1	100	30	10,000
Chromolith Performance x 2	200	60	19,000
Chromolith Performance x 3	300	90	27,000
Chromolith Performance x 4	400	120	35,000
Chromolith Performance x 5	500	150	41,000

- Polymeric monolithic columns offer excellent biocompatibility, a wide pH range, and the ability to be cleaned with caustic mobile phases [71,72,73,74,75]. Ikegami and Tanaka [76] suggest that high performance polymer monolithic columns may occupy a considerable portion of the monolithic column market, especially for biological macromolecules.
- The challenges prompted by miniaturisation of chromatographic systems have lead scientists to explore new avenues in the synthesis of stationary phases. Packed column capillaries in electrochromatography and micro-HPLC have found limited application in routine analysis due to difficulties such as non-specific interactions, increased backpressure in micro-HPLC, gas bubble formation in CEC, column to column irreproducibility, and increased fragility of capillaries, all of which are often attributed to frits. In the search for fritless columns the concept of replacing the particulate packings with a continuous rod has been investigated [77]. In CEC fritless polymer monoliths can play a major role, because they provide high chemical stability and ease of preparation of long columns and often a simple way to design materials that increase EOF (due to the introduction of ionic groups) and selectivity (with various selectors such as molecular imprinting for chiral separations).

#### **1.1.10: Limitations of monolithic columns**

Although the monolithic stationary phases possess a number of unique, beneficial properties compared to traditional stationary phases, some disadvantages and

limitations are inevitable. Most of the current disadvantages of monolithic columns are related to the column production [38, 78].

- As with other silica packings, the working pH range for monolithic silica columns is limited to pH 2-8.
- Individual silica monolithic columns must be prepared and chemically modified on-column one at a time, and as a result, individual preparation and subsequent chemical bonding can lead to problems in reproducibility. When the monoliths are prepared in a mould, column materials such as PEEK are used to enclose the bare silica rod. This seems to be the most difficult step in preparing a monolithic HPLC column, because this type of preparation and subsequent chemical bonding also leads to problems with reproducibility.
- The preparation of monolithic silica columns in a mould limits the length of a column to less than 15 cm, otherwise a straight monolithic column cannot be prepared, and as a result, the generation of a large number of theoretical plates requires a number of monolithic columns to be connected in series [35].

The disadvantages of using polymeric monoliths include [2]:

- The general drawback of these materials, as is typical for polymeric stationary phases, is their lower efficiency compared with silica-based columns. The structure of porous polymers often contains micropores that negatively affect the column efficiency (by causing a large C-term contribution for small molecules) and peak symmetry.
- Most polymers, especially those with a low degrees of cross-linking, will swell or shrink in organic solvents. This behaviour could have dramatic effects upon the chromatographic performance of these monolithic columns, and it frequently leads to a lack of mechanical stability.

#### **1.1.11: Applications of silica monoliths in high-speed chromatographic separations**

According to Sinz and Cabrera [9] “*monolithic silica technology has opened the doors on a new era of dramatically higher sample throughput and added new opportunities to improve separation performance*”. The following Sections will

examine the contribution silica based monolithic columns have made to reducing the run time of complex pharmaceutical and bioanalytical analyses, without compromising separation efficiency, as well as increasing sample throughput and laboratory productivity.

#### **1.1.11.1: Drug and Pharmaceutical analysis**

The reduction of analysis times is becoming increasingly important in many application areas of HPLC, including pharmaceutical analysis in order to increase throughput and reduce costs [79]. Macchia *et al.* [80] have assessed the advantages of a monolithic silica column (Merck Chromolith RP 18e, 100 mm x 4.6 mm i.d.) for the HPLC analysis of heroin samples, with a view to their use in routine analysis. A solution of acetonitrile and phosphate buffer, pH 3.5, was used under both isocratic and gradient conditions, and the total analysis time for the heroin samples was 11 minutes, including re-equilibrium time and reporting. A baseline separation of the compounds found in clandestine heroin, namely morphine, paracetamol, codeine, caffeine, monoacetylmorphine, acetylcodeine, heroin, papaverine and noscapine, was achieved in 7 minutes. A comparison of analytical accuracy was carried out by comparing the monolithic HPLC results for a real sample with those from a GC method currently employed for heroin analysis.

Table 1.3: Comparison of analytical accuracy for a real sample between the monolithic HPLC method and a traditional GC method [80].

<b>Analyte</b>	<b>HPLC (% Analyte in heroin sample)</b>	<b>GC (% Analyte in heroin sample)</b>
monoacetylmorphine	0.58	0.59
heroin	8.01	8.16
acetylcodeine	0.59	0.60
papaverine	0.40	0.39
noscapine	0.55	0.57

The results presented in Table 1.3 show that the monolithic column proved to be a useful tool for providing a routine, rapid and simple method of analysis, which can be used as a powerful, complementary technique in the case of global characterisation of various illicit heroine samples for comparative purposes.

Rocheleau *et al.* [81] have applied a Chromolith Performance RP-18e silica monolithic column (100 mm x 4.6 mm i.d.) to a very challenging HPLC separation, namely the impurity profiling of an analog of Taxol. Analogs of Taxol (paclitaxel) are destined to become used as potential new anticancer drugs. Synthesis of taxanes is typically associated with a large number of impurities, which makes their analysis and impurity profiling particularly challenging. The silica monolith was found to reduce the run time for the impurity profiling of BMS-275183-01 (a Taxol analog) by ~ 30 %, when the flow rate was increased from 1 to 4 mL/min. In addition to this the plate height was ~ 2.5 times lower on the monolithic column than on a previously employed 250 mm x 4.6 mm i.d., 3  $\mu$ m silica particle size, reversed-phase (C<sub>18</sub>) stationary phase. The performance of the Chromolith column was found to be comparable to that of a traditional particle-packed silica column for the separation of a Taxol analog (BMS-275183-01) from its impurities. Only one impurity, 10-methylcarbonate analog, whose structure is very similar to its parent compound BMS-275183-01, could not be separated on the reversed-phase monolith.

Apers *et al.* [82] have investigated the potential of a fast HPLC method, using a reversed-phase (C<sub>18</sub>) silica monolithic column, for the quality control of soy. Owing to the growing evidence suggesting that phytoestrogens might protect against various cancers, cardiovascular diseases and osteoporosis, many various preparations of isoflavone extracts from soy are marketed as nutritional supplements and phytotherapeutic preparations. Two HPLC runs are necessary to determine the total amount of isoflavones, and therefore, analysing samples in duplicate leads to a total analysis time of ~ 4 hours. A method developed by Apers *et al.* was transferred from a LiChrospher RP-18 particle-packed HPLC column (250 mm x 4.6 mm i.d., 5  $\mu$ m particle size), to a Chromolith Performance RP-18e (100 mm x 4.6 mm i.d.). In order to achieve a good separation of the late eluting isoflavones, two Chromolith Performance RP-18e columns were linked together in series. The column efficiency

of these linked monolithic columns (2 x 100 mm) was even better than that of the 250 mm particle-packed column, such that there was a remarkable improvement of the resolution of the late-eluting peaks (see Fig. 11 (a) and (b)). In contrast to the analysis on the conventional reversed-phase, particle-packed silica HPLC column, the peaks of the late eluting isoflavones were baseline resolved on the coupled reversed-phase silica monoliths, up to a flow rate of 3 mL/min. A flow gradient from 3 to 4 mL/min at the end of the run for washing the column was incorporated, reducing the analysis time even further. Analysing samples in duplicate for the determination of isoflavones using the coupled reversed-phase monolithic columns took about 1 hour 40 minutes, instead of 4 hours with conventional particle-packed HPLC silica columns.

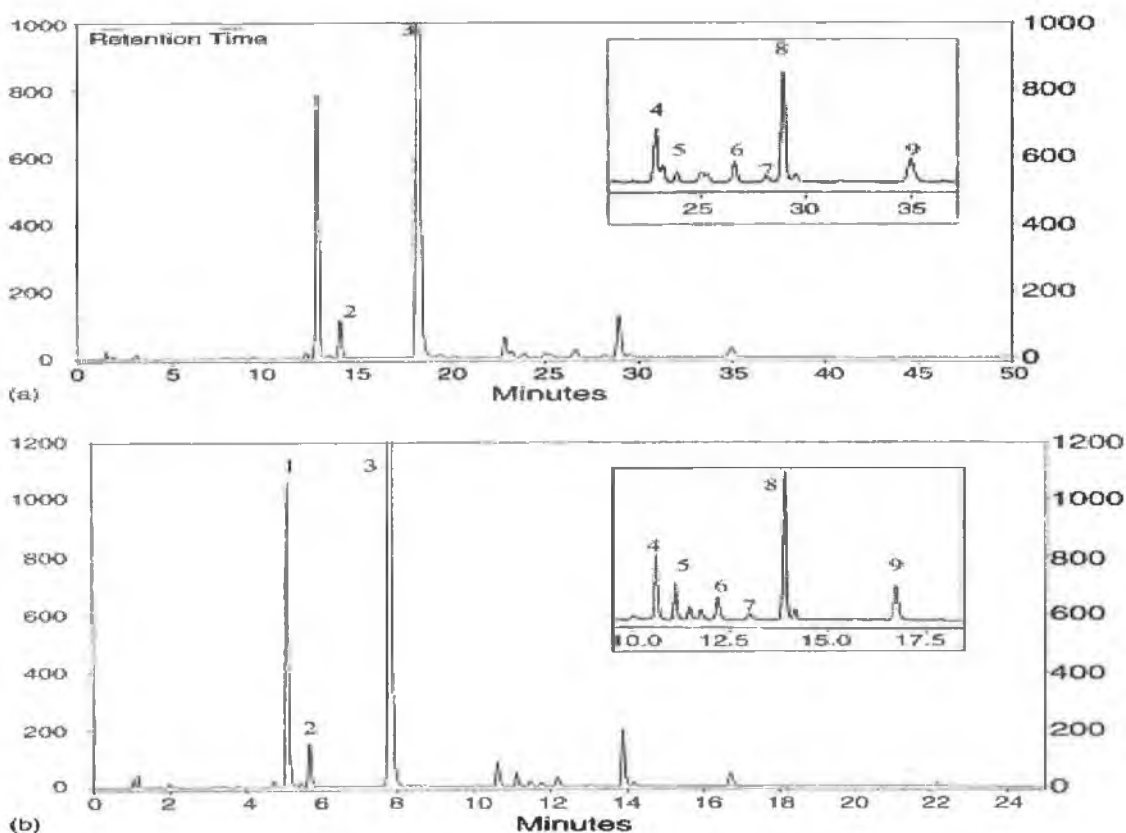


Figure 1.11: Chromatograms of the separation of the isoflavones of a soy extract on (a) a LiChrospher RP-18 (250 mm x 4 mm) and on (b) two linked Chromolith Performance RP-18 (100 mm x 4.6 mm) columns [82].

The importance of enantiomerically pure drugs, intermediates and fine chemicals means that enantioselective HPLC is still a growing field. An enantioselective silica monolithic chiral stationary phase was prepared by Ludba *et al.* [83] using a

procedure developed for the in-situ modification of a bare silica monolithic column (100 mm x 4.6 mm i.d. Chromolith Performance Si) with tert-butyl-carbamoylquinine (t-BUCQN), a chiral anion-exchanger selector. Complex separations require a long column bed to provide the necessary separation efficiency; therefore, Lubda *et al.* coupled six tetra-butylcarbamoylquinine silica monolithic columns in series. The coupling of the six columns was possible due to the low backpressure generated by monolithic columns, and the 60 cm long t-BuCQN silica monolithic column builds up a column backpressure of only 45 bars. By linearly connecting the six tert-butylcarbamoylquinine silica monoliths, Lubda *et al.* increased the efficiency from 7000 plates, for a single 10 cm long t-BuCQN silica monolith, to a total of 30,000, for the 60 cm long t-BuCQN silica monolithic column. In order to reduce the separation time for the analysis of the Suprofen enantiomers, the flow rates were varied from 1 to 4 mL/min using the 60 cm long t-BuCQN silica monolithic column. By increasing the flow rate from 1 up to 4 mL/min the backpressure was observed to increase from 45 to 240 bar, but the overall separation time was reduced to 10 minutes while still achieving a baseline resolution of the Suprofen enantiomers ( $R_s$  of 2.6), see Fig. 1.12.

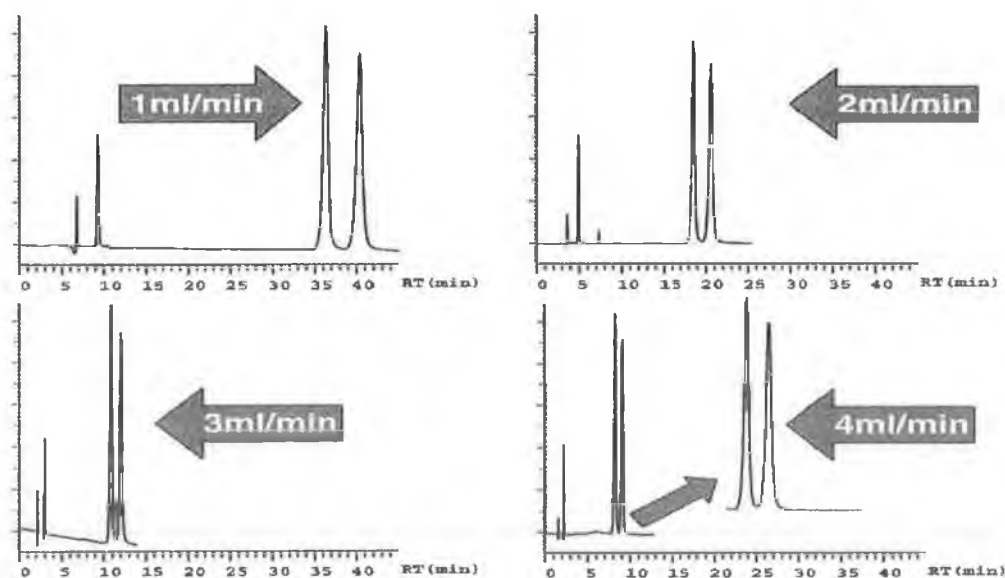


Figure 1.12: Effect of increasing flow rate on the separation of Suprofen using a 60 cm long t-BuCQN modified monolithic silica column. Flow rate 1 to 4 mL/min [83].

Wu *et al.* [84] demonstrated the application of reversed-phase silica monolithic columns for pharmaceutical process development, which included crude drug

substances, reaction mixtures and mother liquors. The analysis time for an in-process sample of a crude drug substance was 3 times shorter on a Chromolith Performance RP-18e monolithic column (100 mm x 4.6 mm i.d) with an eluent flow rate of 5 mL/min when compared to the separation obtained using a Zorbax reversed-phase column (250 x 4.6 mm i.d., 5 $\mu$ m silica particle size), which was operated at only 1.5 mL/min. In addition, the total run time for the monolithic column was also shorter, as only 3 minutes were needed for re-equilibration at 5mL/min, compared to 10 minutes for the packed column at 1.5 mL/min. The average resolution and column efficiencies were observed to be highly comparable. Complicated samples such as mother liquors frequently need to be screened for impurity identification and for tracking mass balance in pharmaceutical process development. By coupling two 100 mm Chromolith Performance RP-18e monolithic columns together in series, approximately 30 peaks including the drug substance and other process impurities, were resolved within 10 minutes, compared to 40 minutes when the 250 x 4.6 mm i.d. Zorbax reversed-phase column (5  $\mu$ m silica particle size) was employed.

Schmidt [85] evaluated the applicability of a reversed-phase monolithic silica column for the rapid separation of ingredients in medicinal plants and their phytopharmaceutical preparations. As in previous studies described, the transfer of an existing method from a 125 mm x 4 mm i.d. Hypersil (5 $\mu$ m silica particle size) to a 100 mm x 4.6 mm i.d. Chromolith Performance RP-18e monolith, meant that the flow rate could be easily increased from 0.8 mL/min (particle-packed column) to 5 mL/min on the monolithic column, and as a result, there was a reduction in the run time from 30 minutes to 5 minutes, without any loss in the resolution of the compound of interest, i.e. iridoid glycoside harpagoside, which is the major pharmacological active ingredient in a plant called *H. procumbens*. The amount of harpagoside in *H. procumbens* was measured with the original method on a conventional particle-packed silica column, and with the adapted method on a monolithic silica column, and a statistical *t*-test showed no significant differences of the variances and the means.

### 1.1.11.2: Bioanalytical separations

The importance of chromatographic separations in molecular biology is increasing rapidly. Therefore, maximising the throughput of assays that support clinical studies is a key process in a bioanalytical laboratory [76].

In a study by Vallano *et al.* [86] reversed-phase monolithic HPLC columns were employed for the determination of the cyclooxygenase II inhibitors roferoxib (I) and 3-isopropoxy-4-(4-methanesulfonylphenyl)-5-5'-dimethyl-5H-furan-2-one (DFP III) in human plasma. Previously, the determination of I in human plasma involved a 96 well SPE plate for sample preparation, followed by reversed-phase HPLC methodology, which required a run time of 10 minutes. Thus, there was a significant disconnect between the throughput of the sample preparation procedure and that of the chromatographic method; more samples could be extracted in a day than could be chromatographed in a 24-hour period. The assay for I was successfully transferred directly from a particle-packed, reversed-phase HPLC silica column (Waters Symmetry C<sub>18</sub> column, 50 x 4.6 mm i.d., 3.5µm silica particle size) with an eluent flow rate of 1.2 mL/min to the reversed-phase monolithic column (Chromolith SpeedROD, 50 mm x 4.6 mm i.d.), with an eluent flow rate of 3 mL/min. Utilisation of the monolithic column together with the increased eluent flow rate allowed the assay run time to be reduced by a factor of 4 from 10 to 2.5 minutes. Both the intra-day accuracy and precision of the monolithic assay results were comparable to those obtained with the conventional particle-packed reversed-phase column previously employed. For the determination of DFP III in human plasma, the eluent flow rate of the established assay was 1.4 mL/min and the run time of the assay was 6 minutes. However, when a flow rate of 6.5 mL/min was used with the monolithic column, total system backpressure was only 160 bar, and the peaks of interest eluted in less than 1 minute, representing a significant increase in assay throughput when compared to the original method.

By exploiting one of the main advantages of monolithic columns, i.e. that the analysis time can be decreased without significantly compromising resolution, Hefnawy *et al.* [87] were able to reduce the analysis time of a HPLC assay for the determination of

mianserin and its metabolites in human plasma. Mianserin (MAN) is a tetracyclic antidepressant drug of the second-generation group of less anticholinergic activity and cardiotoxicity than the tricyclic ADPs. The determination of mianserin and its metabolites (desmethyalmianserin (DMM), 8-hydroxymianserin (HM) and mianserin-N-oxide (MNO)) has been performed using either GC or HPLC methods. However the methods described are time consuming and lack sensitivity for an accurate determination of mianserin and its metabolites in human plasma [87]. In the method developed by Hefnawy *et al.*, each compound together with its internal standard (propranolol) was extracted from the plasma matrix using SPE, and separation of the analytes was performed on a Chromolith SpeedROD monolithic silica column (100 mm x 4.6 mm i.d), and using a flow rate of 3.5 mL/min, the total run time of the assay was less than 5 minutes, with the retention times of 0.69, 1.90, 2.87, 4.21 minutes for mianserin, DMM, HM and MNO.

The applicability of monolithic silica columns in the field of quantitative bioanalysis has also been investigated by Aboul-Enein *et al.* [79] for the development of a rapid HPLC assay for the simultaneous determination of ketamine and its two main metabolites, namely norketamine and dehydronorketamine, in human plasma. Ketamine is an anesthetic agent that has been widely used since 1970 for the induction of anaesthesia and at present the frequency of ketamine abuse is on the increase and numerous fatal ketamine cases have been reported. The successful transfer of a previously developed HPLC assay from a particle-packed, reversed-phase HPLC silica column to a Chromolith Performance RP-18e, 100 x 4.6 mm i.d. monolithic column, facilitated an increase in flow rate, which reduced the run time six-fold, while the chromatographic resolution of the analytes remained unaffected.

#### ***1.1.11.3: Rapid ion chromatography using monolithic silica stationary phases***

In recent years, interest has increased in using monolithic stationary phase media for high performance separations of inorganic and organic ions. According to a review by Paull and Nesterenko [88], the production of monoliths with either bonded or coated ionic sites has led to the development of a number of new approaches to the chromatographic separation of ions. These include low- and medium pressure ion

chromatography (IC), ultra-fast IC, the use of flow gradients and double gradients in IC as well as multi-column and multi-dimensional IC.

In 2002, Hatsis and Lucy [89] reported the separation of common inorganic anions in as little as 15 seconds. Using a Chromolith Speed ROD RP-18e (50 mm x 4.6 mm i.d.), separations were performed using ion-interaction chromatography with tetrabutylammonium-phthalate as the ion-interaction reagent and were monitored using either direct conductivity or indirect absorbance detection, rendering the method universal to all anions. At a flow rate of 4 mL/min, a separation of  $\text{H}_2\text{PO}_4^-$ ,  $\text{Cl}^-$ ,  $\text{NO}_2^-$ ,  $\text{Br}^-$ ,  $\text{NO}_3^-$ ,  $\text{ClO}_3^-$ ,  $\text{I}^-$  and  $\text{SO}_4^{2-}$  was achieved in 1 minute, using an eluent composed of 1.5 mM TBA-1.1 mM phthalate with 5 % (v/v) acetonitrile. However, because at 4 mL/min the pressure drop across the 50 mm Speed ROD monolith was only 50 bar, Hatsis and Lucy increased the flow rate to 8 mL/min (separation time 30 seconds) and even to 16 mL/min (separation time 15 seconds), where the pressure drop at 16 mL/min was still only 170 bar, which is well within the normal HPLC operating conditions. However, in order to achieve the 15-second separation, Hatsis and Lucy had to perform a number of modifications to the HPLC system employed. The eluent flow had to be split 3:1 before the detector flow cell, to protect it from excessive backpressure, and in addition, a prototype detector had to be developed to enable data collection at 20 Hz, as the data acquisition rate of conventional conductivity detectors is often only 5 Hz. In addition to this, it was observed that the use of such extreme flow rates had an adverse effect on peak efficiency such that the resolution between the nitrate and bromide peak was reduced to 0.73, and the variation in peak area and retention time values also increased significantly.

In an effort to combine ultra-fast ion chromatographic separations with high sensitivity detection, Hatsis and Lucy [90] developed an alternative high-speed ion chromatographic separation that employed suppressed conductivity detection. Instead of using the ion-interaction approach, the separation of  $\text{IO}_3^-$ ,  $\text{Cl}^-$ ,  $\text{NO}_2^-$ ,  $\text{Br}^-$ ,  $\text{NO}_3^-$ ,  $\text{HPO}_4^{2-}$  and  $\text{SO}_4^{2-}$  was performed on a reversed-phase monolithic silica column (Chromolith Speed ROD RP-18e, 50 mm x 4.6 mm i.d.), permanently coated with didodecyldimethylammonium bromide (DDAB). The eluent employed was 6 mM cyanophenol (pH 7.0), and at a flow rate of 10 mL/min the separation of the 7 anions was possible in as little as 30 seconds, as shown in Fig. 1.13. The use of a packed bed

suppressor (Metrohm, MSM) was used in this work, because this suppressor was able to withstand pressures up to 200 bar and flow rates as high as 10 mL/min. Hatsis and Lucy have reported detection limits in the parts per billion range for all of the anions studied. Coated columns were observed to be stable for up to 12 hours of continuous use at 5 mL/min.

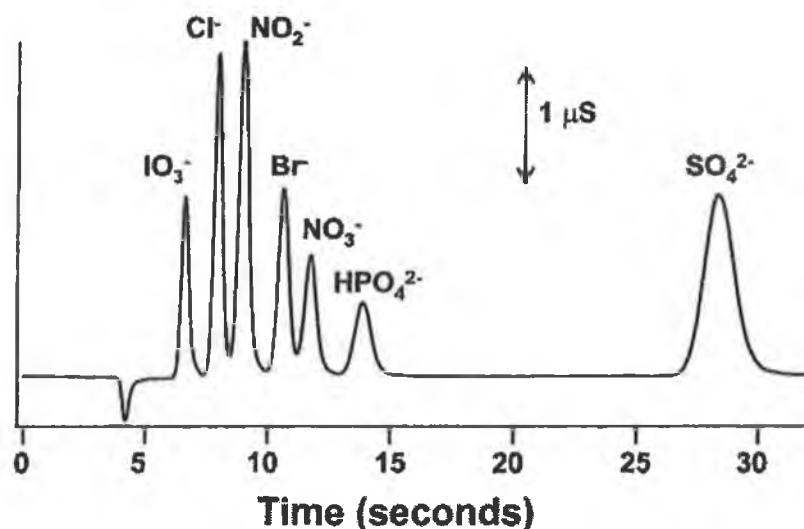


Figure 1.13: The 30-second separation of 7 common anions on a 5 cm monolithic column reported by Hatsis and Lucy [90].

The determination of the acid or base content of some samples is one of the most important tasks in analytical chemistry. Some researchers have tried to use IC to overcome the disadvantages, such as low detection limits, low sensitivity and/or complicated operating steps, of the two frequently used methods, acid-base titration and potentiometry. Although various IC methods have been developed, the excessive run times associated with these methods made them inadequate for actual applications. Xu *et al.* [91] have demonstrated the high-speed determination of acidity using ion chromatography on a monolithic stationary phase. Using a reversed-phase, monolithic silica column (Chromolith Performance RP-18e, 50 mm x 4.6 mm i.d), which was modified with lithium dodecylsulfate, H<sup>+</sup> was eluted as a sharp and highly symmetrical peak before other cations (Na<sup>+</sup>, NH<sub>4</sub><sup>+</sup>, K<sup>+</sup>, Mg (II) and Ca (II)) in less than 1 minute using an acidified solution containing EDTA-2K and Li-DS as the eluent, at a flow rate of 1.5 mL/min. The monolithic column modified with Li-DS was stable for at least 2 months of operation with no evidence of peak area/height changes of the cations under analysis (peak area % RSD < 1.88 %), while for the column to column reproducibility, the column was modified three times and the % RSD of the

chromatographic peak area of the  $H^+$  peak was  $< 1.89\%$ . As the data in Table 1.4 demonstrates, the IC method developed by Xu *et al.* [91] was applied to the determination of acidity in rainwater and deionised water samples.

Table 1.4: A comparison of analytical performance reported by Xu *et al.* [91].

Sample	Detection by IC method		Detection by pH meter	
	pH	% RSD	pH	% RSD
Rainwater	4.716	1.02	4.72	1.96
Deionised water	5.564	1.03	5.56	2.13

Xu *et al.* [92] also demonstrated the high-speed determination of  $H^+$ , Mg (II) and Ca (II) when the Li-DS modified monolith (Chromolith Performance RP-18e, 50 mm x 4.6 mm i.d) was used with an eluent composed of 2 mM ethylenediamine and 0.1 mM Li-DS at pH 6.0. At a flow rate of 4 mL/min,  $H^+ < Mg(II) < Ca(II)$  were well separated within 4 minutes, see Fig. 1.14, and it was possible to analyse rainwater samples directly, with detection limits of  $1\ \mu M$  for  $H^+$  and  $2\ \mu M$  for Mg (II) and Ca (II).

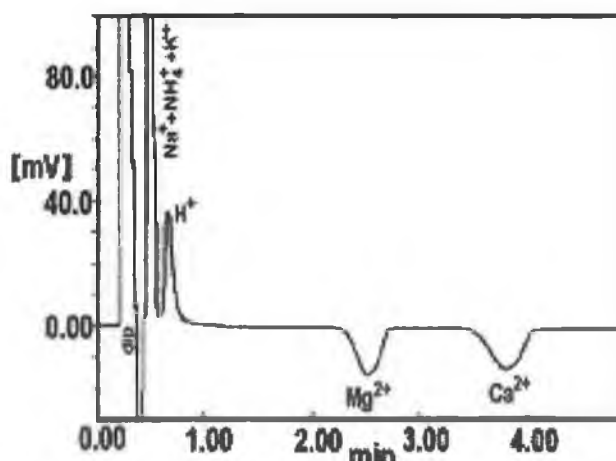


Figure 1.14: A separation of  $H^+$ , Mg (II), Ca (II) using a Li-DS modified reversed-phase silica monolith [92].

For the determination of hydroxide ions Xu *et al.* [93] employed a Chromolith Performance RP-18e monolithic column (100 mm x 4.6 mm i.d.) coated first with a non-ionic surfactant, polyoxyethylene (POE), and then with a cationic surfactant, cetyltrimethylammonium bromide (CTAB), in order to produce more stable and more

efficient columns for the separation of common inorganic and organic ions than produced by simply dynamically coating a reversed-phase silica column with a cationic surfactant alone. When this stationary phase was used in conjunction with a 10 mM sodium sulphate eluent at pH 8.2, OH<sup>-</sup> was observed to elute in under 3 minutes, and was well resolved from other anions such as Cl<sup>-</sup> and NO<sub>3</sub><sup>-</sup>. Solutions of some strong and weak bases were analysed by the developed IC method, and as Table 1.5 demonstrates, the data obtained was in good agreement with results obtained using a potentiometric pH meter.

Table 1.5: A comparison of analytical performance reported by Xu *et al.*[93].

Samples	IC method		Potentiometric pH meter	
	pH	% RSD	pH	% RSD
KOH (1mM)	11.07	1.04	11.06	1.94
CH <sub>3</sub> CH <sub>2</sub> NH <sub>2</sub> (10 mM)	11.39	1.35	11.37	1.98
CH <sub>3</sub> NH <sub>2</sub> (10 mM)	11.40	1.23	11.45	1.93

Connolly *et al.* [94] demonstrated the simultaneous separation of common inorganic and cations on short permanently coated monolithic columns. In this work, two double chained surfactants, one anionic (didodecyldimethylammium bromide DDAB) and one cationic (dioctylsulphosuccinnate, DOSS), were used to coat 25 and 50 mm reversed-phase silica monolithic columns (Chromolith Flash RP-18e). A single eluent was developed which could be used with either column for the separation and conductimetric detection of both cations (indirect detection) and anions (direct detection). The eluent used by Connolly *et al.* was an ethylenediamine/phthalate eluent. Ethylenediamine is a divalent cationic organic base, which has a charge of 2+ at pH values less than 6.99 and phthalate has a charge of 2- at pH values greater than 5.51. Using the ethylenediamine/phthalate eluent, pH 6.2, a separation of 5 anions in under 1.8 minutes using a flow rate of only 2 mL/min was achieved on the 25 mm DDAB coated reversed-phase monolith. An optimised separation of H<sub>2</sub>PO<sub>4</sub><sup>-</sup>, Cl<sup>-</sup>, NO<sub>2</sub><sup>-</sup>, Br<sup>-</sup>, NO<sub>3</sub><sup>-</sup>, IO<sub>3</sub><sup>-</sup>, SO<sub>4</sub><sup>2-</sup> and I<sup>-</sup> was achieved using a 2.5 mM phthalate/1.5 mM ethylenediamine eluent (pH 4.5) at flow rate 4 mL/min. Using the same eluent, the retention of metal ions on the 50 mm reversed-phase monolith coated with DOSS was

investigated. The anion- and cation-exchange monoliths were connected in parallel and the IC system was configured to achieve a relative flow of 0.5/1.5 mL/min through the anion/cation exchange monolith columns, and the eluent flow from both columns were combined and passed through a single conductivity detector. Using this dual column system, the simultaneous separation and detection of  $\text{Cl}^-$ ,  $\text{NO}_2^-$ ,  $\text{Br}^-$ ,  $\text{NO}_3^-$ ,  $\text{Cu (II)}$ ,  $\text{Mg (II)}$ ,  $\text{Ca (II)}$ ,  $\text{Sr (II)}$  and  $\text{SO}_4^{2-}$  was possible in under 6 minutes, and as shown in Fig. 1.15, this method was then applied to the determination of common inorganic anions and cations in drinking water, river water and diluted seawater.

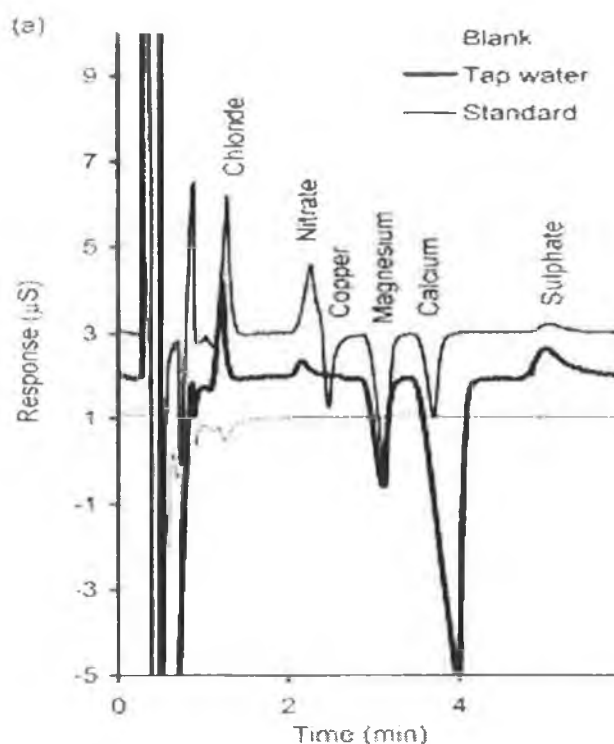


Figure 1.15: Simultaneous separation of anions and cations on two parallel-modified silica column as reported by Connolly *et al.* [94].

According to Paull and Nesterenko [88] the two main advantages of monolithic columns, namely a high permeability, and the ability to maintain good peak efficiencies at elevated mobile-phase flow rates, means that these columns are ideally suited to flow gradient conditions. Ó Ríordáin *et al.* [95] investigated the use of flow gradients (i.e. the flow rate was increased from 2 to 5 mL/min, over the 2<sup>nd</sup> and 3<sup>rd</sup> minute of the run time) for the separation of  $\text{NO}_2^-$ ,  $\text{Br}^-$ ,  $\text{NO}_3^-$ ,  $\text{I}^-$  and  $\text{SCN}^-$  on a 100 mm x 4.6 mm i.d. reversed-phase silica monolith column coated with a carboxybetaine-type zwitterionic surfactant. When the separations obtained using the

flow gradient and a constant flow rate of 4.5 mL/min were compared, it was observed that the gradient separation produced better resolution and detector sensitivity for the early eluting peaks in addition to an improved peak shape for the later eluting I<sup>-</sup> peak. By combining a pH gradient and a flow gradient (1-5 mL/min over the first 5 minutes), Ó Ríordáin *et al.* demonstrated the separation of NO<sub>2</sub><sup>-</sup>, Br<sup>-</sup>, NO<sub>3</sub><sup>-</sup>, I<sup>-</sup> and SCN<sup>-</sup> in under 8 minutes.

When the length of the reversed-phase monolith coated with carboxybetaine was reduced from 100 to 10 mm, this double gradient technique was again applied and a separation of NO<sub>2</sub><sup>-</sup>, NO<sub>3</sub><sup>-</sup>, I<sup>-</sup> and SCN<sup>-</sup> was achieved in less than 3 minutes, see Fig. 1.16 [96]. In addition to the improvement in separation time, the combination of the pH and flow gradients was observed to improve the iodide and thiocyanate peak shape and produce excellent peak efficiencies, above that previously thought possible for such an ultra short monolithic anion-exchanger.

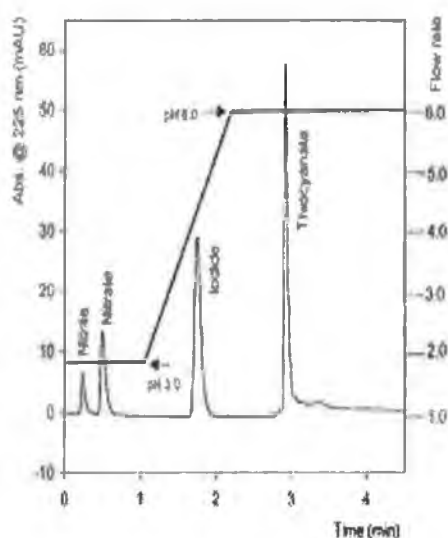


Figure 1.16: The dual gradient separation achieved on the 1 cm carboxybetaine monolithic column [96].

## Section 1.2: Ion Chromatography

Ion chromatography (IC) is an analytical technique for the separation and determination of ionic solutes and a number of IC separation modes have been developed for this purpose, including:

- Ion-exchange chromatography.
- Ion-interaction (or ion-pair) chromatography using reversed-phase columns.
- Chelation IC.
- Zwitterionic IC.

### 1.2.1: Ion-exchange chromatography

#### *1.2.1.1: Ion-exchange stationary phases*

Ion-exchange chromatography is based on dynamic interactions between charged solute ions and stationary phases that have oppositely charged functional groups. Cation-exchange columns have a negative charge to attract cations, while anion-exchange columns have a positive charge to attract anions. Table 1.6 shows the different functional groups found on common ion-exchange stationary phases. The stationary phase is also characterised by the presence of exchangeable counter ions that are attached to the charge bearing functional groups of that ion-exchanger [28, 97, 98].

Table 1.6: A summary of the different functional groups found on common anion- and cation-exchangers.

Cation-Exchangers		Anion-Exchangers	
Type	Functional Group	Type	Functional Group
Sulfonic Acid	$-\text{SO}_3^- \text{H}^+$	Quaternary amine	$-\text{N}(\text{CH}_3)_3^+ \text{OH}^-$
Carboxylic acid	$-\text{COO}^- \text{H}^+$	Quaternary amine	$-\text{N}(\text{CH}_3)_2 (\text{EtOH})^+$
Phosphonic acid	$\text{PO}_3^- \text{H}^+$	Tertiary amine	$-\text{NH}(\text{CH}_3)_2^+ \text{OH}^-$
Phosphinic acid	$\text{HPO}_2^- \text{H}^+$	Secondary amine	$-\text{NH}_2(\text{CH}_3)^+ \text{OH}^-$
Phenolic	$-\text{O}^- \text{H}^+$	Primary amine	$-\text{NH}_3^+ \text{OH}^-$
Arsonic	$-\text{HAsO}_3^- \text{H}^+$		
Selenonic	$-\text{SeO}_3^- \text{H}^+$		

Cation-exchange functional groups can function as such only when they are ionised, therefore they are classified into strong acid and weak acid types. The strong acidic functional groups are ionised over a wide pH range, in contrast to weak acidic functional groups, which are ionised over a limited pH range. Sulfonic acid exchangers are strong acid types, whereas the remaining cation-exchanger functional groups shown in Table 1.6 are weak (in order to retain cations the weak acidic functional group requires the use of pH higher than its  $pK_a$ ). Similarly, anion-exchangers are classified as strong base and weak base exchangers. Quaternary amine functional groups form strong anion-exchangers, whilst less substituted amines form weak base exchangers. The strong base will be positively charged over a wide pH range, therefore will be able to function as an anion-exchanger, in contrast to the weak anion-exchangers, which require pH sufficiently low enough to protonate the amine group [98,99].

### 1.2.1.2: Ion-exchange separation mechanism

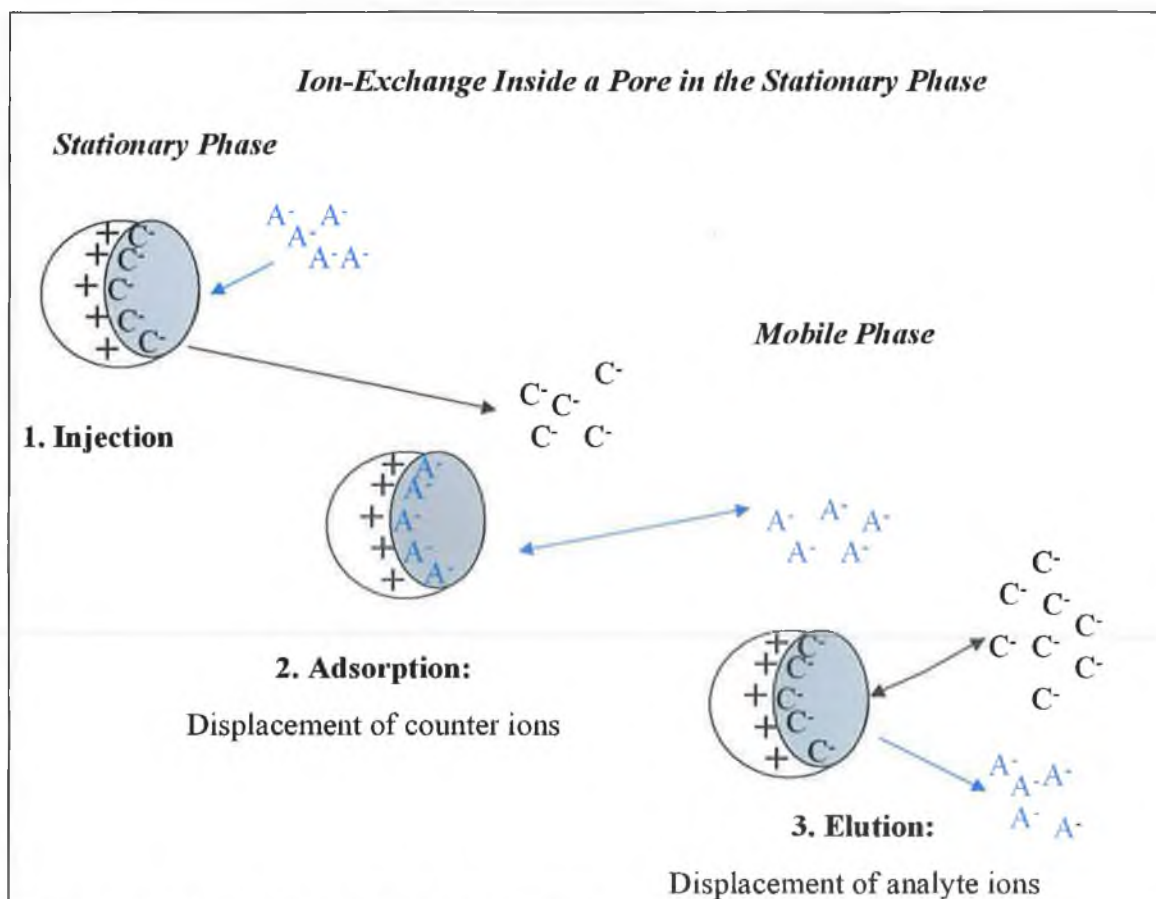


Figure 1.17: The retention of anions by anion-exchange chromatography [98].

In Fig. 1.17 the functional groups on the stationary phase surface are fixed positively charged species (+). At equilibrium these positively charged functional groups are neutralised by the counter ions ( $C^-$ ) from the eluent (mobile phase). In the second and third steps, the solute ions ( $A^-$ ) enter the column and distribute between the stationary phase and the eluent by displacing the counter ions and being displaced by the eluent ions back and fourth. The distribution equilibrium is determined by the competition between the sample components and the eluent anions for the charged sites of the stationary phase.

Primarily, ion-exchange is regulated by electrostatic interactions between the solute ions being exchanged and the eluent ions, with the fixed ions on the stationary phase [100]. Jones and Nesterenko [101] defined ion-exchange as “competitive ionic attraction for the ionic site” and expanded this further to define ion-exchange as “the equivalent exchange of ions between two or more ionised species located in different phases, at least one of which is an ion-exchanger, without the formation of new types of chemical bonds”.

### ***1.2.1.3: Factors affecting selectivity in ion-exchange chromatography***

The properties of the solute ions, the eluent ions and the counter ions that affect the extent of the ionic interactions are the following [102,103]:

- The charge on the solute ion.
- The size of the solvated ion.
- The polarizability of the solute ion.
- The ion-exchange capacity of the stationary phase.
- The type of functional group on the stationary phase.
- The extent of interactions with matrix of the stationary phase support.

However, as a rule, an increase in the charge-density (charge/solvated size) of the solute ion increases its affinity for the stationary phase. Higher charge with smaller solvated ion radius result in higher retention due to higher coulombic interactions, and this trend becomes more pronounced in more dilute eluents.

The relative affinities of cations to strong cation-exchange stationary phases are generally in the following order:

$\text{Pu}^{4+} \gg \text{La}^{3+} > \text{Ce}^{3+} > \text{Pr}^{3+} > \text{Eu}^{3+} > \text{Y}^{3+} > \text{Sc}^{3+} > \text{Al}^{3+} \gg \text{Ba}^{2+} > \text{Pb}^{2+} > \text{Sr}^{2+} > \text{Ca}^{2+} > \text{Ni}^{2+} > \text{Cd}^{2+} > \text{Cu}^{2+} > \text{Co}^{2+} > \text{Zn}^{2+} > \text{Mg}^{2+} > \text{UO}_2^{2+} \gg \text{Tl}^+ > \text{Ag}^+ > \text{Cs}^+ > \text{Rb}^+ > \text{K}^+ > \text{NH}_4^+ > \text{Na}^+ > \text{H}^+ > \text{Li}^+$

The relative affinities of anions on strong anion-exchangers are generally in the following order:

$\text{Citrate} > \text{salicylate} > \text{ClO}_4^- > \text{SCN}^- > \text{I}^- > \text{S}_2\text{O}_3^{2-} > \text{WO}_4^{2-} > \text{MoO}_4^{2-} > \text{CrO}_4^{2-} > \text{SO}_4^{2-} > \text{SO}_3^{2-} > \text{HPO}_4^{2-} > \text{NO}_3^- > \text{Br}^- > \text{NO}_2^- > \text{CN}^- > \text{Cl}^- > \text{H}_2\text{PO}_4^- > \text{CH}_3\text{COO}^- > \text{IO}_3^- > \text{HCOO}^- > \text{BrO}_3^- > \text{ClO}_3^- > \text{F}^- > \text{OH}^-$

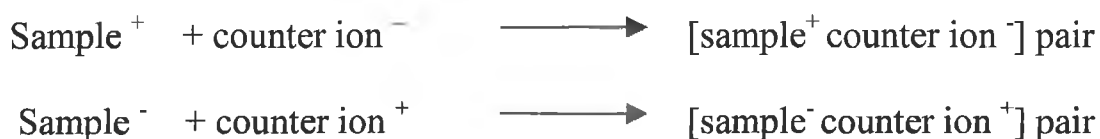
#### ***1.2.1.4: The influence of eluent properties in ion-exchange***

- *Nature of the competing ion:* The affinity of the eluent ions for the stationary phase is governed by the same factors that affect the affinity of the solute ions, i.e., charge density, solvated size, polarizability etc. Eluent ions of higher affinity to the stationary phase result in lower interactions of the sample ions with the stationary phase hence, lower retention times [99].
- *Concentration of the competing ion:* the concentration of the counter ion in the eluent affects the retention of the solute ions as higher concentrations result in stronger competition and displacement of the sample ions from the stationary phase, hence lower retention [97].
- *Eluent pH:* the pH of the eluent can influence the charges on both the eluent ions and the solute ions, if they are weak acid or basic ions. The effect of pH is particularly important in the separation of anions, where it may effect their ionisation, especially in the case of weak acids. The charge on the acid anion increases with pH, so the eluting power of weak acid eluents increase with pH until the acid is completely dissociated. The opposite trend occurs for weak bases in the eluent, where decreasing pH results in a higher degree of protonation and this results in a stronger eluent. Similarly, the degree of ionisation of the solute ions that are derived from weak acids or bases will be pH dependent and in this case, increased solute charge will increase its affinity to the functional groups on the stationary phase, hence increase their retention [100].

- *Eluent buffering capacity*: since both eluent and solute ions can be affected by the pH, the buffering capacity of the eluent is very important in order to maintain a constant eluent pH [99].
- *Ability to complex the ionic sample components*: when metal ion separations are considered, the ability of the eluent salts to complex these metal ions is a very important variable. The complexing agent may form complexes with the metal ions that may alter its effective overall charge. The degree of complexation depends on the concentration of the complexing agent as well as on the pH of the eluent [97].

### 1.2.2: Ion-interaction chromatography

Ion-interaction chromatography is a powerful analytical technique that allows conventional reversed-phase columns to be used for the separation of inorganic and organic ions, with comparable efficiency and resolution to that obtained by conventional reversed-phase HPLC. An organic ionic substance (ion-pair or ion-interaction reagent, IIR) is added to the organic-aqueous eluent and forms an ion-pair with a sample component of opposite charge. This forms a salt, but its chromatographic behaviour is that of a non-ionic organic molecule.



These IIR are typically long-chained alkyl anions or cations that, when added in dilute concentrations to an organic-aqueous eluent, can increase the retention of solute ions on a reversed-phase column. C<sub>5</sub> – C<sub>10</sub> alkylsulfonates are commonly used for the separation of cations; combinations can be used for difficult separations. Tetraalkyl ammonium salts (tetramethyl-, tetrabutyl ammonium salts) or triethyl- (C<sub>5</sub>-C<sub>8</sub>) alkyl ammonium salts are generally used for the separation of anions [104, 105, 106].

Modification of the reversed-phase stationary phase can essentially be performed in two different ways; a dynamic process in which the eluent contains the ion-interaction reagent (IIR) and the eluent itself modifies the surface or, through a process, referred to as permanent coating, in which the modifier agent is firstly adsorbed onto the stationary phase (often dynamically, by passing it through the column for a certain time); then the column is rinsed and used with a different eluent [107].

### ***1.2.2.1: Retention models in ion-interaction chromatography***

According to many authors, the IIR is added to the eluent to form, with the ionic solute, an ion-pair, which due to its increased lipophilicity can be retained on the reversed-phase stationary phase. According to other hypotheses, the IIR added to the eluent, when flowing in isocratic conditions, induces a dynamic modification of the surface of the reversed-phase packing [107]. Kissinger [108] suggested that the ion-interaction reagent partitions strongly onto the stationary phase, modifying its surface charge. This implies an ion-exchange mechanism and this interpretation would appear to be valid when the ion-interaction reagent is very strongly adsorbed on the stationary phase surface.

Bidlingmeyer *et al.* [109] have suggested a third retention model, known as the ion-interaction model, which can be viewed as intermediate between the ion-pair and dynamic ion-exchange models, that incorporates both the electrostatic effects which are the basis of the ion-pair model and the adsorptive effects which form the basis of the dynamic ion-exchange model. The lipophilic IIR ions are considered to form a dynamic equilibrium between the eluent and the stationary phases, and this results in the formation of an electrical double layer at the stationary phase surface. The adsorbed IIR ions are spaced evenly over the stationary phase due to repulsion effects, which leaves much of the stationary phase surface unaltered by the ion-interaction reagent. The adsorbed IIR ions constitute a primary layer of charge, to which is attracted a diffuse, secondary layer of oppositely charged ions. This secondary layer of charge consists chiefly of the counter ions of the IIR. A solute, having an opposite charge to the IIR, can compete for a position in the secondary layer, from which it will tend to move into the primary layer as a result of electrostatic attraction. The

presence of such a solute in the primary layer causes a change in the total charge of this layer, so to maintain charge balance, a further IIR ion must enter the primary layer. This means that the adsorption of a solute ion having opposite charge to the IIR will be accompanied by the adsorption of an IIR ion. The overall result is that solute retention involves a pair of ions (that is, the solute and IIR ions), but not necessarily an ion-pair.

According to Haddad and Jackson [105], both the ion-pair and dynamic ion-exchange modes have certain shortcomings and some significant deviations from the predicted dependences indicate that the actual separation mechanism is more complex. Studies concerned specifically with the retention of inorganic anions and cations in ion-interaction chromatographic systems have concluded that the ion-interaction model is the most appropriate and provides the most consistent agreement with experimental measurement.

#### ***1.2.2.2: Factors affecting selectivity in ion-interaction chromatography***

The factors that affect the adsorption of the IIR onto the stationary phase in ion-interaction chromatography and some factors that influence the retention of solutes include [110, 111]:

- Nature of the stationary phase.
- The lipophilicity of the IIR.
- The concentration of the IIR in the eluent.
- The ionic nature of the eluent.
- The nature of the competing ion in the eluent.
- The concentration of the competing ion in the eluent.
- The eluent pH.

The first four factors will determine the surface concentration of the IIR on the stationary phase, and hence, the surface charge density and the effective ion-exchange capacity. The higher the surface concentration of the ion-interaction reagent, the greater the retention of solutes having a charge opposite to that of the IIR. Therefore, the retention times will increase as the lipophilicity of the IIR is increased and as the % of organic modifier in the eluent is decreased. It has been observed that the solute

retention generally increases with the concentration of the IIR in the eluent, but there is a threshold concentration above which solute retention decreases with further increases in the concentration of the IIR. This is a result of the increased concentration of the IIR counter ion. The nature and concentration of the eluent competing ion (whether it is the counter ion of the IIR or an ion which is added separately) will determine the retention times and elution order for solute ions. Increases in the concentration of the eluent counter ion will result in decreased solute retention. The eluent pH will influence the charges on the counter ions and solute ions if these species are weak acids or bases.

### 1.2.3: Chelation-exchange chromatography

In recent years, the main trend in ion-exchange chromatography has been the development of high efficiency ion-exchange substrates, with the sulphonated group still being the most popular of the cation-exchange groups. However, this approach has resulted in limited scope for changing the selectivity for metal ion separations. This lack of selectivity control limits the versatility of ion-exchange methods, particularly, if there is interest in trace metals eluting in the presence excess amounts of other ionic species [101]. Also, a second emerging trend, towards lower capacity, higher performance cation-exchange substrates, suffers from the vulnerability of separation to changes in sample ionic strength. These limitations could be overcome through the use of a chelating-exchange stationary phase rather than a simple ion-exchange stationary phase. Chelating ion-exchangers can be used in analytical separations just like ion-exchangers, but have the added advantages of selectivity control and less sensitivity to changes in sample ionic strength [112, 113].

In contrast to the sorption mechanism of ion-exchange, which occurs without the formation of new types of chemical bonds, the process of chelation-exchange involves the formation of a co-ordinate bond between the metal cation and the chelating group on the stationary phase surface during the exchange process. Hence chelation-exchange can be considered as a sorption mechanism where the separation is controlled by the thermodynamics and kinetics of metal complex formation and dissociation [101].

### ***1.2.3.1: Principles of complexation***

In a complex, when the central atom is bound to its immediate neighbours via covalent bonds, formed as a result of electron pair acceptance by the metal ion from non-metal atom, it is customary to call the latter the donor atom and the former the acceptor atom. Alternatively, the non-metal atom is termed the co-ordinating atom and the bond between it and the metal atom is called a co-ordinate bond [114]. Several co-ordinating atoms can be incorporated into single ligand molecules. A ligand of this type can form several bonds to the metal centres. If all the bonds are formed with the same centre, then the complex is called a chelate and the ligand is said to be multidentate, i.e.,

- Unidentate ligands:  $\text{Cl}^-$ ,  $\text{F}^-$ ,  $\text{NH}_3$ ,  $\text{H}_2\text{O}$ .
- Bidentate ligands: oxalate, ethylenediamine, glycine.
- Tridentate ligands: iminodiacetic acid.
- Tetridentate ligands: nitrilotriacetic acid.
- Hexadentate ligands: ethylenediaminetetraacetic acid.

Complex formation between a metal ion and a multidentate ligand is called chelation. For a molecule to function as a chelating agent, it must fulfil at least two conditions. Firstly, it must possess at least two donor atoms, which are capable of combining with a metal atom by donating a pair of electrons. Electrons may be contributed by basic co-ordinating groups such as  $\text{NH}_2$  or acidic groups that have lost protons. Some acidic groups that combine with metal atoms by replacement of hydrogens are:  $-\text{COOH}$ ,  $-\text{SO}_3\text{H}$  and  $-\text{OH}$  and other co-ordinating groups include:  $-\text{NH}$ ,  $-\text{NH}_2$ ,  $=\text{NOH}$ ,  $-\text{N}=\text{}$  and  $-\text{S}-$ . Secondly, these functional groups must be so situated in the molecule so that they permit the formation of a ring with a metal atom as the closing number [115, 116]

#### ***1.2.3.1.1: Stability of metal chelates***

The stability of a complex in solution refers to the degree of association between the two species in equilibrium. The greater the degree of association between the metal and ligand, the greater the stability of the compound, and hence, the greater the magnitude of the stability/formation equilibrium constant.



The stepwise stability or formation constant ( $K_n$ ) can be expressed as follows:

$$K_n = [ML_n] / [ML_{n-1}].[L] \quad (\text{Eqn. 1.7})$$

Alternatively, the overall stability constant ( $\beta_n$ ) can be expressed as:



$$\beta_n = [ML_n] / [M].[L]^n \quad (\text{Eqn. 1.9})$$

The stepwise and overall stability constants are related as follows:

$$\beta_n = K_1 \cdot K_2 \cdot K_3 \dots \dots \dots K_n \quad (\text{Eqn. 1.10})$$

Metal complexes may be roughly classified on the basis of the speed with which equilibrium between the metal ion and ligands is attained, with those that attain it rapidly being described as labile, whereas those which attain equilibrium slowly are described as inert or robust [107, 117].

### 1.2.3.2: Chelating stationary phases

As discussed earlier, the use of chelating stationary phases offers alternative selectivities to those achievable when using simple sulphonated or carboxylated ion-exchange stationary phases for metal ion analysis. Another benefit of chelation ion chromatography is the availability of a large and varied number of chelating ligands to functionalise the stationary phase, each offering unique metal ion selectivity [118]. However, the correct choice of chelating functionality is a critical factor for the efficient functioning of the separation system, because the kinetics of chelation-exchange are generally much slower than those of simple ion-exchange. Some frequently used chelating ligands are carbamates,  $\beta$ -diketones, diamines, iminodiacetate and amino acids, various azo- and tri-phenylmethane dyes and 8-hydroxyquinoline [112], see Fig. 1.18. As a rule two- and three dentate ligands, such as 8-hydroxyquinoline and iminodiacetic acid, result in more efficient separations. Ligands of higher denticity are likely to have much slower kinetics of dissociation because the number bonds involved with the metal [112]. In addition, the chelating groups should have a broad spectrum of chelating action and have no special selectivity to one or two separate metals. To date, stationary phases functionalised

with carboxylic acid containing ligands have proven to be the most successful in terms of selectivity, efficiency and range of applications [118].

A number of approaches have been employed to produce chelating stationary phases. Where possible synthetic schemes have been devised for the surface derivatisation of substrates, i.e., silica and polystyrene, as surface-modified substrates demonstrate the best efficiency and peak shape in chelation ion chromatography (CIC). The distribution of bonded groups at the stationary phase surface is also a crucial factor for the improvement of separation efficiency and selectivity. According to Jones and Nesterenko [101], the best distribution of chelating groups providing homogeneous sorption sites can be achieved by impregnation of appropriate substrates. For example, a chelating dyestuff, i.e., xylenol-orange was used by Paull *et al.* [119] to impregnate 10  $\mu\text{m}$  particle size polystyrene-divinylbenzene (PLPRS) neutral resin, and this chelating ion-exchange dye-impregnated resin was used for the determination of trace metals in coastal seawater. A third approach for the formation of a chelating surface is dynamic modification of the substrate where the chelating compound is added to the eluent and the substrate initially has no chelating surface [120, 121, 122].

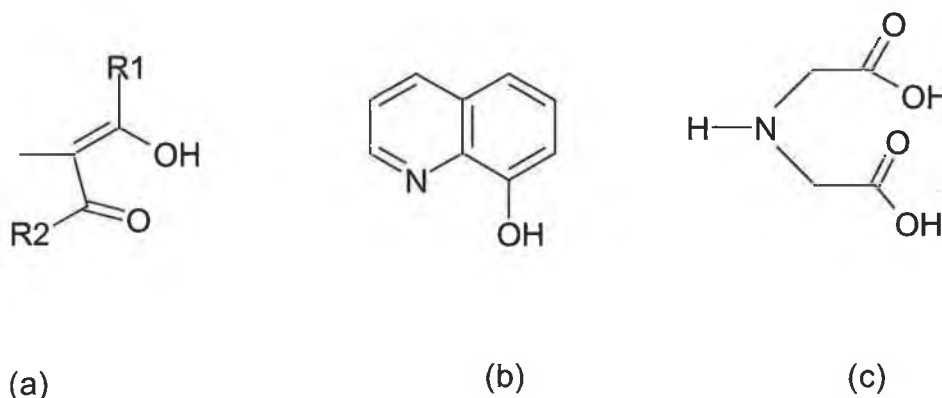


Figure 1.18: Structures of chelating ligands (a)  $\beta$ -diketones, (b) 8-hydroxyquinoline and (c) iminodiacetic acid.

### 1.2.3.3: The effect of eluent parameters on cation retention in chelation ion chromatography

As metal ion retention is based upon the relative conditional stability constants of each metal and the immobilised chelating ligand, retention and selectivity is predominately controlled through eluent pH, although, as in simple ion-exchange

chromatography, a range of eluent parameters can be used to obtain desired changes in selectivity [101, 106, 112].

With simple cation-exchange, the alkali metal ions of the eluent, although having a weaker affinity for the ion-exchange site than the polyvalent analyte ion, will have a major competitive effect as the eluent ionic strength/concentration of the alkali metal ions increases. Competition from the hydrogen ions will be even weaker, not becoming significant until the pH is quite low. However, with chelation-exchange, the alkali metals present in the eluent, form such extremely weak coordinate bonds, such that their interaction with the chelating stationary phase can be neglected. Consequently, the effect of alkali metal concentration will be small. On the other hand, the hydrogen ion concentration will have a major effect on the formation of the polyvalent metal-ligand complex, because most chelating ligands are conjugate bases of weak acid groups and accordingly, will have a very strong affinity for hydrogen ions. The pH, therefore, will be the dominant factor in the separation of metal ions by chelation, as it will determine the values of the conditional stability constants of the metal complexes on the surface of the chelating stationary phase.

For metal cations of the same charge, except the alkali metals, the retention order for chelation exchange is, in general the reverse of simple cation-exchange. Further changes in the retention order between selected metals can also be obtained by:

- Careful choice of ligating atom in the chelating group [101]. Steric effects involving bulky complexing groups can modify the retention order for certain metal species.
- The use of complexing or chelating agents in the eluent [101]. In ion-exchange, the use of complexing agents in the eluent is mainly for the control of the charge on the metal ions, in order to improve the speed and efficiency of the separation. For chelation-exchange, the presence of a complexing agent in the eluent will result in competition between the chelating group in the eluent and the chelating functionality of the stationary phase. When considering the large range of chelating agents available, the number of possible combinations is very large.
- The presence of more than one sorption mechanism on the stationary phase [101]. Pure sorption mechanisms are very rare in chromatography and chelation-

exchange is no exception. The vast majority of chelating compounds contain weak acid groups whose conjugate base forms coordinate bonds with the metal cations. These groups, of course, can act as ion-exchange sites in their own right and are commonly known as weak cation-exchangers. Furthermore, nitrogen-containing ligands will become protonated at low pH values, giving rise to the possibility of anion-exchange if the metal species in the eluent is in the form of anionic complex. Therefore, some analyte metal ions maybe influenced by both simple ion-exchange and chelation-exchange.

#### ***1.2.3.4: The determination of metals in complex matrices using chelation ion chromatography***

The direct analysis of samples such as surface saline waters, biological/geological digests and natural/industrial brines can be extremely difficult by conventional ion-exchange chromatography, and requires matrix elimination/ pre-concentration steps or large sample dilutions before injection. These pre-treatment steps are necessary to prevent an undesired effect known as 'self-elution'. Self-elution occurs when the ionic strength of the matrix is too high, resulting in ion-exchange sites on the stationary phase being swamped by the matrix ions and this seriously affects the separation efficiency [123]. The unique selectivity exhibited by chelating stationary phases i.e., showing little or no affinity for alkali metals, while at the same time being capable of separating many di- and trivalent metal ions, means that direct injection of high ionic strength samples, without any on-line pre-treatment, is possible [101, 123].

A large number of applications involving CIC of complex sample matrices have been performed using silica substrates modified with iminodiacetic acid (IDA) [123, 124, 125, 126, 127, 128]. The popularity and extensive use of the IDA ligand is based on two factors:

- Firstly, the stability constants for alkaline earth and transition transition/heavy metal ions with the IDA ligand are not prohibitively high as to require excessively strong eluents. For many other chelating functionalities studied the selectivity coefficients are often too large to enable multi-elemental separations without complex gradient strategies [124].

- Secondly, chelating ligands with large metal stability constants can produce very broad peaks due to slow dissociation kinetics. However, the complexation/dissociation kinetics of the IDA-metal complex are sufficiently rapid as to produce separation efficiencies comparable with simple ion-exchange [124].

Bonn *et al.* [125] synthesised a stationary phase by covalently binding iminodiacetic acid to a porous silica support and investigated the determination of transition metal ions in alkali and alkaline earth metal-rich matrices, e.g. seawater. Seawater is of major interest because not only is the ionic strength of the matrix relatively high but there is the added complication of the presence of large concentrations of Mg (II) and Ca (II). Using an eluent composed of 10 mM tartaric acid (pH 2.54), a separation of Co (II), Zn (II) and Cd (II) was possible in a solution containing up to 10 % Na and Mg (II). The affinity of the IDA stationary phase toward transition metals, which are retained through complexation between pH 2-3, means that these ions are well separated from Na and Mg (II), which will react with the IDA only by ion-exchange under acidic conditions. Therefore, by exploiting this difference in selectivity, Bonn *et al.* demonstrated the separation of Co (II), Cd (II) and Zn (II) in seawater. Elefterov *et al.* [126] also employed an IDA-bonded silica column to separate transition metals in the presence of fifty fold molar excess of alkali and alkaline earth metals. Using a 0.001 M dipicolinic acid eluent (pH 3.0), the alkali and alkaline earth metals were not retained on the column and hence did not interfere with the determination of Zn (II), Pb (II), Co (II) and Cd (II). The application of this method for the analysis of low mineralised waters e.g., ground waters and wastewater from a galvanic bath was investigated. The results obtained for the determination of Zn (II) and Pb (II) in galvanic bath wastewater showed good agreement with data obtained by flame atomic absorption spectroscopy.

Using an iminodiacetic acid bonded silica column, Bashir and Paull [123] developed a method for the determination of trace levels of Mg (II) and Ca (II) in medicinal NaCl saline solutions and laboratory grade KCl. A number of methods have been developed for the analysis of Mg (II) and Ca (II) in NaCl and KCl brines, however, each method contains a preconcentration/matrix elimination step. Using sensitive post-column reaction detection with *o*-cresolphthalein complexone, it was possible to detect trace

amounts of Ca (II) in a 0.9 % NaCl medical eyewash saline solution, in which there was a 20,000-fold excess concentration of sodium, and trace levels of Mg (II) in a 0.5 M solution of laboratory grade KCl.

Another significant application of the IDA bonded silica chelating stationary phase is the monitoring of trace levels of Be (II), one of the most toxic non-radioactive elements to be found at trace levels in natural and industrial wastewaters. Beryllium metal and its compounds are widely involved in present day technologies and as a consequence of this, Be (II) containing wastewaters from industrial plants and power plants can contaminate natural waters, which may in turn lead to pollution of tap water. Cation-exchange methods for the determination of Be (II) are limited by the lack of desired stationary phase selectivity required for the analysis of anything other than relatively simple sample types such as drinking water and other low ionic strength samples. Voloschik *et al.* [127] compared selectivity of a surface-sulphonated cation-exchanger and an IDA functionalised silica gel column for the separation of Be (II) and other alkaline earth metals. Be (II) eluted as a wide peak before Mg (II), Ca (II), Sr (II) and Ba (II) on the surface-sulphonated cation exchanger and in addition to this, some transition and heavy metal cations eluted before Mg (II) and interfered with the determination of Be (II). However, on the IDA functionalised silica stationary phase, Be (II) forms more stable complexes than other alkaline earth metals with the IDA functional groups. When a dipicolinic acid eluent was used, transition and heavy metal cations form stable complexes, which are not retained on the IDA silica phase. Therefore, Be (II) is fully separated from Mg (II), Ca (II), Al (III) and Fe (III), which are the main matrix components of rock and wastewater samples. The method developed by Voloschik *et al.* was applied to the determination of Be (II) in a geological sample and a number of wastewater samples from a metal plant. Results obtained by Bashir and Paull [128] demonstrated that the retention of Be (II) on an IDA-silica column is predominantly as a result of coordination of the metal ion with N and O donor atoms. Using a 0.4 M KNO<sub>3</sub> eluent, pH 3, alkali and alkaline earth metal ions were not retained on the IDA silica gel column, however, Be (II) eluted as a reasonably sharp peak at 5.5 minutes. Therefore, it was possible to analyse a simulated seawater matrix spiked with trace levels of Be (II), in which the ratios of Be (II) to Na, Mg (II) and Ca (II) were 1:300,000, 1:32,500 and 1:100,000, respectively. The selectivity as regards other transition and heavy ions

was also investigated, as these may be present at high concentrations in natural and industrial wastewaters. Under the eluent conditions described previously, the Be (II) peak was also well resolved from transition and heavy metal ions, which were observed to elute between 10 and 15 minutes.

#### **1.2.4: Complexation ion chromatography**

Complexation ion chromatography, which includes all ion chromatographic modes in which complexation is exploited for the separation and detection of metal ions in different ways, is now a widely accepted method of metal analysis [112,113]. The possible chromatographic variants include:

- Cation chromatography with complex forming eluents and cation chromatography with complex forming stationary phases (CIC).
- Ion-exchange and ion-interaction chromatography of anionic metal chelates with direct conductivity or spectrophotometric detection including post column complexation derivatisation.

These IC methods are distinguished by the complicated retention behaviour of metal ions and their complexed forms in the chromatographic system. This common feature is related to a number of complexation reactions, accompanying the chromatographic process, and/or a complex retention mechanism. One more distinguishing feature, confirming a relationship between the ion chromatographic methods described above, is based on complexation reactions, i.e. the main elution and separation mechanisms are determined by the stability of metal complexes. This basic characteristic is of great importance in regulating interactions between the metal ion, the eluent and stationary phase. Hence the versatility of complexation ion chromatography is due to the vast range of different metal-complexing forms and complex cation equilibria that can be utilised to control resolution. Depending on the particular sample, different chromatographic techniques can be chosen and applied in order to obtain the greatest selectivity. Hence, it would appear that complexation IC techniques complement each other well.

#### ***1.2.4.1: Metal determination using complex ion chromatographic methods***

In most cases, ion-exchangers bearing sulfonated or carboxylic functional groups provide a strictly defined elution order. Often, to change the selectivity of the separation of metal ions, the presence of complexing agents in the eluent is required. By adding a complexing ligand to the eluent, the metal ions to be separated are partially complexed and converted to non-charged or lower-charged metal complexes, while a certain fraction of each metal ion remains as the charged cation. Owing to differences in the fraction that is not complexed, separation of metal ions is enhanced [100]. Eluents can be classified into two main types, depending on their complexing ability, i.e., citric or tartaric acid are described as weak complexing agents while reagents such as pyridine-2,6-dicarboxylic acid (DPA) and nitrilotriacetic (NPA) can be described as strong eluent complexing agents [125].

Ding *et al.* [129] developed a method for the simultaneous determination of Pb (II), Cu (II), Ni (II), Co (II), Cd (II), Mn (II) and Hg (II), which involved the separation of the metal cations as their anionic chelates on a bifunctional ion exchange column (IonPAC CS5A). A mixed bed/bifunctional ion exchange column allows separation of transition metals by cation- or anion-exchange, depending on the complexing agent chosen. The eluent employed, pyridine-2,6-dicarboxylic acid, was found to be of particular interest because it is such a strong complexing agent that heavy and transition metals could be well separated as their anionic chelates  $M(DPA)_2^{2-}$  on the mixed bed resin of the analytical column. Following the separation of the metal chelates by anion-exchange, detection involved post-column reaction with 2-[5-bromo-2-pyridyl]-azo]-5-diethyl-aminophenol to form metal-5-Br-PADAP chelates, which can be sensitively monitored by spectrophotometric detection @ 565 nm. Cordellicchio *et al.* [130] also employed the mixed bed ion exchange column with a 2,6-pyridinedicarboxylic acid eluent, and achieved a separation of Fe (III), Fe (II), Cu (II), Ni (II), Zn (II), Co (II), Cd (II) and Mn (II) in 20 minutes. This method was successfully applied to the analysis of natural and wastewaters related to the maintenance of a sewage treatment plant.

Unmodified silica gel can also be used as a weakly acidic cation-exchanger because of the silanol groups present on the silica surface. The retention of transition metals

on an unmodified silica gel column (Develosil 30-5) was investigated by Ohta *et al.* [131]. An eluent composed of 0.5 mM ethylenediamine-oxalic acid eluent at pH 5.5 resulted in the most efficient separation of both alkaline earth and transition metal ions.

The separation of transition metal ions on porous graphitic carbon using an acidified aqueous eluent and post-column detection, using PAR and spectrophotometric detection, was reported by Merly *et al.* [132]. Using an eluent composed of 0.45 M oxalic acid, pH 1.6, a separation of Ni (II), Cd (II), Pb (II) and Cu (II) was achieved on the Hypercarb column, with the high oxalate concentration assisting the elution of the strongly retained Pb (II) and Cu (II).

As an alternative to conventional ion-exchange chromatography, Jen *et al.* [133] developed an ion-interaction chromatographic method for the determination of metal ions such as Pb (II), Ni (II), Cd (II), Fe (II) and Cu (II) in electroplating wastewaters. In this method, a dynamic anion-exchange bed was created by the sorption of a hydrophobic cation (tetrabutylammonium in the eluent) onto a reversed-phase (C<sub>8</sub>) column. This makes it possible to separate anionic chelates by ion-interaction chromatography. In the work performed by Jen *et al.* metal ions were first chelated with ethylenediaminetetraacetic acid (EDTA), followed by injection into the chromatographic system. EDTA is an excellent chelating agent that is able to form sufficiently stable chelates with 62 different metals. The applications of other commonly used chelates such as dithizone, dithiocarbamates, β-diketones and quinolin-8-ol are limited to specific systems and cannot be used with various metal ions. An eluent consisting of acetonitrile/water mixture (8:92 v/v) containing 0.002 M tetrabutylammonium, as the ion-interaction reagent, was used to separate the anionic chelates on the modified reversed-phase column.

The separation of transition metal ions by reversed-phase HPLC, using on-column complexation, has also been investigated [134, 135]. Neterenko *et al.* [135] employed picolinic acid as a chelating agent for reversed-phase separation of Mn (II), Cu (II), Ni (II), Co (II), Cd (II) and Zn (II). Using a Spherisorb reversed-phase column and an eluent composed of acetonitrile: water (6:94 % v/v) containing  $2 \times 10^{-3}$  M picolinic

acid (pH 7), the determination of Zn (II), Cd (II), Mn (II) and Cu (II) in industrial wastewater from a galvanic bath was possible using spectrophotometric detection at 235 nm.

As discussed in Section 1.2.3.4, an alternative, less commonly used approach is the application of IDA silica chelation ion-exchangers for the separation of transition and heavy metal ions [118, 125, 126]. Bashir and Paull [118] demonstrated that iminodiacetic acid bonded silica gel offered a viable alternative to simple cation-exchange resins for the determination of trace transition metal ions in real samples. Separations of several alkaline earth and transition metal ions using simple inorganic eluents were also obtained through manipulation of the unique stationary phase selectivity.

### **1.2.5: Zwitterionic Ion Chromatography**

The technique termed zwitterionic ion chromatography (ZIC), utilises a bifunctional stationary phase, formed as a result of either chemical modification of the stationary phase or from a hydrophobic zwitterionic surfactant adsorbed onto a hydrophobic chromatographic support material, where cationic and anionic functional groups in close proximity occur on the stationary phase [136]. The idea of combining both anion- and cation-exchange groups within a single ion-exchange site for the purpose of improving selectivity appeared shortly after the initial invention of polymeric ion-exchange resins. In 1951, Stach synthesised a zwitterionic ion-exchange resin containing both sulfonic acid and quaternary ammonium functional groups [137]. Zwitterionic stationary phases have been shown to have a unique selectivity, a tolerance to high ionic strength matrices [138] and the ability to separate ions with only pure water as the eluent [139].

#### ***1.2.5.1: Types of zwitterionic ion-exchanger***

The distribution of the oppositely charged groups can vary considerably and the following types of zwitterionic ion-exchangers have been identified [137]:

- Polyampholyte resins having a continuous distribution of oppositely charged groups in the whole volume of the ion-exchange particle.

- Pellicular resins containing a layer of opposite charge on a charged core, with this layer comprising microparticles, latex microbeads, a polymer film, or a simple treated outer surface of the core for the purpose of adding functional groups of opposite charge sign to the functional group core.
- Ion-exchangers containing functional groups of opposite charge at the outer surface available for interaction with ions, see Fig. 1.19 (a).
- Ion-exchangers in which there are oppositely charged groups present in a single attached or immobilised molecule, see Fig. 1.19 (b).

An observed trend in the development of zwitterionic-exchangers is a decrease in the scale of localisation of oppositely charged groups, and a reduction in the distance between these functional groups on the surface of the substrate, because ion-exchangers formed in this way often exhibit unique ion-exchange selectivity and can therefore be used for separations which may not be possible with other types of ion-exchangers.

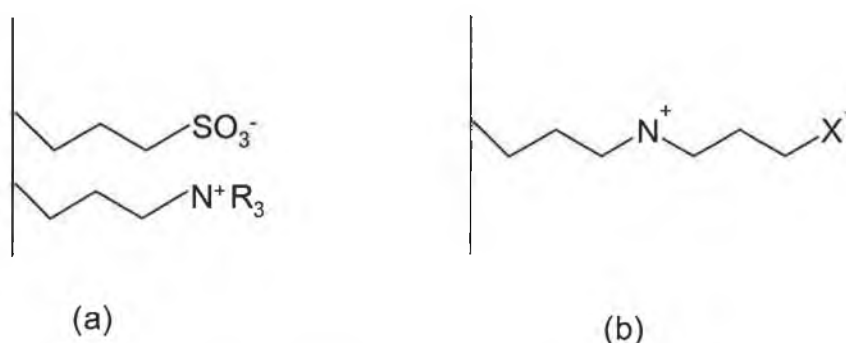


Figure 1.19: Schematic showing zwitterionic ion-exchangers with (a) localisation of oppositely charged groups on the surface and (b) localisation of oppositely charged groups in one molecule attached to the surface.

#### 1.2.5.2: Coated zwitterionic phases

Some factors that will influence the selectivity of coated zwitterionic phases, i.e. a reversed-phase stationary phase coated with zwitterionic surfactants, include the length of the hydrophobic tail region, which will impact upon coating stability and column capacity, the spacing between the cationic and anionic groups within the immobilised zwitterionic molecule, the order of the two ionic groups within the molecule and the relative strength of the two ionic groups [136, 137].

### 1.2.5.3: Proposed separation mechanisms in ZIC

According to Cook *et al.* [136] several explanations have been offered for the ZIC retention mechanism which are based on the following concepts:

- Simultaneous electrostatic attraction and repulsion of solute ions from two oppositely charged functional groups of the zwitterionic stationary phase.
- The formation of “ion-pairs” between oppositely charged ions in solution.
- The establishment of a zwitterionic electrical double layer comprising the accumulation of oppositely charged ions (from the eluent) around the centres of the zwitterion.

Hu [140] proposed the binary electrical double-layer (EDL) mechanism, in which a binary-EDL is established as a result of retention of cations and anions by the negative and positive functional groups on the zwitterionic stationary phase. The unique properties of the binary-EDL can be summarised as:

- Cations and anions are both retained because of the electrostatic attraction by the negative and positive stationary phase functionalities [141].
- However, these solute ions also experience simultaneous forces of attraction and repulsion because of the close proximity of the positive and negative functionalities on the stationary phase [141].
- The combined effects of the above effects results in the achievement of an effective distribution of both the cationic and anionic solute ions from the electrical fields (stationary phase) to the bulk solution (eluent) without the need for a displacing ion, i.e., pure water could be used as the eluent [141].

Hu and Haddad [141] further explained the retention characteristics in terms of an ‘ion-pair’ theory, which was based on the theory that cations and anions are eluted as combinations of ions, which can be described as ion-pair like forms. When a mixture of salts is injected, ‘ion-pairs’ comprising all possible combinations of the solute cations and anions are produced, however the distribution of cations and anions between ‘ion-pairs’ is dependent on a priority order determined by the  $\Delta G$  of the cation and anion in the ‘ion-pair’ [141]. In the case of a zwitterionic stationary phase in which the negative functional group is outermost, i.e., Zwittergent-3-14 shown in Fig. 1.20, analyte anions with a high propensity for forming neutral ‘ion-pairs’ show

strong retention, while those with a low propensity are expelled due to repulsion from the anion-EDL.

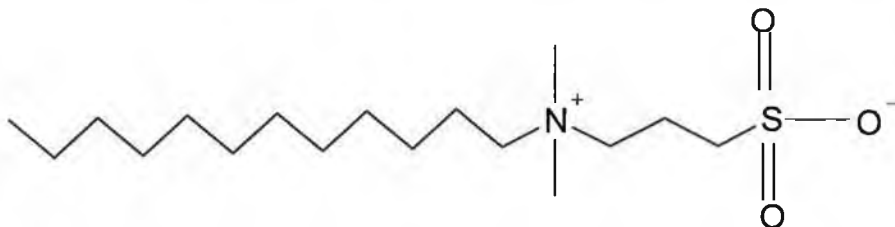


Figure 1.20: The structure of 3-(N,N-dimethylmyristylammonio)propanesulfonate (Zwittergent-3-14).

#### 1.2.5.4: Mechanism of separation in ZIC using electrolytic eluents

Okada and Patil [142] suggested that the introduction of a salt into the eluent in ZIC results in changes in the surface morphology of the zwitterionic stationary phase, which provides solute ions with easier access to charged functional groups. Observations by Cook *et al.* [136] that a rapid initial increase in retention factor ( $k$ ) values for 3 test anions on a Zwittergent-3-14 coated reversed-phase ( $C_{18}$ ) column in going from pure water to a 1 and 2 mM concentration of salt in the eluent supports this theory of an abrupt change in surface morphology. The mechanism proposed by Cook *et al.* comprises two simultaneous effects, one of ion-exclusion and one of chaotropic interaction.

Ion-exclusion: the sulphonate group on the outer part of the zwitterionic stationary phase contributes a negative charge that repels solute anions by acting as a Donnan membrane, however, the magnitude of this negative charge varies depending on how strongly the eluent cations interact with the sulphonate groups and how strongly the eluent anions interact with the quaternary ammonium groups. The situation occurring with a  $NaClO_4$  and a  $CeCl_3$  eluent is depicted in Fig. 1.21. In the case of the  $NaClO_4$  eluent there is a weak interaction between  $Na^+$  and the sulphonate functional group and a strong interaction between the  $ClO_4^-$  and the quaternary ammonium functional groups, and these effects combine to establish a relatively strong negatively charged Donnan membrane, which exerts a strong repulsion on analyte anions. However, there is a strong interaction of  $Ce^{3+}$  with the sulphonate groups and a weak interaction of  $Cl^-$  with the quaternary ammonium groups and this results in a Donnan membrane that

becomes weakly positively charged and as a result all the analyte anions can penetrate relatively freely.

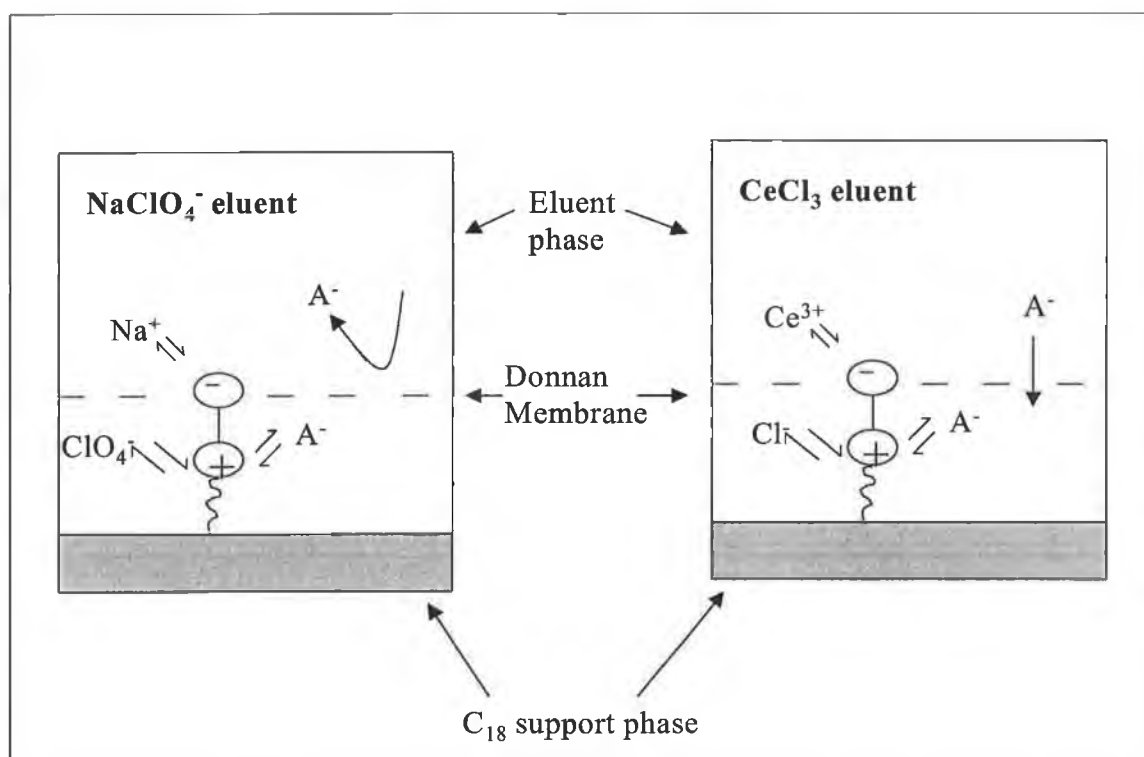


Figure 1.21: A schematic showing the proposed mechanism using a  $NaClO_4$  and a  $CeCl_3$  eluent.

The other part of the mechanism proposed by Cook *et al.* [136] concerns the interaction of sample anions with the quaternary ammonium functional group on the zwitterion. It was observed that the selectivity follows the order of increasing polarizability or chaotropic character, i.e., retention follows the Hofmeister series:



## Section 1.3: Detection methods in ion chromatography

### *1.3.1: Introduction*

In IC, the detector must be able to “pick out or see” sample ions in the presence of eluent ions. There are several methods that can be employed to make this possible. One is to choose a detector that will respond only to the ions of interest, but not the eluent ions. Another method is to use indirect detection, this is where the eluent has a background signal and the presence of sample ions causes a decrease in the concentration of eluent ions through a replacement process. The detector records the absence of eluent ions when the sample ion peak elutes and a corresponding decrease signal is observed [100].

The most widely used detection methods for IC detection involve manipulation of the eluent prior to detection, to make the eluent ions less detectable or make the sample ions more detectable. The most common example of this is the use of chemical suppression with conductometric detection. Another example is post-column reaction with a colour-forming reagent prior to visible-spectrophotometric detection. For example, 4-(2-pyridylazo)-resorcinol (PAR), a colour forming ligand, can be added post-column, to detect metal ions by visible spectrophotometric detection, whereas, the eluent ions in this case don't react with the colour-forming reagent.

Detectors can be classified either as general or selective [100, 143]. A general detector will respond to all or most of the ions that pass through the detector cell. A conductometric detector is classified as a general detector because all ions will conduct electricity (although to different degrees). UV-Vis spectrophotometric, atomic emission and atomic absorption and electrochemical detectors can be considered to be selective detectors because they respond only to certain ions (again by varying degrees). A key advantage of selective detection is the ability to achieve lower detection limits. A selective detector may or may not have a higher sensitivity (signal per unit concentration) for a particular ion. However, lower background signals produced by selective detection will translate into lower detection limits because the signal to noise ratio is improved.

### 1.3.2 Conductivity Detection

Conductivity detection is based upon the electrical conductivity of an ionic solution when placed between two oppositely charged electrodes. The presence of ions in the solution allows electrical current to flow between the electrodes, completing the circuit [144, 145].

#### *1.3.2.1: Conductivity definitions and equations*

Electrolytic conductivity is the ability of an electrolytic solution to conduct electricity between two electrodes across which an electric field is applied. Ohm's law,  $V = IR$ , is obeyed and the magnitude of the current depends, in part, on the magnitude of the applied potential [146]. The conductance,  $G$ , of a solution is expressed in terms of the solution electrolytic resistance. It is measured in reciprocal ohms or the SI unit siemens (S):

$$G = 1/R \quad (\text{Eqn. 1.11})$$

Specific conductance ( $k$ ) takes into account the area of the electrodes ( $A$ ) in  $\text{cm}^2$  and the distance ( $l$ ) between the electrodes. Conductance increases with the area of the electrodes but decreases as the distance between the electrodes is increased:

$$k = G (l/A), \text{ thus } k \text{ has units of } \text{S cm}^{-1} \quad (\text{Eqn. 1.12})$$

The cell constant ( $K$ ) is equal to  $l/A$ , and has units of  $\text{cm}^{-1}$ .

$$k = GK \quad (\text{Eqn. 1.13})$$

Equivalent conductance takes into account the concentration of the chemical solution and is defined by:

$$\Lambda = 1000k/C \quad (\text{Eqn. 1.14})$$

where  $C$  is the concentration in equivalent per L and  $\Lambda$  has units of  $\text{S cm}^2 \text{equiv}^{-1}$ .

Therefore, the equivalent conductance can be related to the measured conductance:

$$G = \Lambda C/1000K \quad (\text{Eqn. 1.15})$$

The ability of the solution to conduct is directly proportional to the salt content and the mobility of the individual cations and anions [145]. As the ionic character of a molecule is increased, the conductivity increases. Small, mobile ions conduct quite readily and to a much greater extent than large, bulky ions. At low ionic concentrations, conductivity is directly proportional to the concentration of

conductive species in the solution. The total ionic concentration of the solution in the cell and the temperature of that solution affect the linearity of the relationship [146].

### ***1.3.2.2: Effect of analyte concentration on conductivity***

The electrical conductance of a solution depends upon the type and concentration of all ions present [145, 147]. Electrical current is carried by both cations and anions in solution. Ideally, conductance increases linearly as the total ionic concentration increases. The degree of dissociation, the mobility of the ions in solution, and the formation of ion pairs in solution limit this linearity.

For weak electrolytes (e.g. weak acid and bases), the primary factor limiting detection linearity is the degree of dissociation or ionisation. For strong electrolytes, e.g. strong acids and bases and their salts, which are by definition completely dissociated in solution, the primary factor limiting detection linearity is ionic mobility. Ionic mobility is defined as the migration velocity of an ion in an electric field in which the potential changes 1 V/cm in the direction of the field. Factors affecting the mobility of an ion are the retardation of ion movement by the solvation sphere surrounding each ion and the total ionic concentration of the solution.

For both weak and strong electrolytes, the detection linearity is influenced by the formation of non-conducting ion pairs in solution. These ion pairs form as a result of electrostatic attraction between oppositely charged ions. Although each ion pair has a finite lifetime, at any instant, the total number of free ions capable of carrying current is lowered by the continual interchange of ions in solution. Under these conditions, a species may be completely ionised, but will not be completely dissociated. As a result, the conductivity of the solution will decrease and the concentration of the detected species will appear lower than it is. In very dilute solutions (below  $10^{-4}$  M), the formation of these ion pairs becomes negligible and solutes are both completely ionised and dissociated.

### 1.3.2.3: The effect of temperature on conductivity

The conductivity of a solution is directly affected by temperature [145, 147]. As the solution conductivity increases, the effect of temperature changes becomes more pronounced. This change is often observed as a regular oscillation in the baseline that is directly related to room temperature. This may in turn, affect the reproducibility and linearity of a determination. Temperature compensation can reduce the effects of temperature by normalising all measured conductivities to 25°C. The detector microprocessor calculates a temperature compensation factor based on a selected temperature coefficient. For most ions in solution, this coefficient is  $\sim 1.7\% / ^\circ\text{C}$ . The temperature coefficient is a measure of the change in the solution conductivity (as a % conductivity at 25°C) per degree C of temperature change.

### 1.3.3: Suppressed Conductivity Detection

In a chromatogram, the baseline is a result of the signal produced by the eluent and the signal produced by the sample ions results in the analyte peak, therefore the larger the difference between the conductance of the eluent and the sample, the larger the sample peak observed. However, as Table 1.7 demonstrates, the limiting ionic conductances of most common electrolytes are high, and as a result, detection proves to be quite insensitive. This has the effect of masking the conductance that would be supplied by the sample ions. To reduce the conductance of the electrolyte, a suppressor is placed in-line after the separation column and before the detector, as shown in Fig.1.22.

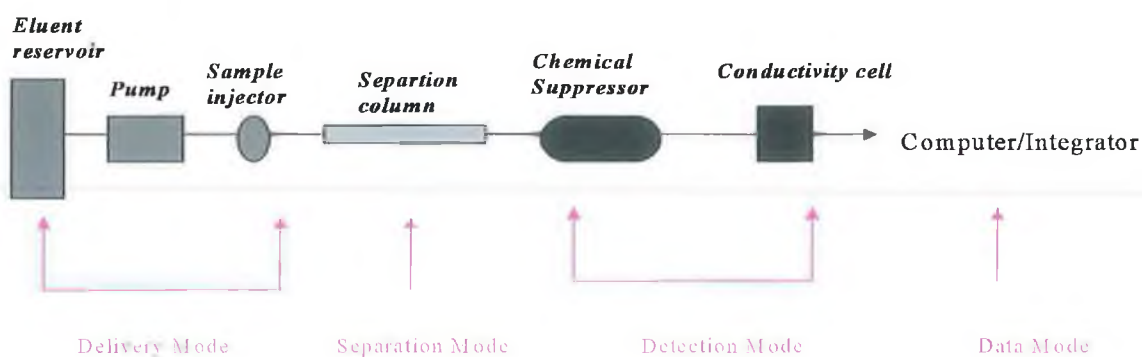


Figure 1.22: Diagram of experimental set-up for suppressed conductivity detection.

In IC, a suppressor device is used to replace the background concentration of highly conductive eluent ions with species that are significantly less conductive.

Table 1.7: Limiting equivalent conductances in aqueous solution at 25°C, units S.cm<sup>2</sup>equiv<sup>-1</sup> [100].

Anions ( $\lambda^-$ )		Cations ( $\lambda^+$ )	
OH <sup>-</sup>	198	H <sup>+</sup>	350
SO <sub>4</sub> <sup>2-</sup>	80	K <sup>+</sup>	74
Br <sup>-</sup>	78	Pb <sup>2+</sup>	71
Cl <sup>-</sup>	76	Ce <sup>2+</sup>	70
NO <sub>2</sub> <sup>-</sup>	72	Fe <sup>3+</sup>	68
NO <sub>3</sub> <sup>-</sup>	71	Ca <sup>2+</sup>	60
PO <sub>4</sub> <sup>3-</sup>	69	Zn <sup>2+</sup>	53
F <sup>-</sup>	54	Mg <sup>2+</sup>	53
HCO <sub>3</sub> <sup>-</sup>	45	Na <sup>+</sup>	50

### 1.3.3.1: Types of suppressor

- Packed column suppressors.
- Hollow fibre membrane suppressors.
- Micromembrane suppressors.

The first used suppressor was an ion-exchange column in the form of H<sup>+</sup> or OH<sup>-</sup>. However, this technique was restricted by the limited capacity of the suppressor, which had to be regenerated periodically off-line. This problem has been overcome with the introduction of the hollow fibre membrane suppressor. However, there was also a limitation with this type of suppressor due to the low surface area of the fibre, resulting in low ion-exchange and suppression capacity. The appearance of the micromembrane suppressor, in which two flat sheets of membrane were inserted into three ion-exchange screens as a sandwich solved these problems [105,148,149]. The surface area available for exchange between eluent and regenerant ions was increased greatly in comparison to the hollow-fibre suppressor, and so was the ion-exchange capacity. This type of suppressor employs diffusion alone for ion transfer. More recently, an electric field was applied to design a more efficient suppressor, known as an electrolytic membrane-based suppressor.

### *1.3.3.2: Operating principles of micro-membrane suppressors*

In an electrolytic micro-membrane suppressor, the eluent passes through a central chamber, which has ion-exchange membrane sheets as the upper and lower surfaces. As Fig. 1.23 shows, the regenerant ( $\text{H}_2\text{O}$ ) flows in a counter direction over the outer surfaces of both membranes. Mesh screens constructed from a polymeric ion-exchange material are inserted into the eluent cavity and also into the cavities, which house the flowing regenerant solution. The entire device is constructed in a sandwich layer configuration with gaskets being used to define the desired flow paths. The volume of the eluent chamber is very small ( $< 50 \mu\text{L}$ ), so band broadening is minimal. Regenerant ions ( $\text{H}^+$  or  $\text{OH}^-$ ) are transferred into the eluent across the membranes, whilst eluent counter ion pass simultaneously into the regenerant. However, unlike the hollow-fibre suppressor, which relies on diffusion to transport the appropriate ions to the membrane surface, the micromembrane suppressor utilises the high capacity ion-exchange screens to perform this tasks. The screens promote ion transport in 2 ways; firstly, the three dimensional over and under square weave pattern of the screens causes a disruption to laminar eluent flow and directs eluent flow to the membrane surface. Secondly, the ion-exchange sites on the screens enable site-to-site transport of the desired ions to the membrane. The latter mechanism of ion transport plays an increasingly important role as the eluent passes from the suppressor inlet towards the outlet. During the passage, the suppressor reaction advances towards completion and there are relatively few eluent ions remaining to react. The transport of these residual eluent ions to the membrane surface is greatly facilitated by the ion-exchange screens [105, 143, 148].

For the suppressed conductivity detection of cations, an acidic, cationic eluent is used to separate the sample cations. The separated cations in the eluate pass directly into the suppressor unit containing an anion-exchange membrane in the hydroxide form. The eluent cation is neutralised and the counter anions associated with the sample metal ions are exchanged for the more highly conducting hydroxide ion, see Fig. 1.23. The background conductivity is very low after the eluent passes through the suppressor unit; theoretically it is that of pure water. The equivalent conductance of sample ions is high; it is the sum of conductances of the alkali metal cation and the

hydroxide counter ion. Suppressors for cation chromatography are limited to those cations that do not form precipitates with the hydroxide ions from the suppressor.

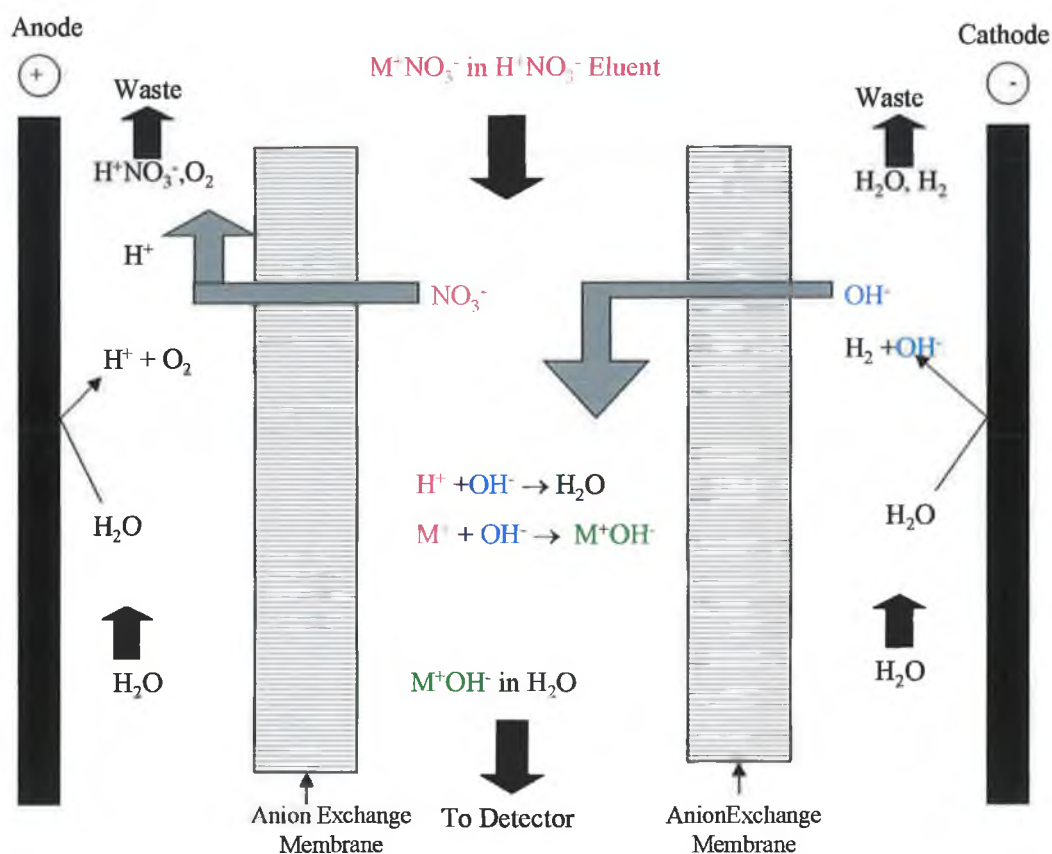
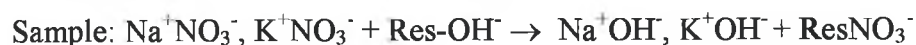


Figure 1.23: Schematic of the mechanism of suppression for a Dionex anion self-regenerating, micro-membrane suppressor [100].

#### 1.3.4: Spectrophotometric Detection

Spectrophotometric detection is a useful detection method for monitoring IC separations because it is selective; yet simply altering the wavelength monitored by the detector can change its selectivity [150]. In addition, the addition of a colour-forming reagent to the eluent or the use of a post-column reagent can increase the versatility of this detector [100].

### ***1.3.4.1: Direct spectrophotometric detection and the Beer-Lambert's Law***

The fundamental law under which the UV-Vis detector operates is the Beer-Lambert Law, which can be described in the following form:

$$A = \epsilon bc$$

A is the absorbance of a species of concentration  $c$  (M) in a cell length  $b$  (cm). The extinction coefficient ( $\epsilon$ ) is characteristic of the substance under analysis and is also a function of the wavelength.

The Lambert-Beer equation is useful for choosing conditions for the separation and detection of ions [26]. The eluent ions should have low absorptivity and the sample ions should have a reasonably high absorptivity. In a special case of indirect detection, this should be the reverse. In this method, the eluent absorbs strongly in the visible or ultra violet spectral region. The wavelength is selected so that the eluent (usually aromatic) absorbs but the sample ions do not absorb. This results in the eluent having an absorption signal and the sample is detected by a decrease of the background signal [150], see Section 1.3.4.2.

However, the Beer-Lambert law is successful in describing the absorption behaviour of dilute solutions only and in that sense it is a limiting law [26]. At analyte concentrations greater than approximately 0.01 M, the average distance between the particles of the absorbing species are diminished to the point where each particle affects the charge distribution of its neighbours. This interaction can alter their ability to absorb a given wavelength of radiation. A similar effect is sometimes encountered in dilute solutions that contain high concentrations of other species, i.e., electrolytes. Deviations from the Beer-Lambert law also arise because the molar absorptivity ( $\epsilon$ ) is dependent upon the refractive index of the solution and if concentration changes cause significant alterations in the refractive index of a solution, departures from the Beer-Lambert law are observed [8]. The Beer-Lambert law is also a limiting law in the sense that it applies only when absorbance is measured with monochromatic radiation. Truly monochromatic light sources, such as lasers, are not practical for routine analytical instrumentation. Instead, a polychromatic, continuous light sources is

employed in conjunction with a grating or a filter that isolates more or less a symmetrical band of wavelengths around the desired wavelength [151].

#### ***1.3.4.2: Indirect spectrophotometric detection***

In the late 1970's a number of workers demonstrated how UV-Vis detection could be effectively used to measure transparent analytes without modifying their chemistry in any way [105, 144]. A major feature of this new approach was the use of light absorbing (usually UV absorbing) eluents, made so by including in the eluent light-absorbing ions with the same charge as the analyte ions. These light absorbing ions have a dual role of selectively displacing the analyte ions from the separator column and also to reveal them in the effluent. The appearance of analytes is signalled by troughs that appear in the base line absorbance as the transparent analytes substituted for the chromophoric displacing ions, see Fig. 1.24.

The sensitivity attainable with this method will depend on a number of factors:

- The absorbance change is increased as the molar absorptivity of the eluent ions increases. Also for solute ions with low molar absorptivities, the absorbance change accompanying solute elution is maximised when the molar absorptivity of the eluent is greatest. This can be achieved by selection of the wavelength of maximum absorption for the eluent ions [105].
- The absorbance change is decreased as the ratio of the charge on the solute ion to that of the eluent ion (i.e.  $x/y$ ) decreases. This ratio has been called the displacement ratio,  $R$ . This suggests that eluent ions of multiple charges are not desirable [105].
- The signal-to-noise ratio for indirect spectrophotometric detection improves as the concentration of the eluent decreases [105].

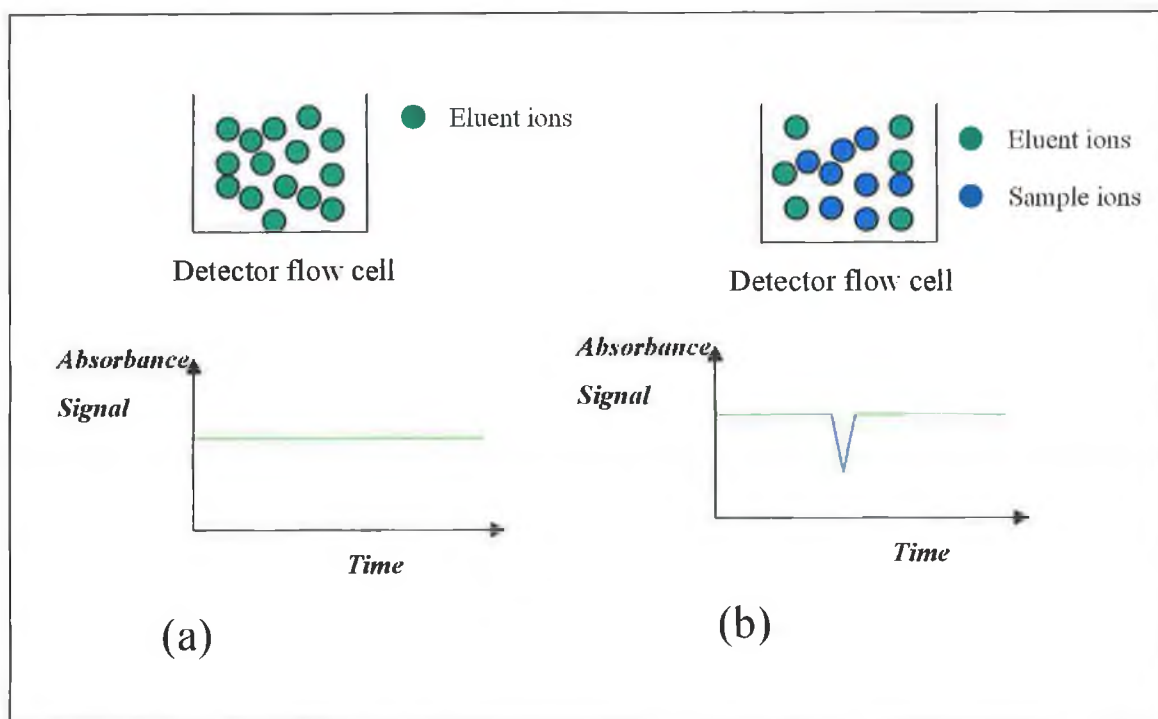


Figure 1.24: Schematic representing indirect UV-Vis detection: (a) shows the background detector response and (b) demonstrates the decrease in background signal due to the presence of the transparent analytes passing through the flow cell.

#### 1.3.4.3: Indirect spectrophotometric detection of anions and cations

The rapid development of indirect spectrophotometric detection of anions since its first introduction in 1978 can be related directly to the rapid increase in the use of eluents containing aromatic acid anions as competing ions in anion-exchange methods employing conductivity detection. These ions also have high molar absorptivities in the UV region and so indirect spectrophotometric detection became possible with the same eluents already in common usage for conductivity detection e.g., eluents such as phthalate, nitrate, sulfobenzoate and benzenetricarboxylate. Aromatic bases, especially those, which are protonated appreciably at neutral pH values, find applications to sensitive indirect spectrophotometric detection of cations. These include species such as 2,6-dimethylpyridine isomers ( $pK_a$  6.72), 2-methylpyridine ( $pK_a$  5.92), 2-phenylethylamine ( $pK_a$  9.84) and 1,4-phenylenediamine ( $pK_a$  6.16) [105].

### 1.3.5: Detection by post-column reaction

A post-column reaction is a reaction between sample ions, following their separation on a column, with a post-column reagent (PCR) or series of reagents on-line, and it is the product of this reaction that is detected by a suitable detector. Post-column reaction offers several advantages as a detection strategy [150]:

- Sample ions that are not easily detected can be converted into products that are easily detected.
- The number of detection options can be increased.
- Detecting the sample ions as the reaction product can increase sensitivity.
- The post-column reaction procedure can be often used to improve the specificity of the detection.

Post-column detection has had a considerable impact in IC, and is widely used with conductivity, spectroscopic and electrochemical detectors. In particular, the use of a suppressor with conductivity detection can be considered one form of post-column reaction. The major type of post-column reaction (excluding suppression techniques) used in IC is one in which the column effluent and a post-column reagent are combined on-line in a post-column mixing chamber, see Fig. 1.25. The sample-PCR mixture may be heated on-line, or provided additional reaction time through the use of a delay/reaction coil, to ensure a favourable reaction before entry into the detector. A second type that can be used is to pass the column effluent through a post-column, packed-bed reactor, in which the analytes undergo a reaction with a post-column reagent that has been physically or chemically bonded to the packed bed material.

The key to successfully using post-column detection is to have an appropriate reaction that yields a product that can be detected with good sensitivity. The % conversion of the analyte into the post-column reaction product needs only to be reproducible, although 100 % conversion is preferred. Finally, the reaction must be controllable, and cause little or no band dispersion and broadening owing to reaction or mixing of the reagents.

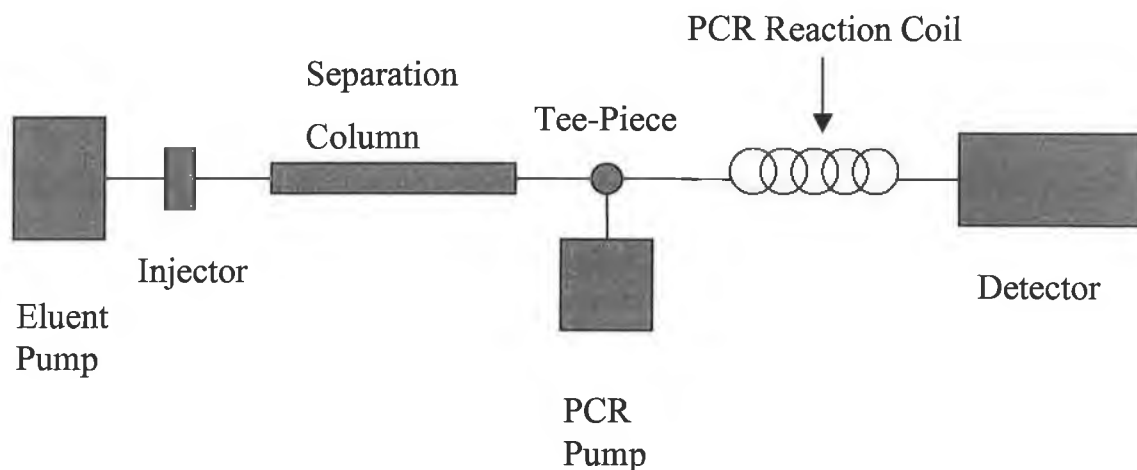


Figure 1.25: Schematic of the post-column reaction experimental set-up for solution post-column detection.

Although as discussed previously, post-column detection is compatible with a wide variety of detectors, it requires more rigid control and operator attention to obtain a sensitive, reproducible and accurate detection [152, 153, 154]:

- The reaction between the sample ions and the post-column reagent must be rapid, complete or reproducible and provide a species suitable for detection.
- Efficient mixing of the post-column reagent and column effluent must be obtained so that the reaction occurs quickly and provides a homogenous solution.
- The reagent must be miscible with the eluent and should not form precipitate in the presence of the eluent.
- The reagent should be stable in order to minimise baseline drift and noise in the detector.
- The reagent should have similar detection properties to that of the eluent so that variations in the degree of mixing of the reagent and the eluent do not cause elevated baseline noise.
- Heat may be required and eluent, reagent and sample ions must be stable at the required temperature.
- Extra tubing or coils may be required between the mixing chamber and detector to provide the necessary reaction time.

(Each of these steps have to be optimised to produce baseline uniformity and thus obtain a good, reproducible S/N and at the same time prevent excessive contributions to band dispersion and broadening, which would also affect detection limits).

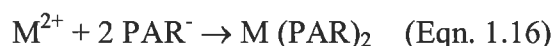
- The reagent must not cause corrosion or other reactions with either the post-column reactor itself or the detector.

#### *1.3.5.1: Post-column detection of inorganic cations*

Post-column detection of inorganic cations, such as alkaline earths, transition metals and lanthanides, has been developed to the point where it can be considered to be the optimal detection mode for most of these species [150]. In the majority of cases, the eluted metal ions are reacted with a colour-forming reagent and spectrophotometric detection is used. However, other detection methods such as fluorescence and amperometry are also applicable.

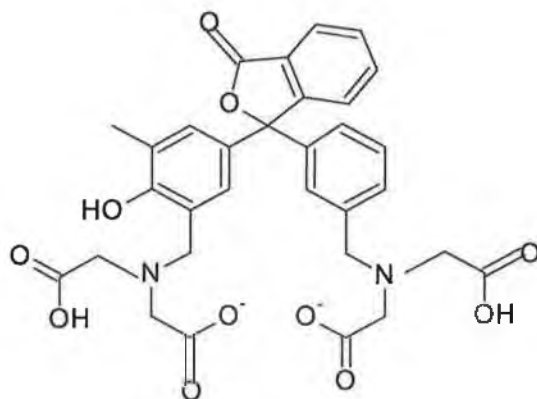
The structures of some commonly employed post-column reagents for the detection of cations are shown in Fig. 1.26. In general, 4-(2-pyridylazo)-resorcinol (PAR) is the preferred reagent for the PCR detection of transition metal ions, whilst 2,7-bis(2-aresonophenylazo)-1,8-dihydroxynaphthalene-3,6-disulfonic acid (arsenazo III) is preferred for lanthanide ions [155]. For the detection of alkaline earth metal ions, the ligand, *o*-cresolphthalein complexone (*o*-CPC) is particularly sensitive to Ca (II) and Mg (II). However, *o*-CPC is not particularly sensitive to Ba (II) and Sr (II). An alternative ligand such as sulfonazo III would be preferable if trace analysis of Ba (II) or Sr (II) is required [123].

Metal ions form a 1:2 complex with PAR according to the following equation:

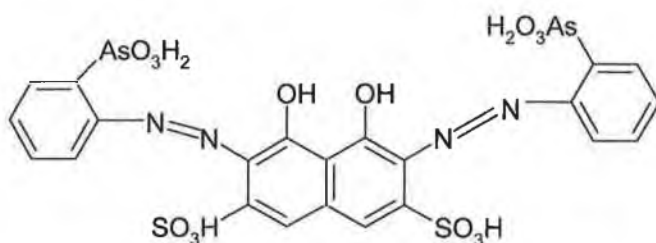


The PCR reagent consists of a dilute PAR solution in an appropriate alkaline buffer, and a detection wavelength in the range 500-540 nm is generally used. The use of PAR for post column detection of transition and heavy metals has proven successful after separation of these species by either ion-exchange [124, 132, 156,157] or ion-interaction chromatography [158].

(a)



(b)



(c)

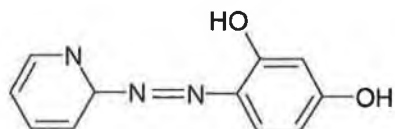


Figure 1.26: The chemical structure of (a) *o*-CPC, (b) arsenazo III and (c) PAR.

Cassidy *et al.* [152] have shown that arsenazo I and arsenazo III are ideal post-column reagents for the detection of lanthanide elements. Reaction with arsenazo dyes and these ions is very rapid at room temperature and detection sensitivity is relatively uniform for the entire lanthanide series. Fritz and Smith [159] have determined Mg (II) and Ca (II) within 3 minutes in hard water using arsenazo I. The selective nature of the ligand meant that it was relatively free from interference and the method was found to be very sensitive with detection limits of 2.3 and 6.3 ng for Mg (II) and Ca

(II). Jones *et al.* [160] developed a system for determining rare earth elements using arsenazo III as the post-column reagent.

Table 1.8: A summary of the reagents for the post-column detection of inorganic cations.

<b>Analytes</b>	<b>Post column reagent</b>	<b>Ref</b>
Al (III)	8-Hydroxyquinoline-5 sulfonate, Tiron	[161,162]
Ca (II), Mg (II)	Arsenazo I	[163]
Co (II)	Luminol	[164]
Fe (II), Fe (III)	PAR, Bathophenanthroline disulfonic acid	[165,166]
Di-, tri-, tetravalent cations	8-Hydroxyquinoline	[167]
Transition metal cations	PAR, Eriochrome Black T, Dithizone	[168,169,170]
Rare earth cations	Arsenazo I and III	[171]

## References

- <sup>1</sup> N. Barbarin, D.B. Mawhinney, R. Black, J. Henion, *J. Chromatogr. B*, 783 (2003) 73.
- <sup>2</sup> D. Lubda, K. Cabrera, W. Kraas, C. Schaefer, D. Cunningham, *LCGC Europe*, December (2001) 18.
- <sup>3</sup> N. Barnett, R. Bos, H. Brand, P. Jones, S. Lim, S. Purcell, R. Russell, *Analyst*, 127 (2002) 45.
- <sup>4</sup> F. Rabel, K. Cabrera, D. Lubda, *J. American Lab.*, 32 (24) (2000) 20.
- <sup>5</sup> N. Tanaka, H. Kobayashi, K. Nakanishi, H. Minakuchi, N. Isizuka, *Anal. Chem.*, 73 (2001), 420A.
- <sup>6</sup> H. H. Willard, L.L Merritt, J. A. Dean, *Instrumental Methods of Analysis*, 5<sup>th</sup> Edition, Van Nostrand (New York) 1974.
- <sup>7</sup> U. D. Neue, *HPLC Columns: Theory, Technology and Practice*, Wiley-VCH (New York) 1997.
- <sup>8</sup> D. C. Harris, *Quantitative Chemical Analysis*, 2nd Edition, W.H. Freeman (San Francisco) 1987.
- <sup>9</sup> K. Sinz and K. Cabrera, *Inter. Labmate*, volume XXV, issue VII, January (2001), 35.
- <sup>10</sup> H. Minakuchi, K. Nakanishi, N. Soga, N. Isizuka, N. Tanaka, *J. Chromatogr. A*, 797 (1998) 121.
- <sup>11</sup> K. Cabrera, G. Wieland, D. Lubda, *TRAC*, volume 17, no.1 (1998) 50.
- <sup>12</sup> P. Hatsis and C.A. Lucy, *Anal. Chem.*, 75 (2003) 995.
- <sup>13</sup> K. Heinig and J. Henion, *J. Chromatogr. B*, 732 (1999) 445.
- <sup>14</sup> B.K. Matauszewki, M.L. Constanzer, C.M. Chavez-Eng, *Anal. Chem.*, 70 (1998) 882.
- <sup>15</sup> H. Moriyama, M. Anegayama, Y. Kato, *J. Chromatogr. A*, 729 (1996) 81.
- <sup>16</sup> H. M. H. Van Eijk, D.R. Rooyakkers, N. E. P. Deutz, *J. Chromatogr. A*, 620 (1993) 143.
- <sup>17</sup> M. W. Dong and A.D. Tran, *J. Chromatogr.* 449 (1990) 125.
- <sup>18</sup> N. D. Danielson and J. J. Kirkland, *Anal. Chem.*, 59 (1987) 2501.
- <sup>19</sup> J. J. Kirkland, F.A. Truszkowski, C.H. Dilks, G.S. Engel, *J. Chromatogr. A*, 890 (2000) 3.

- 
- <sup>20</sup> E. Vidal, C. Pascual, L. Pou, *J. Chromatogr. B*, 736 (199) 295.
- <sup>21</sup> D. Connolly and B. Paull, *J. Chromatogr. A*, 917 (2001) 353.
- <sup>22</sup> D. Connolly and B. Paull, *Anal. Chim. Acta*, 441 (2001) 53.
- <sup>23</sup> H. Poppe, *J. Chromatogr. A*, 778 (1997) 3.
- <sup>24</sup> B. Yan, J. Zhao, J. Brown, J. Blackwell, P. Carr, *Anal. Chem.*, 72 (2000) 1253.
- <sup>25</sup> N. Ishizuka, H. Minakuchi, K. Nakanishi, N. Soga, H. Nagayama, K. Hosoya, N. Tanaka, *Anal. Chem.*, 72 (2000) 1275.
- <sup>26</sup> D. A. Skoog, D. M. West and F. J. Holler, *Fundamentals of Analytical Chemistry*, 7th Edition, Saunders College Publishers (Forth Worth) 1996.
- <sup>27</sup> R. Kellner, J. M. Mermet, M. Otto and H. M. Widmen, *Analytical Chemistry*, Wiley-VCH (Chichester) 1998.
- <sup>28</sup> S. Abieja, *Chromatography and Separation Science, Volume 4, Separation Science and Technology*, Academic Press, USA, 2003.
- <sup>29</sup> J. MacNair, K. Patel, J. Jorgenson, *Anal. Chem.*, 72 (2000) 1353.
- <sup>30</sup> J. D. Thompson and P.W. Carr, *Anal. Chem.*, 74 (2002) 4150.
- <sup>31</sup> N. Ishizuka, H. Minakuchi, K. Nakanishi, K. Hirao, N. Tanaka, *J. Coll. Surf. A*, 187-188 (2001) 273.
- <sup>32</sup> J. MacNair, K. Patel, J. Jorgenson, *Anal. Chem.*, 71 (1999) 700.
- <sup>33</sup> J. MacNair, K. Lewis, J. Jorgenson, *Anal. Chem.*, 69 (1997) 983.
- <sup>34</sup> M. M. Dittmann and G. P. Rozing, *J. Chromatogr. A*, 744 (1996) 63.
- <sup>35</sup> N. Ishizuka, H. Kobayashi, H. Minakuchi, K. Nakanishi, K. Hirao, K. Hosoya, T. Ikegami, N. Tanaka, *J. Chromatogr. A*, 960 (2002) 85.
- <sup>36</sup> H. Minakuchi, K. Nakanishi, N. Soga, N. Ishizuka, N. Tanaka, *J. Chromatogr. A*, 762 (1997) 135.
- <sup>37</sup> M. Miyabe and G. Guichon, *J. Sep. Sci.*, 27 (2004) 853.
- <sup>38</sup> H. Zou, X. Huang, Y. Mingliang, Q. Luo, *J. Chromatogr. A*, 954 (2002) 5.
- <sup>39</sup> A. M. Siouffi, *J. Chromatogr. A*, 1000 (2003) 801.
- <sup>40</sup> Merck KGaA-What is Chromolith?, Merck KgaA, Darmstadt, Germany, viewed 27/6/2004 < [www.chromolith.com/servlet/PB/menu/1210300/index.html](http://www.chromolith.com/servlet/PB/menu/1210300/index.html)>
- <sup>41</sup> F. Svec, *LCGC Europe*, volume 16, no. 6a (2003) 24.
- <sup>42</sup> N. Ishizuka, H. Minakuchi, K. Nakanishi, K. Hirao and K. Tanaka, *J. Coll. Surf A*, 187-188 (2001) 273.
- <sup>43</sup> M. Kubin, P. Spacek, R. Chromeczek, *Czech. Chem. Comm.*, 32 (1967) 3881.

- 
- <sup>44</sup> F. D. Hileman, R. E. Sievers, G. G. Hess, W. D. Ross, *Anal. Chem.*, 45 (1973) 1126.
- <sup>45</sup> D. K. Roper, E.N. Lightfoot, *J. Chromatogr. A*, 702 (1995) 3.
- <sup>46</sup> J. F. Kennedy, M. Paterson, *Polym. Int.*, 32 (1993) 71.
- <sup>47</sup> Y. Yang, A. Velayudhan, C. M. Ladish, M. R. Ladish, *J. Chromatogr.*, 598 (1992) 169.
- <sup>48</sup> S. Hjerten, J. L. Liao, R. Zhang, *J. Chromatogr.*, 473 (1989) 273.
- <sup>49</sup> T. B. Tennikova, F. Svec, B.G. Belekii, *J. Liq. Chromatogr.*, 13 (1990) 63.
- <sup>50</sup> F. Svec and J. M. J. Frechet, *Anal. Chem.*, 64 (1992) 820.
- <sup>51</sup> S. M. Fields, *Anal. Chem.*, 68 (1996) 2709.
- <sup>52</sup> H. Minakuchi, K. Nakanishi, N. Soga, N. Ishizuka, N. Tanaka, *Anal. Chem.*, 68 (1996) 3498.
- <sup>53</sup> M. Al-Bokari, D. Cherrak, G. Guiochon, *J. Chromatogr. A*, 975 (2002) 275.
- <sup>54</sup> N. Tanaka, H. Kobayashi, N. Ishizuka, H. Minakuchi, K. Nakanishi, K. Hosoya, T. Ikegami, *J. Chromatogr. A*, 965 (2002) 35.
- <sup>55</sup> E. C. Peters, F. Svec, J. M. J. Frechet, *Chem. Mater.*, 9 (1997) 1898.
- <sup>56</sup> F. Svec and J. M. J. Frechet, *J. Ind. Engin., Chem. Res.*, 38 (1999) 34.
- <sup>57</sup> F. Svec, *J. Sep. Sci.*, 27 (2004) 747.
- <sup>58</sup> A. ChingWang, F. Svec, J. M. J. Frechet, *Anal. Chem.*, 65 (1993) 2243.
- <sup>59</sup> F. C. Leinweber and U. Tallarek, *J. Chromatogr. A*, 1006 (2003) 207.
- <sup>60</sup> K. Cabrera, *J. Sep. Sci.*, 27 (2004) 843.
- <sup>61</sup> K. Nakanshi and N. Soga, *J. Am. Ceram. Soc.*, 139 (1991) 2518.
- <sup>62</sup> C. Schafer, K. Cabrera, D. Lubda, K. Sinz, D. Cunningham, *Inter. Labmate*, volume XXVI, February (2001) 89.
- <sup>63</sup> F. C. Leinweber, D. Lubda, K. Cabrera, U. Tallarek, *Anal. Chem.*, 74 (2002) 2470
- <sup>64</sup> V. K. Parashar, Raman, O. P. Bahl, *J. Non-Cryst. Solids*, 201 (1996) 150.
- <sup>65</sup> M. T. Anderson, J. E. Martin, J. G. Odinek, P. P. Newcomer, *Microp. Mat.*, 10 (1997) 13.
- <sup>66</sup> K. Nakanishi, H. Minakuchi, N. Soga, N. Tanaka, *J. Sol-Gel Sci. Tech.*, 8 (1997) 547.
- <sup>67</sup> N. Ishizuka, H. Minakuchi, K. Nakanishi, N. Soga, N. Tanaka, *J. Chromatogr. A*, 797 (1998) 133.
- <sup>68</sup> W. Gao, G. Yang, J. Yang, L. Haiyan, *Turk. J. Chem.*, 28 (2004) 379.

- 
- <sup>69</sup> Merck Chromolith<sup>TM</sup> Information Sheet: General Information and Applications, 2002.
- <sup>70</sup> B. Bidlingmaier, K.K. Unger K.K., N. von Doehren, *J. Chromatogr. A*, 832 (1999) 11.
- <sup>71</sup> F. Svec and J. M. J. Frechet, *J. Chromatogr. A*, 702 (1995) 89.
- <sup>72</sup> S. Xie, F. Svec, J. M. J. Frechet, *J. Chromatogr. A*, 775 (1997) 65.
- <sup>73</sup> M. B. Tennikov, N. V. Gazolina, T. B. Tennikova, F. Svec, *J. Chromatogr. A*, 798 (1998) 55.
- <sup>74</sup> S. Xie, R. W. Allington, F. Svec and J. M. J. Frechet, *J. Chromatogr. A*, 865 (1999) 169.
- <sup>75</sup> K. Branovic, A. Buchacher, M. Barut, A. Strancan, D. Josic, *J. Chromatogr. A*, 903 (2000) 21.
- <sup>76</sup> T. Ikegami and N. Tanaka, *Curr. Opin. Chem. Bio.*, 8 (2004) 527.
- <sup>77</sup> G. S. Chirica and V. T. Remcho, *J. Chromatogr. A*, 924 (2001) 223.
- <sup>78</sup> D. V. McCalley, *J. Chromatogr. A*, 965 (2002) 51.
- <sup>79</sup> H. Y. Aboul-Enein and M. M. Hefnaw, *Talanta*, 65 (2005) 67.
- <sup>80</sup> M. Macohia, S. Bertini, C. Mori, C. Orlando, C. Papi., G. Placania, *IL Farmaco*, 59 (2004) 237.
- <sup>81</sup> M. Rocheleau, C. Jean, J. Bolduc, D. Carazzato, *J. Pharm. Biomed. Anal.*, 31 (2003) 191.
- <sup>82</sup> S. Apers, T. Naessens, K. Van Den Steen, F. Cuyckens, M. Claeys, L. Pieters, A. Vlietinck, *J. Chromatogr. A*, 1038 (2004) 107.
- <sup>83</sup> D. Lubda and W. Lindner, *J. Chromatogr. A*, 1036 (2004) 135.
- <sup>84</sup> N. Wu, J. Dempsey, P.M. Yehl, A. Dovletoglou, D. Ellison, J. Wyvratt, *Anal. Chim. Acta*, 523 (2004) 149.
- <sup>85</sup> A. H. Schmidt, *J. Chromatogr. A*, 1073 (2005) 377.
- <sup>86</sup> P. T. Vallano, R. S. Mazenko, E. J. Woolf, B. K. Matuszewski, *J. Chromatogr. B*, 779 (2002) 249.
- <sup>87</sup> M. M. Hefnawy and H. Y. Abold-Enein, *Anal. Chim. Acta*, 504 (2004) 291.
- <sup>88</sup> B. Paull and P. N. Nesterenko, *TRAC*, 24, no. 4 (2005) 295.
- <sup>89</sup> P. Hatsis and C. A. Lucy, *Analyst*, 127 (2002) 451.
- <sup>90</sup> P. Hatsis and C. A. Lucy, *Anal. Chem.*, 75 (2003) 995.

- 
- <sup>91</sup> Q. Xu, K. Tanaka, M. Mori, M. Helaleh, W. Hu, K. Hasebe, H. Toada, J. Chromatogr. A, 997 (2003) 183.
- <sup>92</sup> Q. Xu, M. Mori, K. Tanaka, M. Ikedo, W. Hu, J. Chromatogr. A, 1026 (2004) 191.
- <sup>93</sup> Q. Xu, M. Mori, K. Tanaka, M. Ikedo, W. Hu, P.R. Haddad, J. Chromatogr. A, 1041 (2004) 5.
- <sup>94</sup> D. Connolly, D. Victory, B. Paull, J. Sep. Sci., 27 (2004) 912.
- <sup>95</sup> C. Ó Ríordáin, P. N. Nesterenko, B. Paull, J. Chromatogr. A, 1070 (2005) 71.
- <sup>96</sup> B. Paull, C. Ó Ríordáin, P. N. Nesterenko, Chem. Comm., 2005, 215.
- <sup>97</sup> H. F. Walton, Ion-exchange Chromatography, Benchmark Papers in Analytical Chemistry, Volume 1, Hutchinson and Ross (Stroudsburg) 1976.
- <sup>98</sup> Dr. S. Lewis, Analytical Dept., Medtechnica, Israel, Ion Chromatography, viewed 25/2/2005 < [www.forumsci.co.il/HPLC/ion-chrm.html](http://www.forumsci.co.il/HPLC/ion-chrm.html) >
- <sup>99</sup> Dr. H. Bungay, Rensselaer Polytechnic Institute, Troy, New York, Theory of Ion-Exchange, date viewed 31/01/2005 < [www.rpi.edu/dept/chem-eng/Biotech-Environ/DUDAS/theory.html](http://www.rpi.edu/dept/chem-eng/Biotech-Environ/DUDAS/theory.html) >
- <sup>100</sup> J. Fritz and D.T. Gjerde, Ion Chromatography, 3rd Edition, Wiley-VCH (Germany) 2000.
- <sup>101</sup> P. Jones and P. N. Nesterenko, J. Chromatogr., 789 (1997) 413.
- <sup>102</sup> A. Braithmaite and F. J. Smith, Chromatographic Methods, 4 th Edition, Chapman and Hall (New York) 1985.
- <sup>103</sup> M. Lederer, Chromatography for Inorganic Chemistry, J. Wiley (Chichester) 1994.
- <sup>104</sup> V. R. Meyer, Practical High-Performance Liquid Chromatography, Wiley and Sons (England) 1994.
- <sup>105</sup> P. R. Haddad and P. E. Jackson, Ion Chromatography: Principles and Practices, Journal of Chromatography library, Volume 46., Elsevier Science Publishers (The Netherlands) 1990.
- <sup>106</sup> C. Sarzanini, J. Chromatogr. A, 850 (1999) 213.
- <sup>107</sup> M. C. Gennaro and S. Angelino, J. Chromatogr. A, 789 (1997) 181.
- <sup>108</sup> P. T. Kissinger, Anal. Chem., 48 (1977) 883.
- <sup>109</sup> B. A. Bidlingmeyer, S. N. Deming, W. P. Price, B. Sachok, M. Petrussek, J. Chromatogr., 186 (1979) 419.
- <sup>110</sup> L. R. Snyder, J. L. Glajch, J. J. Kirkland, Practical HPLC Method Development, J. Wiley (New York) 1988.

- 
- <sup>111</sup> A. Pryde and M. T. Gilbert, *Applications of High Performance Liquid Chromatography*, Chapman and Hall (London) 1979.
- <sup>112</sup> K. Obards, P. Starr, E. Patsalides, *Analyst*, 61 (1991) 1247.
- <sup>113</sup> A. R. Timberaev and G. K. Bonn, *J. Chromatogr. A*, 640 (1993) 195.
- <sup>114</sup> Prof. R.J. Lanachire, Dept. of Chemistry, University of West Indies, Jamaica, *Stability, Chelation and the Chelate Effect*, date viewed 17/11/2003 <[www.chem.uwimona.edu.jm:1104/courses/chelate.html](http://www.chem.uwimona.edu.jm:1104/courses/chelate.html)>
- <sup>115</sup> S. M. Owen and A.T. Brooker, *A Guide to Modern Inorganic Chemistry*, Wiley: Long Scientific and Technical (New York) 1991.
- <sup>116</sup> F. A. Cotton, G. Wilkinson, P. L. Gauss, *Basic Inorganic Chemistry*, 3<sup>rd</sup> Edition, Wiley (New York) 1995.
- <sup>117</sup> C.G. Enke, *The Art and Science of Chemical Analysis*, Wiley (New York) 2001.
- <sup>118</sup> W. Bashir and B. Paull, *J. Chromatogr. A*, 942 (2002) 73.
- <sup>119</sup> B. Paull, M. Foulkes, P. Jones, *Analyst*, 119 (1994) 937.
- <sup>120</sup> B. Paull, P. N. Nesterenko, P. R. Haddad, *Anal. Chim. Acta*, 375 (1998) 117.
- <sup>121</sup> B. Paull and P. R. Haddad, *TRAC*, 18 no. 2 (1999) 107.
- <sup>122</sup> M. J. Shaw, S. J. Hill, P. Jones, *Anal. Chim. Acta.*, 401 (1999) 65.
- <sup>123</sup> W. Bashir and B. Paull, *J. Chromatogr. A*, 907 (2001) 191.
- <sup>124</sup> P. Jones and P. N. Nesterenko, *J. Chromatogr. A*, 770 (1997) 129.
- <sup>125</sup> G. Bonn, S. Reiffenstuhl, P. Jandik, *J. Chromatogr.*, 44 (1990) 669.
- <sup>126</sup> A. I. Elefterov, S. N. Nosal, P. N. Nesterenko, O. A. Shipgun, *Analyst*, 119 (1994) 1329.
- <sup>127</sup> I. N. Voloschik, M. L. Litvina, B. A. Rudenko, *J. Chromatogr. A*, 706 (1995) 315.
- <sup>128</sup> W. Bashir and B. Paull, *J. Chromatogr. A*, 910 (2001) 310.
- <sup>129</sup> X. Ding, S. Mou, K. Liu, Y. Yan, *J. Chromatogr. A*, 883 (2000) 127.
- <sup>130</sup> N. Cardellicchio, P. Ragone, S. Cavalli, J. Riviello, *J. Chromatogr. A*, 770 (1007) 185.
- <sup>131</sup> K. Ohta, K. Tanaka, B. Paull, P.R. Haddad, *J. Chromatogr. A*, 770 (1997) 219.
- <sup>132</sup> C. Meryl, B. Lynch, P. Ross, J. D. Glennon, *J. Chromatogr. A*, 804 (998) 187.
- <sup>133</sup> J-F. Jen and C-S. Chem, *Anal. Chim. Acta*, 270 (1992) 55.
- <sup>134</sup> C. Ohtsuka and K. Matsuzaua, *Anal. Chim. Acta*, 252 (1991) 181.
- <sup>135</sup> P. N. Nesterenko, G. Amirova, T.A. Bol'shova, *Anal. Chim. Acta*, 285 (1994) 161.
- <sup>136</sup> H. A. Cook, W. Hu, J. S. Fritz, P. R. Haddad, *Anal. Chem.*, 73 (2001) 3022.

- 
- <sup>137</sup> P. N. Nesterenko and P. R. Haddad, *Anal. Sci.*, 16 (2000) 565.
- <sup>138</sup> W. Hu, P. R. Haddad, K. Hasebe, K. Tanaka, P. Yong, C. Khoo, *Anal. Chem.*, 71 (1999) 1617.
- <sup>139</sup> W. Hu, T. Takeuchi, H. Haraguchi, *Anal. Chem.*, 65 (1993) 2204.
- <sup>140</sup> W. Hu, *Langmuir*, 15 (1999) 7168.
- <sup>141</sup> W. Hu and P. R. Haddad, *TRAC*, 17 no. 2 (1998) 73.
- <sup>142</sup> T. Okada and J. M. Patil, *Langmuir*, 14 (1998) 6241.
- <sup>143</sup> D. A. Skoog, F. J. Holler, T. A. Nieman, *Principles of Instrumental Analysis*, 5<sup>th</sup> Edition, Harcourt Brace College Publishers (USA) 1998.
- <sup>144</sup> H. Small, *Ion Chromatography*, Plenum Press (New York) 1989.
- <sup>145</sup> *Conductivity Detector II Operators Manual*, Dionex series 4500 Chromatography system manual, March 1988.
- <sup>146</sup> S. Lindsay, *High performance liquid chromatography*, 2nd Edition (ACOL Series), J. Wiley and Sons (Chichester) 1992.
- <sup>147</sup> G. Schwedt, *Chromatographic Methods in Inorganic Analysis*, Huthig (Heidelberg) 1981.
- <sup>148</sup> D. Pu, *Advances in Ion Chromatography*, A literature seminar, department of chemistry, University of Alabama, 10<sup>th</sup> February 2004.
- <sup>149</sup> H. Engelhardt, *Practice of High-Performance Liquid Chromatography: Applications, Equipment and Quantitative Analysis*, Springer-Verlag (Germany) 1986.
- <sup>150</sup> E. Katz, R. Eksten, P. Schoenmakers, N. Miler, *Handbook of HPLC*, Volume 78, *Chromatographic Science Series*, Marcel Dekker (New York) 1998.
- <sup>151</sup> B. E. Lendi and V. R. Meyer, *LCGC Europe* 18 (3) (2005) 2.
- <sup>152</sup> R. M. Cassidy, S. Elchuk, N. L. Elliott, L.W. Green, C. H. Knight, B. M. Recoskie, *Anal. Chem.*, 58 (1986) 1181.
- <sup>153</sup> J. H. Knox, *High-Performance Liquid Chromatography*, 1<sup>st</sup> Edition, Edinburgh University Press (Edinburgh) 1980.
- <sup>154</sup> E. Heftmann, *Chromatography* 5<sup>th</sup> Edition: *Fundamentals and Applications of Chromatography and Related Differential Migration Methods. Part A: Fundamentals and Techniques*, *Journal of Chromatography library- Volume 51A*, Elsevier Science Publishers (The Netherlands) 1992.

- 
- <sup>155</sup> G. Lunn and L. C. Hellwig, *Handbook of Derivatisation Reactions for HPLC*, J. Wiley (New York) 1998.
- <sup>156</sup> N. Cardellicchio, P. Ragone, S. Cavalli, J. Riviello, *J. Chromatogr. A*, 770 (1997) 185.
- <sup>157</sup> E. Santoyo, S. Santyo-Guiterrez, S. P. Verma, *J. Chromatogr. A*, 884 (2000) 229.
- <sup>158</sup> N. Vachirapatama, M. Macka, B. Paull, C. Munker, P. R. Haddad, *J. Chromatogr. A*, 850 (1999) 257.
- <sup>159</sup> D. Smith and J. Fritz, *Anal. Chim. Acta*, 204 (1988) 87.
- <sup>160</sup> E. Jones, H. Bezuidenhout and J. Van Staden, *J. Chromatogr. A*, 537 (1991) 277.
- <sup>161</sup> P. Jones, L. Ebdon, T. Williams, *Analyst*, 113 (1988) 641.
- <sup>162</sup> P. M. Bertsch and M. A. Anderson, *Anal. Chem.*, 61 (1989) 535.
- <sup>163</sup> D. L. Smith and J. S. Fritz, *Anal. Chim. Acta*, 204 (1988) 87.
- <sup>164</sup> P. Jones, T. Williams, L. Ebdon, *Anal. Chim. Acta.*, 217 (1989) 157.
- <sup>165</sup> C. O. Moses, A. T. Herlihy, J. S. Herman, A. L. Mills, *Talanta*, 35 (1988) 15.
- <sup>166</sup> H. Saitoh and K. Oikawa, *J. Chromatogr.*, 329 (1985) 247.
- <sup>167</sup> B. D. Karcher, I. S. Krull, R. G. Schleicher, S. B. Smith, *J. Chromatographia*, 24 (1987) 705.
- <sup>168</sup> H. Hojabri, A. G. Lavin, G. Wallace, J. M. Riviello, *Anal. Proc.*, 23 (1986) 26.
- <sup>169</sup> H. Hojabri, A. G. Lavin, G. Wallace, J. M. Riviello, *Anal. Chem.*, 59 (1987) 54.
- <sup>170</sup> P. J. Hobbs, P. Jones, L. Ebdon, *Anal. Proc.*, 20 (1983) 613.
- <sup>171</sup> D. J. Barkley, M. Blanchette, R. M. Cassidy, S. Elchuk, *Anal. Chem.*, 58 (1986) 2222.

## **Chapter 2**

***Alkali and alkaline earth metal ion selectivity  
on an IDA functionalised silica monolith***

## ***2.1: Introduction***

The recent development and successive commercial introduction of monolithic silica columns has motivated many scientists, from both academia and industry, to study their use in HPLC [1]. The unique properties of monoliths, in particular their tolerance to high flow rates, while maintaining excellent peak efficiencies, and the rapid speed of chromatographic separations that can be achieved at acceptable backpressures, make the monolithic column format superior in some applications to the more commonly used packed columns [2].

However because monoliths are still rather “young”, the number of different stationary phases, separation mechanisms and methods developed with them remains much smaller than that available for packed columns [2], although the belief is that it is only a matter of time before the range of monolithic technology will be developed and extended to successfully compete with other well established separation technologies.

Silica-based monolithic HPLC columns have received much attention in recent years, particularly those modified for reversed-phase separations. However, for ion-exchange separations, monolithic-based silica columns have only received limited attention. To date, as demonstrated by Table 2.1, the approach used for the separation of anions and cations on monolithic silica columns is to either dynamically modify or permanently coat reversed-phase (RP 18) monoliths with ion-exchangers, e.g. cetyltrimethylammonium bromide (CTAB), polyoxyethylene (POE), didodecyldimethylammonium bromide (DDAB), dioctylsulphosuccinate (DOSS), lithium dodecylsulfate (Li-DS), cetylpyridinium chloride (CPC) and (dodecyldimethyl-amino) acetic acid (carboxybetaine).

Table 2.1: Summary of the ion chromatographic separations achieved on modified reversed-phase silica monolithic columns.

Column	Eluent Conditions	Separated ions	Ref
100 x 4.6 mm Chromolith RP18e coated with DDAB	6 mM <i>o</i> -cyanophenol (pH 7.0), flow rate 10 mL/min	IO <sub>3</sub> <sup>-</sup> , Cl <sup>-</sup> , NO <sub>2</sub> <sup>-</sup> , Br <sup>-</sup> , NO <sub>3</sub> <sup>-</sup> , HPO <sub>4</sub> <sup>2-</sup> , SO <sub>4</sub> <sup>2-</sup> separated in 30s	[3]
100 x 4.6 mm Chromolith RP18e coated with CTAB-POE	10 mM Na <sub>2</sub> SO <sub>4</sub> (pH 10.5), flow rate 1 mL/min	OH <sup>-</sup> , Cl <sup>-</sup> , NO <sub>3</sub> <sup>-</sup> separated in 20-30 min	[4]
100 x 4.6 mm Chromolith RP18e coated with carboxybetaine	10 mM KCl-10 mM Na <sub>2</sub> PO <sub>4</sub> <sup>-</sup> buffer, 0.2 mM carboxybetaine. pH gradient: pH 6-8, over 5 min Flow gradient: 1 to 5 mL/min over first 5 min	NO <sub>2</sub> <sup>-</sup> , Br <sup>-</sup> , NO <sub>3</sub> <sup>-</sup> , I <sup>-</sup> , SCN <sup>-</sup> , separated in under 8 min.	[5]
50 x 4.6 mm Chromolith RP18e coated with Li-DS	2 mM ethylenediamine-0.1 mM LiDS (pH 6.0), flow rate 4 mL/min	H <sup>+</sup> , Mg (II) and Ca (II) separated in 4.5 min	[6]
	5 mM potassium salt of EDTA- 0.1 mM LiDS (pH 4.80), flow rate 1.5 mL/min	H <sup>+</sup> , Li <sup>+</sup> , Na <sup>+</sup> , Ca (II), Mg (II) separated in 30 min	[7]
50 x 4.6 mm Chromolith RP18e coated with DOSS	2.54 mM phthalate, 1.5 mM ethylenediamine, (pH 4.5), flow rate 8 mL/min	Cu (II), Mg (II), Ca (II), Sr (II), Ba (II) in 100 s	[8]

Table 2.1 continued.

Column	Eluent Conditions	Separated ions	Ref
2.5 x 4.6 mm Chromolith RP18e coated with DDAB	2.54 mM phthalate, 1.5 mM ethylenediamine, (pH 4.5), flow rate 4 mL/min	$\text{PO}_4^{3-}$ , $\text{Cl}^-$ , $\text{NO}_2^-$ , $\text{Br}^-$ , $\text{NO}_3^-$ , $\text{ClO}_4^-$ , $\text{SO}_4^{2-}$ , $\text{I}^-$ separated in 100 s	[8]
25 x 4.6 mm Chromolith RP18e coated with CPC	10 mM $\text{Na}_2\text{SO}_4$ , flow rate 3 mL/min 1.5 mM phthalate (pH 7.0), flow rate 3 mL/min	Acetate, $\text{NO}_2^-$ , $\text{Br}^-$ , $\text{NO}_3^-$ , $\text{WO}_4^{2-}$ , $\text{CrO}_4^{2-}$ separated in 50 s $\text{Cl}^-$ , $\text{NO}_2^-$ , $\text{Br}^-$ , $\text{NO}_3^-$ , $\text{SO}_4^{2-}$ , $\text{CrO}_4^{2-}$ separated in 55 s	[9]
10 x 4.6 mm Chromolith RP18e coated with DDAB	2 mM p-hydroxybenzoate, increasing to 5 mM over 5-20 min, flow rate 0.33 mL/min	$\text{F}^-$ , $\text{Cl}^-$ , $\text{NO}_2^-$ , $\text{Br}^-$ , $\text{NO}_3^-$ , $\text{SO}_4^{2-}$ separated in 30 min	[10]
10 x 4.6 mm Chromolith RP18e coated with carboxybetaine	10 mM $\text{KCl}$ -10 mM $\text{Na}_2\text{PO}_4^-$ buffer (pH3.0), 0.2 mM carboxybetaine. Flow gradient: 1 mL/min for first minute, then increased to 6 mL/min between 1 and 2 min	$\text{NO}_2^-$ , $\text{Br}^-$ , $\text{NO}_3^-$ , $\text{I}^-$ , $\text{SCN}^-$ , separated in 6.5 min	[11]

The potential disadvantages of either dynamically modifying or permanently coating reversed-phase monoliths with ion-exchangers include the possible variations in coating stability and intolerance of coated phases to changes in the composition of the eluent and column temperature. These potential problems can be overcome through the use of monolithic columns with chemically bonded ion-exchange groups. In this work, a chelating ion-exchanger, iminodiacetic acid (IDA), was covalently bonded to a bare silica monolith using on-column modification.

The selectivity, and mode of retention, of alkali and alkaline earth metal ions on iminodiacetic acid (IDA) functionalised silica gel columns has been thoroughly investigated in recent years in a number of detailed studies [12-15], with Bashir and Pauli [16] demonstrating that IDA-silica behaves somewhat differently to other polyfunctional ion-exchangers, i.e. a dual retention mechanism is responsible for the changes in selectivity observed with the IDA silica stationary phase. Iminodiacetic acid (IDA) is a tridentate ligand, which exhibits two possible methods of metal uptake:

- Chelation of metal ions with the nitrogen and carboxyl groups on the IDA as ligands.
- The other possible type is simple ion-exchange of cations that are electrostatically attracted to the negatively charged carboxylate groups.

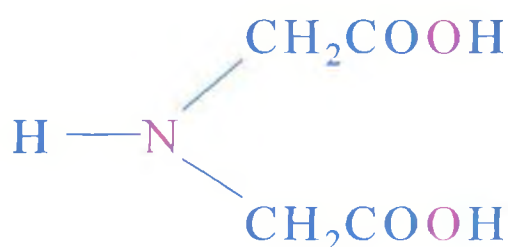


Figure 2.1: Structure of iminodiacetic acid (IDA).

### 2.1.1: Objective

In this Chapter, the retention of alkali and alkaline earth metal ions on the IDA functionalised silica monolith was characterised. The effects of both eluent ionic strength and pH on cation selectivity were investigated, and the selectivity of the 10 cm IDA silica monolith was compared to a 25 cm IDA silica gel particle-packed HPLC column. In addition, the contribution of the residual, unfunctionalised silanol

groups to the retention of both alkali and alkaline earth metal ions on the IDA silica monolith was also studied.

## **2.2: Experimental**

### **2.2.1: Modification of silica monolith**

A PEEK lined bare monolithic silica column (Performance Si), of 10 cm length and 4.6 mm i.d. was purchased from Merck KGaA (Damstadt, Germany). According to the manufacturer the silica monolith has a surface area of 300 m<sup>2</sup>/g, with a 2 μm macroporous and 13 nm mesoporous structure. Before modification, the surface of the silica monolith was activated by washing the column with DIW whilst placed in a thermostated water bath at 60 °C for 4 hours. The modification of the column with IDA groups<sup>1</sup> was performed at 70 °C, by recycling 80 mL of a water solution containing a mixture of γ-glycidoxypropyltrimethoxysilane and IDA through the column (both from Fluka Chemie GmbH, Buchs, Switerland). The recycling system consisted of a glass beaker containing the above reagents, a Waters Model 510 HPLC pump (Waters, Milford, USA) and the thermostated monolithic silica column. The reagent mixture was pumped at a flow rate 0.5 mL/min for 6 hours. Then the column was then washed with 0.01 M nitric acid for approximately 1 hr and equilibrated with the eluent before use.

### **2.2.2: Instrumentation**

A Dionex Model GPM2 Gradient Pump Module (Sunnyvale, CA, USA) was used to deliver the eluent (1– 4 mL/min). An automated injection valve, fitted with a 20 μL injection loop was used for the introduction of standards and samples. The particle type silica IDA (8 μm particle size, 130 Å pore size) used for comparison with the IDA-monolith was packed in either 250 x 4.0 mm I.D. or 30 x 4.6 mm I.D. columns and was supplied by BioChemMack ST (Moscow, Russia). A pressure driven Dionex Reagent Delivery Module was used for introduction of the post-column reagent (PCR) where required, which was mixed at room temperature with the eluent using a 0.5 m PEEK reaction coil (0.25 mm i.d.). For eluent flow rates greater than 4 mL/min a Waters model 510 HPLC pump (Waters, Milford, USA) was used to deliver the

---

<sup>1</sup> (The proposed structure of the IDA functionalised monolith is shown in Appendix I, Fig. 1.1A).

PCR. A Waters model 486 UV/Vis detector (Kyoto, Japan) was used at 570 nm to monitor the resultant chromatograms. For non-suppressed and suppressed conductivity detection a Dionex conductivity detector was used, with a CSRS Ultra 4 mm membrane suppressor where required. Data acquisition was at a rate of 10 Hz with processing of chromatograms performed using a PeakNet 6.0 chromatography workstation (Dionex).

### **2.2.3: Reagents**

The eluent and post-column reagent (PCR) solutions were prepared using DIW from a Millipore Milli-Q water purification system (Bedford, MA, USA). Where post-column reaction (PCR) detection was required, the reagent used for the detection of alkaline earth metals was 0.4 mM *o*-cresolphthalein complexone (*o*-CPC), 0.25 M boric acid (adjusted to pH 10 using NaOH). The *o*-CPC was purchased from Sigma-Aldrich (Gillingham, Dorset, UK), and used without further purification (monitored at 570 nm). Potassium nitrate, potassium chloride and sodium nitrate salts were all obtained from Fluka Chemie (Buchs, Switzerland), as was the methanesulfonic acid (MSA) and nitric acid used for suppressed and indirect conductivity eluents, and also for control of eluent pH. All eluents, reagents and standard solutions prepared were filtered through a 0.45 µm filter and degassed using sonication. Low level standard solutions of all metal ions were generally made up freshly each day from stock solutions prepared from nitrate or chloride salts (1000 ppm) and stored in 1% nitric acid.

## 2.3 Results and discussion

### 2.3.1. Physical analysis

The ion-exchange capacity, i.e. the number of ionic sites on the stationary phase that can participate in the ion-exchange process of the IDA modified monolith (~75  $\mu\text{mol}$  IDA per 10 cm monolith) was determined through the use of breakthrough studies. This value compares reasonably well to the value of 185  $\mu\text{mol}$ , determined at the same conditions for a 25 cm IDA silica gel particles column [16]. As the monolithic silica was functionalised 'on-column' by recycling reactants through the monolith, evaluation of the degree of surface coverage along the length of the monolith was only possible by destroying the column and analysing sections of the de-packed monolith. This was carried out at the end of the study using elemental analysis, the results of which are shown in Table 2.2.

Table 2.2: Elemental and surface analysis of the 10 cm IDA functionalised silica monolith.

Theoretical ratio <sup>a</sup>	C	H	N	Cu adsorption (AAS) <sup>b</sup>	Cu adsorption (EDX) <sup>b</sup>
	0.800	0.107	0.093		
<b>Elements found as % of theoretical ratio</b>					
Monolith section	<b>C</b>	<b>H</b>	<b>N</b>		
Start	110	75	43	100	100
Middle	103	163	0	101	129
End	107	133	0	43	64

<sup>a</sup>As calculated for the attached residue  $-(\text{CH}_2)_3\text{OCH}_2\text{CH}(\text{OH})\text{CH}_2\text{N}(\text{CH}_2\text{COOH})_2$ .

<sup>b</sup>% adsorption relative to adsorption at start of column.

As can be seen from Table 2.2, the elemental analysis data was inconclusive. The presence of nitrogen at the start of the monolith indicates the presence of the attached IDA groups. However the concentration of these groups at the middle and end of the column were obviously below the sensitivity of the elemental analysis system. To

further check for the presence of IDA groups on each section of the monoliths, the individual sections were saturated with a  $\text{CuSO}_4$  solution and then washed with DIW. After drying and weighing each of the sections the Cu (II) was desorbed using 10 mM  $\text{HNO}_3$  and the Cu (II) concentration determined using atomic absorption spectroscopy (AAS). The results showed little difference between the Cu (II) adsorption on the start and middle sections of the monolith, but this dropped off to approximately 40 % on the end section. These results were then further verified with energy dispersive X-ray microanalysis (EDX), which gave a qualitative evaluation of surface adsorbed Cu (II) levels on the three sections of modified monolith. As with the AAS analysis, EDX showed non-uniform capacity along the length of the monolith, with the middle section actually showing higher levels of surface Cu (II) compared to the start, whereas the end section showed 30 – 40 % less. These results would appear to indicate the need to increase the time used to functionalise the monolith, or continuously alternate the direction of reagent flows during the modification process, when preparing future modified monoliths in this way.

### ***2.3.2: Ion-exchange chromatography on a chelation stationary phase***

Although IDA-silica based stationary phases show ion-exchange properties as well as strong chelating abilities, only a few reports discuss the use of IDA derivatised stationary phases as weak cation-exchangers [13, 15, 17]. Chelating-exchangers with covalently bonded iminodiacetic acid functional groups have been shown to react with alkaline earth metal ions by simple ion-exchange at pH values below 4, and by chelation-exchange at pH values above 6 [14]. In the case of the silica based substrates it has been shown that when using low-ionic strength acidic eluents, such as mineral acids, ion-exchange is the dominant mechanism for both alkali and alkaline earth metal ions. This ion-exchange capacity originates from residual silanols as well as the attached carboxylic acid groups [18].

Elefterov *et al.* [19] simultaneously determined alkali and alkaline earth metal using a column packed with IDA bonded silica. Elefterov *et al.* found that the IDA-silica sorbent exhibited high selectivity, i.e.  $\text{Na} < \text{K} < \text{Mg (II)} < \text{Ca (II)} < \text{Ba (II)}$ , which agrees with the selectivity series for alkali and alkaline earth metals for carboxylic cation-exchangers and with the stability constants for alkaline earth metal complexes

of IDA. Therefore, the initial sections of this Chapter will deal with results obtained for the separation of alkali and alkaline earth metal ions on the IDA functionalised silica monolith, using a low ionic strength, acidic eluent in conjunction with suppressed conductivity detection.

### ***2.3.2.1: Separation of alkali metals on an IDA functionalised silica monolith.***

Initially the chromatographic behaviour of alkali and alkaline earth metal ions on the IDA functionalised silica monolith was investigated using a dilute nitric acid eluent and suppressed conductivity detection. The elution order of  $\text{Li} < \text{Na} < \text{K} < \text{Cs}$  was expected using a cation-exchange column. It has been shown previously that IDA silica exhibits similar behaviour to other weak cation-exchangers for alkali metal cations [20]. However, it is clear from the results presented in Table 2.3, that the IDA silica monolith offers poor selectivity for the alkali metal cations. The IDA silica monolith was compared with a 25 x 0.4 cm IDA functionalised silica gel column for selectivity and retention of alkali metal cations using weak nitric acid eluents, 0.5 – 5.0 mM. The IDA silica gel has a higher overall capacity than the IDA monolith, and so, as expected, the retention of alkali metals was greater on the IDA silica gel column (see Table 2.4). In terms of differences in selectivity, the selectivity exhibited by the lower capacity monolithic phase was poor over the range of eluent strengths investigated, such that a separation of more than two alkali metals was not possible.

Table 2.3: The effect of  $\text{HNO}_3$  eluent concentration on the retention of alkali and alkaline earth metal ions on a 10 cm, IDA functionalised silica monolithic column. Eluent flow rate 1 mL/min.

Analyte	Retention factor ( <i>k</i> )				
	5 mM $\text{HNO}_3$	4 mM $\text{HNO}_3$	3 mM $\text{HNO}_3$	2 mM $\text{HNO}_3$	1 mM $\text{HNO}_3$
Li	0.3	0.3	0.5	0.8	1.7
Na	0.3	0.3	0.5	0.8	1.7
K	0.4	0.4	0.5	0.9	1.8
Cs	0.4	0.4	0.7	1.1	2.1
Mg (II)	1.1	1.4	2.8	5.8	19.0
Ca (II)	1.2	1.6	3.2	6.6	21.7

Table 2.4: The selectivity exhibited for alkali metal ions on a 25 cm IDA functionalised silica gel column and a 10 cm IDA functionalised silica monolithic column<sup>2</sup>.

Column	Selectivity	Slope <sup>a</sup>			
		Li <sup>+</sup>	Na <sup>+</sup>	K <sup>+</sup>	Cs <sup>+</sup>
IDA silica gel	Li < Na < K < Cs (1 mM HNO <sub>3</sub> )	-0.66	-0.67	-0.60	-0.71
IDA monolith	Li = Na < K < Cs (1 mM HNO <sub>3</sub> )	-0.63	-0.62	-0.56	-0.57

<sup>a</sup>Slopes for plots of  $\log k$  versus  $\log [E^+]$  were determined over 0.5 to 5.0 mM HNO<sub>3</sub> (n=4) for the IDA silica gel column and 1.0-5.0 mM HNO<sub>3</sub> (n=5) for the IDA silica monolith.

### 2.3.2.2: Ion-exchange properties of a bare silica monolith.

The chemical properties of silica are due to the presence of surface silanols, i.e. the hydroxyl acidity is responsible for the acid/base properties of silica. According to a review by G. B. Cox [21], studies of chromatography on silica concluded that the principle mechanism of retention was ion-exchange chromatography on the acidic silanol groups. In a review of the properties of silica, Berthod [22] concluded that the acidic character of surface silanols confers some ion-exchange properties on the porous silica.

Using a 10 cm bare silica monolithic (Chromolith Performance Si) column, the ion-exchange properties were investigated for the alkali and alkaline earth metal ions. It is important to investigate the ion-exchange properties of the bare silica, because when a similar silica monolithic column was functionalised with IDA, only a certain fraction of the silanol groups are available to be functionalised, due to steric reasons. Hence, the IDA functionalised silica monolith will have some silanol groups present on its surface, which may also contribute to the retention of cations through their inherent ion-exchange properties. For this study, a weak LiCl eluent (0.1 – 1 mM) was

<sup>2</sup> (For the plots of  $\log k$  versus  $\log [E^+]$  for alkali metals on a 10 cm IDA silica monolith and 25 cm IDA silica particulate column, see Appendix I, Fig. 1.2A)

employed. Fig. 2.2 demonstrates the results obtained for the retention of alkali metal ions on a bare silica monolithic column. It is clear that there is a degree of retention of the alkali metal ions, which can be attributed to the ion-exchange properties of the surface silanol groups, previously demonstrated by Cox [21] and Berthod [22]. As expected for an ion-exchange mechanism, the order of elution observed was  $\text{Na} < \text{K} \ll \text{Cs}$ . However, the low affinity of  $\text{NH}_4$ , which is eluted before the  $\text{Na}$ , would not be typical of a weak cation-exchanger, although this trend was observed over the range of eluent ionic strengths investigated.

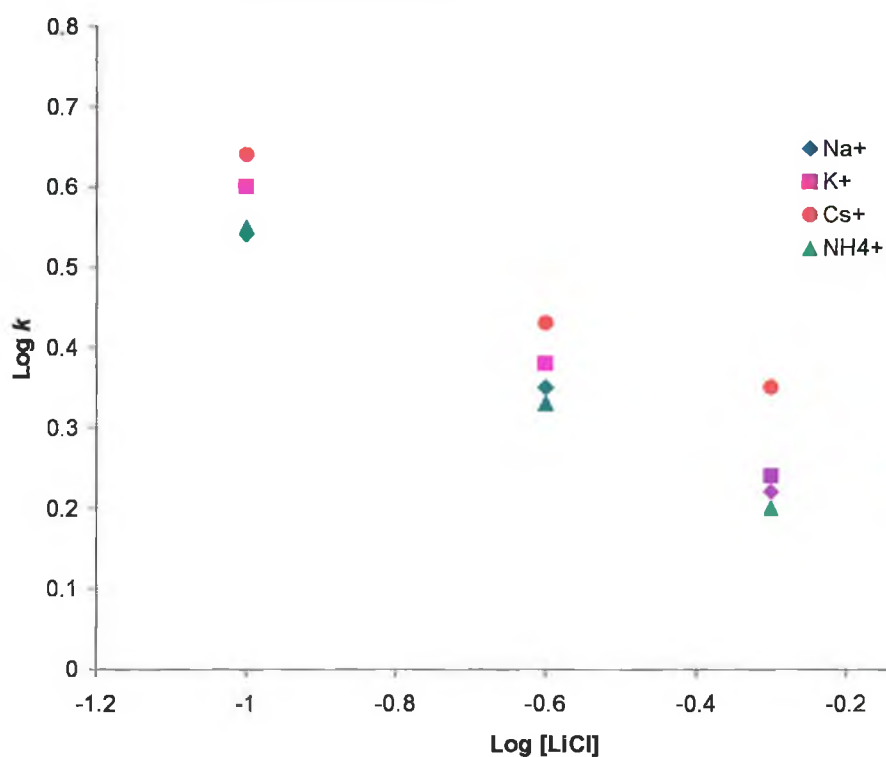


Figure 2.2: The effect of LiCl eluent concentration on the retention of alkali metal ions on a 10 cm bare silica monolith.

The data in Table 2.5 compares differences in selectivity observed for alkali cations on the 10 cm bare silica and the IDA functionalised monolith columns. It is clear, that the presence of surface silanol groups on the IDA silica monolith, which could not be functionalised due to steric reasons, may also contribute to the retention of alkali metal ions, via an ion-exchange mechanism, under non-acidic eluent conditions.

Table 2.5: The selectivity exhibited for alkali metal ions on a 10 cm bare silica monolith and a 10 cm IDA functionalised silica monolithic column.

Column	Selectivity	Slope <sup>a</sup>				
		Li <sup>+</sup>	Na <sup>+</sup>	K <sup>+</sup>	NH <sub>4</sub> <sup>+</sup>	Cs <sup>+</sup>
Bare silica monolith	NH <sub>4</sub> < Na < K < Cs (0.5 mM LiCl)	-	-0.43	-0.41	-0.47	-0.35
IDA monolith	Li = Na < K < Cs (1 mM HNO <sub>3</sub> )	-0.63	-0.62	-0.56	-	-0.57

<sup>a</sup>Slopes for plots of  $\log k$  versus  $\log [E^+]$  were determined over 1.0-5.0 mM HNO<sub>3</sub> (n=5) for the IDA silica monolith and 0.1 to 1 mM LiCl (n=5) for the bare silica monolith.

### 2.3.2.3: Separation of alkaline earth metals on an IDA silica monolith using low-ionic strength acidic eluents

A range of low-ionic strength, acidic eluents were prepared (1 to 5 mM methansulfonic acid), and the selectivity of the IDA silica monolith for Mg (II), Ca (II), Sr (II) and Ba (II) was studied. With ion-exchange, counter ions present in the eluent (H<sup>+</sup>), although having weaker affinity for the ion-exchange sites than the divalent analyte ions, will have a major competitive effect as the concentration of the eluent increases, see data in Table 2.6.

Table 2.6: The effect of methansulfonic acid (MSA) eluent concentration on the retention of alkali and alkaline earth metal ions on a 10 cm, IDA functionalised silica monolithic column. Eluent flow rate 1 mL/min.

MSA (mM)	Retention factor ( <i>k</i> )			
	Mg (II)	Ca (II)	Sr (II)	Ba (II)
1	20.3	22.8	23.3	27.7
2	8.2	9.3	9.3	10.4
4	5.4	6.6	6.5	7.4
5	1.3	1.7	1.6	1.8

In general, under acidic conditions, when ion-exchange was the dominant retention mechanism, the difference in selectivity between observed for the alkaline earth metal

cations on IDA silica was poor, particularly Ca (II) and Sr (II). Retention of the alkaline earth metals on the IDA monolith was investigated using both nitric and methansulfonic acid eluents, see Table 2.7. Selectivity using both eluents was similar to that shown previously with IDA silica gel and HNO<sub>3</sub> eluents [16], although slightly better resolution was obtained using the methansulfonic acid eluent.

Table 2.7: The selectivity exhibited for alkali cation on a 25 cm IDA functionalised silica gel column and a 10 cm IDA functionalised silica monolithic column<sup>3</sup>.

Column	Selectivity	Slope <sup>a</sup>			
		Mg(II)	Ca(II)	Sr(II)	Ba(II)
IDA silica gel	Mg= Sr < Ca < Ba (10 mM HNO <sub>3</sub> )	-0.73	-0.71	—	---
IDA monolith	Mg < Ca = Sr < Ba (2 mM HNO <sub>3</sub> )	-0.99	-1.0	—	—
	Mg < Ca = Sr < Ba (2 mM MSA)	-0.99	-0.94	-0.97	-0.99

<sup>a</sup>Slopes for plots of log *k* versus log [E<sup>+</sup>] were determined over 3.0-10 mM HNO<sub>3</sub> (n=3) for the IDA silica gel column and 1.0 –5.0 mM HNO<sub>3</sub> (n=5) and 1.0 to 5.0 mM methansulfonic acid (n=4) for the 10 cm IDA silica monolith.

The results of the analysis of alkali (Section 2.3.2.1) and alkaline earth metals (Section 2.3.2.3) illustrate the limited intra-group selectivity IDA offers under acidic conditions, compared to alternative weak cation-exchangers. They also show IDA does offer good inter-group selectivity, which sees a narrow separation window for all alkali metal cations, well removed from the separation window for all of the alkaline earth metal cations. As the results in Table 2.3 demonstrate, the retention of Ca (II) and Mg (II) is much greater than the alkali metal ions. Elefterov *et al.* [19] also encountered this significantly stronger retention of the alkaline earth metal ions compared to the alkali metal ions. The explanation put forward by Elefterov *et al.* was that alkaline earth metal ions may also interact with the iminodiacetic acid groups on the surface of the stationary phase through complexation, and that results in an additional contribution to retention.

<sup>3</sup> (For the plots of log *k* versus log [E<sup>+</sup>] for alkaline earth metals on a 10 cm IDA silica monolith and 25 cm IDA silica particulate column, see Appendix I, Fig. 1.3A and Fig. 1.4A)

Hence, as Fig. 2.3 demonstrates, this makes IDA phases suitable for separation of alkaline earth metals in the presence of excess alkali metals. Under the conditions described above, all the alkali metals elute at roughly the same time as potassium, illustrating both the unusually large difference in selectivity IDA exhibits towards alkaline earth metals over alkali metal cations, and the reduced absolute retention of Ba (II) relative to Mg (II) and Ca (II), particularly when compared to alternative weak (e.g. Dionex CS12) and strong cation-exchangers (e.g. Dionex CS10)

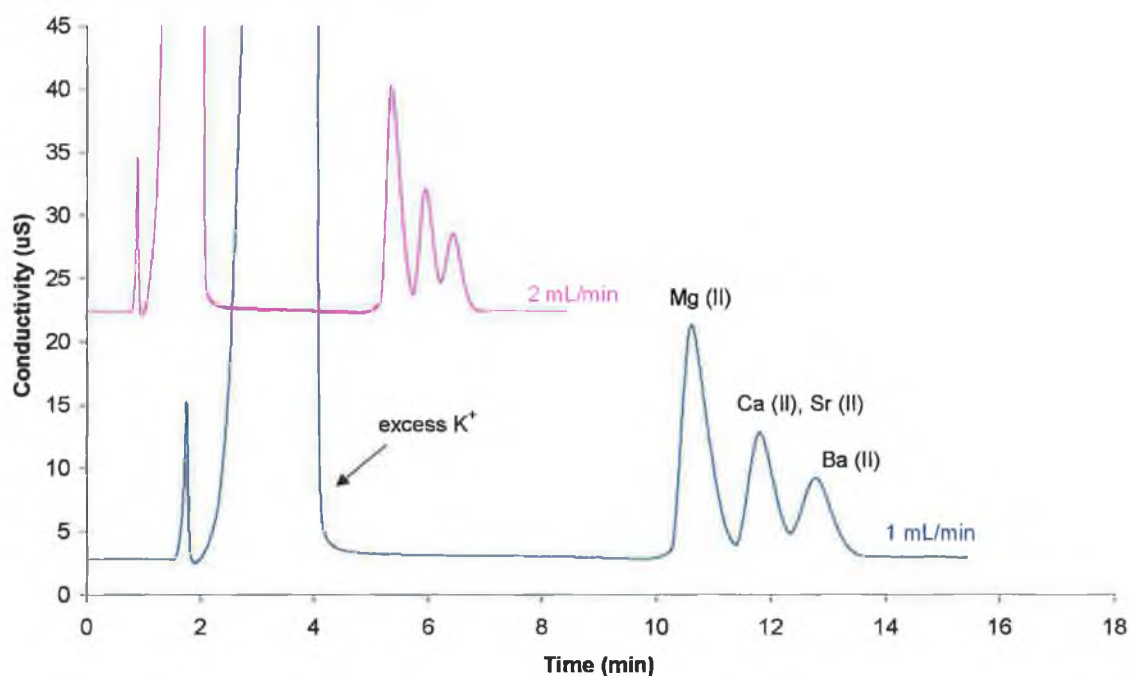


Figure 2.3: The analysis of Mg (II), Ca (II), Sr (II) and Ba (II) in the presence of excess  $K^+$  on a 10 cm IDA functionalised silica monolith. Eluent conditions: 2 mM methansulfonic acid at flow rates of 1 mL/min and 2 mL/min, monitored using suppressed conductivity detection.

#### 2.3.2.4: *The effect of complexing agents on alkaline earth metal selectivity*

In an attempt to overcome the problem of Ca (II) and Sr (II) co-elution, a series of chelating organic acids were added to the methansulfonic acid eluent. By adding a weak complexing ligand such as tartrate, citrate or oxalate to the eluent, the metal ions to be separated are partially complexed and converted to uncharged or lower charged metal complex. A certain fraction of each metal ion remains as the charged cation. The net effect is that the metal ions elute more rapidly. Owing to differences in the

fraction that is not complexed, separation of the sample ions is enhanced. Separation of metal ions may now be based on differences in partial complexation, and on differences in the selectivity of the ion-exchanger for free metal ions. The ligand selected, the concentration and the pH of the eluent should be chosen so that complexation of the metal ions is only partial. If the metal ions are too strongly complexed, they will move to rapidly and no separation will occur [23].

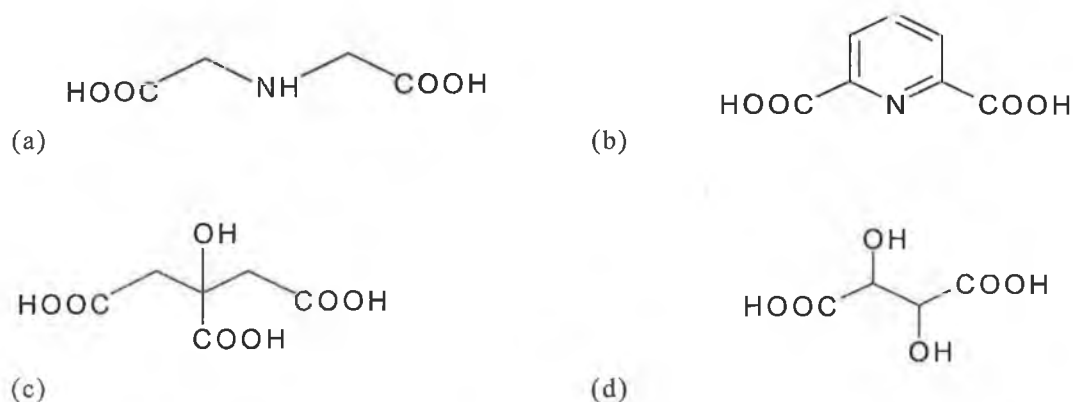


Figure 2.4: Structures of complexing ligands used in ion chromatography, (a) iminodiacetic acid (IDA), (b) dipicolinic acid (DPA), (c) citric acid and (d) tartaric acid.

Elefterov *et al.* [19] added complexing agents to the eluent in an effort to reduce the analysis time for alkaline earth metal ion separations, because by adding a chelating reagent to the eluent, this reagent would result in a decrease in the effective charge of the cations. In the case of the addition of citric and tartaric acids to a perchloric acid eluent, it was observed that an increase in the amount of chelating reagent lead to a greater decrease in the retention time of the alkaline earth metal ions. However, the retention order ( $\text{Na} < \text{K} < \text{Mg (II)} < \text{Ca (II)} < \text{Ba (II)}$ ), was not affected.

A difference was observed for the dependence of the retention of alkaline earth metal cations on the concentration of dipicolinic acid (DPA) added to the eluent. Because the  $\text{Ca (II)}$  complex of DPA is more stable than the  $\text{Mg (II)}$  complex, addition of the DPA to the mobile phase was observed to result in a change in the elution order for the  $\text{Mg (II)} - \text{Ca (II)}$  pair. The structure of iminodiacetic acid (IDA), pyridine-2,6-dicarboxylic acid (dipicolinic acid, DPA), citric acid and tartaric acid are shown in Fig 2.4 (a)-(d). Both IDA and DPA have 3 centres involved in complexation, i.e. 2 carboxylate groups and a nitrogen atom, which are similarly arranged within the

molecules. Nevertheless, the IDA molecule has a flexible structure, whereas the nitrogen atom of the DPA is part of an aromatic system, which rigidly holds two carboxylate groups in a position coplanar to the pyridine ring, thus favouring bond formation. Normally, the tendency of the ligand to bind a proton parallels its complexation ability. If a double log scale is employed, the values for IDA, tartaric acid and citric acid lie on a straight line (see Fig. 2.5), showing that the stability of metal complexes is in direct proportion to the affinity of the ligand for protons. The DPA acid anion, on the other hand, shows a chelating ability higher than would be expected from its basicity, which is a result of the steric effect discussed above [13].

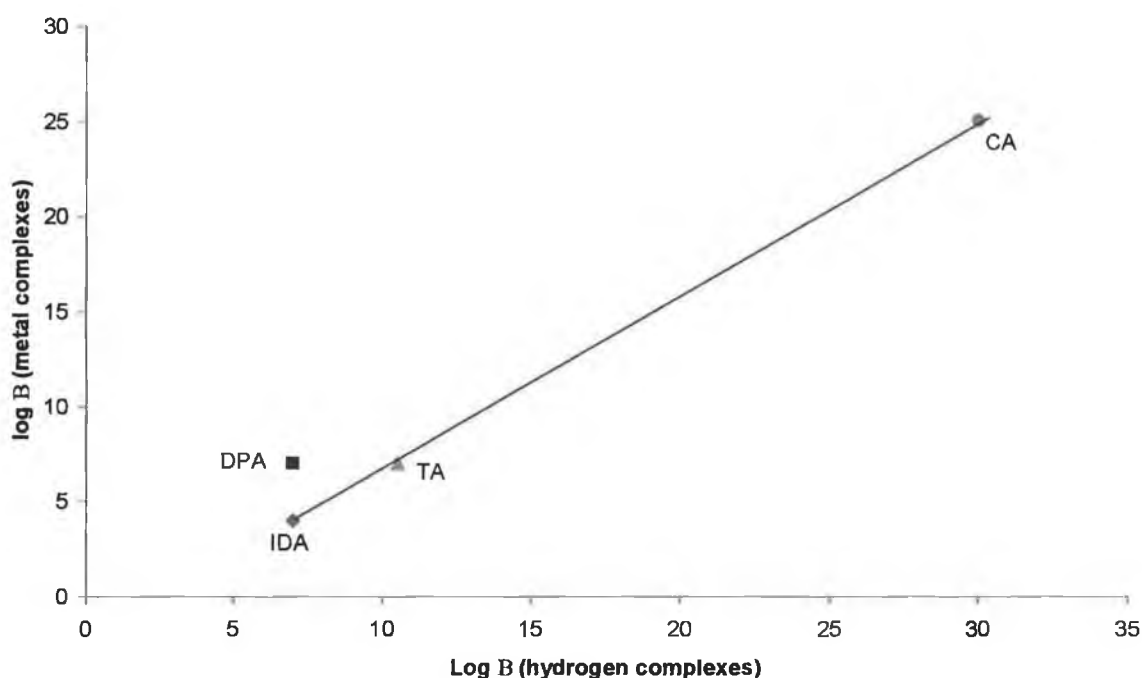


Figure 2.5: A plot showing the correlation between basicity and stability of Co (II) complexes. IDA= iminodiacetic acid, DPA= dipicolinic acid, TA= tartaric acid and CA= citric acid [13].

However, when citric acid, tartaric acid and dipicolinic acid were added to the methansulfonic acid eluent, the presence of these complexing agents in the methansulfonic acid eluent did not impact on the selectivity of the IDA functionalised silica monolith for the alkaline earth metal ion. In fact the column showed no improvement of the separation of the four alkaline earth metal ions, which was

obtained with just the methansulfonic acid eluent (see Fig. 2.3). Another interesting point to note is that unlike the observations discussed by Bonn *et al.* [13], there was very little difference between the separations obtained using tartaric acid and dipicolinic acid eluents. The co-elution of Ca (II) and Sr (II) was still observed with each of the methansulfonic acid-complexing agents eluents (see Fig. 2.6). A possible reason for this, was that the concentration of each complexing agent added to the methansulfonic acid was limited to 2 mM for the citric and tartaric acid, and 0.5 mM for the dipicolinic acid. Low concentrations of the complexing agents in the eluent were necessary to protect the membrane in the suppressor unit employed for the method of suppressed conductivity detection. However, these concentrations may not have been sufficient for the complexing agents to impact the separation selectivity.

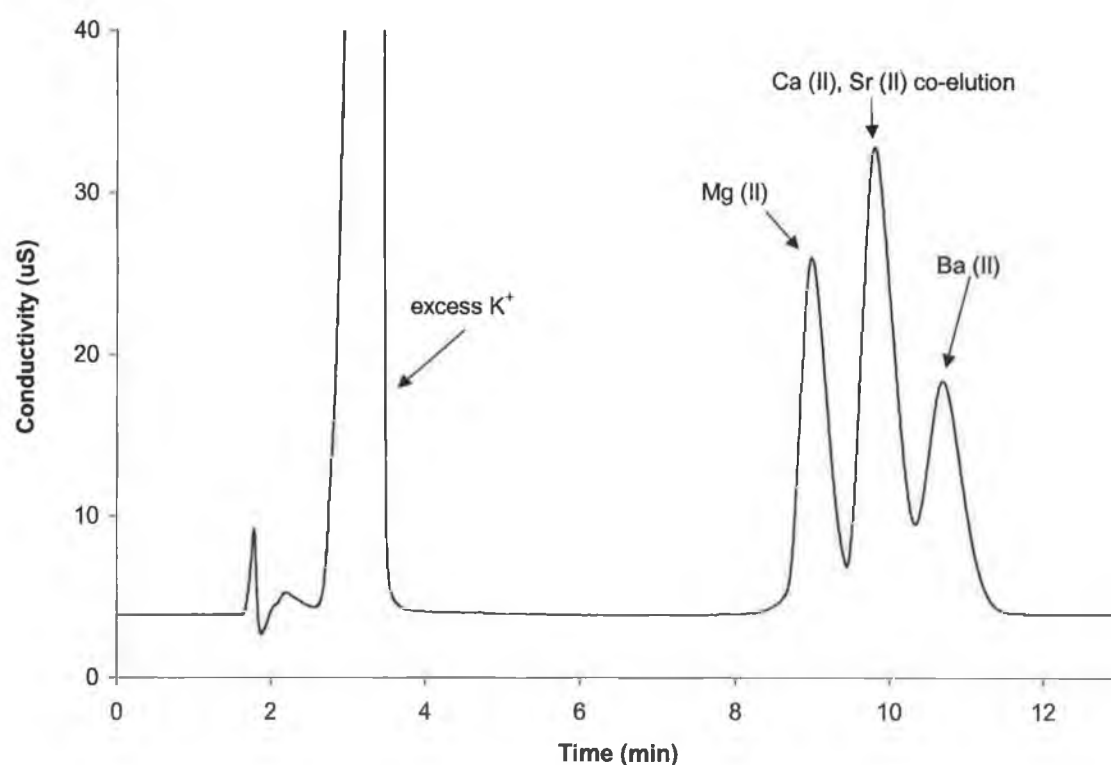


Figure 2.6: The selectivity obtained for a mixture of 10 ppm Mg (II), Ca (II), Sr (II) and Ba (II) on a 10 cm IDA functionalised silica monolithic column. Eluent conditions: a mixture of 0.5 mM dipicolinic acid and 2.5 mM methansulfonic acid, flow rate 1 mL/min, and analysis was monitored using suppressed conductivity detection.

### ***2.3.2.5: Fast separations of alkaline earth metals using low ionic strength acidic eluents with suppressed conductivity detection***

With the addition of the complexing agents (citric acid, tartaric acid and dipicolinic acid) failing to resolve the problem of the Ca (II) and Sr (II) co-elution, the work focussed on the separation of Mg (II), Ca (II) and Ba (II), with a view of achieving a rapid separation of these three cations. However, the use of suppressed conductivity detection limited the eluent flow rate to less than 2 mL/min.

The separation of the three alkaline earth metal ions (Mg (II), Ca (II) and Ba (II)) was performed on the IDA functionalised silica monolith using both a 2 mM and a 2.5 mM methansulfonic acid eluent, at flow rates of 1, 1.5 and 2 mL/min. The optimum conditions for the fast separation of Mg (II), Ca (II) and Ba (II), based on the results presented in Table 2.8, are a flow rate of 2 mL/min using a 2.5 mM methansulfonic acid eluent concentration. However, the use of the 2.5 mM eluent did result in a reduction in the resolution of the alkaline earth metal ions, even at 1 mL/min.

Table 2.8: The effect of eluent concentration on the retention and resolution of Mg (II), Ca (II) and Ba (II) on the IDA silica monolith.

<b>Analyte</b>	<b>Retention factor (<i>k</i>)</b>	<b>Resolution</b>
<b>Eluent: 2 mM MSA, 2 mL/min</b>		
Mg (II)	5.0	
Ca (II)	5.7	1.5
Ba (II)	6.1	1.1
<b>Eluent: 2.5 mM MSA, 2 mL/min</b>		
Mg (II)	2.7	
Ca (II)	3.0	1.2
Ba (II)	3.3	1.1

### 2.3.3: Separation of alkaline earth metal ions by chelation ion-exchange

#### 2.3.3.1: Effect of eluent ionic strength

The data in Table 2.9 demonstrates that a dual retention mechanism, i.e. a combination of ion-exchange and chelation, is responsible for the retention of alkaline earth metals on the IDA functionalised silica monolith.

Table 2.9: The effect of KNO<sub>3</sub> eluent (pH 4.85) concentration on of the alkaline earth metal ion retention, flow rate 1 mL/min.

KNO <sub>3</sub> Conc.	Retention factor ( <i>k</i> )			
	Mg (II)	Ca (II)	Sr (II)	Ba (II)
0.1 M	8.5	20.2	14.2	17.7
0.2 M	2.8	4.9	4.1	4.7
0.3 M	1.5	2.8	2.2	2.4
0.4 M	1.1	2.1	1.4	1.5
0.5 M	0.9	1.9	1.1	1.1
1.0 M	0.4	0.7	0.4	0.4

At 0.1 M KNO<sub>3</sub>, the selectivity shown is not typical of either simple ion-exchange or chelation (Mg (II)  $K_1 = 2.94$ , Ca (II)  $K_1 = 2.59$ , Sr (II)  $K_1 = 2.23$  and Ba (II)  $K_1 = 1.67$  (0.1 M KNO<sub>3</sub>, 25 °C)) [24], but would appear to be a combination of both. However, the dominance of the ion-exchange retention mechanism with the 0.1 M eluent is evident from the selectivity shown, which matches very closely, the selectivity expected from simple ion-exchange on carboxylic acid exchangers, i.e. Mg (II) < Sr (II) < Ba (II). However, as Fig. 2.7 demonstrates, the retention of Ca (II) is unusually high; indicating that some degree of complexation may be responsible for this increased retention of Ca (II) compared to the remaining alkaline earth metal ions. Also, Ca (II) elutes last under higher ionic strength eluent conditions, indicating the strongest degree of complexation. It is clear that chelation-exchange is not totally insensitive to changes in ionic strength. The concentration of the background electrolyte will have an effect on the activities of the ions, and therefore, on the

stability constants. Ba (II) is most affected by changing the eluent ionic strength, thus indicating the dominance of ion-exchange as the sorption mechanism in this case. The transition of Ba (II) in the elution order, as the eluent ionic strength increased, demonstrates how the ion-exchange capacity of IDA-silica can be effectively switched off through the use of high ionic strength eluents. An increase in ionic strength will increase the ratio of chelation-to-ion exchange and, at very high salt concentrations, ion-exchange will become very small or insignificant. The optimum ionic strength of the eluent for use when chelation-exchange is required as the dominant retention mechanism is between 0.5 and 1.0 M.

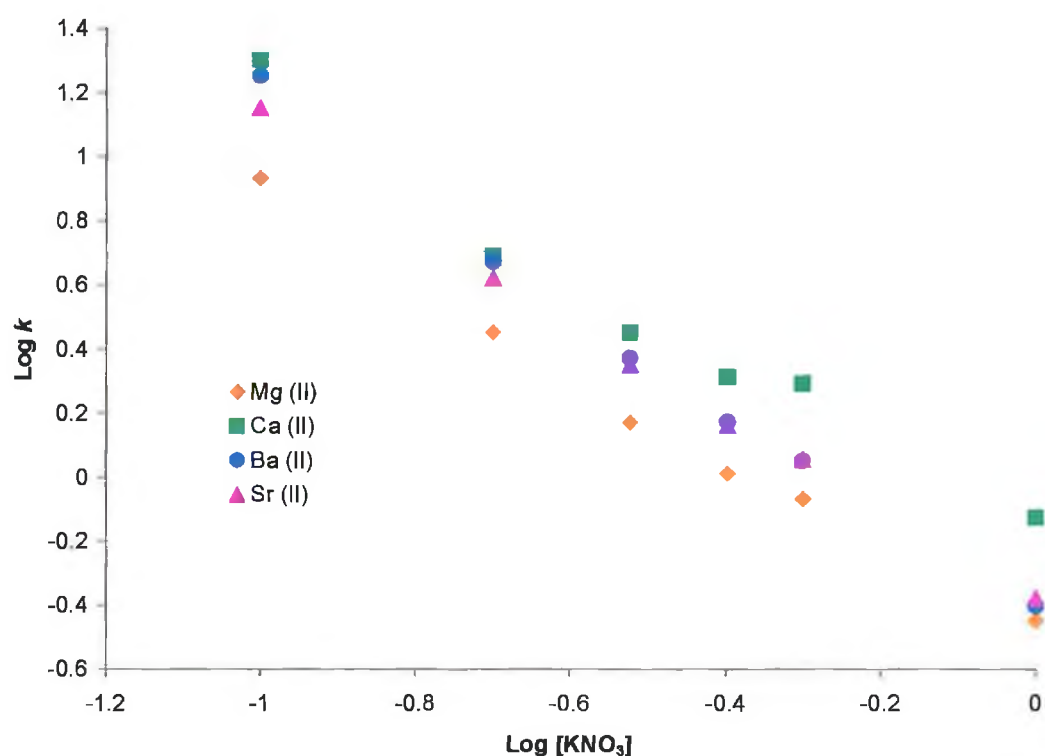


Figure 2.7: Effect of increasing the KNO<sub>3</sub> eluent concentration (pH 4.85) on the alkaline earth metal ion retention factors ( $k$ ), retained on a 10 cm IDA functionalised silica monolith. Flow rate 1 mL/min. Detection conditions: 0.4 mM *o*-CPC in 0.25 M boric acid, pH 10.5, was employed as the post-column reagent and the resultant *o*-CPC- metal complexes were monitored at 570 nm.

### ***2.3.3.2: Comparison of alkaline earth selectivity for an IDA silica gel packed column and the IDA functionalised silica monolithic column.***

Unlike silica gel type stationary phases, modification of silica monoliths can only be carried out 'on- column'. Therefore it was important to evaluate the new monolithic IDA column for capacity and selectivity in comparison with a commercially available IDA modified silica gel column. This was carried out to determine whether surface coverage of the silica skeleton was of an order similar to that of silica gel type phases, and if the silica structure had a substantial affect upon selectivity for metal ions.

Figure 2.8 (a) and (b), shows the chromatograms obtained for the alkaline earth metals, using similar eluents, with the new 10 cm IDA functionalised silica monolithic column and those obtained by Bashir and Paull [18] using a standard 25 cm silica gel IDA column. The eluents used consisted of (a) 0.3 M  $\text{KNO}_3$ , adjusted to pH 4.2 for the silica gel column and pH 4.85 for the monolithic column (the difference in pH reflects a lower total column capacity for the monolithic phase:  $\sim 75\mu\text{mol}$  IDA per monolith compared to  $\sim 185\mu\text{mol}$  IDA on the silica gel column, although given the difference in the lengths of the two columns, the actual surface coverage of the monolithic phase should be very similar), and (b) the 0.5 M  $\text{KNO}_3$ , adjusted to pH 4.2 for the silica gel column and pH 4.85 for the monolith column. As can be seen from the chromatograms in Fig. 2.8, the monolithic IDA column exhibits remarkably similar selectivity and efficiency to the modified silica gel column. As described in Section 2.3.3.1, eluents ranging from 0.1 to 1 M  $\text{KNO}_3$  were investigated with the monolithic column, with the resulting selectivity changes being identical to those reported by Bashir and Paull [16] with the silica gel column. These similarities made it clear that the retention mechanism for the alkaline earth metal ions on the monolithic IDA column was the same combination of ion-exchange and chelation as demonstrated by the silica gel IDA column.

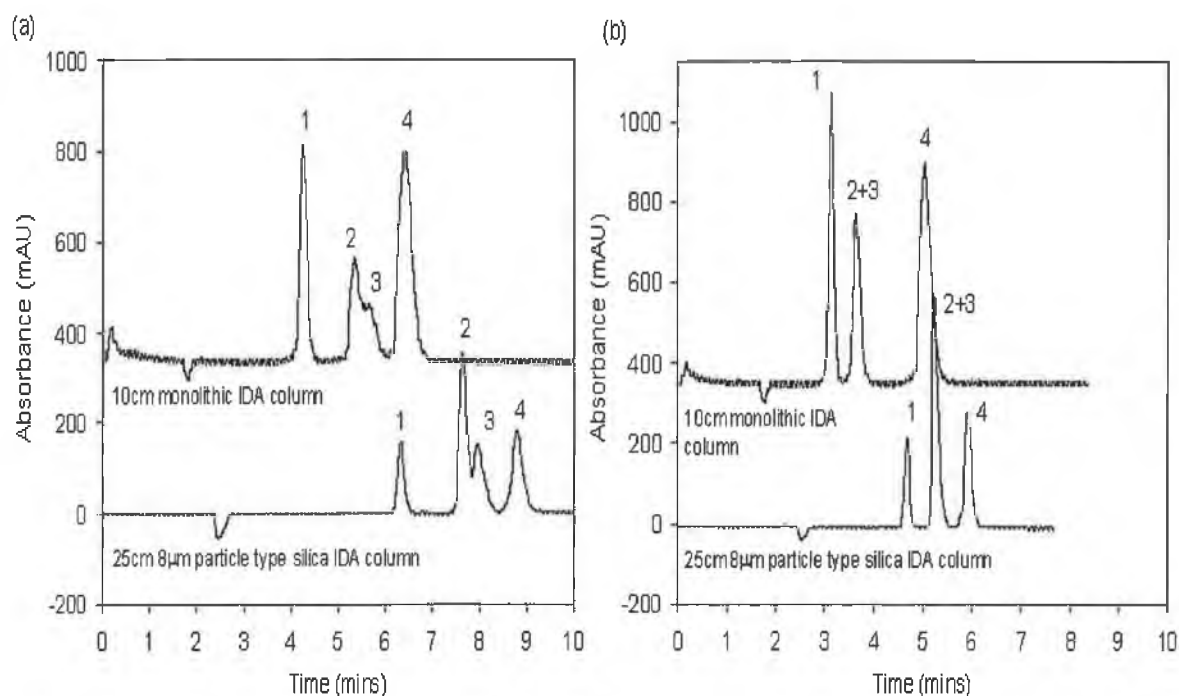


Figure 2.8: Chromatograms showing the separation of 1-Mg (II), 2-Sr (II), 3-Ba (II) and 4-Ca (II), using an eluent (a) 0.3 M KNO<sub>3</sub>, adjusted to pH 4.2 for the silica gel column and pH 4.85 for the monolithic column, and (b) 0.5 M KNO<sub>3</sub>, adjusted to pH 4.2 for the silica gel column and pH 4.85 for the monolithic column. Flow rate 1 mL/min. Detection conditions: 0.4 mM *o*-CPC in 0.25 M boric acid, pH 10.5, was employed as the post-column reagent and the resultant *o*-CPC-metal complexes were monitored at 570 nm.

### 2.3.3.3: The effect of eluent pH on alkaline earth metal ion selectivity

As Fig. 2.9 demonstrates, pH is undoubtedly the most important of the elution parameters controlling the separation of metal ions in chelation exchange. In the absence of hydrolysis and complexed forms of the metal ions, other than the stable hydrated form, increased retention of metal cations is usually observed on increasing the pH of the eluent. The dissociation of the acid groups on the immobilised chelating ligand produces a sharp increase in the conditional stability constants of surface metal complexes. When any ion-exchange sorption is swamped or suppressed by using a high ionic strength eluent, the increase in pH of the eluent means that the retention occurs only through chelation on the surface. The retention and selectivity is defined solely by the values of stability constants [25]. Once again Ca (II) exhibited differing

behaviour to the remaining alkaline earth metals ions, showing a rapid increase in retention at  $\sim$  pH 5 and above. It is clear from Fig. 2.9 that complexation begins to dominate retention  $>$  pH 5 for Ca (II) and  $>$  pH 6 for the remaining alkaline earth ions, especially Sr (II).

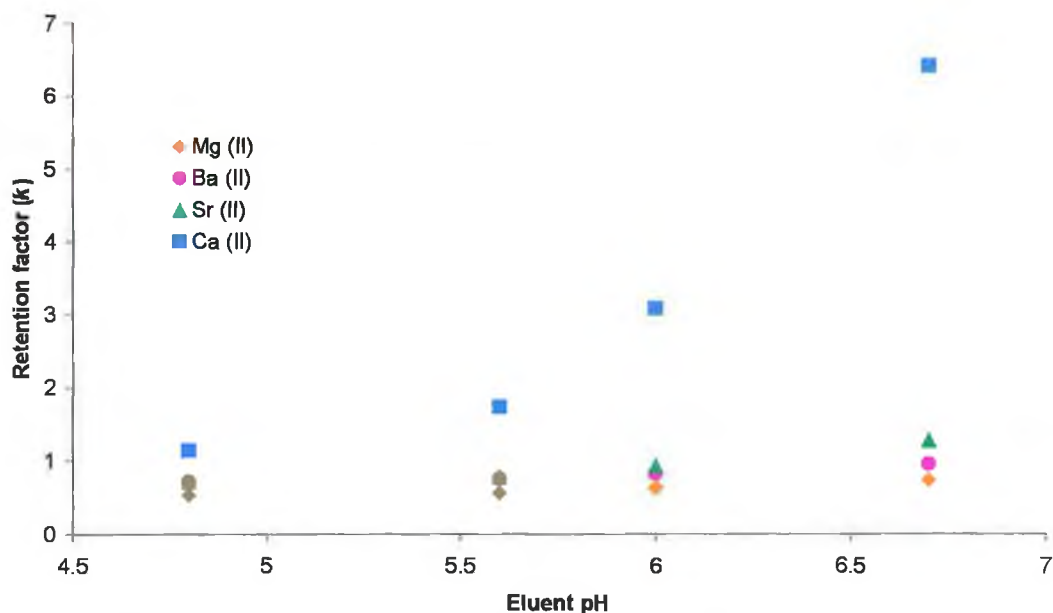


Figure 2.9: Effect of increasing the eluent pH (0.5 M  $\text{KNO}_3$ ) on the alkaline earth metal ion retention factors ( $k$ ), retained on a 10 cm IDA functionalised silica monolith. Flow rate 1 mL/min.

Using a 0.4 M KCl, pH 6.7 eluent, a baseline separation of the four alkaline earth metals was achieved, each exhibiting different selectivity, see Fig. 2.10. The selectivity shown differs remarkably from that seen with simple ion-exchange (see Fig. 2.3), and allows Ca (II) to be selectively retained. As the results in Chapter 3 will demonstrate, the IDA monolith is ideally suited to the analysis of samples with very high Ca (II) levels. The separation shown in Fig. 2.10 also shows the clear advantages in using the IDA silica column for the separation of alkaline earth metal ions compared to a simple cation-exchanger, which would normally require the presence of a complexing eluent to achieve the desired selectivity for the alkaline metal ions [16].

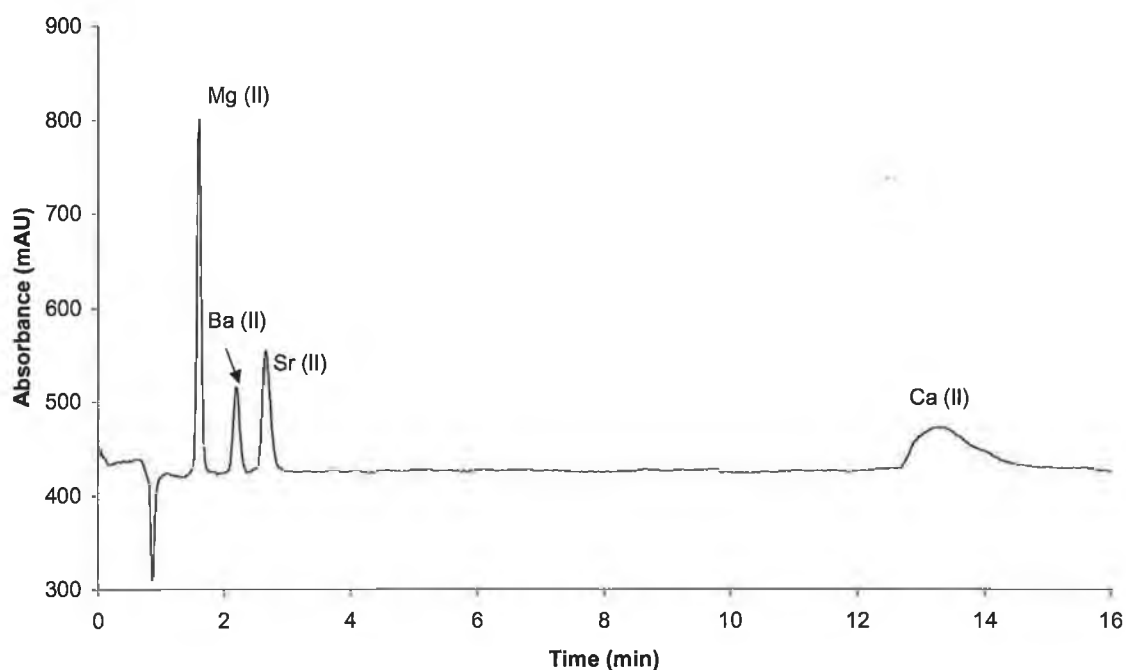


Figure 2.10: A separation of Mg (II), Ba (II), Sr (II) and Ca (II) on a 10 cm IDA functionalised silica monolith. Eluent Conditions: 0.4 M KCl, pH adjusted to 6.7, flow rate 2 mL/min. Detection conditions: 0.4 mM *o*-CPC in 0.25 M boric acid, pH 10.5, was employed as the post-column reagent and the resultant *o*-CPC- metal complexes were monitored at 570 nm.

#### ***2.3.3.4: The effect of eluent pH on the retention of alkaline earth metal ions on a bare silica monolithic column***

When considering the effect of increasing eluent pH on the retention of cations on IDA, two aspects must be considered. As mentioned earlier, increasing the pH results in the dissociation of acid groups on the immobilised chelating ligands, producing a sharp increase in the conditional stability constants of the surface metal complexes. However, the dissociation of weak acid groups will also cause an increase in the ion-exchange capacity depending on the values of the acid dissociation constant,  $K_a$ . Therefore, an important aspect that tends to be overlooked in pH studies of chelating-exchangers is the effect of secondary equilibria connected with the ionisation of some groups at the surface of the chelating-exchanger (e.g. silanol groups at the silica surface) [26].

The aim of this experiment was to demonstrate that the unique selectivity of the IDA silica for the alkaline earth metal ions presented in Section 2.3.3.3, was as a result of complexation with the IDA groups, and was not affected to any great extent by the presence of surface silanol groups, which act like weak cation-exchangers. The relationship between eluent pH and analyte retention is presented in Fig. 2.11. If the pH effects shown in Fig. 2.9 and 2.11 are compared, it is clear that ion-exchange alone could not produce the selectivity necessary to separate the alkaline earth metal ions or the unique selectivity observed for Ca (II) on the IDA silica monolith at pH values > 5. The bare silica monolith did show significant retention of alkaline earth metals over the latter half of the pH range investigated, although selectivity was poor. However, the separation shown in Fig. 2.12 demonstrates that a simple separation of Mg (II) and Ca (II) could be obtained on the bare silica monolithic column.

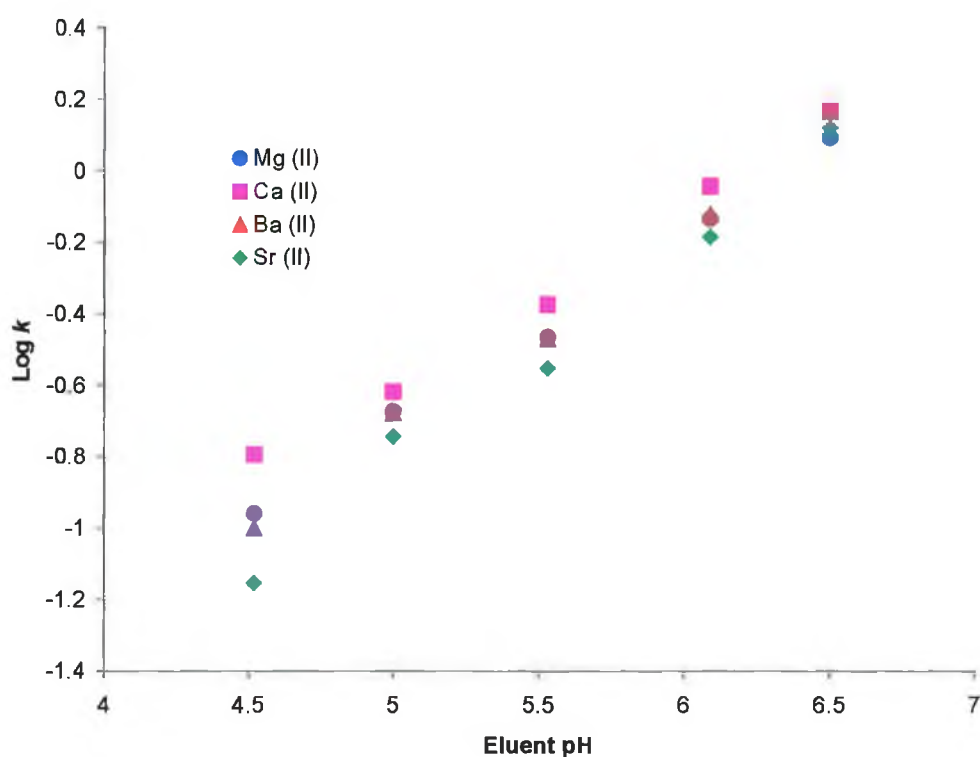


Figure 2.11: The effect of eluent pH on the retention of alkaline earth metal ions on a 10 cm bare silica monolith. Eluent conditions: 5 mM KCl (prepared in 10 mM sodium acetate buffer), pH 6.0, flow rate 1 mL/min.

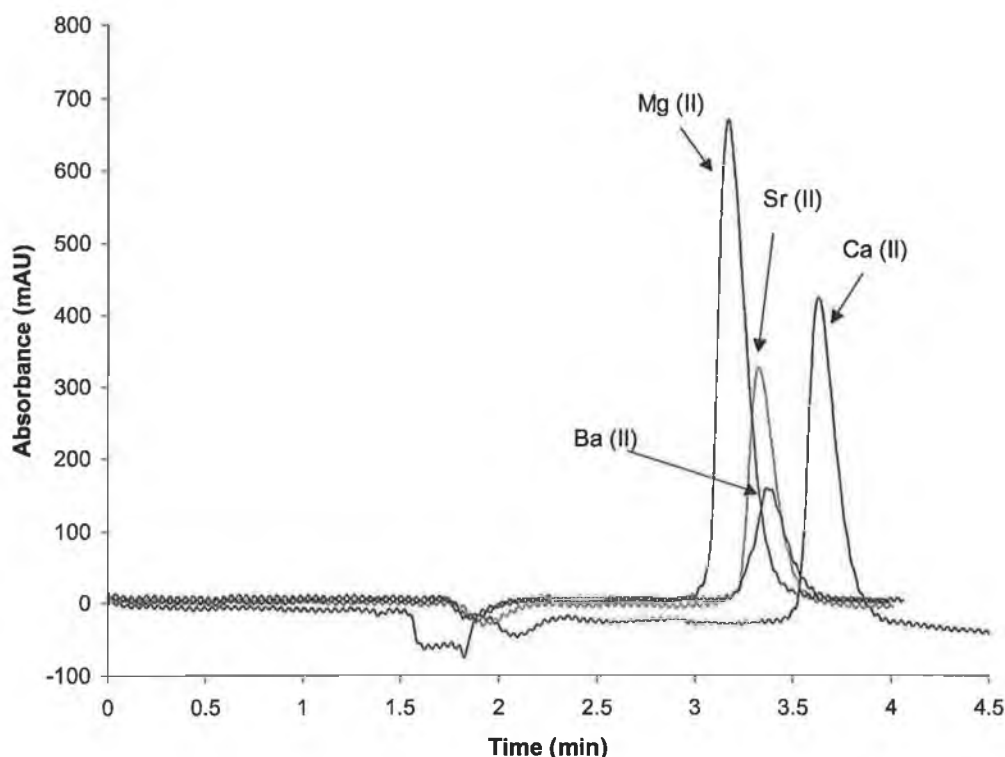


Figure 2.12: The separation of alkaline earth metal cations a 10 cm bare silica monolith. Eluent conditions: 5 mM KCl (prepared in 10 mM sodium acetate buffer), pH 6.0, flow rate 1 mL/min. Detection conditions: 0.4 mM *o*-CPC in 0.25 M boric acid, pH 10.5, was employed as the post-column reagent and the resultant *o*-CPC-metal complexes were monitored at 570 nm.

## 2.4: Conclusion

A 10 cm silica monolith has been functionalised on-column with IDA groups and the retention of alkali and alkaline earth metal cations on the IDA silica monolith has been investigated over a range of eluent ionic strength and pH values. The results obtained for the analysis of alkali and alkaline earth metal cations on the IDA silica monolith were compared to the performance of a 25 cm IDA silica gel column, with a view to identifying possible differences in selectivity, and other specific properties, between stationary phases consisting of the same chemistry of attached functional groups but differing in the nature of the porous substrate.

The surface concentration of attached IDA groups on the monolithic phase was found to be non-homogeneous and approximately half that seen with the silica gel phase, and therefore, it was observed that the higher capacity IDA silica particulate phase exhibited better selectivity for alkali metal ions, and stronger retention of alkaline earth metal ions. As in the case of the IDA silica gel particulate column, the IDA silica monolith exhibited both ion-exchange and chelation-exchange properties and it was possible to manipulate the selectivity of the IDA silica monolith by varying different mobile phase parameters. Using a weak acidic eluent, a limited separation of alkaline earth metal ions was observed. However, under conditions of high ionic strength and eluent pH, it was possible to achieve a baseline resolution of Mg (II), Ca (II), Sr (II) and Ba (II) on the IDA silica monolith.

Finally, the contribution of surface silanol groups to the ion-exchange properties exhibited by the IDA silica monolith was also investigated, and it was demonstrated that limited retention of both alkali and alkaline earth metal ions was possible on a bare silica monolithic column.

## References

1. K. Cabrera, *J. Sep. Sci.*, 27 (2004) 843.
2. F. Svec, *LCGC Europe*, 16, 6a (2003) 24.
3. P. Hatsis, C.A. Lucy, *Anal. Chem.* 75 (2003) 995.
4. Q. Xu, M. Mori, K. Tanaka, M. Ikedo, W. Hu, P.R. Haddad, *J. Chromatogr. A*, 1041 (2004) 95.
5. C. Ó Ríordáin, P. N. Nesterenko, B. Paull, *J. Chromatogr. A*, 1070 (2005) 71.
6. Q. Xu, M. Mori, K. Tanaka, M. Ikedo, W. Hu, *J. Chromatogr. A*, 1026 (2004) 191.
7. Q. Xu, K. Tanaka, M. Mori, M. I. Helaleh, M. Ikedo, W. Hu, K. Hasebe, H. Toada, *J. Chromatogr. A*, 997 (2003) 183.
8. D. Connolly, D. Victory, B. Paull, *J. Sep. Sci.*, 27 (2004) 912.
9. Y. Guo, Z. Yan, J. S. Fritz, High-speed ion chromatography on monolithic columns coated with cationic surfactant, in: *IICS Symposium, Trier, Germany, 2004*, p 52.
10. D. Victory, P. N. Nesterenko and B. Paull, *Analyst*, 129 (2004) 700.
11. B. Paull, C. Ó Ríordáin, P. N. Nesterenko, *Chem. Comm.*, (2005) 215.
12. P. N. Nesterenko, P. Jones, *J. Chromatogr. A*, 770 (1997) 129.
13. G. Bonn, S. Reiffenstuhl, P. Jandik, *J. Chromatogr.*, 449 (1990) 669.
14. I. N. Voloschik, M. L. Litivina, B. A. Rudenko, *J. Chromatogr. A*, 706 (1995) 315.
15. P. N. Nesterenko, P. Jones, *J. Chromatogr. A*, 804 (1998) 223.
16. W. Bashir and B. Paull, *J. Chromatogr. A*, 907 (2001) 191.
17. C. Sarzanini and E. Mentasti, *J. Chromatogr. A*, 850 (1999) 213.
18. M. G. Kolpachnikova, N. A. Penner, P. N. Nesterenko, *J. Chromatogr. A*, 826 (1998) 15.
19. A. I. Elefterov, P. N. Nesterenko, O. A. Shpigun, *Anal. Chem.*, 51 (1996) 887.
20. B. Paull and W. Bashir, *Analyst*, 128 (2003) 335.
21. G. B. Cox, *J. Chromatogr. A*, 656 (1993) 353.
22. A. Berthod, *J. Chromatogr. A*, 54 (1991) 1.
23. J. S. Fritz and D. T. Gjerde, *Ion Chromatography*, 3<sup>rd</sup> Edition, Wiley-VCH (Germany) 2000.

24. A. E. Martell, *Stability Constants of Metal Ion Complexes: Supplement 1: The Chemical Society of London, Alden Press (Oxford) 1971.*
25. P. Jones and P. N. Nesterenko, *J. Chromatogr. A*, 789 (1997) 413.
26. K. Robards, P. Starr, E. Patsalides, *Analyst*, 116 (1991) 1247.

## **Chapter 3**

### ***Determination of alkaline earth metal ions in complex matrices***

### 3.1: Introduction

The determination of trace metals in complex matrices remains one of the most complicated areas in analytical chemistry [1]. IC has a proven track record in the determination of inorganic, and organic, anions and cations in complex matrices, i.e. solutions of high ionic strength or samples containing large disparities between the concentrations of the analyte ions and other species present within the sample [2].

To date, only a few reports exist in the literature where monolithic columns have been applied to the analysis of complex samples in IC. A 10 cm reversed-phase silica monolith was coated with carboxybetaine-type surfactant, and used by Ó Ríordáin *et al.* [3] for the analysis  $\text{NO}_2^-$  and  $\text{NO}_3^-$  in estuarine water and seawater. An ion chromatographic method for the determination of  $\text{ClO}_4^-$  in the presence of a high ionic matrix containing 1000 ppm of  $\text{Cl}^-$ ,  $\text{CO}_3^{2-}$  and  $\text{SO}_4^{2-}$  using an anion-exchange monolithic column has been developed by Methrom AG [4]. Xu *et al.* [5] modified a 5 cm reversed-phase silica monolith with lithium dodecylsulfate (Li-DS) for the rapid separation of  $\text{H}^+$  from other mono- and divalent cations, such as Na,  $\text{NH}_4$ , K, Mg (II) and Ca (II), and applied the developed method to the analysis of acid rain samples.

According to Paull and Nesterenko [2], the key to the determination of analytes in the most challenging complex matrices is the ability to manipulate selectivity through the control of stationary phase chemistry, mobile phase chemistry and choice of detection method. In particular, the nature of the stationary phase plays a very significant role in controlling selectivity in IC [6,7]. In Chapter 2 it was shown that the IDA silica monolith exhibits a 'dual retention mechanism', which provides scope to manipulate the retention of target analytes through control of various eluent conditions, such as eluent pH, and not just eluent concentration. In addition, it was shown that the IDA silica monolith showed little or no affinity for alkali metals, while at the same time being capable of separating alkaline earth metal ions, which means that direct injection of high ionic strength samples, without any on-line pre-treatment would be possible.

### **3.1.1: Objective**

The aim of this Chapter was the development of rapid and efficient separations of alkaline earth metal ions in complex matrices, using the 10 cm IDA functionalised silica monolith and post-column reaction detection.

## **3.2: Experimental**

### **3.2.1: Modification of silica monolith**

As detailed in Section 2.2.1, Chapter 2.

### **3.2.2: Instrumentation**

As detailed in Section 2.2.2, Chapter 2.

### **3.2.3: Reagents**

The eluent and post-column reagent (PCR) solutions were prepared using DIW from a Millipore Milli-Q water purification system (Bedford, MA, USA). Where post-column reaction (PCR) detection was required, the reagent used for the detection of alkaline earth metals was 0.4 mM *o*-cresolphthalein complexone (*o*-CPC), 0.25 M boric acid (adjusted to pH 10 using NaOH). The *o*-CPC was purchased from Sigma-Aldrich (Gillingham, Dorset, UK), and used without further purification (monitored at 570 nm). Potassium and sodium nitrate salts were obtained from Fluka Chemie (Buchs, Switzerland) and potassium, sodium, cesium and lithium chloride salts were all obtained from Sigma-Aldrich (Tallaght, Dublin). All eluents, reagents and standard solutions prepared were filtered through a 0.45 µm filter and degassed using sonication. Low level standard solutions of all metal ions were generally made up freshly each day from stock solutions prepared from chloride salts (1000 ppm) and stored in 1% nitric acid.

### 3.3: Results and discussion

#### 3.3.1: *The determination of Sr (II) and Ba (II) in complex matrices.*

There is a great deal of interest in the determination of Ba (II) and Sr (II) in certain environmental and biological samples. The presence of either, or both, of the above often occurs in samples containing much larger concentrations of alkali and other alkaline earth metals, which can cause problems in several commonly used analytical techniques. The use of atomic spectroscopy for the determination of Ba (II) and Sr (II) in a variety of sample types has been reported. However, the presence of Ca (II) and Mg (II) at much higher concentrations caused severe interferences when using AAS and also AES [8]. When using traditional cation-exchange chromatography, Mg (II) elutes first, followed by Ca (II), Sr (II) and finally Ba (II). Therefore, the presence of excess Ca (II) or Mg (II) in the sample matrix can result in large peaks that will mask the signal for Sr (II) and Ba (II). Dilution of the sample prior to injection could result in a loss in the signal for Sr (II) and Ba (II) completely.

Jones *et al.* [9] evaluated high performance chelation ion chromatography involving dye-coated resins for the determination of trace amount of Ba (II) and Sr (II) in environmental samples containing high levels of other alkali and alkaline earth metals, particularly Ca (II). However, it was also possible to exploit the unusually high selectivity observed for Ca (II) on the IDA silica monolith, demonstrated in Chapter 2, for the determination of Sr (II) and Ba (II) in samples containing excess amounts of Ca (II).

Using an eluent composed of 0.4 M KCl, pH 6.7, chelation-exchange provided the necessary selectivity required to achieve an efficient separation of Mg (II), Ba (II) and Sr (II), in a matrix containing 1000 ppm Ca (II), on the IDA silica monolith. With an eluent pH of 6.7, Mg (II), Sr (II) and Ba (II) were baseline resolved in 2.5 minutes, while there was a separation window of 1.5 minutes between the Sr (II) peak and the elution of the 1000 ppm Ca (II) peak. The peak efficiency values calculated for Mg (II), Ba (II) and Sr (II) peaks, i.e. 20,920 N/m, 19,080 N/m and 17,060 N/m respectively, were impressive considering the complex sample matrix. It should be

noted that the Ba (II) and Sr (II) peaks are well suited to the window between chromatographic peaks of Mg (II) and Ca (II), which is useful for practical analysis of different natural waters, where Mg (II) and Ca (II) are usually present in excess.

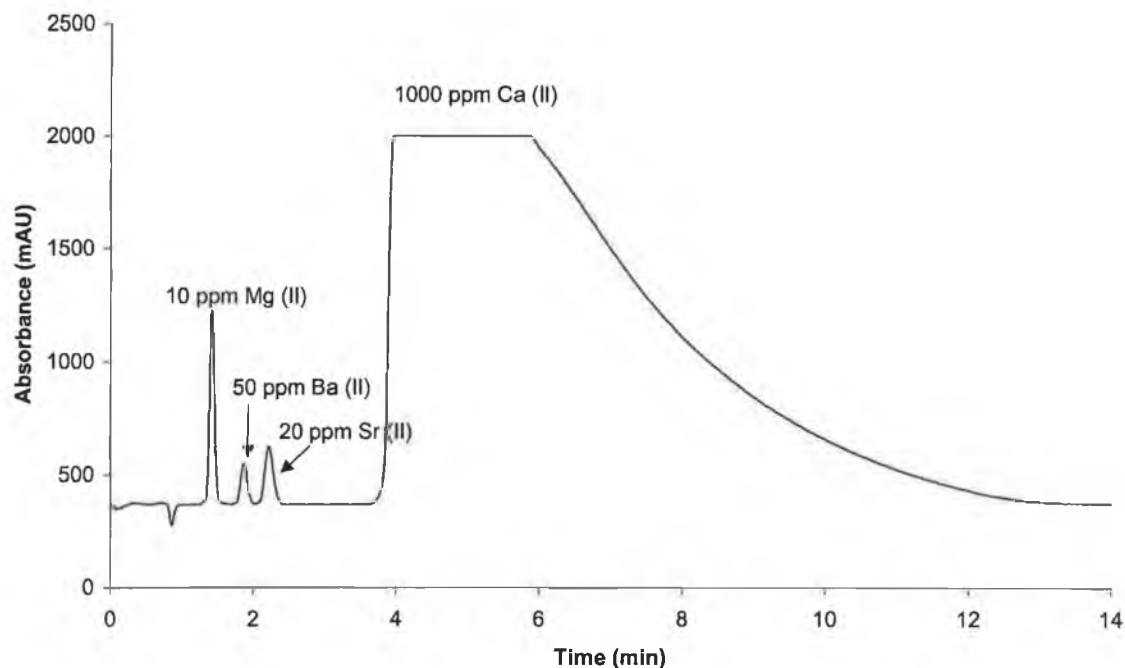


Figure 3.1: A separation of Mg (II), Ba (II), Sr (II) and Ca (II) on a 10 cm IDA functionalised silica monolith. Eluent conditions: 0.4 M KCl, eluent adjusted to pH 6.7, flow rate 2 mL/min. Detection conditions: 0.4 mM *o*-CPC in 0.25 M boric acid, pH 10.5, was employed as the post-column reagent and the resultant *o*-CPC- metal complexes were monitored at 570 nm.

### 3.3.2: Determination of Mg (II) and Ca (II) in high ionic strength samples

As previously discussed, chelation-exchange provides the selectivity necessary for the separation of alkaline earth metal ions in high ionic strength samples. Therefore, an eluent concentration of 1 M was employed to ensure that the ion-exchange properties of the IDA silica monolith were suppressed, and that chelation-exchange was the dominant retention mechanism.

### 3.3.2.1: Selection of a suitable eluent

The separation of Mg (II) and Ca (II) in high ionic strength samples, on the 10 cm IDA functionalised silica monolith, was achieved using an eluent composed of 1M  $\text{KNO}_3$ , pH 4.85. In order to determine the effect of the sample matrix upon the separation achieved and to determine the correct eluent to use, the separation of Mg (II) and Ca (II) prepared in DIW, 1M KCl and 1 M NaCl matrices was investigated. In the case of the 1M NaCl matrix, a matrix peak was observed due to a detector disturbance as a result of the matrix eluting at the eluent dip. However, no such system disturbance was observed when analysing a mixture prepared in the KCl matrix, using a  $\text{KNO}_3$  eluent, see Fig. 3.2. Therefore, it is clear, that to eliminate these system disturbances, the eluent cation had to match that of the sample cation. Using a 1 M  $\text{KNO}_3$  eluent, it was possible to inject samples containing up to 2 M KCl without any system peak interfering with the Mg (II) or Ca (II) peaks.

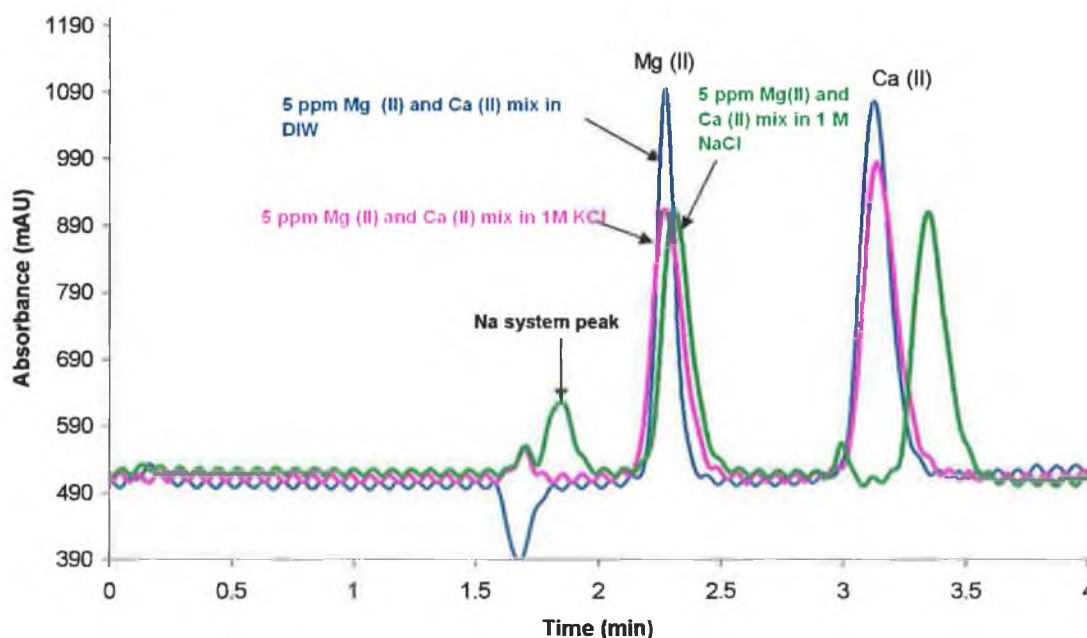


Figure 3.2: The separation of a 5ppm Mg (II) and Ca (II) mixture prepared in the following matrices; DIW (navy trace), 1 M KCl (pink trace) and 1 M NaCl (green trace) on a 10 cm IDA silica monolith. Eluent conditions: 1 M  $\text{KNO}_3$ , pH 4.85, flow rate 1 mL/min. Detection conditions: 0.4 mM *o*-CPC in 0.25 M boric acid, pH 10.5, was employed as the post-column reagent and the resultant *o*-CPC- metal complexes were monitored at 570 nm.

When the separation of the 5 ppm mixture of Mg (II) and Ca (II) in DIW and a 1 M KCl matrix are compared, two observations can be made. As explained above, there is a lack of any matrix peak from the KCl matrix. Secondly, the retention times of the analyte peaks are identical, as opposed to the noticeable variation in retention times of the Ca (II) peak in the 1M KCl and 1M NaCl brines, which can be seen in Fig. 3.2. The reason for this unusual behaviour is unclear, but may be related to the greater affinity the IDA phase demonstrates for potassium over sodium and other alkali metals, under strong eluent conditions on IDA silica gel columns.

### ***3.3.2.2: Investigation of sample matrix effects using a commercial IDA silica gel column***

The difference in the retention time observed for Ca (II) peak, prepared in 1 M KCl and NaCl matrices was further investigated using a 25 cm IDA silica gel particle-packed column. A series of 10 ppm Mg (II) and Ca (II) mixtures were prepared in the following matrices: DIW, 1 M KCl, 1 M NaCl, 1 M CsCl and 1 M LiCl.

For the particle-packed IDA silica column a variation in the retention time of Ca (II) was also observed for the 1 M NaCl, 1 M CsCl and 1 M LiCl sample matrix. However, identical retention times for the Ca (II) peak were observed for 1 M KCl matrix and the DIW. This effect was similar to the results obtained using the monolith IDA silica column, and the results confirm that other alkali chloride matrices, e.g. CsCl and LiCl, and not only the NaCl matrix, resulted in a slight increase in the retention time of Ca (II), see Fig. 3.3. The chromatogram for Mg (II), Ca (II) mixture prepared in the 1M LiCl matrix was not included in Fig. 3.3, because of the presence of a large matrix peak, which swamped the signal for Mg (II).  $\text{Li}^+$  behaves differently to other alkali metals, namely  $\text{K}^+$  and  $\text{Na}^+$ , in that it is known to form weak complexes with certain metallochromic ligands, including *o*-CPC [7].

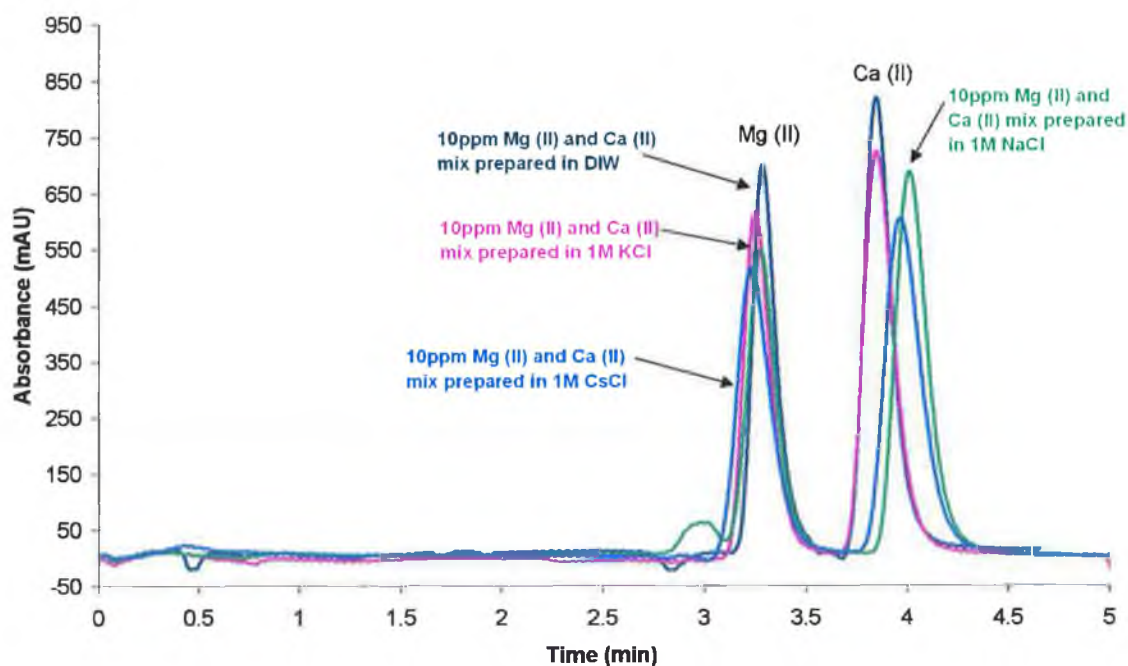


Figure 3.3: Separation of 10 ppm Mg (II) and Ca (II) mixture prepared in DIW (navy trace), 1 M KCl (pink trace), 1 M NaCl (green trace) and 1 M CsCl (blue trace), on a 25 cm IDA silica gel particle-packed column. Eluent conditions: 1 M KCl eluent, pH 4.85, flow rate 1 mL/min. Detection conditions: 0.4 mM *o*-CPC in 0.25 M boric acid, pH 10.5, was employed as the post-column reagent and the resultant *o*-CPC- metal complexes were monitored at 570 nm.

### 3.3.2.3: Matrix effects on separation efficiency

The lower backpressure associated with the IDA silica monolithic column allowed faster chromatographic separations to be performed than were previously possible with particle packed columns. However, it was necessary to study the effect of using elevated flow rates on the efficiency of the Mg (II) and Ca (II) peaks.

The separations presented in Fig. 3.4 exhibit no evidence of a matrix peak because the eluent cation ion matched the sample cation, but there was a reduction in sensitivity observed at the higher flow rates, due to the problem of introducing the post-column reagent (PCR) using the pressure driven Dionex Reagent Delivery Module, at elevated eluent flow rates. However, the PCR used was highly sensitive and selective for Mg (II) and Ca (II) ions, resulting in an approximate detection limit of 0.2 mg/L for each ion in the 1 M brine solution.

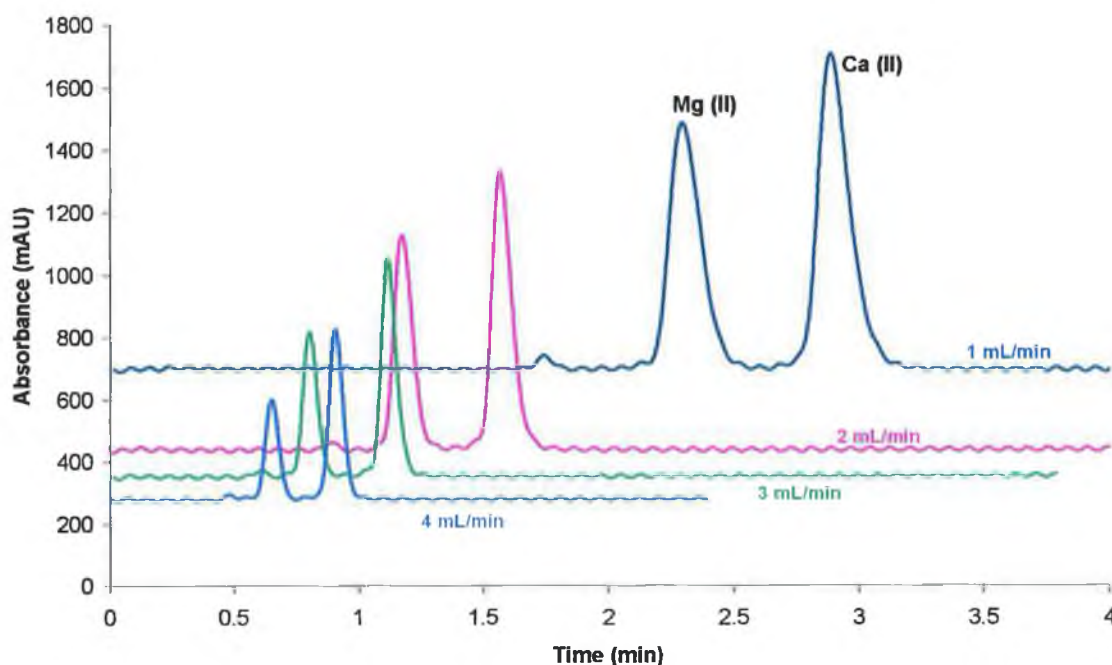


Figure 3.4: Separation of 10 ppm Mg (II) and Ca (II) in 1 M KCl matrix on a 10 cm IDA functionalised monolith. Eluent conditions: 1 M KNO<sub>3</sub> eluent, pH 4.85, flow rate 1 to 4 mL/min. Detection conditions: 0.4 mM *o*-CPC in 0.25 M boric acid, pH 10.5, was employed as the post-column reagent and the resultant *o*-CPC- metal complexes were monitored at 570 nm.

The efficiency of the IDA functionalised silica monolithic column was evaluated at eluent flow rates between 1 and 4 mL/min, and the results of this study are presented in Fig. 3.5 (a) and (b). For this study, the maximum eluent flow rate investigated was 4 mL/min, because this was sufficient to allow a rapid separation of Mg (II) and Ca (II), without causing excessive back pressure (< 120 bar) or significant problems with the mode of detection being applied, namely post-column detection.

In accordance with the van Deemter equation, the expected loss of efficiency at the elevated flow rates, due to an increase in the mass transfer term, was observed for both samples prepared in water and 1 M KCl. However, the loss in efficiency is much more pronounced for the Ca (II), and in particular, the Mg (II) standards prepared in the 1 M KCl brine solution. As the sample matrix and eluent cations are both K<sup>+</sup> and are both present at the same concentration (i.e. 1 M), this effect could be a result of the high matrix Cl<sup>-</sup> concentration, causing increased band broadening at the higher flow rates. There, this effect must be considered when analysing high ionic strength

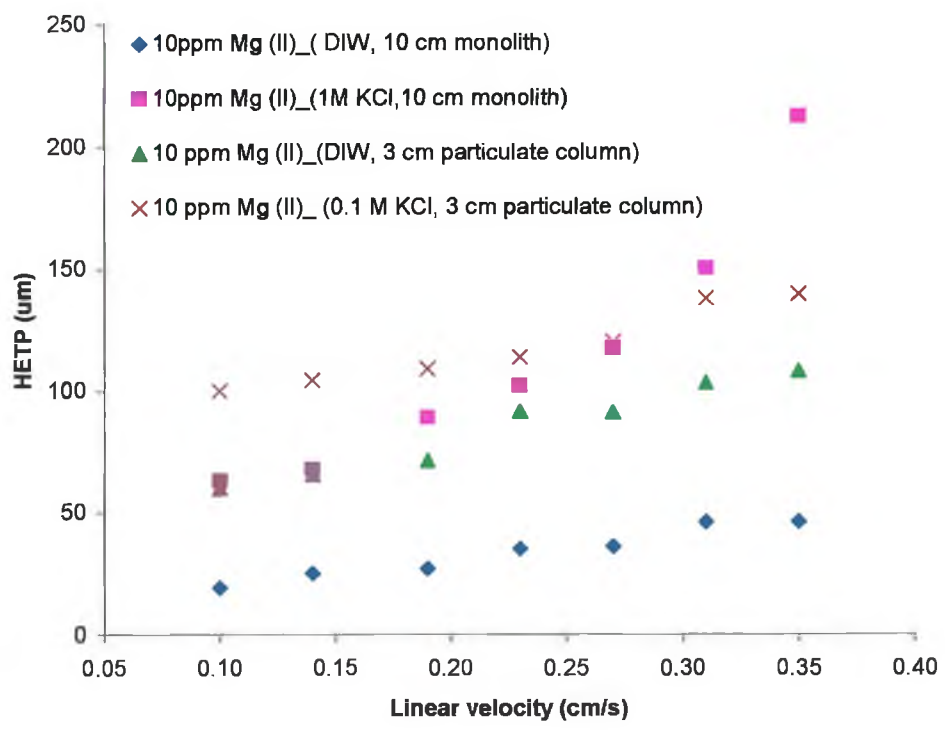
samples at higher flow rates, and standard addition calibration should be used for quantitative analysis. It is very interesting to note, that for the standards prepared in deionised water, the van Deemter curves appear to be levelling off at the higher eluent flow rates, with this being particularly evident with the Ca (II) peak. The results obtained for the separation of Mg (II) and Ca (II) in the DIW indicate that for low ionic strength samples, this IDA functionalised monolithic column could be used at even higher flow rates (4–10 mL/min) without further substantial loss in efficiency, provided a suitable detection method could be found.

***3.3.2.4: Comparison of efficiency studies performed on a 10 cm IDA silica monolithic column and a 3 cm IDA silica particle-packed column.***

In Section 3.3.2.3, the effect of the sample matrix on the efficiency of the Mg (II) and the Ca (II) peaks was demonstrated. In order to substantiate these results, a similar experiment was performed using a 3 cm silica IDA particle-packed column. However, for Mg (II) and Ca (II) to be retained on the lower capacity IDA silica particle-packed column, the eluent concentration had to be reduced from 1 M to 0.08 M KCl (pH 4.85). Using this lower ionic strength eluent, there would be a larger contribution from the ion-exchange mechanism of the IDA functionality, as opposed to the chelation-exchange mechanism, which was the dominant mechanism when the 1 M KNO<sub>3</sub> eluent was employed. Due to the decrease in eluent concentration, the ionic strength of the sample matrix that could be successfully analysed was limited to less than 0.1 M KCl. A more concentrated matrix would result in possible losses in efficiency, as a result of matrix ions swamping the ion-exchange sites.

A 10 ppm mixture of Mg (II) and Ca (II) was prepared in both DIW and a 0.1 M KCl matrix, and the separation of Mg (II) and Ca (II) was achieved with a 0.08 M KCl eluent, pH 4.85, using flow rates between 1 and 4 mL/min. When a particle-packed column is employed, it is necessary to use a short column when high flow rates are required, otherwise the excessive backpressure associated with particle-packed columns is a limiting factor as to the speed at which the separation can be achieved.

(a)



(b)

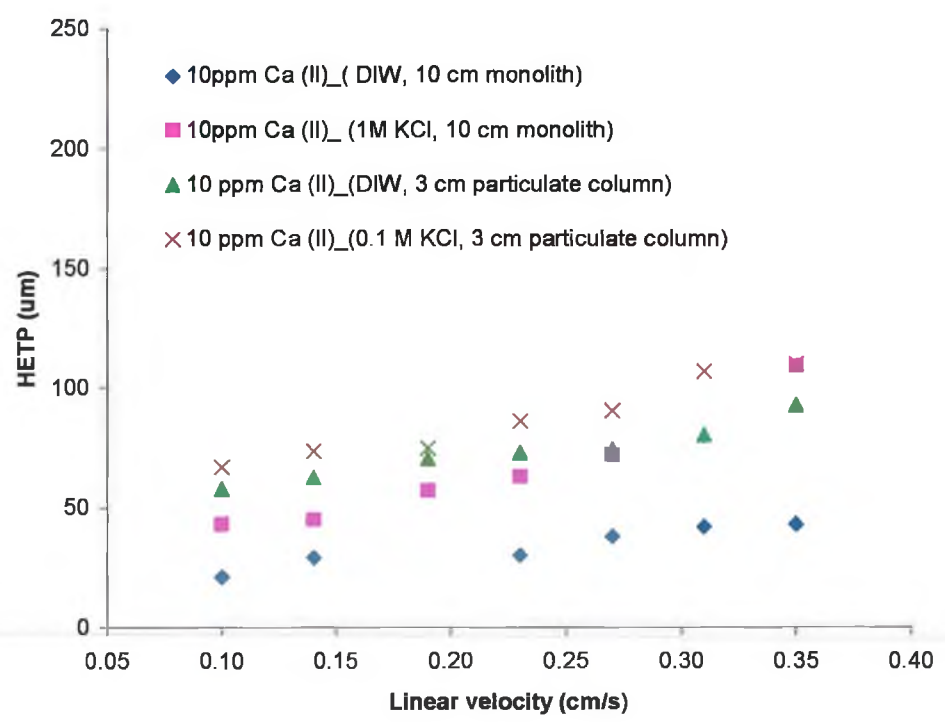


Figure 3.5: Overlay of (a) the Mg (II) van Deemter curves and (b) the Ca (II) van Deemter curves obtained on a 10 cm IDA silica monolith and a 3 cm particle-packed IDA silica gel column.

The van Deemter curves for Mg (II), using both the 10 cm monolithic and 3 cm particle-packed IDA silica columns were overlaid, see Fig. 3.5 (a), and the Ca (II) van Deemter plots for both columns and the different sample matrices were also overlaid, see Fig. 3.5 (b). In the case of the Mg (II) van Deemter plots, two observations can be made. Firstly, as expected, the efficiency of the Mg (II) analyte peak on the monolithic column was greater than the values observed for the 3 cm particle-packed column, because mass transfer in monoliths is controlled by convection instead of diffusion [10]. In contrast to diffusion, for which the concentration gradient is the driving force, convection uses flow to dramatically accelerate the mass transfer of solutes. As a direct result of the convective flow of the solution through the pores of monolithic columns, the mass transfer resistance is reduced tremendously [11]. Secondly, the matrix effect is clearly visible for both the 3 cm particle-packed and 10 cm monolithic column, i.e. the samples prepared in the KCl matrix demonstrated a significantly greater loss of peak efficiency with increasing flow rate, than observed for the Mg (II) standard prepared in DIW alone.

The efficiency values for the Ca (II) peaks analysed on both columns were observed to exhibit an overall improvement when compared to the results presented in the Mg (II) van Deemter curves. A possible reason for this observation could be due to the much smaller interaction time experienced by the early eluting Mg (II) with the IDA silica phases, therefore, increasing the flow rate would lead to more significant decreases in peak efficiency. As in the case of the Mg (II) results, the Ca (II) samples prepared in both the 0.1 M KCl (for the 3 cm particle-packed column), and 1 M KCl (for the 10 cm monolithic column) matrices showed decreased peak efficiency compared to the Ca (II) samples prepared in DIW alone.

### 3.3.2.5: A sub-minute separation of Mg (II) and Ca (II) in 1 and 2 M KCl brines

By exploiting the fact that monolithic stationary phases can operate at elevated flow rates, with associated low column back pressures, the possibility of achieving a sub-minute separation of Mg (II) and Ca (II) in the high ionic strength KCl brines was investigated.

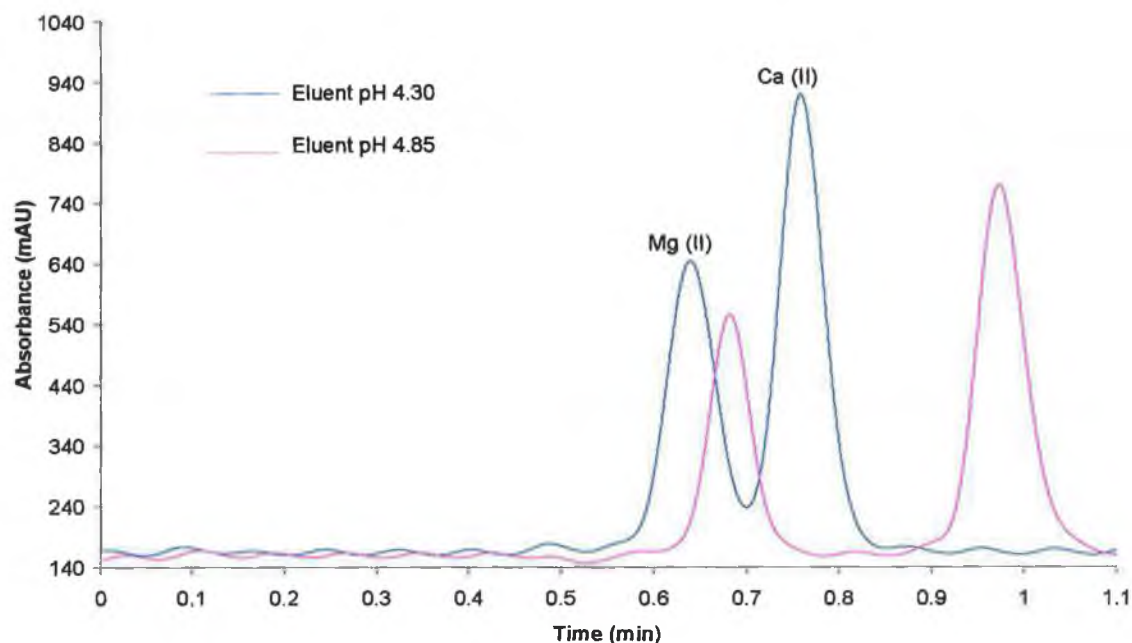


Figure 3.6: The separation of a 10 ppm mixture of Mg (II) and Ca (II) prepared in a 1 M KCl matrix. Eluent conditions: 1 M KNO<sub>3</sub> eluent adjusted to pH 4.30 (blue trace) and pH 4.85 (pink trace), flow rate 4 mL/min. Detection conditions: 0.4 mM *o*-CPC in 0.25 M boric acid, pH 10.5, was employed as the post-column reagent and the resultant *o*-CPC-metal complexes were monitored at 570 nm.

Using a 1 M KNO<sub>3</sub> eluent (pH 4.85), the separation of a 10 ppm mixture of Mg (II) and Ca (II) in a 1 M KCl matrix was possible in 66 seconds, using a flow rate of 4 mL/min. A faster separation of Mg (II) and Ca (II) was achieved by decreasing the eluent pH to 4.30, see Fig. 3.6. The reduction in eluent pH resulted in a decrease in the retention time of Mg (II), and in particular, Ca (II), as the retention of Ca (II) was previously shown in Chapter 2, to be dominated by chelation. At a flow rate of 4 mL/min, using the 1M KNO<sub>3</sub> eluent (pH 4.30), the run time for the separation of Mg (II) and Ca (II) was 50 seconds.

Although the decrease in eluent pH resulted in a sub-minute separation of Mg (II) and Ca (II), the data presented in Table 3.1 demonstrates that baseline resolution of the Mg (II) and Ca (II) peaks was not observed at pH 4.30.

Table 3.1: The resolution values obtained for the 10 ppm Mg (II), Ca (II) mixture prepared in both 1 and 2 M KCl brines, separated using 1 M KNO<sub>3</sub> eluent, with a flow rate of 4 mL/min.

Analyte	Eluent pH 4.30	Eluent pH 4.85
	<b>Resolution</b>	
10ppm Mg, Ca in 1M KCl	1.26	2.61
10ppm Mg, Ca in 2 M KCl	1.08	2.20

Therefore, instead of decreasing the eluent pH, the run time of the Mg (II) and Ca (II) separation was reduced by further increasing the eluent flow rate. However, if a flow rate of 5 mL/min was to be successfully employed, an additional HPLC pump was required to deliver the PCR, as the pressure driven Reagent Delivery Module could not provide sufficient PCR flow. Although the introduction of the second pump did cause some obvious additional 'pump noise', Fig. 3.7 shows the separation of a mixture of 10 ppm Mg (II) and Ca (II) in both 1 and 2 M KCl brines, and the analyte peaks were clearly visible and well resolved in less than 40 seconds.

It is important to point out the significance of the separation presented in Fig. 3.7. In this chromatogram, the sample presented has a ratio of matrix ion to analyte ion of ~ 8000:1 and direct injection of this sample was possible without any pre-treatment. Also, because the run time is less than 40 seconds, the analysis rate is greater than 90 samples per hour, which is considerably faster than previously published methods, including those employing spectrophotometry and FIA.

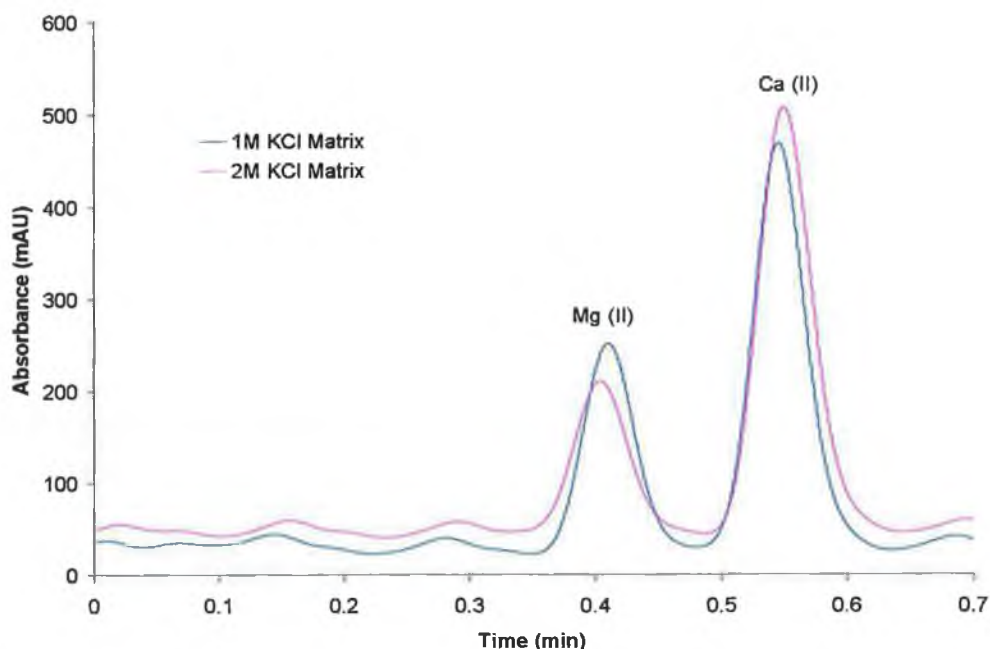


Figure 3.7: Separations of a 10 ppm Mg (II) and Ca (II) mixture prepared in 1 M KCl matrix (blue trace) and 2 M KCl matrix (pink trace) on a 10 cm IDA functionalised silica monolith. Eluent conditions: 1 M KCl eluent, pH 4.85, flow rate 5 mL/min. Detection conditions: 0.4 mM *o*-CPC in 0.25 M boric acid, pH 10.5, was employed as the post-column reagent and the resultant *o*-CPC- metal complexes were monitored at 570 nm.

### 3.3.2.6: Analytical Performance Data

The quantitative performance of the described system was evaluated under elevated eluent flow conditions using a 1 M KNO<sub>3</sub> eluent, adjusted to pH 4.85.

**Precision study:** at a flow rate of 4 mL/min, nine repeat injections for a 6 ppm Mg (II) and Ca (II) mixture prepared in 1 M KCl, resulted in average retention times of 0.6 minutes for Mg (II) and 0.8 minutes for Ca (II), with % RSD values of 1.2 % and 0.8 % respectively. For the peak area precision study, the % RSD for the Mg (II) peak area was determined to be 3.3 % and for the Ca (II) peak area, a % RSD value of 2.0 % was calculated. The effect of sample matrix on precision was also studied. Ten repeat injections of a 2 ppm Mg (II) and Ca (II) mixture prepared in both 1 and 2 M KCl were performed at a flow rate of 3 mL/min. For the 1 M KCl matrix, the % RSD values calculated for the retention time and peak area of Mg (II) are 0.3 % and 4.1 %, respectively.

and for the Ca (II) peak, the % RSD for the retention time was determined to be 0.2 % and 2.5 % for peak area precision. When the sample matrix concentration was increased to 2 M KCl, there was a decrease in the quality of the analytical performance data. The % RSD for retention time and peak area of Mg (II) increased to 1.6 and 4.5 % respectively and in the case of the Ca (II) peak, the % RSD for the retention time increased to 1.2 % and 3.0 % for the peak area precision.

**Linearity Study:** Linearity was determined over the range 2-10 ppm (n=5) for Mg (II) and Ca (II) mixture prepared in both 1 and 2 M KCl, at a flow rate of 4 mL/min. The correlation coefficients obtained for the Mg (II) calibration curves were  $R^2=0.9952$ , for the Mg (II) standards prepared in 1 M KCl, and  $R^2=0.9848$  for the 2 M KCl sample matrix. For the Ca (II) standards prepared in 1 M KCl, the correlation coefficient value obtained was  $R^2=0.9952$ , and  $R^2=0.9918$  for the 2 M KCl sample matrix. The resolution of the Mg (II) and Ca (II) peaks was also calculated for each mixed standard injection and found to range from 2.56 to 2.79 for the standards prepared in 1 M KCl, and from 2.10 to 2.38 for the standards prepared in the 2 M KCl. This linearity study was repeated at a flow rate of 3 mL/min, over the same range, 2 to 10 ppm (n=5), for the mixture of Mg (II) and Ca (II) prepared in 1 and 2 M KCl. In the case of the Mg (II) standard curves, there was a similar decrease in the correlation coefficient values, with  $R^2=0.9935$  obtained for the standards prepared in 1 M KCl and  $R^2=0.9818$  for the standards prepared in 2 M KCl. For the Ca (II) standard curves, once again, there was little difference between the correlation coefficients for the 1 and 2 M KCl matrices, with the values obtained being  $R^2=0.9976$  and  $R^2=0.9915$  respectively.

Therefore, the use of elevated flow rates does not dramatically affect the quality of the linearity coefficients obtained for either Mg (II) or Ca (II). However, a slight decrease in  $R^2$  values for both Mg (II) and Ca (II) was observed when the KCl sample matrix was increased from 1 to 2 M.

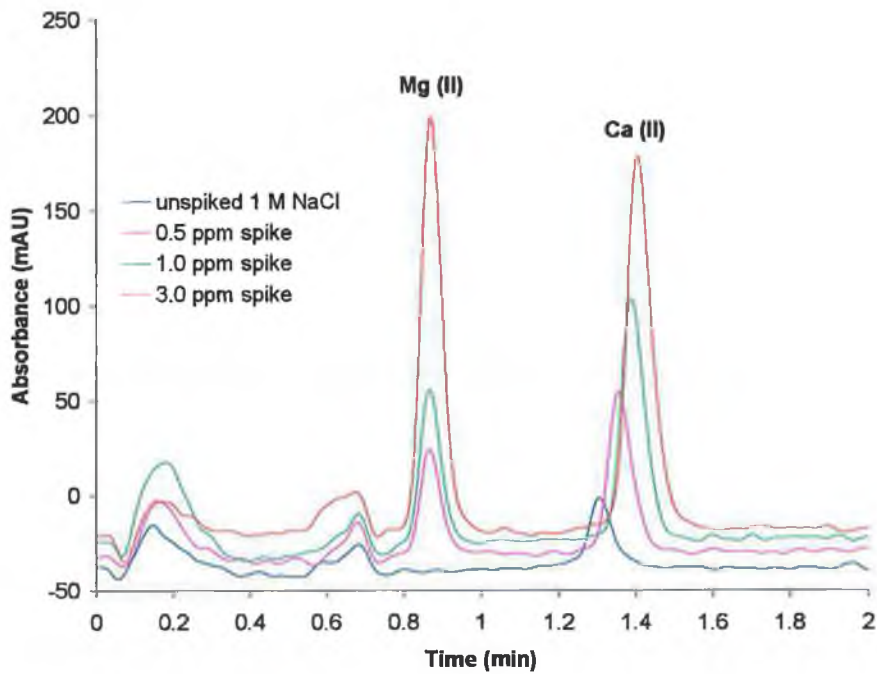
Table 3.2: Summary of analytical performance data for the 10 cm IDA silica monolith.

	<b>Mg (II)</b>	<b>Ca (II)</b>
<b>Reproducibility (% RSD), (n=9)</b>		
Retention time	1.2 %	0.8 %
Peak area	3.3 %	2.0 %
<b>Linearity (n=5)</b>		
2 - 10 mg/L, in 1 M KCl matrix	$R^2 = 0.9952$	$R^2 = 0.9945$
2 - 10 mg/L, in 2 M KCl matrix	$R^2 = 0.9848$	$R^2 = 0.9918$
<b>Standard Addition (n=6)</b>		
0.25 -10 mg/L, in 1 M KCl matrix	$R^2 = 0.9994$	$R^2 = 0.9921$
0.25 -10 mg/L, in 1 M NaCl matrix	$R^2 = 0.9982$	$R^2 = 0.9883$
<b>Resolution</b>		
Sample matrix: 1 M KCl	2.6 - 2.8	
Sample matrix: 2 M KCl	2.1 - 2.4	

### 3.3.2.7: Quantitative determination of laboratory grade KCl and NaCl salts

Laboratory grade KCl and NaCl salts (1M solutions) were analysed using standard addition for Mg (II) and Ca (II) impurities, see Fig. 3.8 and 3.9. Due to the unavailability of KNO<sub>3</sub> for eluent preparation, 1 M NaNO<sub>3</sub> was used as a suitable eluent replacement. In the case of the KCl salt samples, a matrix peak due to excess potassium in the sample could interfere with the accurate quantitation of the Mg (II) analyte peak at elevated flow rates. However, no such matrix peak would be expected for the NaCl samples, because the eluent cation matches that of the sample. Therefore, the eluent pH was increased by 0.5 pH units to 5.30. This increase in pH was necessary to eliminate the problem of the matrix peak interfering with the accurate quantitation of the Mg (II) peak in the 1 M KCl samples.

(a)



(b)

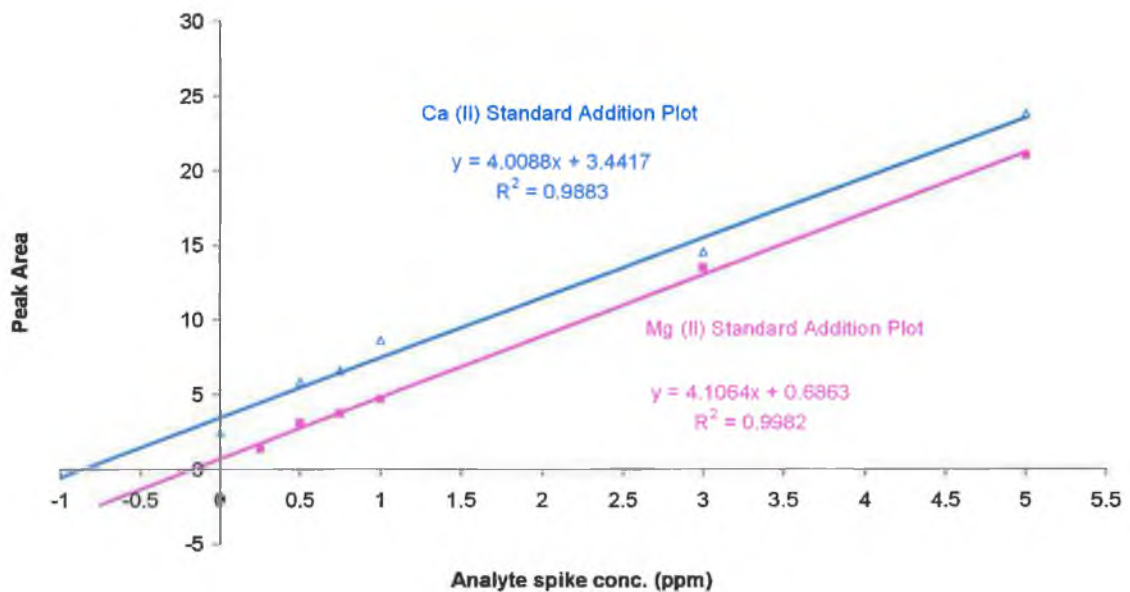
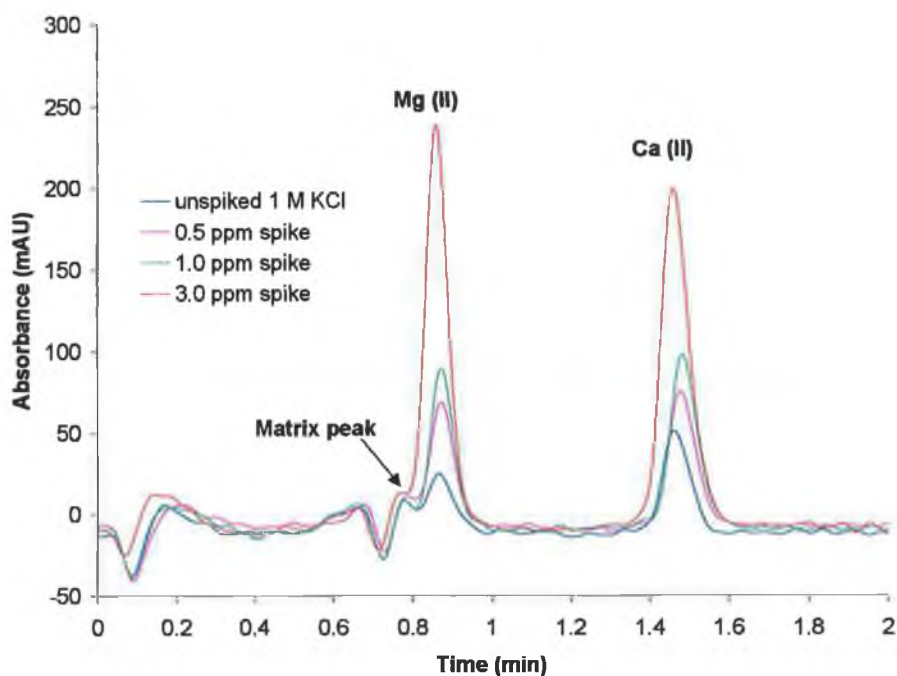


Figure 3.8: a) Overlay of unspiked 1 M NaCl and 1 M NaCl samples spiked with 0.5, 1.0 and 3.0 ppm Mg (II) and Ca (II), b) Standard addition calibration curves for Mg (II) and Ca (II) in a 1M laboratory grade NaCl sample. Eluent conditions: 1M NaNO<sub>3</sub> eluent, pH 5.30, flow rate 2.5 mL/min.

(a)



(b)

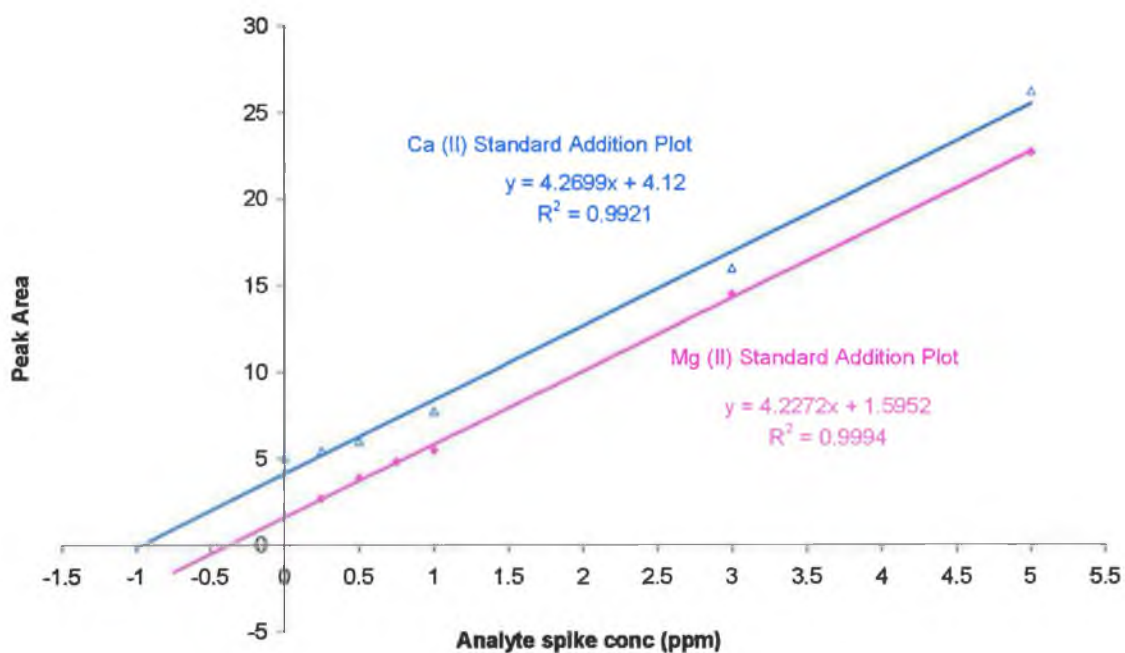


Figure 3.9: a) Overlay of unspiked 1 M KCl and 1 M KCl samples spiked with 0.5, 1.0 and 3.0 ppm Mg (II) and Ca (II), b) Standard addition calibration curves for Mg (II) and Ca (II) in a 1M laboratory grade KCl sample. Eluent used 1M NaNO<sub>3</sub>, pH 5.30, flow rate 2.5 mL/min.

Standard additions ranging from 0.25 to 5 ppm Mg (II) and Ca (II), (n=6) were investigated. A linear response was obtained for the standard addition calibration graphs constructed for each sample solution. For the 1 M NaCl sample, the resulting correlation coefficient obtained for the Mg (II) standard addition curve was  $R^2=0.9982$ , while for the Ca (II) standard addition curve the value obtained was  $R^2=0.9883$ . When the 1 M KCl sample was analysed, correlation coefficient values of  $R^2=0.9994$  and  $R^2=0.9921$  were obtained for the Mg (II) and Ca (II) calibration curves respectively.

Using these standard addition calibration curves, the concentration of Mg (II) was determined to be 0.37 ppm in the 1 M KCl laboratory grade solution and  $< 0.2$  ppm in the 1 M NaCl laboratory grade solution. The quantitative analysis of the 1 M KCl and 1 M NaCl laboratory grade sample solutions yielded Ca (II) concentrations of 0.85 ppm and 0.26 ppm respectively.

### ***3.4: Conclusion***

The application of a novel chelating-exchanger for the rapid and efficient separation of alkaline earth metal ions in high ionic strength matrices has been demonstrated. Using this IDA silica monolithic column, the determination of traces of alkaline earth metal ions in NaCl and KCl brines (up to 2 M) was achieved in less than 40 seconds, and the Mg (II) and Ca (II) impurities present in laboratory grade KCl and NaCl were also determined. The separation of Mg (II), Sr (II) and Ba (II) in the presence of excess amounts of Ca (II), i.e. 1000 ppm Ca (II), was also demonstrated.

Once again, differences in efficiency and selectivity between the IDA silica monolith and IDA silica particle packed columns were investigated. Peak efficiencies for the IDA monolith were found to be superior to the particle packed column for the alkaline earth metals. The results also indicated some unusual behaviour for the effect of sample ionic strength on peak efficiency at elevated flow rates, and also how the sample matrix marginally affected the selectivity, this effect being common to both IDA monolithic and IDA silica gel particle-packed columns.

## ***References***

1. P. N. Nesterenko and P. Jones, *J. Chromatogr. A*, 770 (1997) 129.
2. B. Paull and P. N. Nesterenko, *Analyst* 130 (2005) 134.
3. C. Ó Ríordáin, P. N. Nesterenko, B. Paull, *J. Chromatogr. A*, 1075 (2005) 71.
4. S. Unger, D. Schmitz, K. H. Viehweger, Determination of trace levels of perchlorate using IC with conductivity detection and a special monolithic column: IICS Symposium, Trier, Germany, 2004, p 29.
5. Q. Xu, K. Tanaka, M. Mori, M. I. Helaleh, M. Ikedo, W. Hu, K. Hasebe, H. Toada, *J. Chromatogr. A*, 997 (2003) 183.
6. P. Jones and P. N. Nesterenko, *J. Chromatogr. A*, 789 (1997) 413.
7. W. Bashir and B. Paull, *J. Chromatogr. A*, 907 (2001) 191.
8. M. Macka, B. Paull, P. Anderson, P. R. Haddad, *J. Chromatogr. A*, 767 (1997) 303.
9. P. Jones, M. Foulkes, B. Paull, *J. Chromatogr. A*, 673 (1994) 173.
10. S. Xie, *Retention Times (Newsletter of Separation Science)*, XI (2002) issue 3.
11. H. Zou, X. Huang, Y. Mingliang, Q. Luo, *J. Chromatogr. A*, 954 (2002) 5.

## **Chapter 4**

### ***Chelation-exchange of transition and heavy metal ions on an IDA functionalised silica monolithic column***

## ***4.1: Introduction***

The analysis of soils, water and air for transition and heavy metals has received increasing attention in recent years, as a result of accelerated industrialisation combined with the rapid increase in population growth [1-3]. For the analysis of transition and heavy metals, chelation-exchange is a specialised ion chromatographic technique, where separation is controlled by the thermodynamics and kinetics of the metal-ligand complex formation and dissociation.

High stability and separation efficiency, with optimal selectivity for transition metals, have been demonstrated for chelating-exchangers with iminodiacetic acid (IDA) functionality bonded to silica [4-7]. The popularity of silica stationary phases with IDA functional groups can be attributed to the fact that many of the other chelating functions studied give selectivity coefficients that are too large to enable multi-element separations, without gradient elution strategies. Furthermore, chelating ligands with large metal stability constants can produce very broad peaks due to slow dissociation kinetics. The IDA functional group produces good performance in high performance chelation ion chromatography because it generates reasonably fast kinetics combined with selectivity coefficients that are not too large. However, although silica bonded with IDA groups form kinetically labile surface complexes with most transition metals, the high stability of complexes of transition metals with the IDA groups demands the use of strong eluents for the chromatographic separation of metals [4,8,9].

### ***4.1.1: Objective***

In this Chapter, the chromatographic behaviour of selected transition and heavy metal ions using simple inorganic salts, as opposed to complexing agents in the eluent, was studied. Hence, the aim of this study was to determine the true selectivity of the IDA functionalised silica monolith for transition and heavy metal ions. In addition, the use of elevated flow rates was employed to achieve rapid separations of selected transition and heavy metal ions, without the need for complex gradient elution.

## ***4.2: Experimental***

### ***4.2.1: Modification of silica monolith***

As detailed in Section 2.2.1, Chapter 2.

### ***4.2.2: Instrumentation***

As detailed in Section 2.2.2, Chapter 2.

### ***4.2.3: Reagents***

The eluent and post-column reagent (PCR) solutions were prepared using DIW from a Millipore Milli-Q water purification system (Bedford, MA, USA). Where post-column detection was required for the detection of transition/heavy metal ions, 4-(2-pyridylazo) resorcinol (PAR) was used (Sigma-Aldrich). The PCR solution consisted of 0.1 mM PAR, 100 mM NaHCO<sub>3</sub>, 5 mM Na<sub>2</sub>CO<sub>3</sub> adjusted to pH 9.8 (monitored at 495 nm). Potassium nitrate, potassium chloride and sodium chloride salts were all obtained from Fluka Chemie (Buchs, Switzerland), as was the nitric acid used to control of eluent pH. All eluents, reagents and standard solutions prepared were filtered through a 0.45 µm filter and degassed using sonication. Low level standard solutions of all metal ions were generally made up freshly each day from stock solutions prepared from nitrate, chloride or sulphate salts (1000 ppm) and stored in 1% nitric acid.

## ***4.3: Results and discussion***

### ***4.3.1: Separation of transition and heavy metal ions using a non-complexing eluent***

The chromatographic behaviour of transition and heavy metal ions on the IDA functionalised silica monolithic column, using a 0.035 M KCl and 0.065 M KNO<sub>3</sub> eluent, pH 2.5, was compared to the results obtained by Bashir and Paull [7] using identical eluent conditions and 25 cm particle packed IDA silica gel column. As Fig. 4.1 demonstrates, the cation elution order on the monolithic column was Mn (II), followed by Co (II), Cd (II) and Zn (II). In addition, the Co (II) peak appeared to be

split (this peak splitting may be as a result of unknown redox chemistry,  $\text{Co (II)} \leftrightarrow \text{Co (III)}$  taking place within the monolith), with the Co (II) artefact eluting immediately after Cd (II).

However, on the particle-packed IDA silica gel column, the Cd (II) peak was observed to elute before the Co (II) peak, using an eluent composed of 0.035 M KCl and 0.065 M  $\text{KNO}_3$  (pH 2.5), with retention times of approximately 6 and 10 minutes respectively [7]. Another difference observed between the separations obtained on monolithic and particle-packed IDA silica columns was the shape of the Zn (II) peak. Even though the Zn (II) peak had a longer retention time on the particle-packed IDA silica column (~20 minutes), a sharper peak was observed than the peak observed in the separation on the monolithic column, where Zn (II) was observed to elute as an extremely broad peak after 15 minutes. To try and eliminate the observed problems for the Co (II) and Zn (II) peaks, the 10 cm IDA silica monolith was washed with a solution of 10 mM dipicolinic acid, to remove any metal cations bound to the IDA silica surface. However, this regeneration procedure did not improve the Zn (II) peak shape or the problem of the Co (II) peak splitting.

To investigate the problems encountered with the split Co (II) peak in the separation of the mixture shown in Fig. 4.1 (a) above, a series of Mn (II), Co (II) and Cd (II) standard mixtures were prepared, each spiked with increasing amounts of the Co (II) standard, and injected using identical experimental conditions. Fig. 4.1 (b) demonstrates that, as the concentration of the Co (II) standard increased (20 to 40  $\mu\text{M}$ ), there was a corresponding increase in the size of the peak observed eluting after the Cd (II) peak, while as expected, the Mn (II) and Cd (II) peak areas were observed to remain constant. As the result of this split Co (II) peak, the speed at which the separation could be performed was limited, as an increase in flow rate led to a decrease in the resolution between the Cd (II) peak and the split Co (II) artefact. Above a flow rate of 2 mL/min, the co-elution of the Cd (II) and the second Co (II) peak occurred, and therefore, accurate integration of the Cd (II) concentration was not possible.

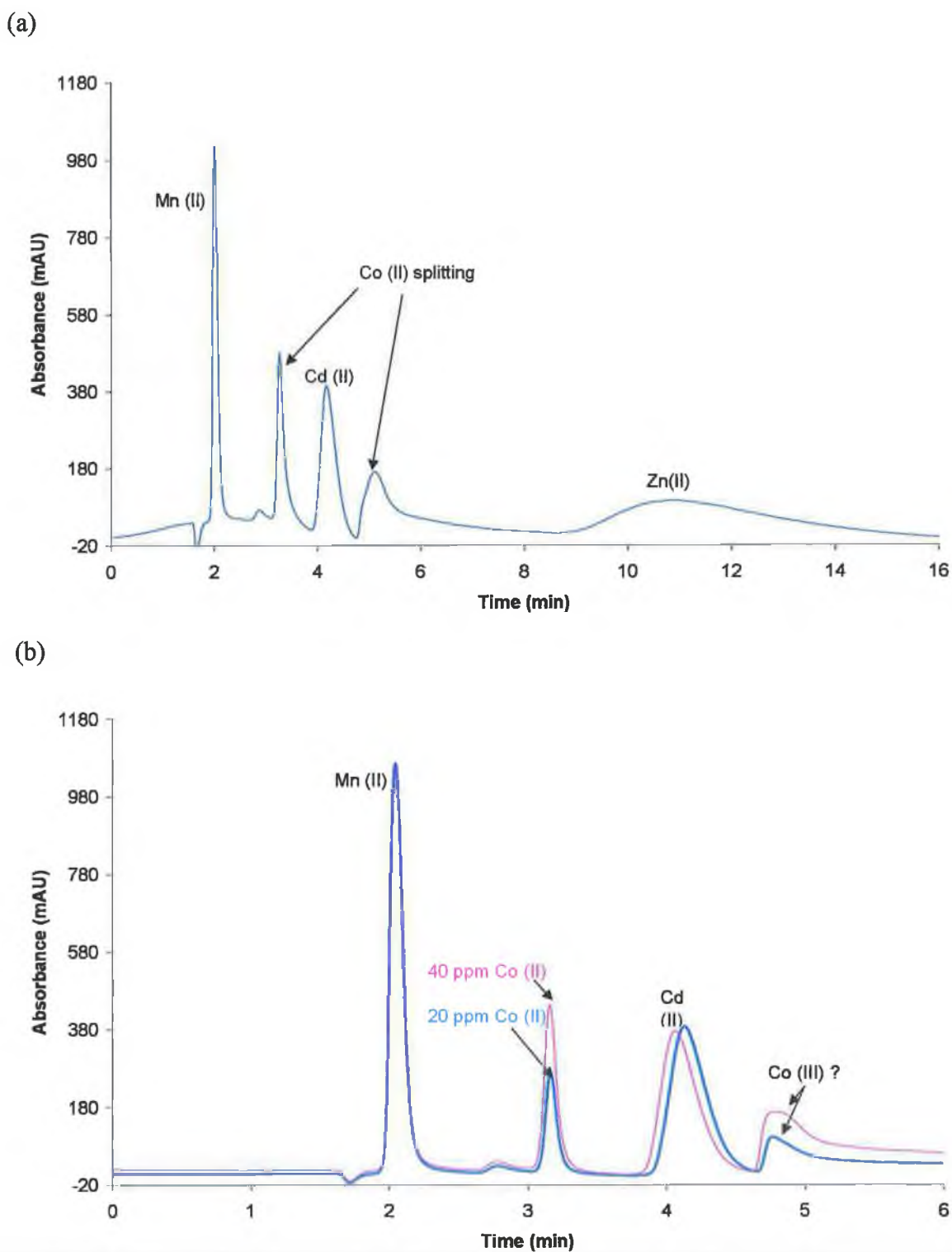


Figure 4. 1: The separation of (a) Mn (II), Co (II), Cd (II) and Zn (II) on a 10 cm IDA functionalised silica monolith and (b) Mn (II), Co (II) and Cd (II) mixture spiked with 20ppm and 40 ppm Co (II). Eluent conditions: 0.035 M KCl and 0.065 M KNO<sub>3</sub>, pH 2.5, flow rate 1 mL/min. Detection conditions: post-column reaction with 0.1 mM PAR, 100 mM NaHCO<sub>3</sub>, 50 mM Na<sub>2</sub>CO<sub>3</sub>, pH 9.8, monitored at 495 nm.

#### ***4.3.2: Simultaneous separation of alkaline earth and transition metals ions***

To achieve a simultaneous separation of alkaline earth and transition metal ions, two eluent parameters had to be optimised, namely the ionic strength of the eluent and the eluent pH. An optimised separation of Mg (II), Ca (II), Mn (II), Cd (II), Co (II) and Zn (II) was demonstrated by Bashir and Paull [7], using an eluent of 0.035 M KCl and 0.065M KNO<sub>3</sub>, adjusted to pH 2.5. Under these eluent conditions, Mg (II) and Ca (II) were unretained on the IDA silica monolith. By decreasing the ionic strength below 0.1 M, increased retention of Mg (II) and Ca (II) through ion-exchange should be possible. In previous studies involving IDA-silica stationary phases it has been shown that considerable retention of alkali and alkaline earth metal ions could be achieved through simple ion-exchange interactions with the dissociated carboxylic acid groups of the IDA ligand ( $pK_{a1}$  1.76,  $pK_{a2}$  2.70) [10].

Using a 0.1 M KNO<sub>3</sub> eluent, Mg (II) and Ca (II) were retained, but not resolved. In order to facilitate the separation of Mg (II) and Ca (II), the ionic strength had to be decreased to 0.08 M KNO<sub>3</sub> and the pH had to be adjusted to pH 4.0. Fig. 4.2 shows the resulting separation of Mg (II), Ca (II) and Mn (II). The weak response of the Mg (II) and Ca (II) signals is a result of the use of 4-(2-pyridylazo)-resocriinol (PAR) as the post-column reagent. Although a separation of Mg (II), Ca (II) and Mn (II) was achieved, the increase in pH resulted in excessive retention of the other analytes, namely Co (II), Cd (II) and, especially, Zn (II). The addition of a complexing agent, e.g. citric or tartaric acid, to the KNO<sub>3</sub> eluent would be required for the elution of Co (II), Cd (II) and Zn (II).

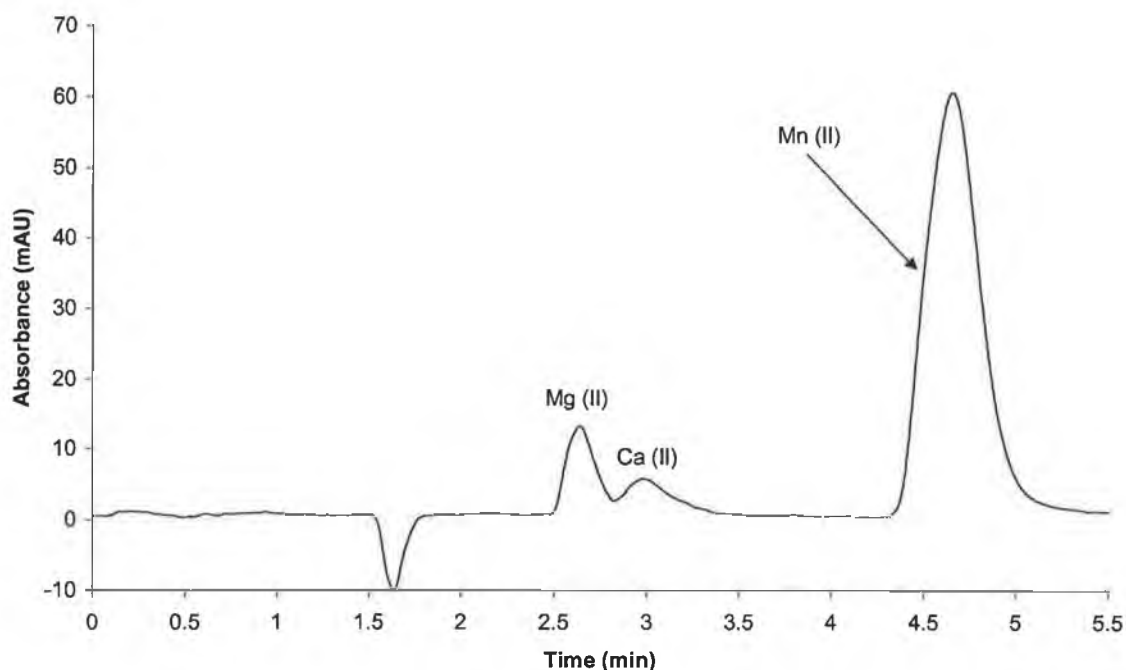
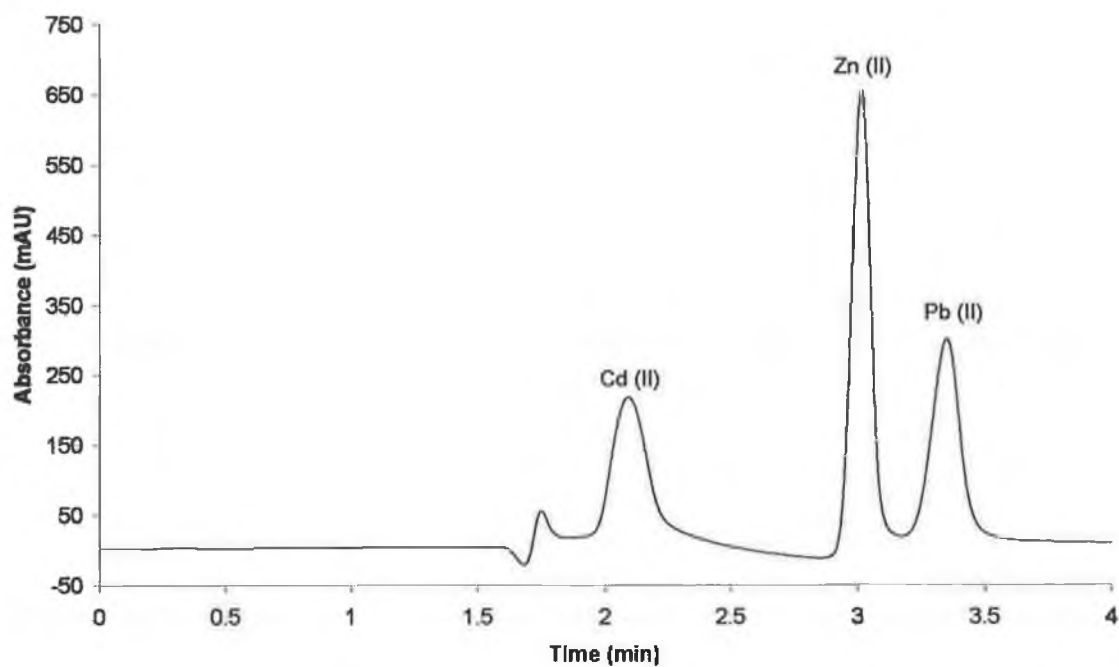


Figure 4.2: The separation of Mg (II), Ca (II) and Mn (II) on a 10 cm IDA functionalised silica monolith. Eluent conditions: 0.08 M KNO<sub>3</sub>, pH 4.0, flow rate 1 mL/min. Detection conditions: post-column reaction with 0.1 mM PAR, 100 mM NaHCO<sub>3</sub>, 50 mM Na<sub>2</sub>CO<sub>3</sub>, pH 9.8, monitored at 495 nm.

#### 4.3.3: Optimisation of Mn (II), Cd (II), Co (II), Zn (II) and Pb (II) separation

As Fig. 4.3 (a) demonstrates, the separation of a 2 ppm mixture of Cd (II), Zn (II) and Pb (II) was achieved using a 0.4 M KCl eluent, adjusted to pH 2.05. Although Cd (II) was only retained for just over 2 minutes, there was significant peak broadening relative to the later eluting Zn (II) and Pb (II) peaks. A consequence of this peak broadening was the significant loss of peak efficiency observed for the Cd (II) peak, compared to the Zn (II) and Pb (II) peak efficiencies. The effect of eluent flow rate on peak efficiency is demonstrated by the van Deemter curves presented in Fig. 4.3 (b). When the eluent flow rate was increased to 3 mL/min, the separation of Cd (II), Zn (II) and Pb (II) was possible in less than 90 seconds. However, at flow rates greater than 2 mL/min, the resolution between Zn (II) and Pb (II) was greatly reduced and a reduction in peak efficiency was observed, particularly in the case of the Cd (II) peak.

(a)



(b)

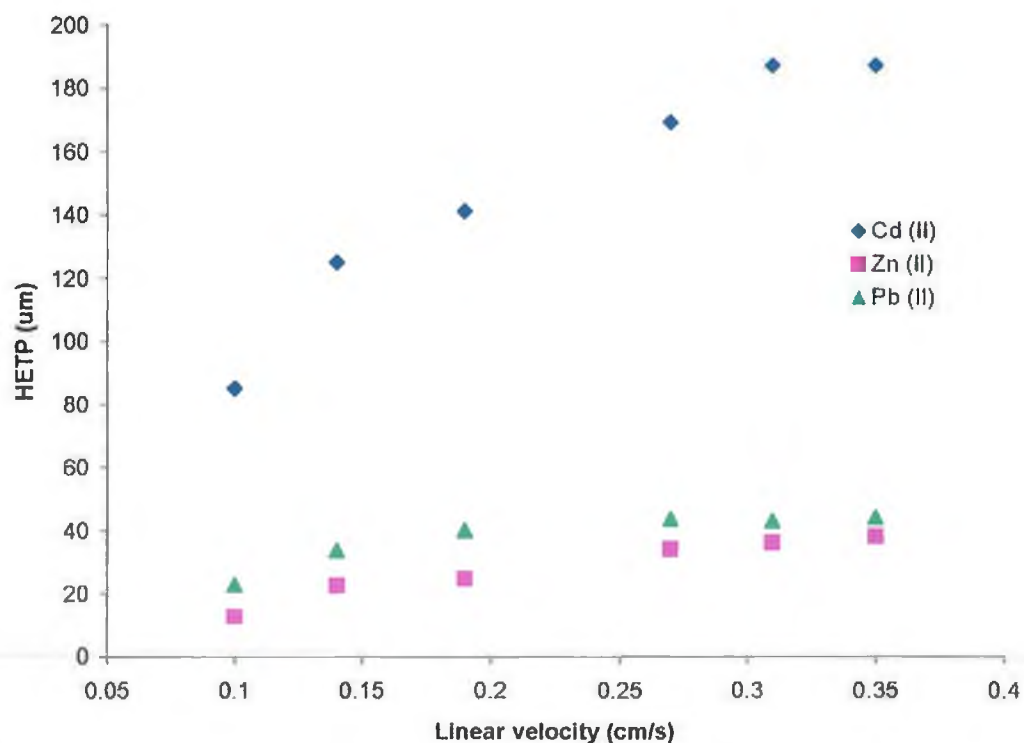


Figure 4.3: (a) The separation of Cd (II), Zn (II) and Pb (II) on a 10 cm IDA silica monolith. Eluent conditions: 0.4 M KCl eluent, adjusted to pH 2.05, flow rate 1 mL/min and (b) van Deemter plot for Cd (II), Zn (II) and Pb (II).

Eluent parameters described in Fig. 4.3 (a) were re-optimised to facilitate the separation of Mn (II), Co (II), Cd (II), Zn (II) and Pb (II). Initially, a reduction of the eluent ionic strength was investigated, because the Mn (II), Co (II) and Cd (II) peaks were observed to co-elute under the eluent conditions of 0.4 M KCl, adjusted to pH 2.05. Table 4.1 shows the results obtained when the ionic strength was reduced from 0.4 to 0.2 M KCl, pH 2.05. Only the retention time of the Pb (II) peak was significantly affected by the change in eluent ionic strength. The reason for the behaviour of the Pb (II) can be attributed to the strong tendency of Pb (II) to form chloro-complexes. This will be discussed in more detail in Section 4.4. The results presented in Table 4.1 demonstrate that the decrease in eluent ionic strength had no impact on the resolution observed between the Mn (II), Co (II) and Cd (II) peaks due to the insensitivity of these analytes to changes in eluent ionic strength.

Table 4.1: The effect of KCl eluent concentration (pH 2.0) on the retention of Co (II), Cd (II), Zn (II) and Pb (II) on a 10 cm IDA functionalised silica monolith, flow rate 1 mL/min.

Analyte	Retention factor ( <i>k</i> )			
	0.4 M KCl	0.35 M KCl	0.3 M KCl	0.2 M KCl <sup>1</sup>
5ppm Co (II)	0.1	0.1	0.1	0.1
5ppm Cd (II)	0.2	0.2	0.2	0.3
2 ppm Zn (II)	0.7	0.8	0.8	0.8
20ppm Pb (II)	1.0	1.2	1.5	2.2

Therefore, to separate the Mn (II), Co (II) and Cd (II) peaks, the eluent pH was increased from pH 2.05 to 2.5. As discussed previously, pH is most important factor governing selectivity in chelation-exchange. It is clear from the results shown in Table 4.2 and Fig. 4.4, that this increase in pH allowed the separation of Mn (II), Cd (II), Co (II), Zn (II) and Pb (II) to be performed on the IDA silica monolith. The observed elution order reflects the increase in stability constant for the complexation of the metal cations with IDA, i.e. Cd (II)  $K_1 = 5.73$ , Co (II)  $K_1 = 6.97$ , Zn (II)  $K_1 = 7.27$ , Pb (II)  $K_1 = 7.45$ , Ni (II)  $K_1 = 8.19$  and Cu (II)  $K_1 = 10.65$  (0.1 M KNO<sub>3</sub>, 25 °C) [11].

<sup>1</sup> 2 ppm Mn (II) was added to the four cation mixture at 0.2 M KCl, and the retention time was found to be 1.8 minutes, retention factor = 0.1.

Table 4.2: The effect of KCl eluent concentration (pH 2.5) on the retention of Mn (II), Co (II), Cd (II), Zn (II) and Pb (II) on a 10 cm IDA functionalised silica monolith, flow rate 1 mL/min.

Analyte	Retention factor ( <i>k</i> )			
	0.4 M KCl	0.3 M KCl	0.2 M KCl	0.1 M KCl
2 ppm Mn (II)	0.1	0.1	0.1	0.1
5ppm Co (II)	0.2	0.2	0.4	0.4
5ppm Cd (II)	0.4	0.6	0.6	0.7
2 ppm Zn (II)	2.9	3.0	3.1	3.8
20ppm Pb (II)	3.6	6.4	10.3	18.1

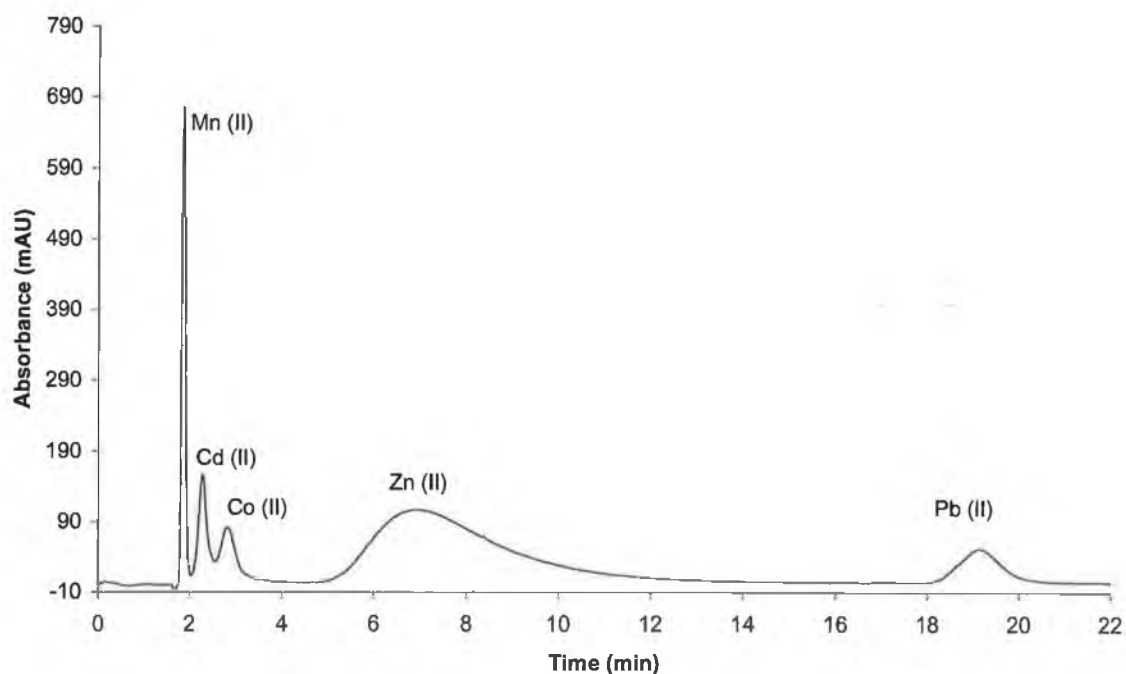


Figure 4.4: The separation of Mn (II), Cd (II), Co (II), Zn (II) and Pb (II) on a 10 cm IDA functionalised silica monolith. Eluent conditions: 0.2 M KCl eluent, adjusted to pH 2.5, flow rate 1 mL/min. Detection conditions: post-column reaction with 0.1 mM PAR, 100 mM NaHCO<sub>3</sub>, 50 mM Na<sub>2</sub>CO<sub>3</sub>, pH 9.8, monitored at 495 nm.

It is interesting to note that when the 0.2 M KCl eluent (pH 2.5) was used, Cd (II) eluted before the Co (II) peak, which is the reverse of the elution order obtained using

the 0.035 KCl, 0.065 M KNO<sub>3</sub>, pH 2.5 eluent. Using the lower ionic strength eluent, Co (II) was seen to elute before the Cd (II), while Co (II) also exhibited a split peak. No such difficulties with split Co (II) peaks were encountered in this separation, using only the KCl as the eluent salt. However, the increase in eluent pH from 2.05 to 2.5, was observed to have a detrimental effect on the Zn (II) peak shape. As Fig. 4.4 demonstrates, Pb (II) had a retention time of approximately 19 minutes, but still exhibited an acceptable peak shape, compared to the earlier eluting Zn (II) peak. Therefore, this broadening of the Zn (II) peak is believed to be as a result of some form of specific secondary interaction with the IDA monolith.

#### 4.3.3.1: Comparing IDA silica monolithic and silica gel columns

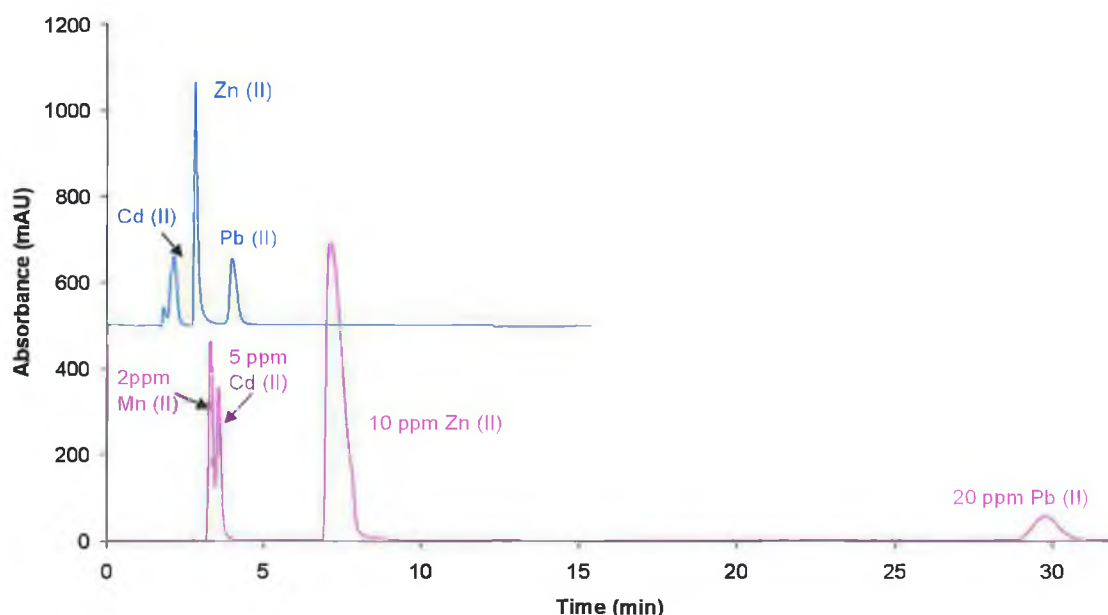


Figure 4.5: Overlays of the separation of selected transition and heavy metal cation on a 10 cm IDA functionalised silica monolith (blue trace) and a 25 cm IDA functionalised silica gel column (pink trace). Eluent conditions: 0.2 M KCl eluent, pH 2.02, flow rate 1 mL/min. Detection conditions: post-column reaction with 0.1 mM PAR, 100 mM NaHCO<sub>3</sub>, 50 mM Na<sub>2</sub>CO<sub>3</sub>, pH 9.8, monitored at 495 nm.

One of the most significant differences between the IDA silica monolithic and IDA silica gel particle-packed column was the behaviour of the Zn (II) peak. When the separation of Mn (II), Cd (II), Zn (II) and Pb (II) was performed on the 25 cm

commercially packed IDA silica gel column, the broadening of the Zn (II) peak was not observed when the eluent pH was increased from 2.02 to 2.5, see Fig. 4.5 and 4.6.

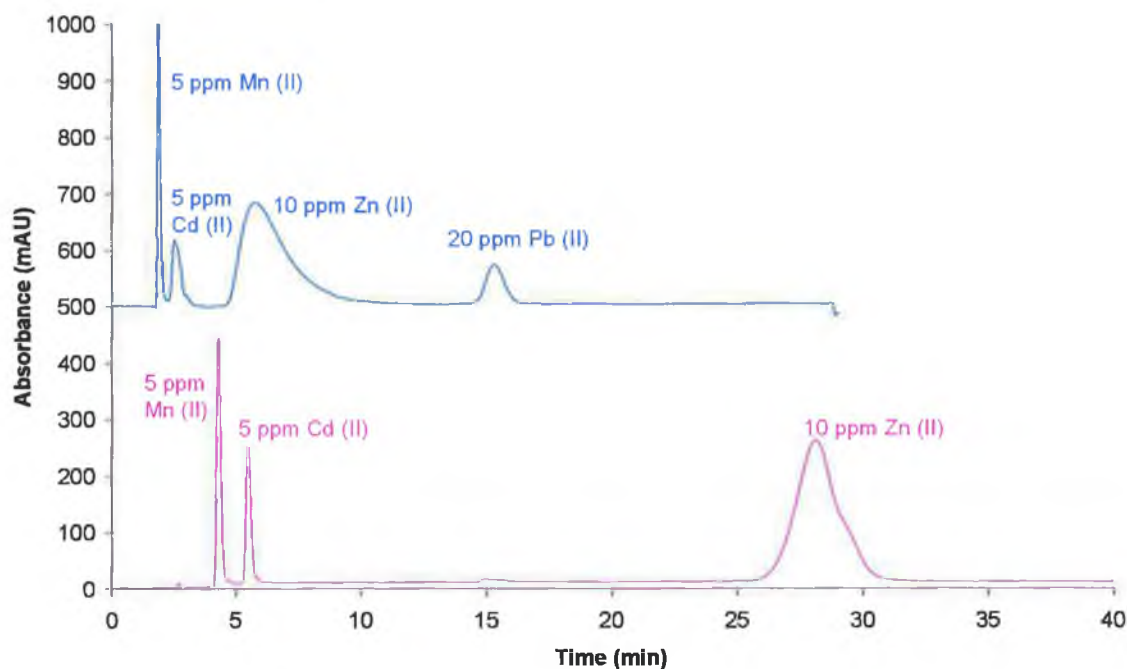


Figure 4.6: Overlays of the separation of selected transition and heavy metal cation on a 10 cm IDA functionalised silica monolith (blue trace) and a 25 cm IDA functionalised silica gel column (pink trace). Eluent conditions: 0.2 M KCl eluent, pH 2.50, flow rate 1 mL/min. Detection conditions: post-column reaction with 0.1 mM PAR, 100 mM NaHCO<sub>3</sub>, 50 mM Na<sub>2</sub>CO<sub>3</sub>, pH 9.8, monitored at 495 nm.

An increase in the pH of the 0.2 M KCl eluent, from pH 2.0 to 2.5, improved the resolution between Mn (II) and Cd (II) on the IDA silica gel particle-packed column. However, this increase in eluent pH also increased the Zn (II) retention time to ~ 30 minutes, which resulted in an expected broadening. However, this peak broadening was not as acute as observed in the case of the retention of Zn (II) on the monolithic IDA silica column, using 0.2 M KCl, pH 2.5. For the particle-packed IDA silica gel column, the separation was allowed to run for > 70 minutes, during which time, no Pb (II) peak was observed, which suggests that the Pb (II) was retained on the particle-packed IDA silica gel column.

As a result of the differences in selectivity for transition and heavy metal ions exhibited by the two IDA functionalised columns, it is clear that the lower capacity monolithic phase has the advantage that strongly retained metal ions, such as Pb (II), can be determined in the same run as Cd (II) and Zn (II), without the need for gradient elution. At pH 2.5, Pb (II) is completely retained on the IDA silica gel particle-packed column, but elutes as a well-defined peak at approximately 15 minutes on the IDA monolith, whilst still allowing the separation of Mn (II), Cd (II) and Zn (II).

#### 4.3.3.2: Investigation into the formation of chloro-complexes by Cd (II) and Pb (II)

Different inorganic eluents were investigated to determine their effect on the separation of Mn (II), Cd (II), Zn (II) and Pb (II). The overlaid chromatograms shown in Fig. 4.7 demonstrate that there was very little difference in selectivity when using either the sodium or potassium form of the nitrate salt in the eluent. However, there was a very significant difference between the chromatograms obtained with the potassium nitrate and potassium chloride eluents.

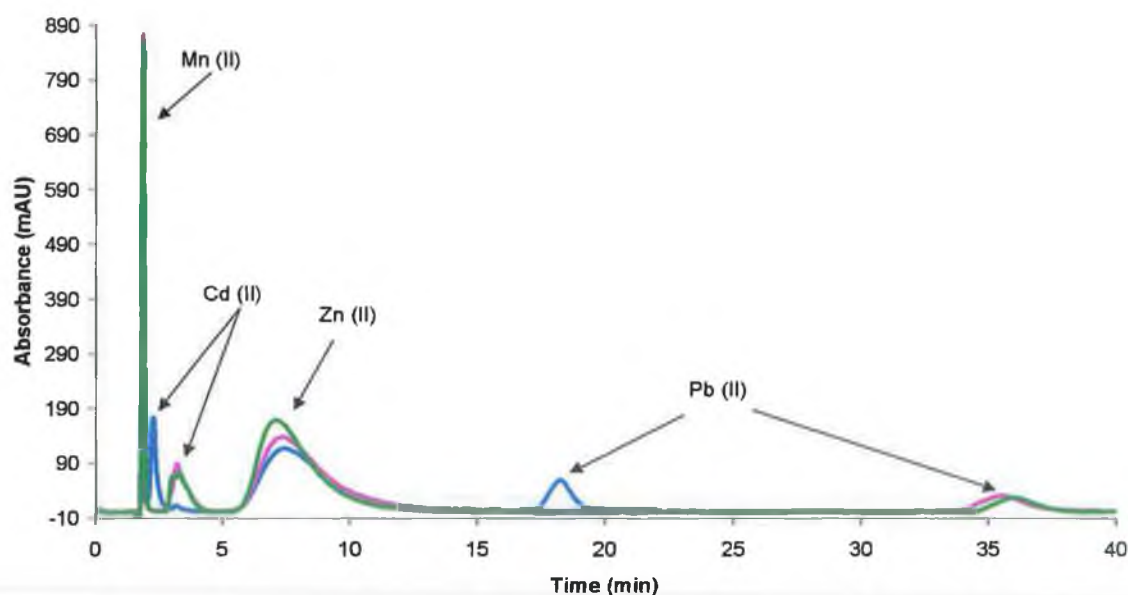


Figure 4.7: Overlays of the separation of 2 ppm Mn (II), 5 ppm Cd (II), 10 ppm Zn (II) and 20 ppm Pb (II) on a 10 cm IDA functionalised silica monolith, using 0.2 M KCl (blue trace), KNO<sub>3</sub> (pink trace) and NaNO<sub>3</sub> (green trace) eluents, adjusted to pH 2.5, flow rate 1 mL/min. Detection conditions: post-column reaction with 0.1 mM PAR, 100 mM NaHCO<sub>3</sub>, 50 mM Na<sub>2</sub>CO<sub>3</sub>, pH 9.8, monitored at 495 nm.

With the chloride eluent, the retention of Pb (II) was significantly reduced. Using the 0.2 M KCl eluent, the Pb (II) was retained for less than 20 minutes. However, when 0.2 M KNO<sub>3</sub> or NaNO<sub>3</sub> was used, the run time in each case was > 35 minutes. Fig. 4.7 also demonstrates that the retention of Cd (II) is reduced using the KCl eluent as opposed to the nitrate eluents, and the Cd (II) peak shape was also observed to deteriorate when the NaNO<sub>3</sub> or KNO<sub>3</sub> eluent was employed. These observations are expected when one considers the stronger tendency of chloride ions to form chloro-complexes with both Pb (II) and Cd (II), relative to the remaining metal ions ( $K_{I(ZnL)} = 0.11$ ,  $K_{I(PbL)} = 1.18$ ,  $K_{I(CdL)} = 1.38$ , medium 1M NaClO<sub>4</sub>, 25°C) [12].

Table 4.3: The effect of different inorganic eluents on the retention of transition metals on the 10 cm IDA silica monolith, flow rate 1 mL/min.

	Retention factor, ( <i>k</i> )		
	0.4 M	0.3 M	0.2 M
<b>Eluent: KNO<sub>3</sub>, pH 2.5</b>			
Mn (II)	0.1	0.1	0.1
Cd (II)	0.7	0.7	0.8
Zn (II)	2.4	2.8	3.0
Pb (II)	9.8	13.6	17.7
<b>Eluent: KCl, pH 2.5</b>			
Mn (II)	0.1	0.1	0.1
Cd (II)	0.2	0.2	0.4
Zn (II)	2.9	3.0	3.1
Pb (II)	3.6	6.6	10.3

#### 4.3.3.3: The effect of different inorganic eluents on Cd (II) and Pb (II) efficiency

The van Deemter plot, shown in Fig. 4.8, demonstrates the detrimental effect on the efficiency of the Cd (II) peak, when the 0.2 M KCl eluent was replaced with 0.2 M KNO<sub>3</sub> (pH 2.5). The separation achieved with the KNO<sub>3</sub> eluent resulted in the highest HETP values, indicating the worst peak efficiency values. In the case of Pb (II), the effect on peak efficiency was not as significant as in the case of Cd (II). However, as demonstrated in previous sections, the use of the nitrate eluents resulted in

excessively long Pb (II) retention times when compared to the run time obtained using the chloride eluent. Therefore, the optimum conditions for the rapid and efficient separation of Mn (II), Cd (II), Zn (II) and Pb (II) was 0.2 M KCl, pH 2.5.

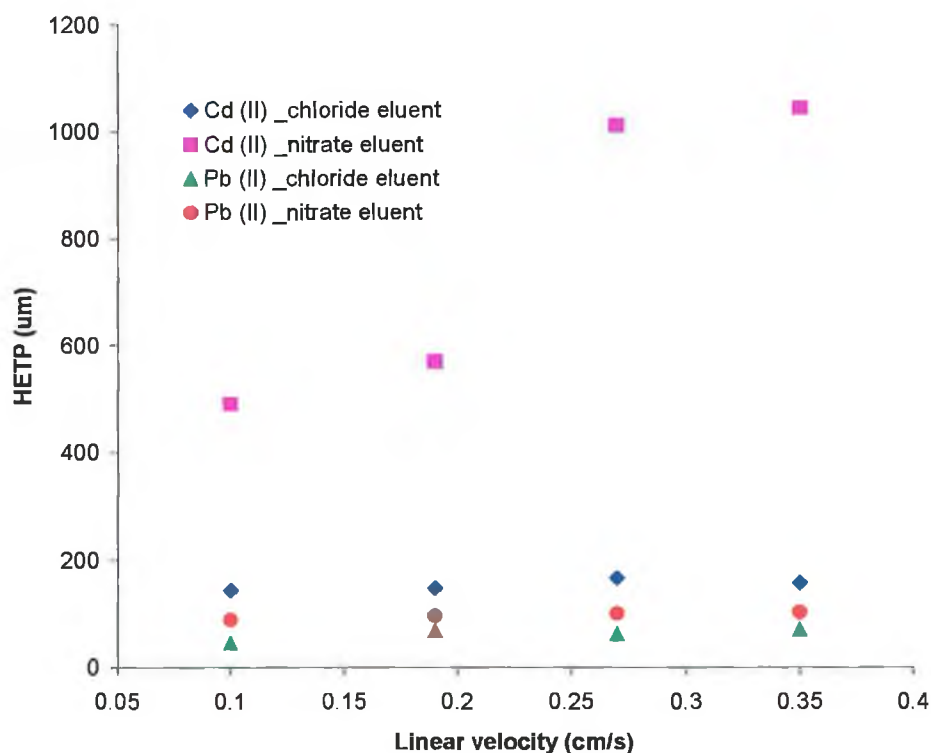


Figure 4.8: van Deemter plots for Cd (II) and Pb (II) obtained with the 10 cm IDA silica monolithic column using 0.2 M KCl and KNO<sub>3</sub> eluents, pH 2.5.

#### 4.3.3.4: Fast separation of Mn (II), Cd (II), Zn (II) and Pb (II)

Using an eluent flow rate of 1 mL/min, the run time required for the separation of Mn (II), Cd (II), Co (II), Zn (II) and Pb (II), using the 0.2 M KCl eluent (pH 2.5), was approximately 20 minutes. It was envisaged, that by exploiting the high porosity of monolithic columns, elevated flow rates could be employed without being limited by high column backpressure, to achieve a rapid cation separation. However, when flow rates greater than 2 mL/min were employed, a dramatic loss in resolution between the Cd (II) and Co (II) analyte peaks was observed, and so, only the separation of Mn (II), Cd (II), Zn (II) and Pb (II) was studied at elevated flow rates. Using the 0.2 M KCl eluent (pH 2.5), a separation of Mn (II), Cd (II), Zn (II) and Pb (II) was performed in approximately 6.5 minutes, using a flow rate of 3 mL/min, see Fig. 4.9 (a). Increasing

the eluent flow rate > 3 mL/min, had a negative impact on Mn (II) and Cd (II) resolution. The results of the flow rate study (see the van Deemter curve, Fig. 4.9 (b)) illustrated the impact of the Zn (II) peak broadening on peak efficiency. The Zn (II) peak exhibited HETP values 4 times greater than the HETP values calculated for remaining metal cations separated on the IDA silica monolith.

Finally, 10 replicate injections of the Mn (II), Cd (II), Zn (II) and Pb (II) mixture were performed on the 10 cm IDA functionalised silica monolith, using the 0.2 M KCl eluent, pH = 2.5, at a flow rate of 3 mL/min, and the % RSD values for analyte retention time and peak area were calculated, as shown in Table 4.5. For Mn (II), Cd (II) and Pb (II), the % RSD for retention time was ~ 0.6 % and for peak area, the % RSD did not exceed 5.0 %. However as the results in Table 4.4 demonstrate, the precision data obtained for Zn (II) was particularly poor. The large % RSD observed for the Zn (II) peak area can be attributed to the broadness of the Zn (II) peak, as well as associated difficulties of accurately integrating such a broad peak.

Table 4.4: Precision data for 10 repeat injections of a mixture of 2 ppm Mn (II), 2 ppm Cd (II), 10 ppm Zn (II) and 20 ppm Pb (II) on the 10 cm IDA silica monolith, using a 0.2 M KCl eluent, pH 2.5, flow rate 3 mL/min.

	%RSD values			
	Mn (II)	Cd (II)	Zn (II)	Pb (II)
<i>Retention Time</i>	0.5 %	0.8 %	1.2 %	0.6 %
<i>Peak Area</i>	3.0 %	4.3 %	13.9 %	4.9 %

In Section 4.3.3.2, when the KCl eluent was replaced with KNO<sub>3</sub> eluent, the retention times of both Cd (II) and Pb (II) were observed to increase, relative to Mn (II) and Zn (II). Therefore, using the KNO<sub>3</sub> eluent (pH 2.5), it was possible to achieve a baseline separation of all four analytes at 4 mL/min, see Fig. 4.10. However, although there was an improvement in the Mn (II), Cd (II) resolution, (see Table 4.5), there were disadvantages of using KNO<sub>3</sub> as the eluent salt, which included the excessive Pb (II) retention, and in particular, the negative impact on Cd (II) peak efficiency, as shown by the van Deemter curve in Fig. 4.8, Section 4.3.3.2.

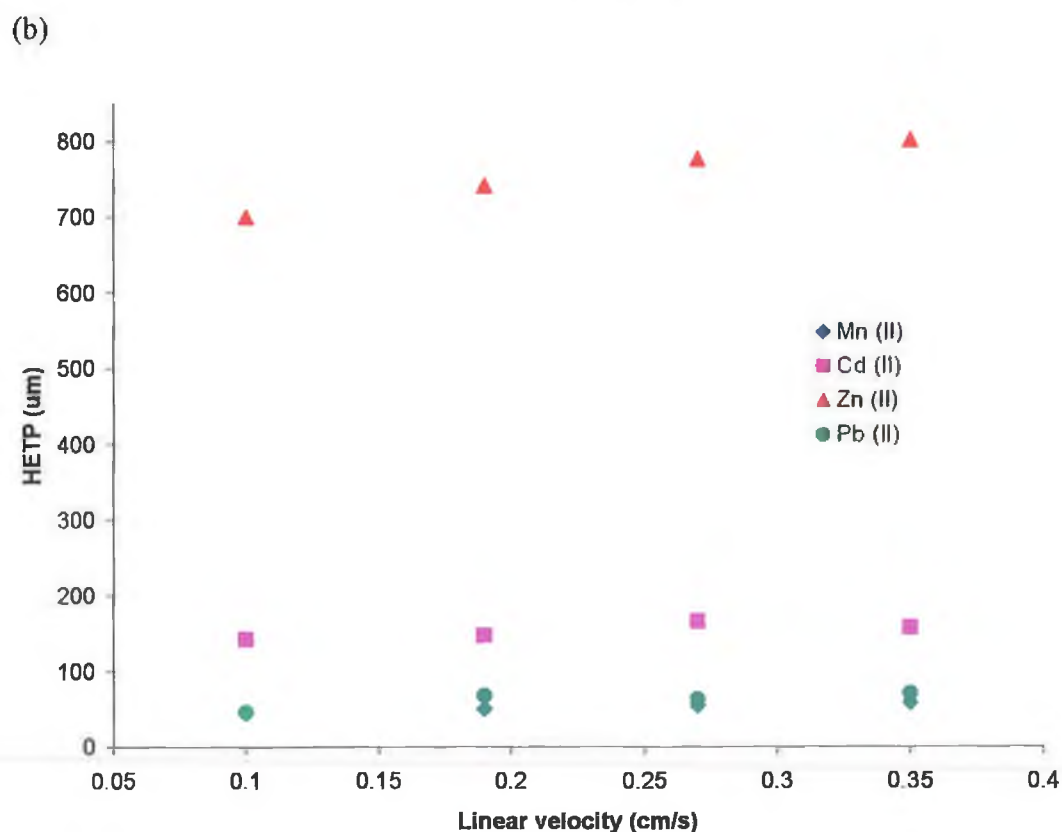
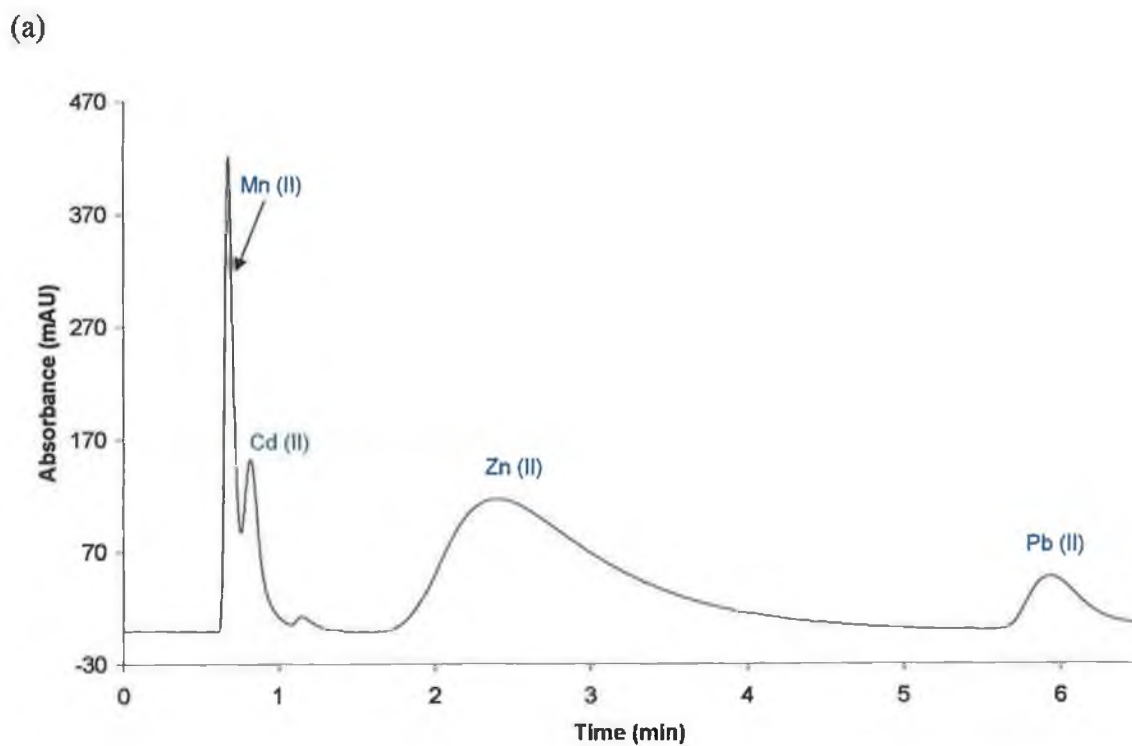


Figure 4.9: (a) The separation of Mn, (II), Cd (II), Zn (II) and Pb (II) on a 10 cm IDA functionalised silica monolith. Eluent conditions: 0.2 M KCl eluent, pH 2.5, flow rate 3 mL/min, and (b) van Deemter plots for Mn, (II), Cd (II), Zn (II) and Pb (II).

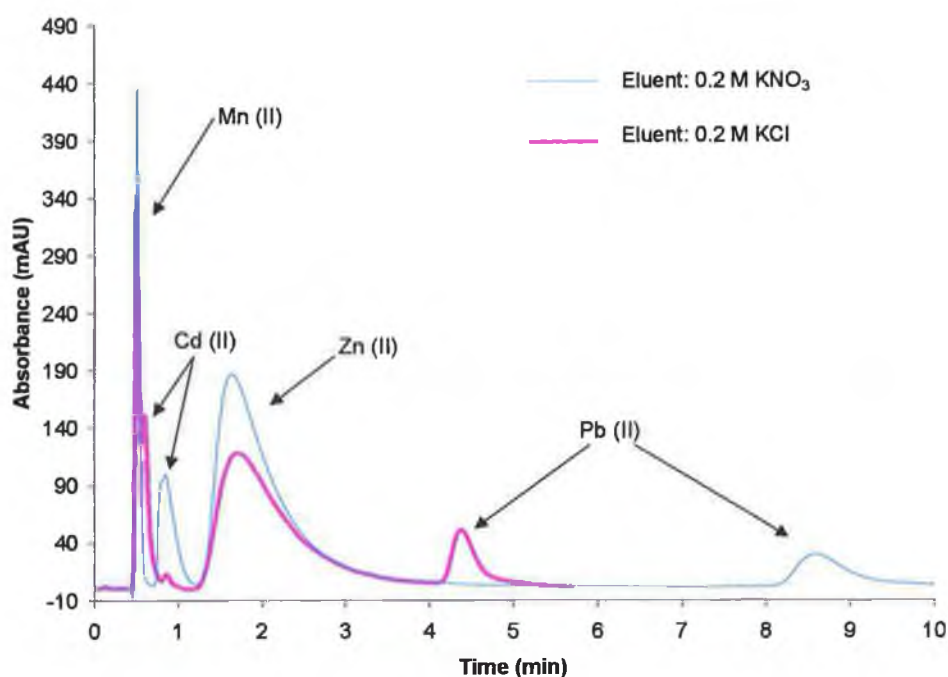


Figure 4.10: Overlays of separations of 2 ppm Mn (II), 2 ppm Cd (II), 10 ppm Zn (II) and 20 ppm Pb (II) on a 10 cm IDA functionalised silica monolithic column, using a 0.2 M KCl eluent (pink trace) and a 0.2 M KNO<sub>3</sub> eluent (blue trace) at 4 mL/min. Detection conditions: post-column reaction with 0.1 mM PAR, 100 mM NaHCO<sub>3</sub>, 50 mM Na<sub>2</sub>CO<sub>3</sub>, pH 9.8, monitored at 495 nm.

Table 4.5: The resolution data for Mn (II) and Cd (II) on the 10 cm IDA silica monolith using 0.2 M KCl and 0.2 M KNO<sub>3</sub> eluents, pH 2.5, flow rate 1-4 mL/min.

Flow Rate	Mn (II), Cd (II) Resolution	
	Eluent: 0.2 M KCl	Eluent: 0.2 M KNO <sub>3</sub>
1	1.7	4.0
2	1.4	2.1
3	1.3	1.9
4	1.1	1.6

#### ***4.4: Conclusion***

It has been demonstrated that the unique selectivity of the IDA functionalised silica monolith can be manipulated, to produce separations of several transition and heavy metal ions, using simple inorganic eluents. A separation of Mn (II), Cd (II), Zn (II) and Pb (II) was achieved in less than 7 minutes, using a flow rate of 3 mL/min, without the problems of excessive backpressure or the requirement of a gradient, usually associated with particle-packed HPLC columns.

Both the eluent pH and type of inorganic salt used in the preparation of the eluent were found to impact upon both the retention time and the efficiency of the analyte peaks. Increasing the eluent pH from 2.0 to 2.5 resulted in an unexpected broadening of the Zn (II) peak on the IDA silica monolith, which was not observed on the IDA silica gel particle-packed column. The use of the nitrate form, as opposed to the chloride form, of the potassium salts resulted in increased retention of Pb (II) and had a negative impact on the efficiency of both Pb (II), and in particular, Cd (II) due to the tendency of chloride ions to form chloro-complexes with both Pb (II) and Cd (II), relative to the other metal ions.

## *References*

1. X. Ding, S. Mou, K. Liu, Y. Yan, *J. Chromatogr. A*, 883 (2000) 127.
2. H. Lu, S. Mou, Y. Yan, S. Tong, J. M. Riviello, *J. Chromatogr. A*, 800 (1998) 247.
3. E. Santoya, S. Santoy-Guiterrez, S. P. Verma, *J. Chromatogr. A*, 884 (2000) 229.
4. G. Bonn, S. Reiffenstuhl, P. Jandik, *J. Chromatogr.*, 449 (1990) 669.
5. P. Jones and P. N. Nesterenko, *J. Chromatogr. A*, 789 (1997) 413.
6. A. I. Elefterov, S. N. Nosal, P. N. Nesterenko, O. A. Shpigun, *Analyst*, 119 (1994) 1329.
7. W. Bashir and B. Paull, *J. Chromatogr. A*, 942 (2002) 73.
8. A. R. Timberaev and G. K. Bonn, *J. Chromatogr. A*, 640 (1993) 195.
9. A. I. Elefterov, P. N. Nesterenko, O. A. Shpigun, *Anal. Chem.* 51 (1996) 887.
10. M. G. Kolpachnikova, N. A. Penner, P. N. Nesterenko, *J. Chromatogr. A*, 826 (1998) 15.
11. A. E. Martell, *Stability Constants of Metal Ion Complexes: Supplement 1: The Chemical Society of London, Alden Press (Oxford) 1971.*
12. E. Hogfeldt, *Stability Constants of Metal Ion Complexes Part A. Inorganic Ligands, Pergamon Press (Oxford) 1982.*

## **Chapter 5**

### ***Cation and anion selectivity on a L-lysine functionalised silica monolithic column***

## 5.1: Introduction

Although monolithic silica technology has opened the doors on a new era of dramatically higher sample throughput, and has added new opportunities to improve separation performance [1], the fact still remains that monoliths are still rather “young,” and the number of different stationary phases and separation mechanisms remains much smaller than that available for particle-packed columns [2]. Previous Chapters have demonstrated the results obtained using an IDA functionalised silica monolith and this Chapter will focus on the ion-exchange properties of a silica monolith functionalised with L-lysine.

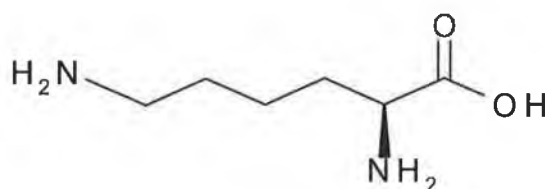


Figure 5.1: Structure of L-lysine amino acid.

According to Kolpachnikova *et al.* [3], a clear trend in IC is the development of a new generation of cation-exchangers containing carboxylic acid functional groups attached to the surface of either silica or polymer. Carboxylic cation-exchangers have demonstrated an optimal selectivity for the separation of alkali and alkaline earth metal cations and also increased affinity to some transition metals due to the complexing properties of the carboxylic groups. The application of weakly acidic, i.e. carboxylic cation-exchangers, for the simultaneous separation and determination of differently charged ions (alkali and alkaline earth metals in particular) is more promising than the use of sulfonic cation-exchangers, because the former present wider possibilities for varying the selectivity of the separation [4].

Recently, good selectivity and ion chromatographic performance was also demonstrated for a number of amino acids chemically bound to the silica surface. Depending on the structure of the amino acids attached to the silica surface the

prepared ion-exchanger could have cation-, anion- or zwitterion-exchange properties, as a result of the occurrence of oppositely charged groups in a single ion-exchange site. [3,4].

$\alpha$ -Amino acids are the simplest available zwitterionic molecules, which can be easily attached to a silica surface. Naturally occurring amino acids can be subdivided into four groups:

1. Monoaminocarboxylic acids, containing 1 primary amino group and one carboxylic acid group.
2. Diaminocarboxylic acids, such as lysine and arginine.
3. Monoaminodicarboxylic acids, such as aspartic and glutamic acid.
4. Heterocyclic amino acids, containing a secondary amino and one carboxylic acid group, eg. proline and hydroxyproline.

In work by Nesterenko *et al.* [5] a number of ion-exchange stationary phases were prepared by the immobilisation of amino acids of different structure (Asp, Glu, Val, Try, Pro, Hypro, Arg and Lys) on the silica surface. In aqueous solutions, the amino acids behave as inner salts and are generally both weak acids and weak bases. However, the attachment of amino acids to the surface of silica leads to a change in their ion-exchange properties owing to the interactions of the amino groups of the bonded molecule with residual silanols and an increase in the basicity of amino groups after linkage with a 3-glycidoxypropyl spacer. Taking these and multiple acid base equilibria in bonded molecules into account, it is only possible to approximately evaluate the relative affinities of amino acid-bonded phases for different ions. Nesterenko *et al.* [6,7] studied the anion-exchange properties of L-hydroxyproline bonded silica and L-proline-bonded silica, and cation-exchange properties were reported for silicas with attached arginine, valine and tyrosine.

According to Nesterenko *et al.* [5], the retention of ionogenic solutes depends on both the ion-exchange capacity of the sorbents and the nature of the bonded functional groups. From studying the retention of ionogenic compounds on the different amino acid bonded silica stationary phases, it was observed that only cyclic amino acids bonded to silica could be considered as zwitterionic-exchangers. The sorbents containing bonded amino acids of other types behave as weak or strong cation-

exchangers. The results of a study of the ion-exchange selectivity for cations demonstrated strong cation-exchange ability for bonded monocarboxylic acids (aspartic acid and glutamic acid) and, curiously, for bonded amino acids containing at least two basic groups, with bonded lysine and arginine showing a reasonable selectivity for the separation of monovalent and divalent cations.

Elefterov *et al.* [4] investigated the separation of alkali and alkaline earth metal cations on a particle-packed lysine bonded silica column using a 3 mM perchloric acid eluent and indirect conductivity detection. A linear dependence of  $\log k$  versus  $\log [E^+]$  was observed, and this indicated that ion-exchange was the predominant mechanism of metal separation. According to Elefterov *et al.* [4], the lysine-silica sorbent exhibited a lower affinity for the alkaline earth metals than other known carboxylic or sulfonic cation-exchangers. This allows the use of eluents with lower concentration and a reduction in analysis time, with the separation of  $Li < Na < NH_4 < K < Mg (II) < Ca (II) < Ba (II)$  using 3 mM perchloric acid as the eluent possible in under 15 minutes. Elefterov *et al.* concluded that silica with covalently bonded lysine groups does not rank below existing carboxylic cation-exchangers in terms of selectivity for the separation of cations of alkali and alkaline earth metals. A possible explanation for this is the fact that the acidity of the carboxylic group in the molecule is not changed after their attachment to the silica surface. Hence one could hope that attachment to silica of amino acids having a carboxylic acid group with relatively low  $pK_a$  value would produce such a kind of ion-exchanger. However, this is not completely correct for the molecules having an  $\alpha$ -amino group. Owing to the specific interactions with the residual silanol groups, the basicity of amino groups is changed, which induces uncertain alterations in the acidity of the carboxylic group and in the selectivity of the ion-exchanger [5].

### **5.1.1: Objective**

In this work a bare silica monolithic column has been covalently modified with lysine using on-column modification to produce a high performance monolithic ion-exchanger. The cation- and anion-exchange properties of this functionalised monolith were investigated and compared to the results previously reported for lysine functionalised silica particle-packed columns.

## **5.2: Experimental**

### **5.2.1: Column modification.**

A PEEK lined bare silica monolithic column (Performance Si) of 10 cm length and 4.6 mm i.d. was purchased from Merck KgaA (Damstadt, Germany). According to the manufacturer, the silica monolith has a surface area of 300 m<sup>2</sup>/g and a bimodal porous structure. The mesopores constitute 80% of the measurable pores with pore diameters centred around 12 nm, and provide the high specific area of 300 m<sup>2</sup>/g to the silica skeleton. Before modification the surface of the silica monolith was activated by washing the column with DIW whilst placed in a thermostated water bath at 60°C for 4 hours. The modification of the column<sup>1</sup> was performed at 70°C by recycling 80 mL of a water solution containing a mixture of  $\gamma$ -glycidoxypropyltrimethoxysilane and lysine (both from Fluka Chemie GmbH, Buchs, Switerland) through the column. The recycling system consisted of a glass beaker containing the above reagents, a Waters Model 510 HPLC pump (Waters, Milford, USA) and the thermostated monolithic silica column. The reagent mixture was pumped at a flow-rate of 0.5 mL/min for 6 hours and the column was then washed with 0.01 M nitric acid for ~ 1 hour and equilibrated with eluent before use.

### **5.2.2: Instrumentation**

An Applied Biosystems 400 Solvent Delivery System (Foster City, CA, U.S.A.), was used to deliver the eluent for the majority of the work involving low to moderate flow rates work, while for the work requiring flow rates greater than 4.9 mL/min or the use of a pH gradient, a Waters Model 600E Multisolvent Delivery System (Waters, Milford, MA, U.S.A.) was used. Samples were injected manually using a Rheodyne injector fitted with a 20  $\mu$ l injection loop. A 1050 series, Hewlett Packard (Palo Alto, CA, U.S.A) UV-Vis spectrophotometric detector was used for the detection of anions and cations. A Gilson pump, Model 302 (Anachem, Luton, Scotland) was used for the introduction of the post-column reagent (PCR) for transition metal work, which was mixed at room temperature with the eluent using a 0.5 m PEEK reaction coil (0.25  $\mu$ m i.d.). For suppressed conductivity detection, a Dionex conductivity detector (Dionex

---

<sup>1</sup> (The proposed structure of the lysine functionalised monolith is shown in Appendix II, Fig. 2.1A)

series 4500i) was used in conjunction with a CSRS Ultra 4 mm membrane suppressor (Dionex). Data acquisition was at a rate of 10 Hz with processing of chromatograms performed using a PeakNet 6.0 chromatography workstation (Dionex).

### **5.2.3: Reagents**

All chemicals used were of analytical reagent grade, and were supplied by Sigma-Aldrich (Tallaght, Dublin, Ireland). All eluents and standard solutions were prepared using DIW from a Millipore Milli-Q water purification system (Bedford, MA, U.S.A.), and were filtered through a 0.45  $\mu\text{m}$  filter and degassed by sonication. For indirect spectrophotometric detection,  $\lambda = 279 \text{ nm}$ , a phthalate eluent (phthalic acid (Aldrich), pH adjusted to 6.5) was employed. Both KCl (Aldrich) and phosphate buffer solutions were used as eluents for direct spectrophotometric detection,  $\lambda = 225, 214 \text{ nm}$ . Phosphate buffer solutions (1- 50 mM) were prepared using monobasic-, dibasic sodium phosphate (Aldrich) and phosphoric acid (85 %, Riedel-de Haën, Hanover, Germany) in the appropriate ratios to give the required pH values. For conductivity detection, a nitric acid (Fisher Chemicals, AGB Scientific, Dublin 11), eluent was employed. Dilute solutions of NaOH and HCl were used to adjust the pH of the eluents. The PCR reagent used for the detection of cations consisted of a mixture of 0.4 mM 4-(2-pyridylazo) resorcinol and 0.5 M ammonia, adjusted to pH 10.5. Low-level standard solutions of metal cations and anions were generally made up freshly each day from stock solutions (1000 ppm).

### **5.3: Results and discussion**

#### **5.3.1: Cation selectivity**

##### **5.3.1.1: Separation of alkali and alkaline earth metal ions on the L-lysine silica monolith**

Results obtained by Elefterov *et al.* [4] indicate that cation-exchange was the predominant retention mechanism for the alkali and alkaline earth metal ions on a particle-packed lysine bonded silica gel column. At the concentration of perchloric acid used (pH 2.5-2.9), both the amino groups of the bonded lysine were assumed to be protonated ( $pK_{a1} = 9.2$  and  $pK_{a2} = 10.7$ ), giving the lysine molecule an overall charge of approximately +1. With this in mind, it is clear that the spatial accessibility of the carboxylic acid groups is such that the repulsion effect of the protonated amino groups is small enough to still allow cation-exchange to take place. According to Nesterenko *et al.* [5] when studying lysine bonded silica gels, the phase exhibited mainly cation-exchange properties because of the formation of a three-layer sandwich structure:

1. The inner layer is formed by negatively charged residual silanol groups.
2. The middle positively charged layer is formed by the protonated amino groups of the bonded amino groups.
3. Lastly, the negatively charged carboxylic groups result in the external layer.

However, when the cation selectivity of the L-lysine silica monolith was investigated using a dilute nitric acid eluent (3-0.5 mM) and suppressed conductivity detection, very little retention and limited selectivity was observed. Even a reduction in the concentration of nitric acid in the eluent did not result in any increase in cation retention or improve the selectivity exhibited towards cations by the L-lysine monolith. This immediately indicated either a much lower capacity column or a change in the charge distribution of the attached lysine molecule on the monolithic surface. The latter could be attributed to the less acidic properties of the silica matrix of the Chromolith column used and subsequent weakened ability to coordinate amino groups of bonded lysine molecule. However the limited selectivity shown by the new monolithic column for the alkali metal ions did match that shown by Elefterov *et al.*,

namely  $\text{Na} < \text{NH}_4 < \text{K}$  (see Fig. 5.2) indicating some limited cation-exchange capacity, although the retention order for the alkaline earth metal cations differed distinctly, with the observed elution order of  $\text{Ba}(\text{II}) < \text{Mg}(\text{II}) < \text{Ca}(\text{II})$  (see Fig. 5.3). Such a retention order for alkaline earth metal ions has been shown previously with alternative aminocarboxylic acid groups, where complexation has played a role in cation retention [8]. Lysine in acid-neutral solutions is known to bind cations through the  $\alpha$ -carboxylate and  $\alpha$ -amino groups to form  $\text{M}(\text{HL})_n$  complexes [9] and if this is the case it would suggest non-hindered access to both the carboxylic acid groups and the amino group in the bonded ligand, which would obviously reduce apparent cation-exchange capacity, particularly for the alkali metal ions.

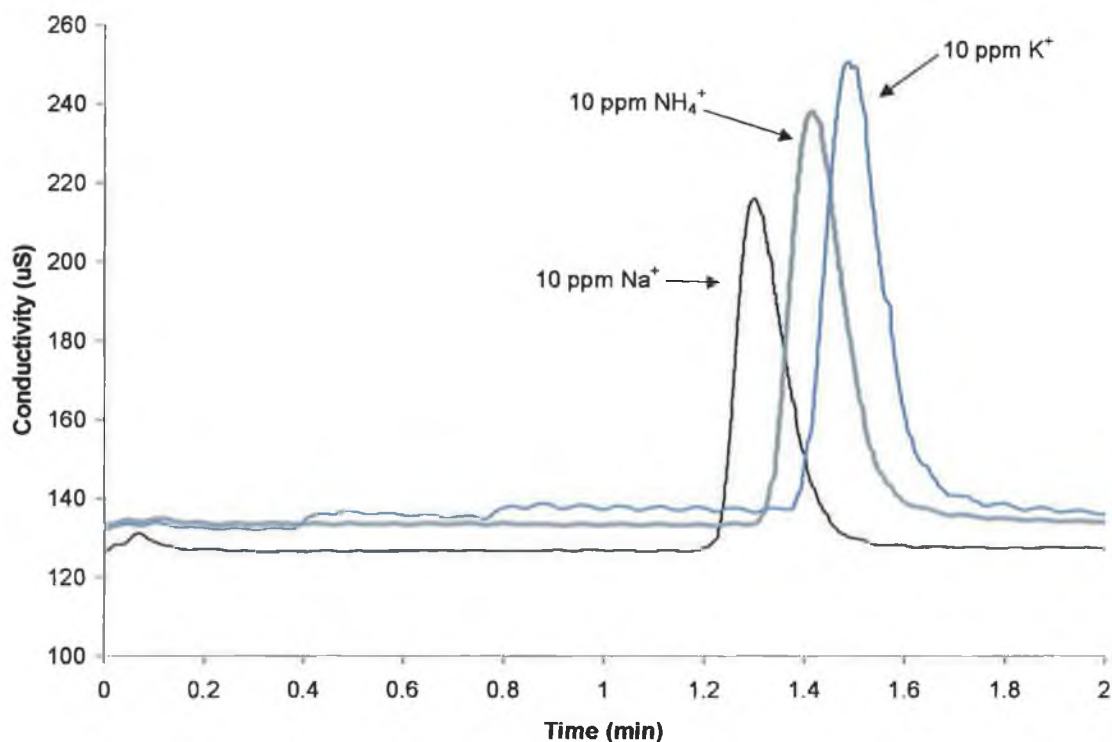


Figure 5.2: Overlay of alkali metal standards on a 10 cm L-lysine functionalised silica monolith. Eluent conditions: 3 mM  $\text{HNO}_3$ , flow rate 1 mL/min. Detection method employed: suppressed conductivity detection.

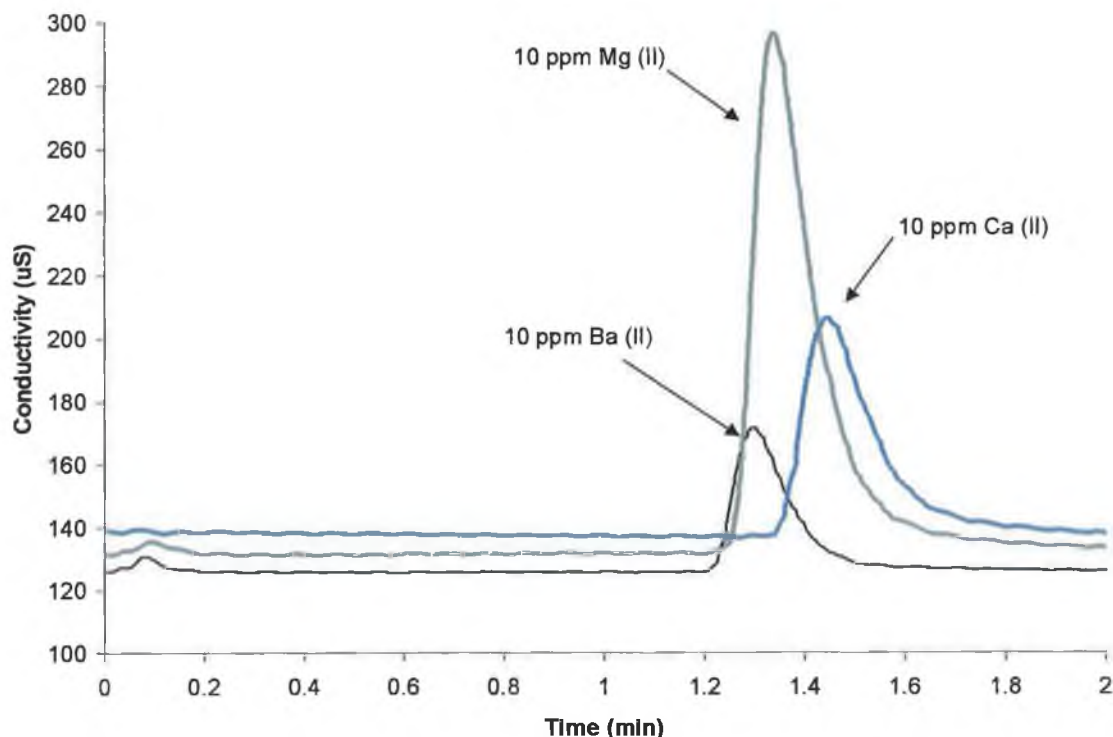


Figure 5.3: Overlay of alkaline earth metal standards on a 10 cm L-lysine functionalised silica monolith. Eluent conditions: 3 mM HNO<sub>3</sub>, flow rate 1 mL/min. Detection method employed: suppressed conductivity detection.

### 5.3.1.2: Transition and heavy metal cation selectivity

The selectivity of the lysine monolith was evaluated for selected transition metal ions using a simple KCl eluent. The metal ions investigated included Mn (II), Co (II), Cd (II), Zn (II) and Pb (II). Using eluent concentrations above 5 mM KCl (pH 2.5) resulted in the rapid elution of all metal cations except Zn (II) and Pb (II). The selectivity of lead shown by the lysine monolith was particularly strong with Pb (II) being retained for >30 minutes when using an 80 mM KCl eluent (pH 2.5).

Complexation between the metal ions and the lysine groups resulted in the selectivity shown and so eluent pH was varied to manipulate selectivity. Table 5.1 shows the retention data for the metal ions using a 5 mM KCl eluent adjusted to pH 4.0, 4.5 and 5.1. Once again the retention order shown matches that previously observed with alternative aminocarboxylic acid phases [10], and is consistent with published stability constant data for M(HL) type lysine-metal complexes (Mn (II),  $K_1 = 2.18$

(20°C); Co (II),  $K_1 = 3.62$  ( 25°C, 1.0 M KCl); Cd (II),  $K_1 = 3.70$  ( 30°C, 1.0 M KNO<sub>3</sub>); Zn (II),  $K_1 = 4.06$  (25°C, 0.2 M KCl)) [9].

Table 5.1: The effect of 5 mM KCl eluent pH on the retention factors of selected transition and heavy metal cations retained on a 10 cm L-lysine functionalised silica monolith, flow rate 2 mL/min.

	Mn (II)	Co (II)	Cd (II)	Zn (II)	Pb (H)
Eluent pH	Retention factor ( <i>k</i> )				
4.0	0.15	0.81	2.24	3.57	retained
4.5	0.24	1.09	2.81	6.24	-
5.1	0.24	3.29	4.61	28.1	-

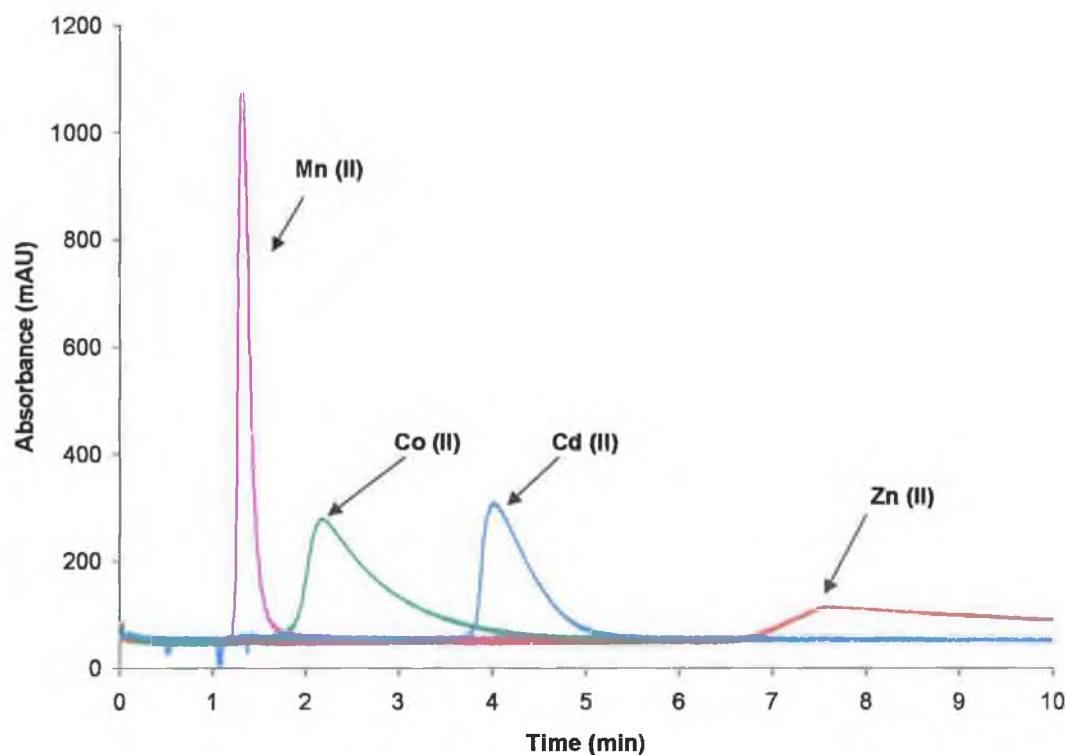


Figure 5.4: Overlay of Mn (II), Co (II), Cd (II) and Zn (II) standards retained on a 10 cm L-lysine functionalised silica monolith. Eluent conditions: 5 mM KCl eluent, pH 4.51, flow rate 2 mL/min. Detection conditions: post-column reaction with 0.4 mM PAR, 0.5 M ammonia, pH 10.5, monitored at 510 nm.

The data shown in Table 5.1 shows the strong pH dependence exhibited by the column and the strong affinity for both Zn (II) and Pb (II). Peak shapes broadened rapidly with retention, particularly Zn (II), again indicating that surface complexation was the dominant retention mechanism. This unusual broadening of the Zn (II) peak has also been observed on the IDA silica monolith in Chapter 4. Fig. 5.4 shows an overlay of chromatograms of low ppm standards obtained using a 5 mM KCl eluent, pH 4.5, at flow rate 2 mL/min.

### 5.3.1.3: Cation-exchange capacity

During the eluent pH study it was noted that retention data varied with sample concentration, for example when injecting mixed standards. Combined with poor peak shapes, this indicates a low overall capacity. Therefore, the column capacity was determined and compared to an unmodified silica monolithic column of similar dimensions (100 x 4.6 mm Merck Chromolith Si) to ascertain the capacity due to complexation with bound lysine groups under non-acidic conditions.

Columns were initially washed with a 10 mM dipicolinic acid solution for 30 minutes at 1 mL/min to remove any bound cations. The columns were then washed with 1 M KCl solution for 30 mins to convert the columns to the potassium form, and finally washed with deionised water for 30 minutes, before the 1mM ZnCl<sub>2</sub> or the 1 mM CdCl<sub>2</sub> solutions were pumped through the lysine and bare silica monoliths at 1 ml/min and the resultant break-through curves are presented in Fig. 5.5 (a) and (b). The results obtained showed the bare silica monolith itself exhibited a very small ion-exchange capacity<sup>2</sup> equivalent to between 1.5 and 3.0 μmoles Me<sup>2+3</sup> (in Chapter 2 it was demonstrated that under non-acidic conditions some retention of alkali and alkaline earth metal ions was possible on a bare silica monolith). The ion-exchange capacity increased to 5.1 – 6.5 μmoles Me<sup>2+</sup> for the lysine modified column.

---

<sup>2</sup> (Ion-exchange capacity is defined as the number of ionic sites on the stationary phase that can participate in the ion-exchange process)

<sup>3</sup> (Me<sup>2+</sup> refers to a divalent metal cation)

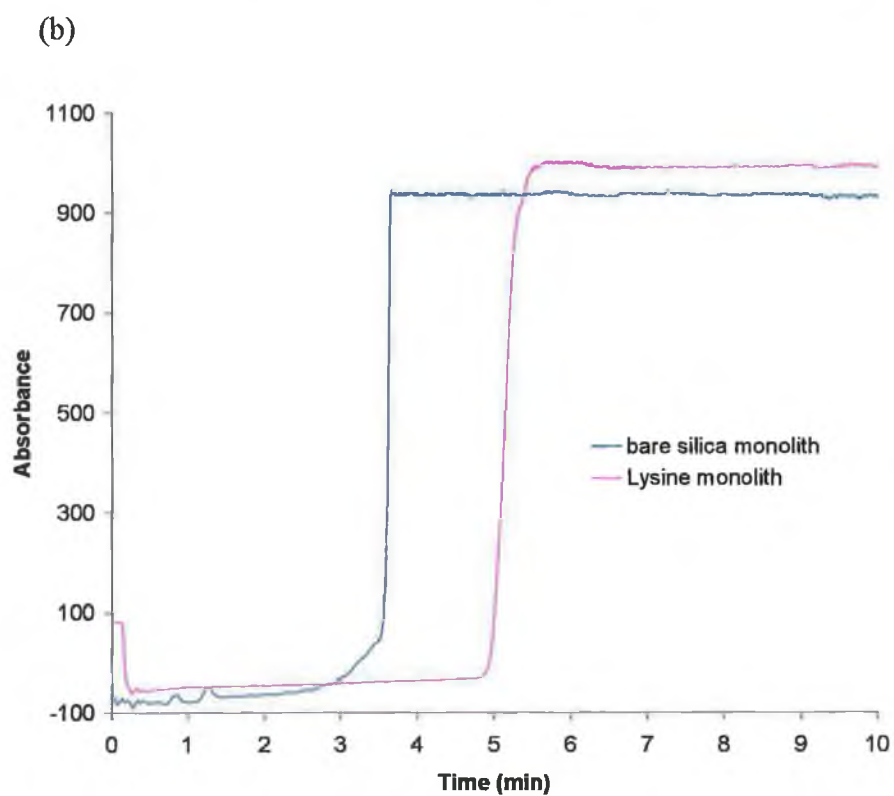
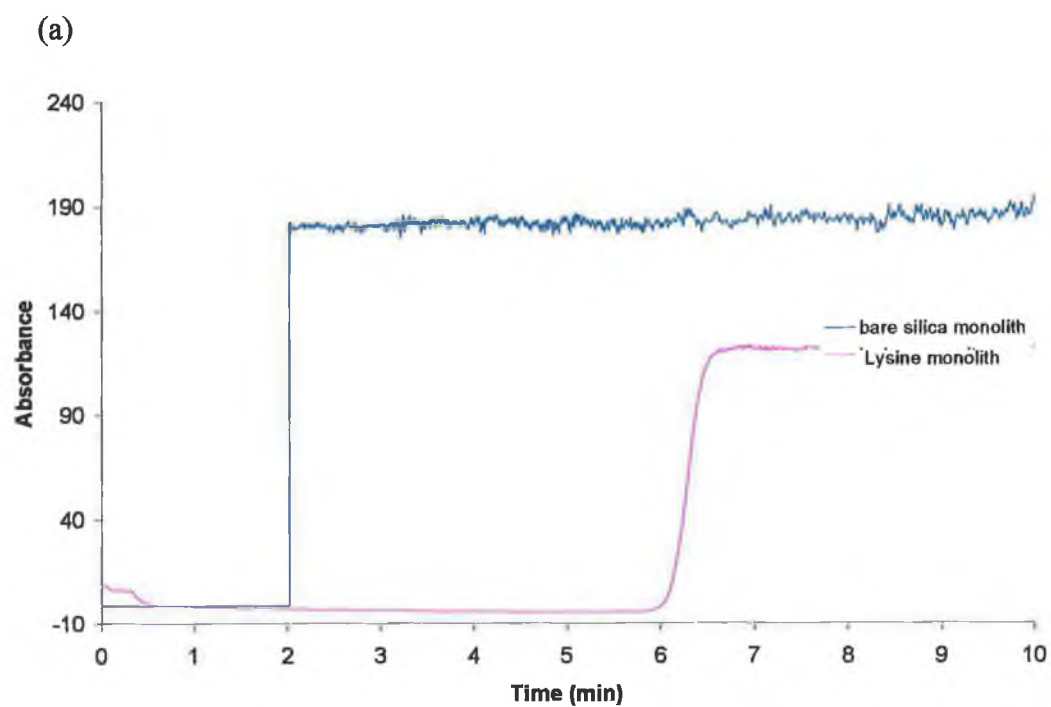


Figure 5.5: Overlays of cation-exchange capacity studies performed on both a 10 cm lysine silica monolith and a 10 cm bare silica monolith using (a) 1 mM  $\text{CdCl}_2$  and (b) 1 mM  $\text{ZnCl}_2$  at a flow rate of 1 mL/min.

### 5.3.2: Anion selectivity

Based on the results obtained by Elefrov *et al.* [4] and Nesterenko *et al.* [5] it was expected that the L-lysine modified monolith would exhibit cation-exchange properties, but as Section 3.1.2 demonstrated, the cation-exchange capacity of the lysine monolithic column was only marginally higher than that of a bare silica column. The zwitterionic nature of lysine means the modified monolith should exhibit a degree of anion selectivity, due to the net positive charge on the molecule under acidic and neutral pH conditions. If this is the case it is clear that under acid-neutral conditions the deprotonation of the carboxylic acid group ( $pK_a = 2.16$ ) will also play a role in the observed selectivity due to repulsive effects, and this contribution towards selectivity should vary with eluent pH.

#### 5.3.2.1: Anion retention on an L-lysine silica monolith

Following on from the limited cation retention observed for the L-lysine monolith, the anion selectivity was investigated using a simple KCl eluent and direct UV detection at 225 and 214 nm. It was possible to separate nitrite (13.9 minutes), nitrate (15.3 minutes), iodide (18.7 minutes) and thiocyanate (24.2 minutes) using a 0.5 mM KCl eluent (pH 6.0), flow rate 2mL/min. The ionic strength of the eluent was increased from 0.5 to 3 mM KCl, (above 2 mM KCl the resolution of nitrite and nitrate decreased substantially) and a plot of  $\log k$  versus  $\log [E^-]$  demonstrated a linear relationship, see Table 5.2. This indicated that ion-exchange is the predominant mechanism of anion separation.

Table 5.2: Slope and  $R^2$  values calculated from the plot of  $\log k$  versus  $\log [KCl]$ .

Analyte	Slope	$R^2$ value
Nitrite	1.1632	0.9953
Nitrate	1.1811	0.9948
Iodide	1.1978	0.9927
Thiocyanate	1.1918	0.9918

Although many anions absorb UV radiation at detection wavelengths above 200 nm, others such as  $F^-$ ,  $SO_4^{2-}$ ,  $PO_3^{3-}$ ,  $ClO_4^-$  and  $CN^-$  do not show appreciable absorption except at lower wavelengths [11]. To further characterise the anion-exchange properties of the lysine monolith, the anion selectivity of the lysine monolith was investigated using a phthalate eluent and indirect spectrophotometric detection (279 nm).

Using a 2 mM phthalate eluent (pH 6.5), the elution order was determined to be:



Although  $F^-$ ,  $Cl^-$ ,  $NO_2^-$  and  $Br^-$  were observed to co-elute, the lysine monolithic column demonstrated good selectivity for  $NO_3^-$ ,  $I^-$ ,  $SCN^-$  and was observed to be highly selective for  $SO_4^{2-}$ , with complete retention of the sulphate anion observed when the eluent concentration was decreased below 0.5 mM, see data in Table 5.3 below.

Table 5.3: The effect of phthalate eluent concentration (pH 6.5) on anion retention using a 10 cm L-lysine silica monolith, flow rate 1 mL/min.

Eluent Conc.	Retention factor ( <i>k</i> )							
	Cl <sup>-</sup>	F <sup>-</sup>	Br <sup>-</sup>	I <sup>-</sup>	NO <sub>2</sub> <sup>-</sup>	NO <sub>3</sub> <sup>-</sup>	SCN <sup>-</sup>	SO <sub>4</sub> <sup>2-</sup>
2 mM	0.6	0.7	0.7	0.9	0.6	0.7	1.2	3.2
0.5 mM	1.6	1.5	1.4	1.9	1.4	1.5	2.4	10.6
0.25 mM	1.9	1.9	1.9	2.5	2.0	2.1	3.2	retained
0.1 mM	3.1	3.2	2.9	4.0	3.1	3.3	4.8	retained

### 5.3.2.2: Rapid separations and speciation studies

Using a simple KCl eluent and an elevated flow rate of 4.9 mL/min it is possible to achieve rapid separations of nitrite, nitrate, iodide and thiocyanate in under 2 minutes, as well as separations of bromate and bromide in 1.5 minutes and iodate and iodide in just over 1 minute; see Fig. 5.6-5.8.

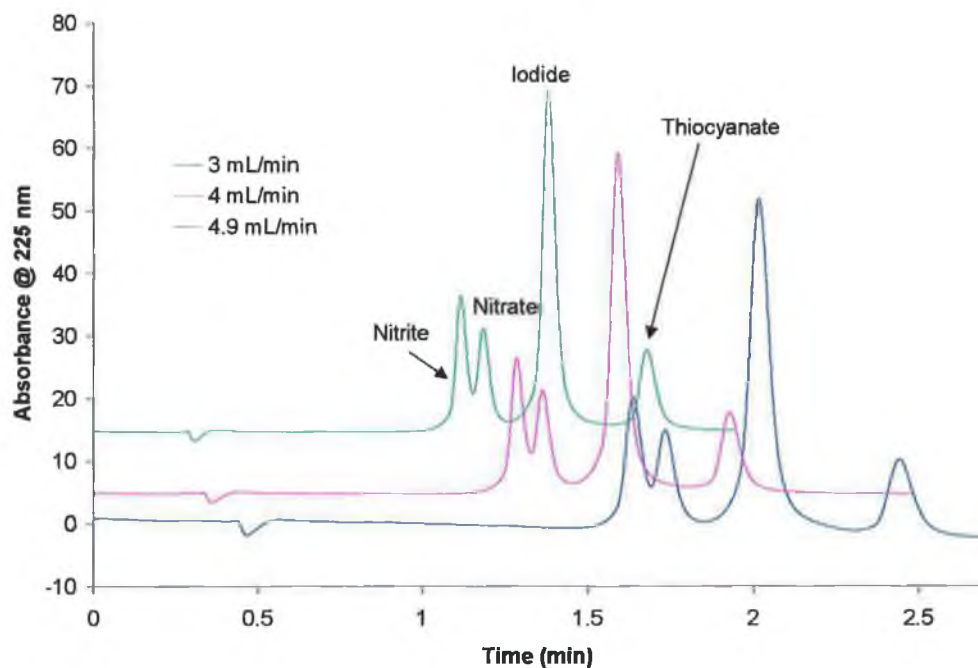


Figure 5.6: Separations of nitrite, nitrate, iodide and thiocyanate on a 10 cm L-lysine monolith at flow rates of 3 mL/min (blue trace), 4 mL/min (pink trace) and 4.9 mL/min (green trace). Eluent conditions: 3 mM KCl, pH 6.0 and the analytes were monitored using direct UV detection at 225 nm.

Simple inorganic speciation methods are particularly important in the monitoring of environmental process and also in the analysis of natural and treated wastewaters. For example, nitrate and nitrite levels in natural waters are important indicators of water quality [12]. Nitrite can be formed during the biodegradation of nitrate, ammoniacal nitrogen and other nitrogenous organic matter and is an important indicator of faecal pollution of natural water systems. Nitrate and nitrite are both intimately involved in the overall nitrogen cycle of soil and higher plants; leaching of nitrate from fertilisers added to soils can result in elevated levels of nitrate in ground and surface water. When nitrate-contaminated water supplies are used as a source of drinking water, adverse human health effects are of great concern. Relative to nitrite, nitrates are

compounds of lower toxicity, representing a danger only when ingested in excess doses or converted to nitrites. Nitrites however can have severe adverse effects on human health.

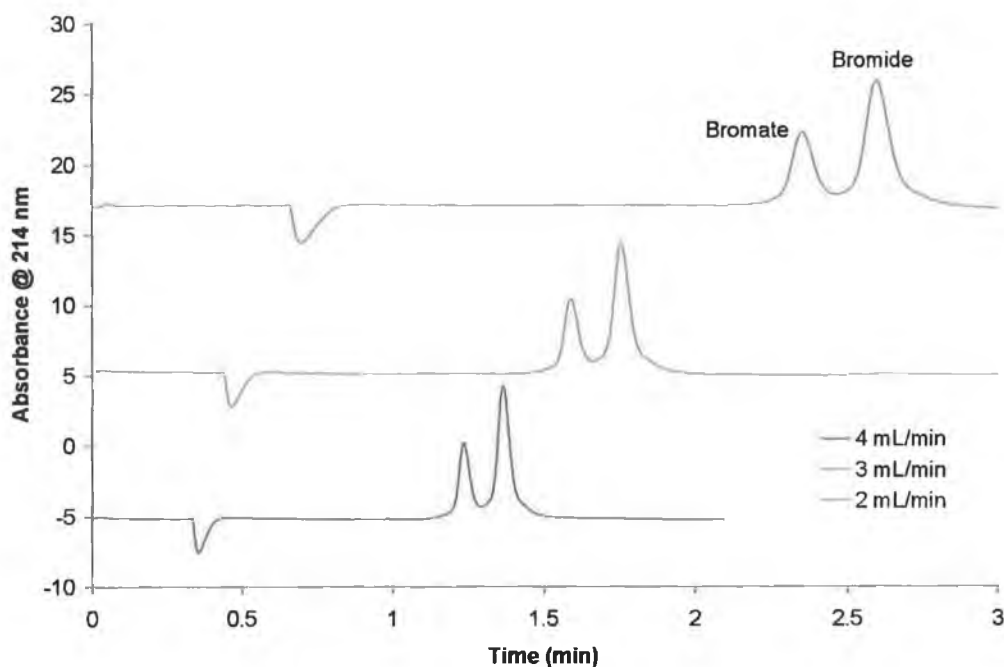


Figure 5.7: Separation of bromate and bromide on a 10 cm L-lysine silica monolith at 2 mL/min (green trace), 3 mL/min (pink trace) and 4 mL/min (blue trace). Eluent conditions: 3 mM KCl eluent, pH 6.0. Analytes were detected by direct UV detection at 214 nm.

During the 1970's it was realised that the chlorination of drinking water produced carcinogenic disinfection by-products, such as trihalomethanes [13]. Since the, alternative disinfection methods that minimise the production of toxic by-products have been investigated. Ozonation has emerged as one of the most promising alternatives to chlorination. However, this method tends to oxidise bromide to bromate. This presents a potential health risk since bromide occurs naturally in source waters and bromate is classified as a group 2B probable human carcinogen by the International Agency for Research on Cancer [13].

Although iodate may also be formed during ozonation of source waters containing iodide, currently however, there is no regulation regarding iodate levels in drinking water [14]. The biological and environmental importance of iodine species, the most dominant species being iodide and iodate, is due to the element's function as an

essential micronutrient and marker of geochemically or biologically active process.

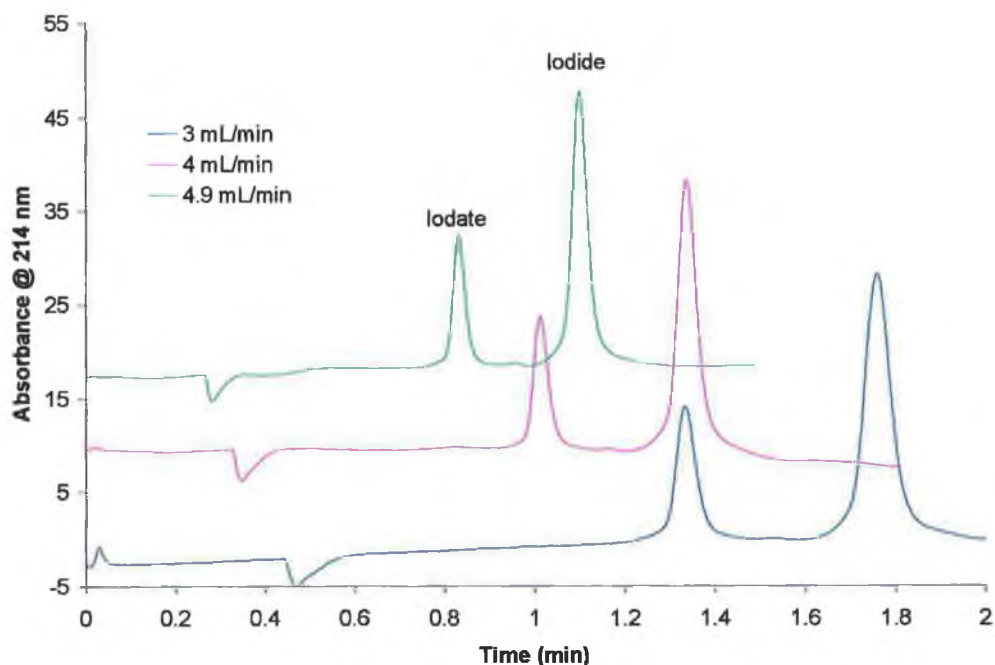


Figure 5.8: Separation of iodate and iodide on a 10 cm L-lysine functionalised silica monolith at 3 mL/min (blue trace), 4 mL/min (pink trace) and 4.9 mL/min (green trace). Eluent conditions: 3 mM KCl eluent, pH 6.0. Analytes were detected using direct UV detection at 214 nm.

Although rapid separations of nitrite, nitrate, iodide and thiocyanate (see Fig. 5.6), as well bromate and bromide (Fig. 5.7) and iodate and iodide (see Fig. 5.8) were possible, the selectivity of the L-lysine monolithic did not allow the separation of a mixture of iodate, bromate, bromide, nitrite and nitrate. Bromide and nitrate were observed to co-elute using the 3 mM KCl, pH 6.0 eluent, and likewise the retention times of iodate, bromate and nitrite were observed to overlap.

As the van Deemter curve presented in Fig. 5.9 shows, the use of elevated flow to achieve rapid separations did not have a negative impact on the efficiency of the analyte peaks, in fact the HETP values were higher at a flow rate of 1 mL/min than at a flow rate of 4 mL/min for bromate and bromide and 4.9 mL/min for nitrite, nitrate, iodate, iodide and thiocyanate.

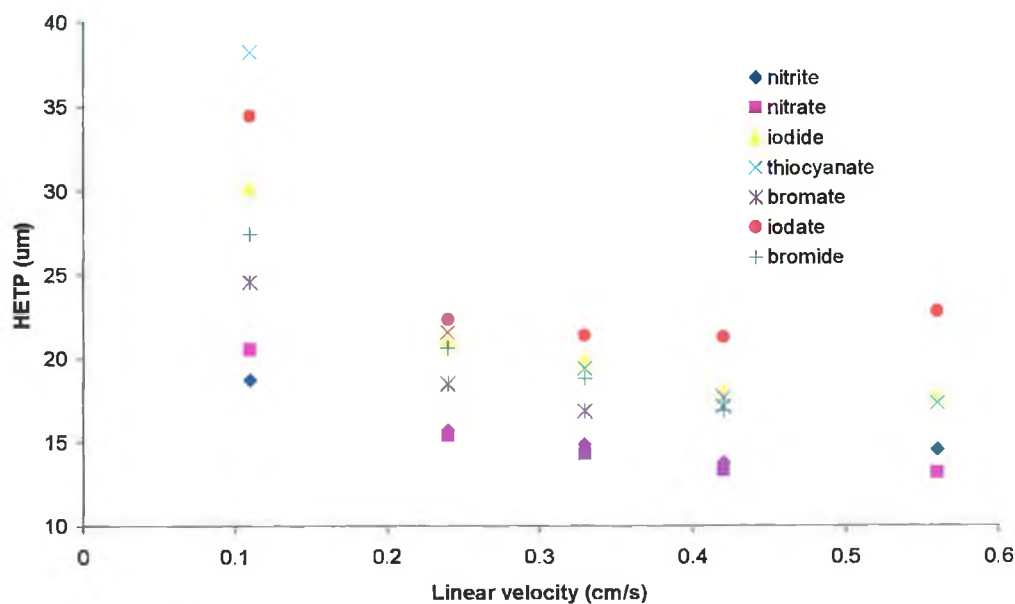


Figure 5.9: van Deemter curves showing the effect of eluent flow rate on anion peak efficiency using a 10 cm L-lysine functionalised silica monolith.

### 5.3.2.3: Effect of pH on anion selectivity and anion-exchange capacity.

To study the effect of eluent pH, phosphoric acid/phosphate buffer solution replaced the KCl solution, and the eluent pH was varied over the range 3.0-6.5. A clear dependence between retention data and eluent pH is evident from the data presented in Fig. 5.10. However, because the elution strength of the eluent varied towards the extremes of the pH range investigated, Fig. 5.10 represents a combination of stationary phase and eluent effects.

It is clear from examining the relationship between anion retention and eluent pH that decreasing the eluent pH caused an increase in the retention of the analytes, perhaps as a result of a decrease in the degree of dissociation of the carboxylic acid group on the lysine. However, below pH 3.5, the retention of nitrite was observed to decrease again, while the other remaining anions continued to exhibit an increase in retention. The unusual behaviour of nitrite can be explained by its  $pK_a$  of 3.15, resulting in the formation of nitrous acid and the resultant reduction in retention at that point.

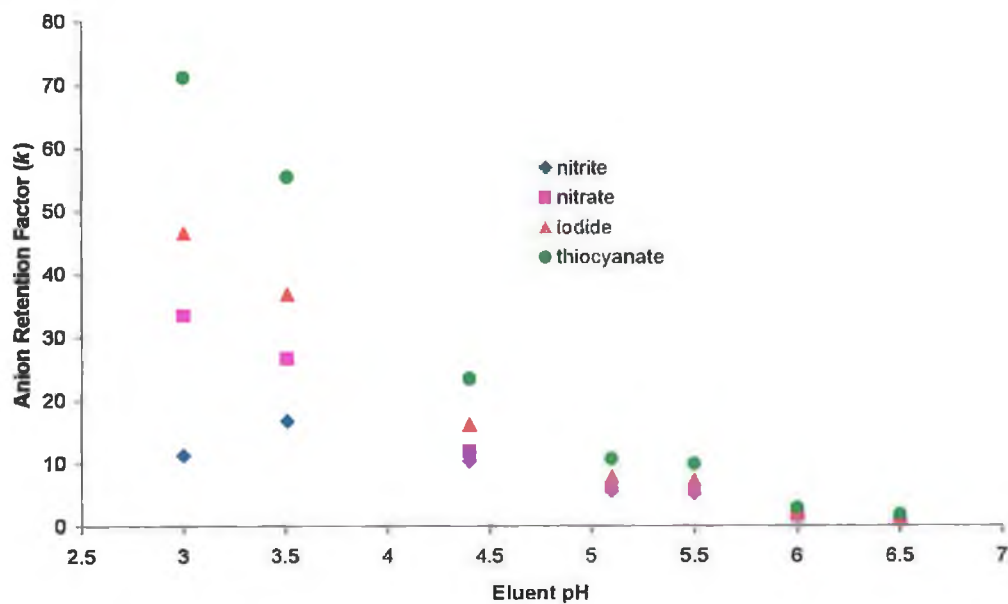


Figure 5.10: The effect of phosphate buffer eluent pH on anion retention factor, on a 10 cm L-lysine monolithic silica column.

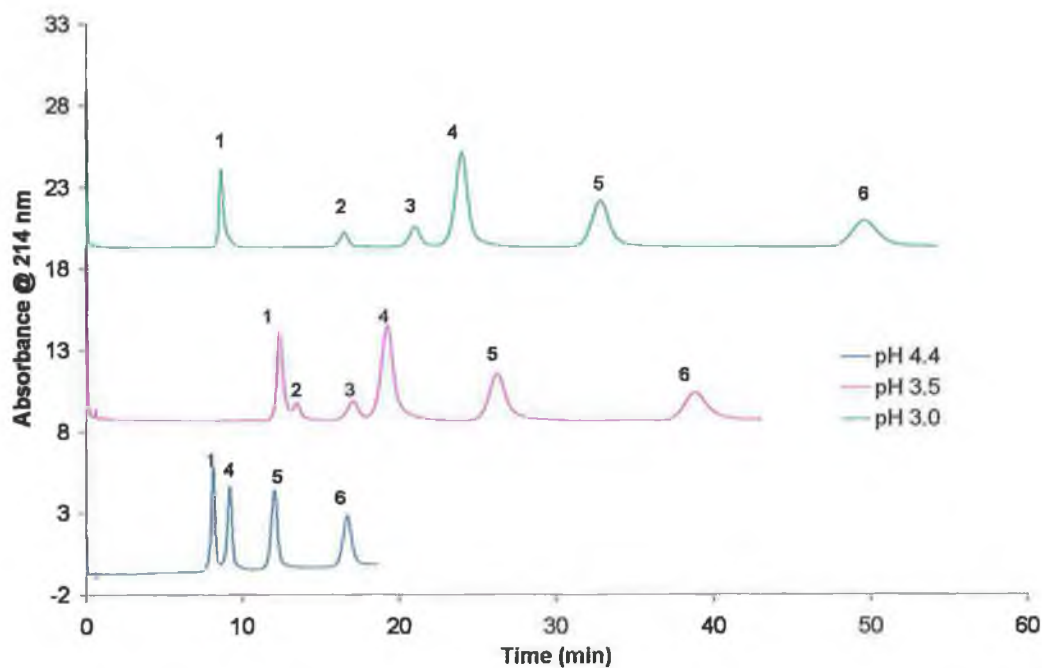


Figure 5.11: Effect of phosphate buffer eluent pH on anion selectivity using a 10 cm L-lysine silica monolith, flow rate 2 mL/min. Elution order: 1-nitrite, 2-bromate, 3-bromide, 4-nitrate, 5-iodide and 6-thiocyanate.

As Fig. 5.11 demonstrates, when the eluent pH was adjusted to 3.5, a separation of nitrite, bromide, nitrate, iodide and thiocyanate was possible. By further reducing the eluent pH by 0.5 pH units, the unusual behaviour of the nitrite ion facilitated the baseline resolution of a mixture of 6 anions; namely, nitrite, bromate, bromide, nitrate, iodide and thiocyanate. It was not possible to incorporate iodate into the separation of the 6 anions described, as iodate and bromate co-elute at pH 3.0, using a 2 mM phosphate eluent. The eluent pH was not reduced below pH 3.0, as the run time for the separation of the 6 anions even at 2 mL/min is greater than 50 minutes.

At each eluent pH, the separation of nitrite, nitrate, iodide and thiocyanate was monitored over a range of flow rates, i.e. 1 to 4.9 mL/min. From the data presented in the van Deemter curves for the 4 anions, it is clear that the highest efficiency achieved over the flow rate range studied was obtained for both nitrite and nitrate using the eluent pH 6.11. In the case of iodide and thiocyanate, between 1 and 2.5 mL/min, the lowest HETP values were observed when the eluent pH 5.5 was employed. However, above 2.5 mL/min, once again for the eluent pH 6.11, the greatest efficiency was observed. The overall trend evident from Fig. 5.12-5.15 was that over the pH range investigated; the efficiency at the higher flow rates (3-4 mL/min) was equal to or greater than the efficiency values observed at 1 and 2 mL/min.

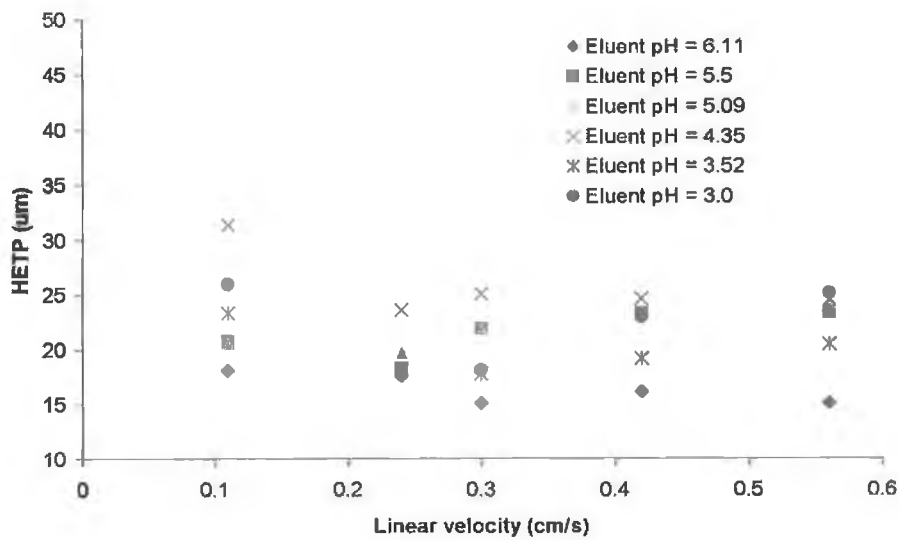


Figure 5.12: Nitrite van Deemter curve showing the effect of eluent flow rate on nitrite efficiency, over the eluent pH range 3.0 – 6.11.

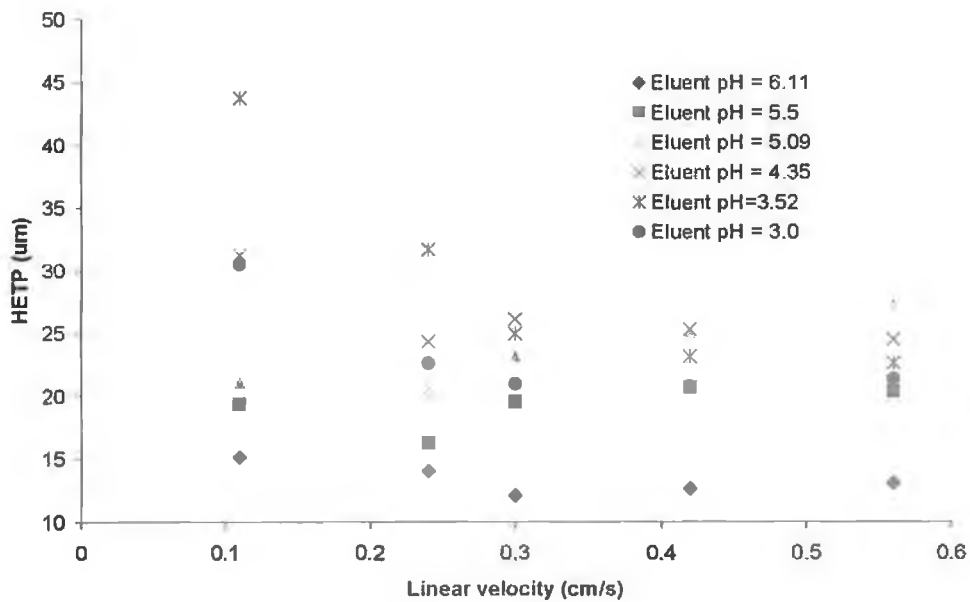


Figure 5.13: Nitrate van Deemter curve showing the effect of eluent flow rate on nitrate efficiency, over the eluent pH range 3.0 – 6.11.

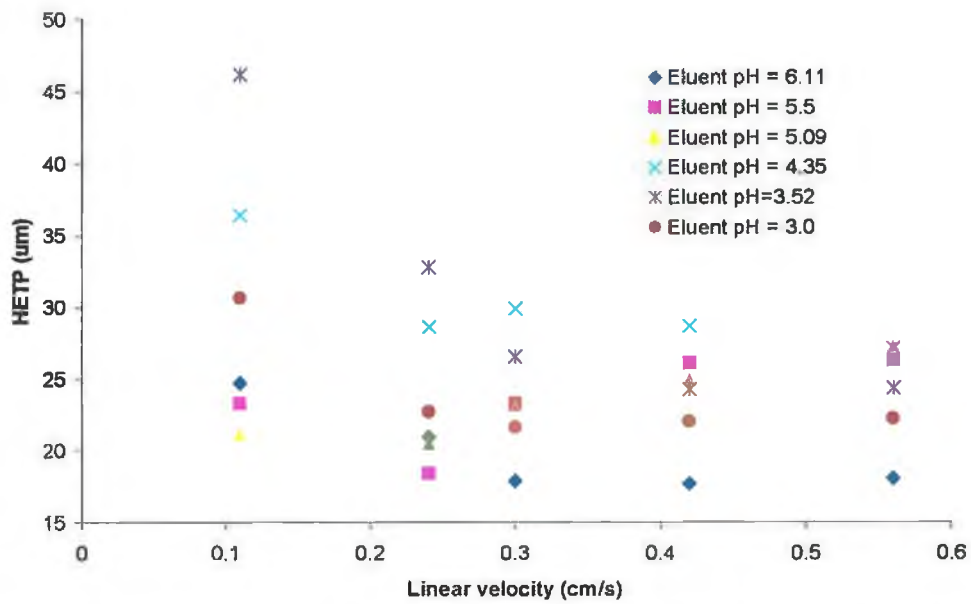


Figure 5.14: Iodide van Deemter curve showing the effect of eluent flow rate on iodide efficiency, over the eluent pH range 3.0 – 6.11.

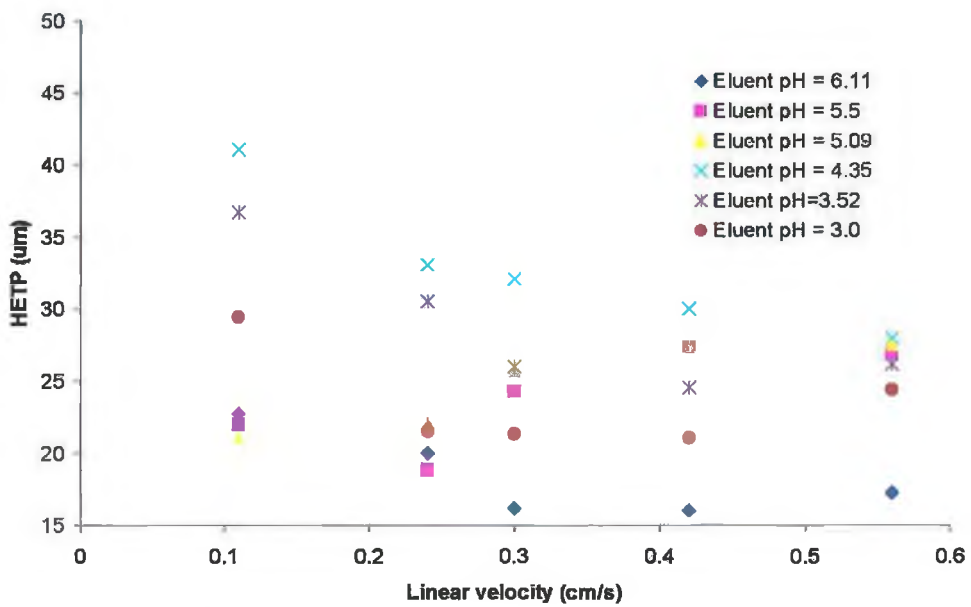


Figure 5.15: Thiocyanate van Deemter curve showing the effect of eluent flow rate on thiocyanate efficiency, over the eluent pH range 3.0 – 6.11.

To evaluate the effect of pH upon the effective anion-exchange capacity, the ion-exchange capacity<sup>4</sup> of the lysine functionalised monolith was re-evaluated. The anion-exchange capacity of the column was determined by initially washing the monolith with 1 M KCl (pH 6.0) for 30 minutes, followed by distilled water for 30 minutes, and then a 1 mM KI solution (pH 6.0) was passed through the monolith at 1 mL/min, and as Fig. 5.16 below shows, the break-through curve was monitored at 225 nm. Subsequent to this, the anion-exchange capacity was once again determined. However, this time the 1 M KCl wash solution, the distilled water and the 1 mM KI solution were all adjusted to pH 3.0. In each case, the capacity study was repeated at least three times, and the results are presented in Table 5.4.

Table 5.4: Summary of results obtained for the anion-exchange capacity studies performed on a 10 cm lysine functionalised silica monolith.

	<b>mL of 1 mM KI required to saturate column</b>	<b>mL of 1 mM KI required to saturate column</b>
	<b>(pH 6.0)</b>	<b>(pH 3.0)</b>
Capacity study 1	4.3 mL	9 mL
Capacity study 2	3.7 mL	14 mL
Capacity study 3	5.4 mL	13 mL
Capacity study 4	-	12 mL

It can be seen from the breakthrough curves presented in Fig. 5.16 (a) and (b) that the effective capacity at pH 6.0 was found to be approximately 30 % of that at pH 3.0. At pH 3.0 the capacity of the modified monolith was found to be equivalent to between 12 and 13  $\mu$ moles I. The difference in the effective capacities determined in this study, show how the lysine functionality and the terminal weak acid group produce a variable capacity cation-exchanger.

<sup>4</sup> (Ion-exchange capacity is defined as the number of ionic sites on the stationary phase that can participate in the ion-exchange process)

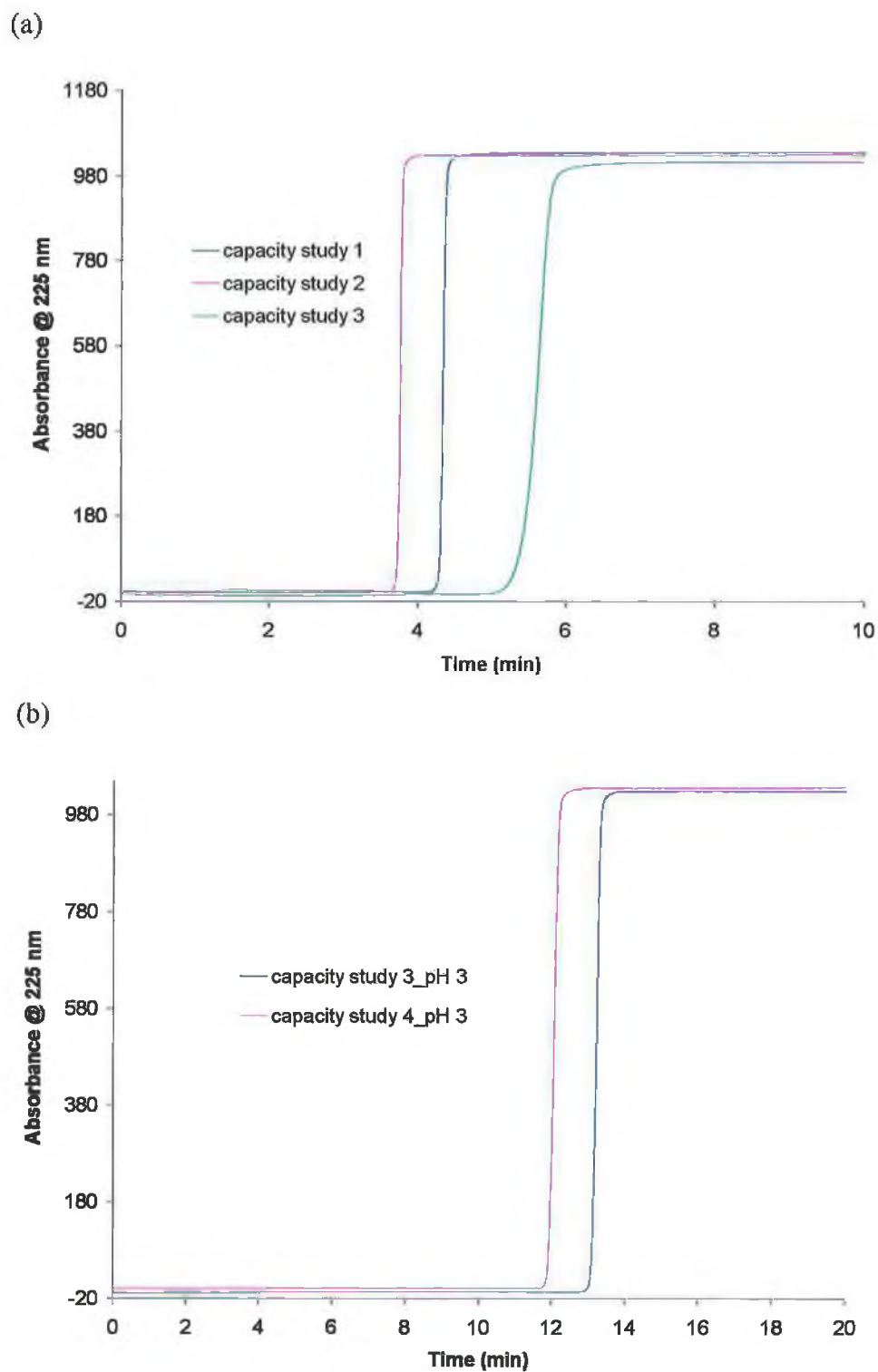


Figure 5.16: Overlays of anion capacity studies performed on a 10 cm lysine silica monolith using 1 mM KI, at (a) pH 6 and (b) pH 3, at a flow rate of 1 mL/min.

#### 5.3.2.4: Effect of eluent concentration on anion retention.

In order to reduce the excessive run times, which result at eluent pH 3.0, the eluent phosphate concentration was increased to reduce run time, while still maintaining the anion resolution.

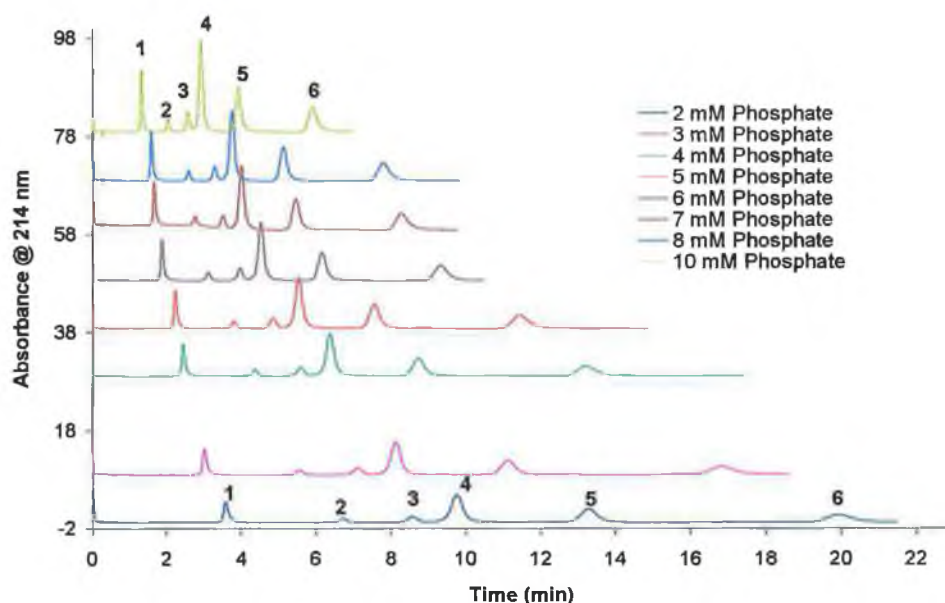


Figure 5.17: Overlays of the separations of 1-nitrite, 2-bromate, 3-bromide, 4-nitrate, 5-iodide and 6-thiocyanate on a 10 cm L-lysine functionalised silica monolith. Eluent conditions: 2 – 10 mM phosphate buffer eluent, pH 3.0, flow rate 4.9 mL/min, monitored at 214 nm.

Using a 10 mM phosphate buffer eluent, pH 3.0, the selectivity of the L-lysine functionalised silica monolith for an increased range of common UV absorbing anions was investigated, and the results are presented in Table 5.5. However, it was not possible to achieve resolution of more than the 6 UV absorbing anions shown in Fig. 5.17, as the peak shape for formate was very broad. In addition, as the results in Table 5.5 demonstrate, chloride and iodate, chlorate and bromide, as well as sulphite and nitrate co-eluted under the above eluent conditions.

Over the course of the experimental work undertaken, the concentration of phosphate buffer eluent (pH 3.0) was increased from 2 to 50 mM (n=11) and the effect of increasing the eluent concentration on the retention of the anions is presented in Fig.

5.18. The linear dependence of  $\log k$  on the  $\log [E^-]$  demonstrated that pure ion-exchange was the predominant mechanism of anion separation.

Table 5.5: The retention data obtained for a selection of UV absorbing anions on the 10 cm L-lysine functionalised silica monolithic column. Eluent conditions: 10 mM phosphate buffer, pH 3.0, flow rate 2 mL/min.

Anion	Rt (min)	Retention factor ( $k$ )	Efficiency (N/m)	Asymmetry
Formate	1.7	1.4	288	2.10
Nitrite	3.2	3.6	4752	1.37
Bromate	5.2	6.4	5195	0.97
Iodate	5.2	6.4	5587	0.97
Chloride	5.4	6.7	4770	0.86
Chlorate	6.2	7.9	4516	1.15
Bromide	6.6	8.4	4712	0.93
Sulphite	7.4	9.6	4539	1.03
Nitrate	7.6	9.9	4523	1.01
Iodide	9.8	13.0	4233	1.12
Thiocyanate	14.9	20.3	4096	1.21

Table 5.6: The values of both the slope and  $R^2$  values calculated for each of the anions shown in Fig. 5.18.

Analyte	Slope	$R^2$ value
Nitrite	-0.8045	0.9958
Bromate	-0.9101	0.9958
Bromide	-0.9021	0.9951
Nitrate	-0.8859	0.9960
Iodide	-0.8839	0.9953
Thiocyanate	-0.8744	0.9946

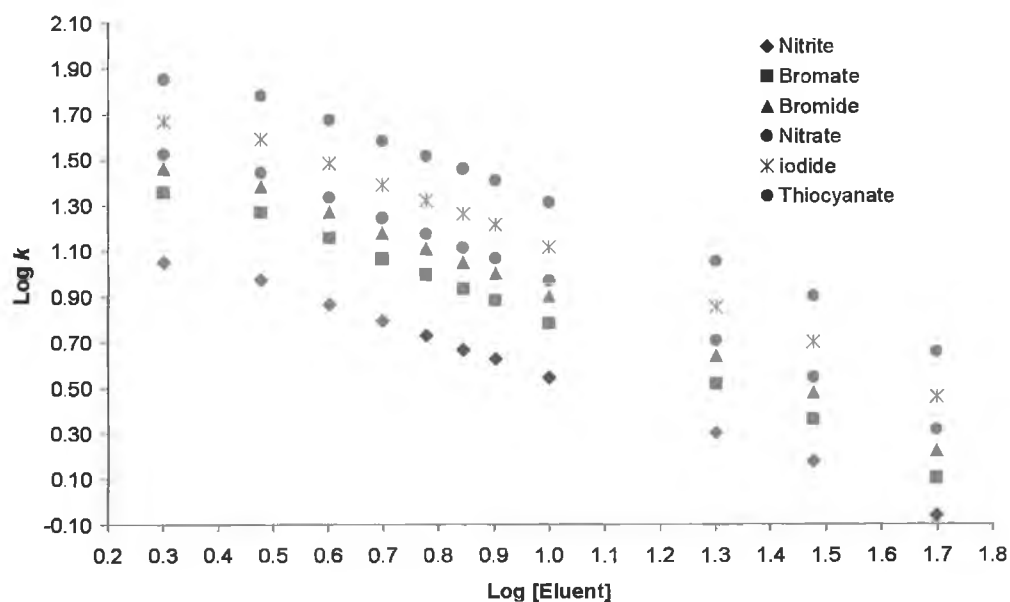


Figure 5.18: Plot of  $\log k$  versus  $\log [E^-]$  showing the dependence of anion retention on the eluent ionic strength.

### 5.3.3: Optimising rapid anion separations

#### 5.3.3.1: The use of a pH gradient

A number of approaches were employed to try and reduce the run time required for the separation of the 6 anions mixture at the optimum eluent pH 3.0:

1. The use of a pH gradient.
2. The use of elevated flow rates, i.e., up to 6 mL/min.
3. Increasing the eluent ionic strength from 10 to 50 mM phosphate.
4. The use of flow gradients.

It is evident from Fig. 5.17 that even at elevated flow rates, i.e. 4.9 mL/min the time in which the separation of the 6 anions can be achieved, i.e. 7 minutes, was limited by the excessive retention of the thiocyanate relative to the other 5 anions at pH 3.0. Hence, if it was possible to apply a pH gradient to the separation, an increase in pH could result in the faster elution of iodide and in particular thiocyanate, which would drastically speed up the separation. However, the baseline separation of the first 4 eluting anions, i.e. nitrite, bromate, bromide and nitrate, was only possible if the pH is maintained at pH 3.0. However, even at pH 6, it was still possible to achieve a separation of nitrate, iodide and thiocyanate. Therefore, the pH gradient was designed

to maintain the eluent pH 3.0 for the first 3 minutes, then following the elution of the first 4 anions, the pH was increased to 6.0 between  $t_1 = 3$  and  $t_2 = 5$  minutes. It is clear from Fig. 5.19 that the use of such a gradient, because it was employed at an elevated flow rate of 5 mL/min, resulted in a high phosphate background when the eluent pH was increased from 3.0 to 6.0 over the 2 minute period and as a result, the signal due to the thiocyanate peak was completely swamped.

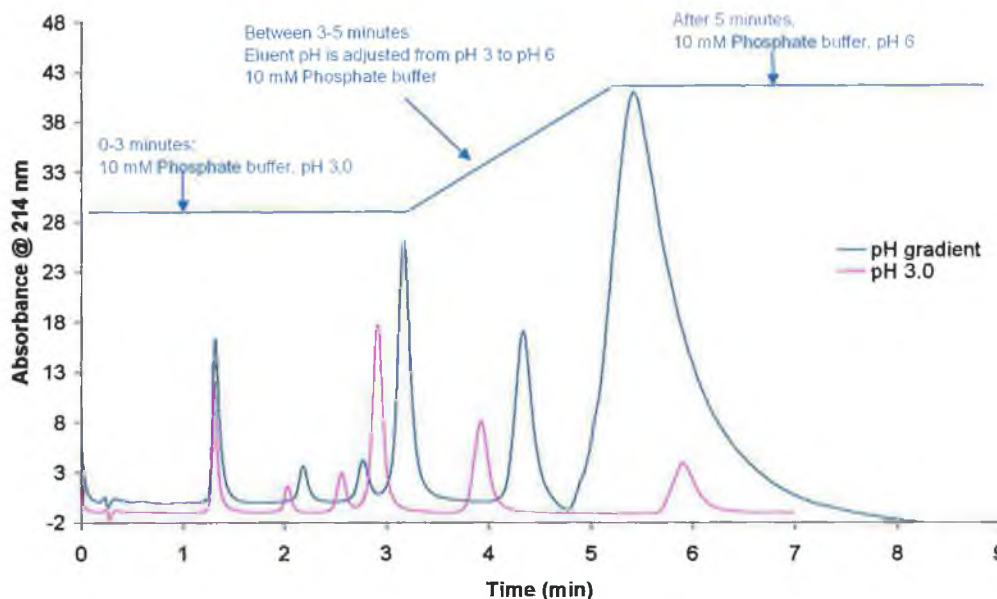


Figure 5.19: Overlays of the separation of the 6 test anions on the 10 cm L-lysine functionalised monolith analysed by 1) an isocratic separation using 10 mM phosphate eluent, pH 3.0, flow rate 5 mL/min (pink trace) and 2) the separation achieved when a pH gradient was applied to increase the pH from pH 3.0 to pH 6.0 at  $t_1 = 3$  minutes and  $t_2 = 5$  minutes (blue trace). Analytes were monitored by direct UV detection at 214 nm.

### 5.3.3.2: The use of elevated flow rates

Following the investigation of the pH gradient, the next approach undertaken was the use of elevated flow rates to achieve a rapid separation of nitrite, bromate, bromide, nitrate, iodide and thiocyanate. Up until this point in the work, an Applied Biosciences 400 delivery system was employed and the rate of mobile phase delivery was limited to 4.9 mL/min. Using a different system, the Waters Multi-Solvent delivery system, flow rates of 5.5 and 6 mL/min were possible. As well as increasing the flow

rate, the concentration of the eluent was increased from 10 to 20 mM phosphate (pH 3.0), and using this eluent and a flow rate of 6 mL/min, the separation of the 6 anions was possible in just over 3 minutes.

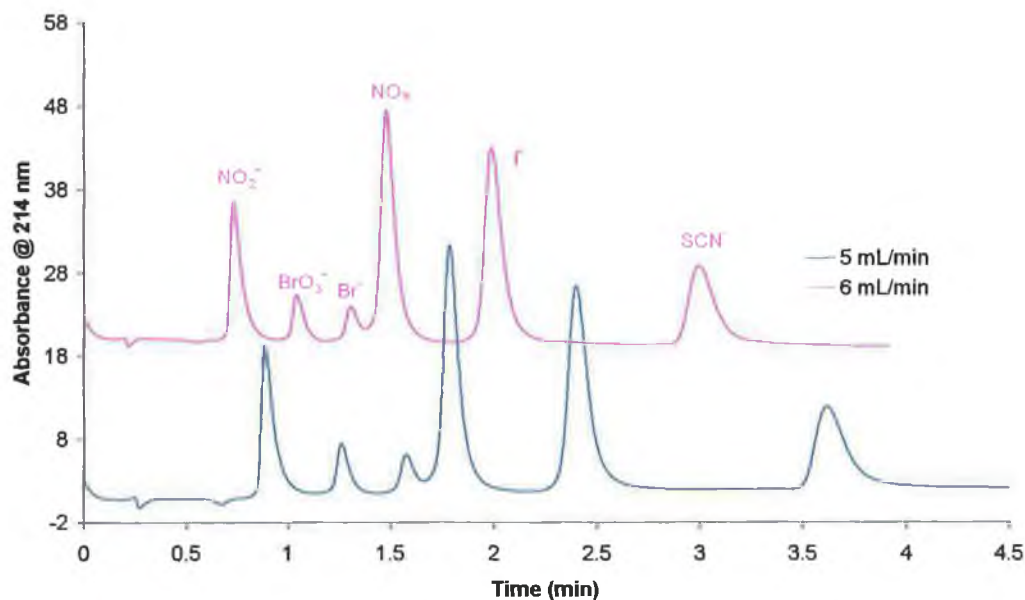


Figure 5.20: Separation of the 6-test anions mixture on a 10cm L-lysine functionalised silica monolithic column. Eluent conditions: 20 mM phosphate buffer eluent, pH 3.0, at flow rates of 5 mL/min (blue trace) and 6 mL/min (pink trace). Analytes were monitored by direct UV detection at 214 nm.

However, although the use of elevated flow rates decreased the run time, the effect of using flow rates up to 6 mL/min on the separation efficiency had to be investigated. It is clear from the van Deemter curve presented in Fig. 5.21 that increasing the flow rate above 5 mL/min resulted in a reduction in the efficiency of all analyte peaks, particularly for nitrite. For example, the HETP value for the nitrite peak at 6 mL/min was 3 times greater than the value reported for a flow rate of 5 mL/min. Paull *et al.* [15] reported that in a study of the effect of eluent flow rate upon peak efficiencies, using a 1cm carboxybetaine modified reversed-phase silica monolith, it was observed that for early eluting species such as nitrite and nitrate, increasing flow rate caused a continuous decrease in peak efficiency. A possible reason for this observation was due to the extremely small interaction time for the early elution species with the actual stationary phase, because at 6 mL/min, the retention time of nitrite on the 1 cm coated column was only 6 sec. Perhaps at 6 mL/min, a similar, if not diminished type of effect comes into play on the lysine monolithic which could account for the large

decrease in peak efficiency values for the first eluting peak, nitrite ( $R_t=0.7$  minutes), and also to a lesser extent, the bromate peak ( $R_t = 1.04$  minutes), which is second in the elution order.

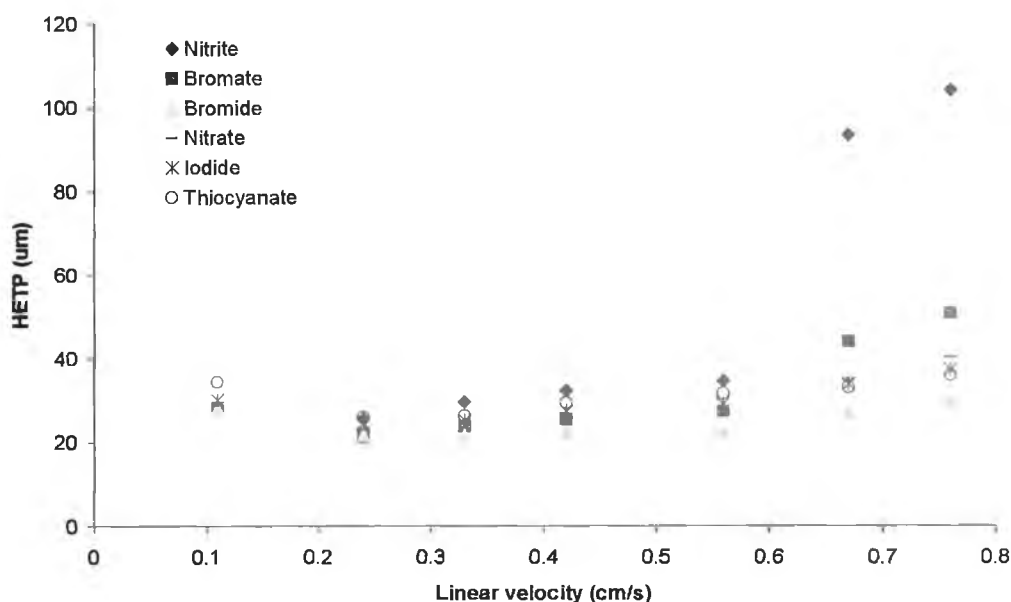


Figure 5.21: van Deemter curves showing the effect of elevated flow rates on anion peak efficiency on the 10 cm L-lysine functionalised silica monolith.

However, when the HETP values for all the anions studied are examined between flow rates of 1 to 5 mL/min, the clear advantage of monolithic columns over traditional particle-packed column is obvious. The trend observed with van Deemter curve for particle-packed columns is a sharp increase in HETP values with increasing flow rates, but for the lysine monolithic there is very gradual increase in HETP values for all of the anions up to flow rates of at least 5 mL/min.

### 5.3.3.3: The effect of eluent concentration on peak efficiency.

As neither a pH gradient nor the application of elevated flow rates results in an optimal, high speed separation of the 6 anions, the next approach investigated was the use of higher eluent concentrations, i.e., up to 50 mM phosphate. As Fig. 5.22 demonstrates, the separation of the 6 anions is possible in 2 minutes using the 50 mM phosphate eluent, pH 3.0, with a flow rate of 5 mL/min, however, there is a notable decrease in the resolution of bromide and nitrate peaks. The retention times for than analytes are as follows: nitrite elutes after 0.6 minutes, followed by bromate at 0.7

minutes, then bromide at 0.8 minutes, nitrate at 0.9 minutes, with iodide being retained for 1.2 minutes and thiocyanate for 1.7 minutes. Although a fast IC separation is now possible, i.e. run time less than 2 minutes, it is important to investigate what impact the increase in eluent concentration has on the efficiency of the separation.

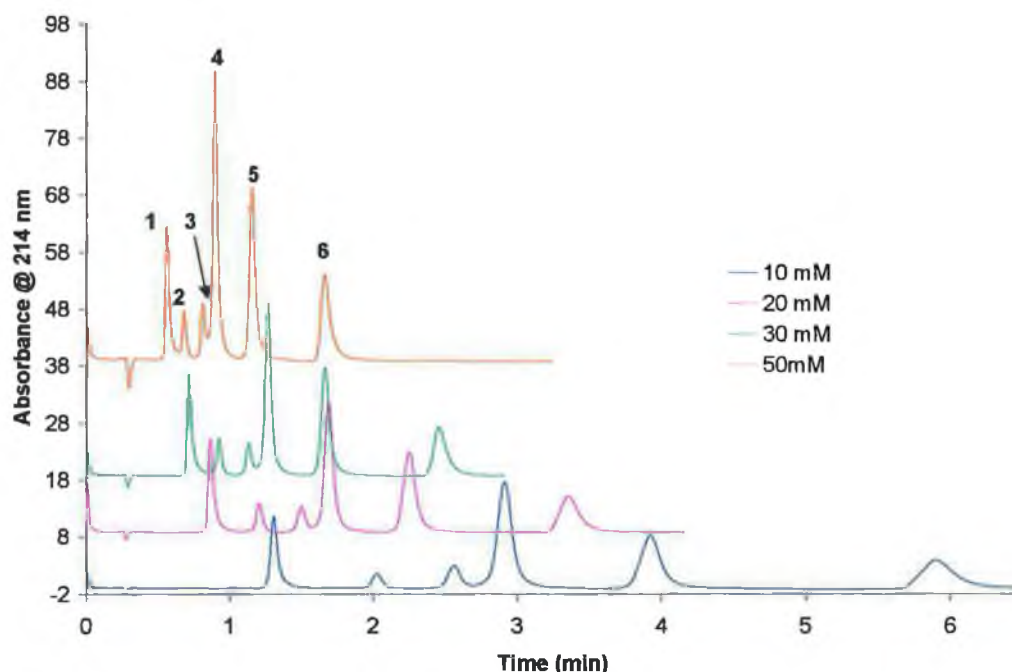


Figure 5.22: Overlays of the separation of 1-nitrite, 2-bromate, 3-bromide, 4-nitrate, 5-iodide and 6-thiocyanate using 10 mM (blue trace), 20 mM (pink trace), 30 mM (green trace) and 50 mM (orange trace) phosphate buffer eluent, pH 3.0, flow rate 4.9 mL/min. Analytes were monitored by direct UV detection at 214 nm.

The HETP values for each analyte peak were calculated at each phosphate buffer (pH 3.0) eluent concentration, i.e. 2-50 mM phosphate. Fig. 5.23 (a) and (b), once again demonstrate the significant difference in the behaviour of the nitrite analyte peak compared to the remaining 5 analytes. At both 1 mL/min and 4.9 mL/min, the nitrite HETP values were observed to increase as the eluent concentration was increased > 10 mM phosphate, with the effect being, once again, more pronounced at the elevated flow rates. However, the optimum eluent concentration in terms of minimising HETP values of the other anions, apart from nitrite, while maintaining a sufficiently rapid separation, would appear to lie between 30 and 50 mM phosphate, flow rate 4.9 mL/min.

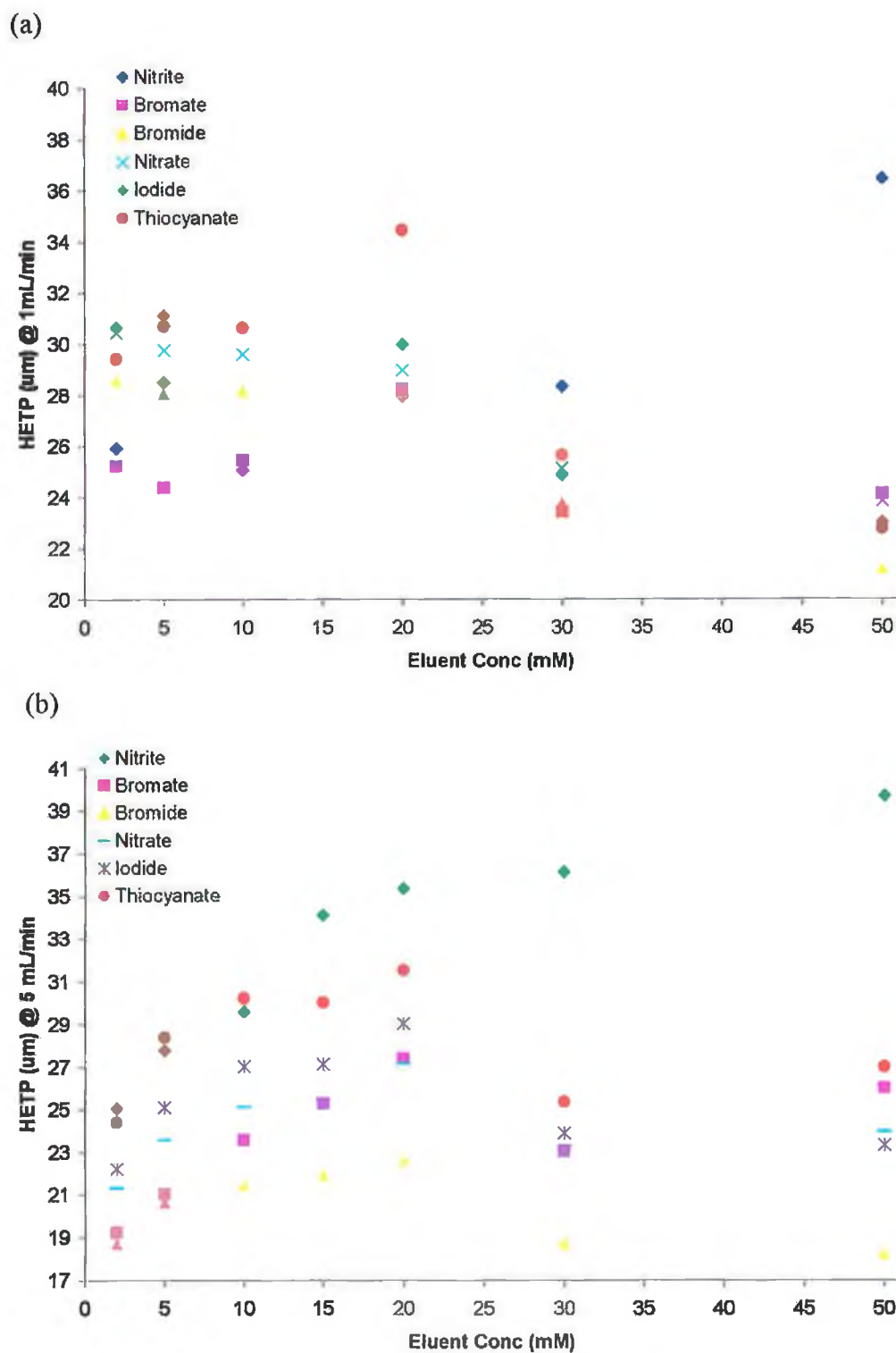


Figure 5.23: The effect of phosphate buffer eluent concentration (pH 3.0) on anion peak efficiencies analysed on the 10 cm L-lysine functionalised silica monolithic column, using flow rates of (a) of 1 mL/min and (b) 4.9 mL/min.

#### 5.3.3.4: Application of flow gradients to separation of nitrite, bromate, bromide, nitrate, iodide and thiocyanate

As is evident from the previous section, the use of elevated flow rates, i.e. 6 mL/min, was not a viable option when attempting to reduce the analysis time, due to the negative impact on peak efficiency of flow rates greater than 4.9 mL/min. Gradient elution can also be employed to reduce the time of the chromatographic analysis. A rarely used alternative approach of flow programming has very limited applications in HPLC with particle-packed columns because of the sharp increase of the associated column backpressure, which limits the flow rate to a relatively narrow range [16]. However, this is less of a problem with the monolithic stationary phase. According to Paull *et al.* [15] the high permeability of monolithic columns provides the analyst with a new option to optimise separations of solutes having very different affinities to the stationary through the use of continuous flow gradient separations. Using a 1 cm coated C<sub>18</sub> monolithic column Paull *et al.* applied a flow gradient to reduce the separation of nitrite, bromide, nitrate, iodide and thiocyanate from 18 minutes at 1 mL/min to a separation in under 7 minutes when the eluent was delivered at 1 mL/min for the first minute and increased to 6 mL/min between t = 1 min and t = 2 min. Schafer *et al.* [17] also considered flow gradient elution on monolithic silica based Chromolith columns. In this instance the use of a sharp increase in flow rate was employed to speed up the elution of one or two strongly retained peaks, which are widely separated from others on an isocratic chromatogram.

Using a 20 mM phosphate buffer, pH 3.0, the separation of the 6 UV absorbing anions was monitored between 1 and 4.9 mL/min. It was observed that a flow rate of 2 mL/min demonstrated the highest peak efficiency values for all 6 analyte peaks. However, the run time at 2 mL/min was greater than 8.5 minutes with iodide eluting over a minute later than nitrate, and there was almost 3 minutes between the elution of iodide and thiocyanate. Therefore, to speed up the elution of iodide and especially thiocyanate, the flow rate was increased from 2 to 5 mL/min over 5 minutes (the flow rate was increased by 0.1 mL/min every 10 sec), which resulted in thiocyanate being eluted in less than 5.5 minutes. When the gradient was applied over 4 minutes (8 sec intervals) thiocyanate was observed to elute after 4.7 minutes and finally thiocyanate

eluted after 4.4 minutes when the gradient was applied over 3 minutes (6 sec intervals).

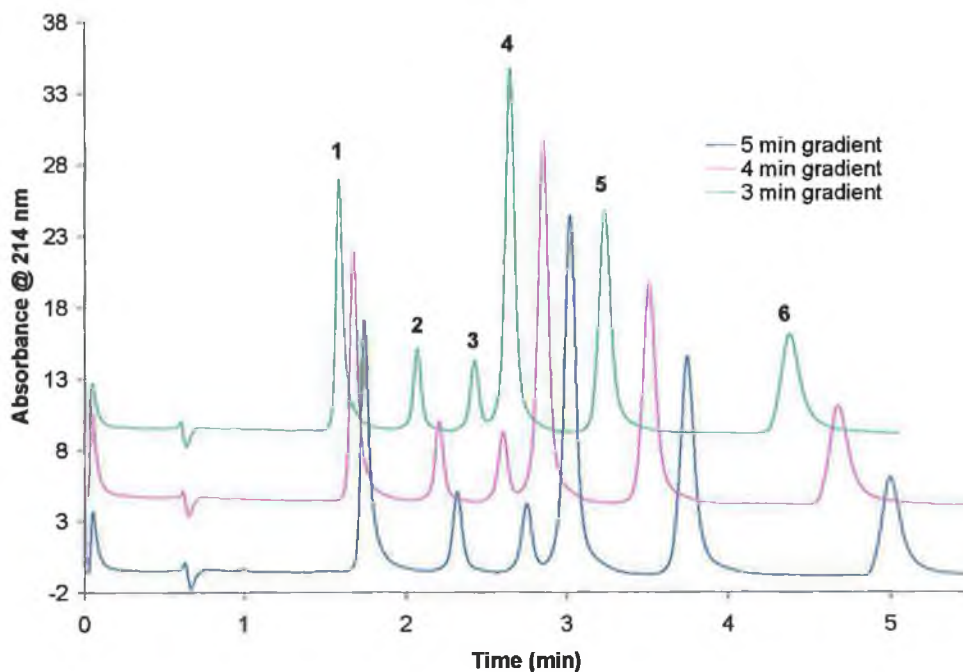


Figure 5.24: Overlays of 1-nitrite, 2-bromate, 3-bromide, 4-nitrate, 5-iodide and 6-thiocyanate separations on a 10 cm L-lysine functionalised silica monolith using a flow gradient, i.e., the eluent flow rate was increased from 2 - 4.9 mL/min over 5 minutes (blue trace), 4 minutes (pink trace) and 3 minutes (green trace). Eluent conditions: 20 mM phosphate buffer eluent (pH 3.0).

It is clear from Fig. 5.24 that the use of flow gradients has the potential to reduce the analysis time because the sharp increase in flow rate resulted in faster elution of iodide and the strongly retained thiocyanate. In an effort to further increase the speed of the separation of the 6 anions, the ionic strength of the eluent was increased to 30 mM phosphate buffer (pH 3.0). Once again, when a van Deemter plot was constructed for the separation of the 6 anions between 1 and 4.9 mL/min, the optimum flow rate in terms of peak efficiency was again found to be 2 mL/min. At 2 mL/min, run time required to separate the 6 anions was 6.5 minutes using the 30 mM eluent. But as Fig. 5.25 demonstrates, when the flow rate was increased from 2 to 4.9 mL/min over a 2 minute period (4 second intervals), the run time of the separation was decreased to just over 3 minutes.

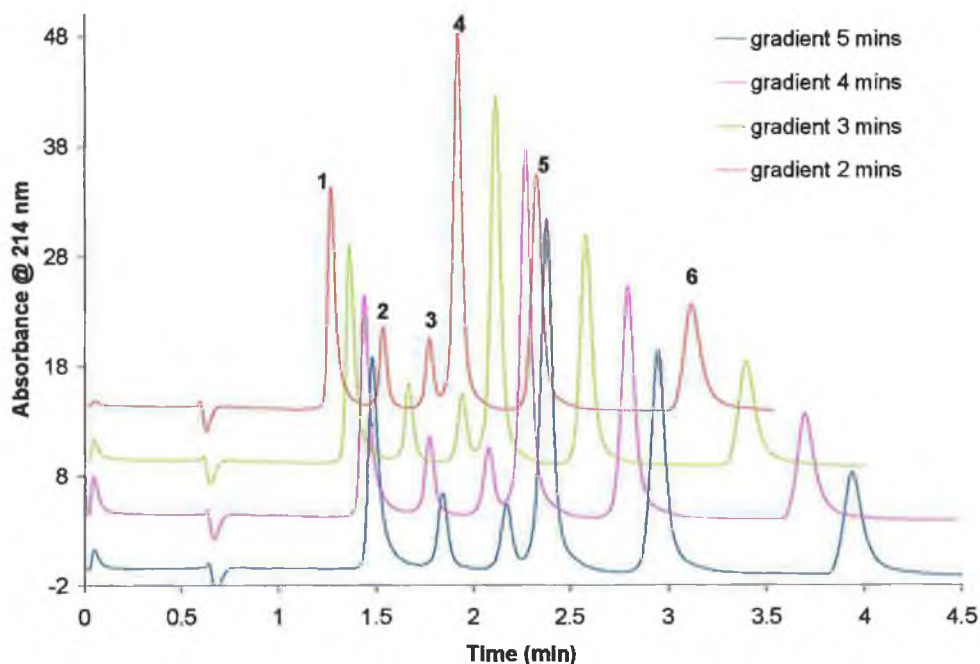


Figure 5.25: Overlays of 1-nitrite, 2-bromate, 3-bromide, 4-nitrate, 5-iodide and 6-thiocyanate separations on a 10 cm L-lysine functionalised silica monolith using a flow gradient, i.e., the eluent flow rate was increased from 2 - 4.9 mL/min over 5 minutes (blue trace), 4 minutes (pink trace), 3 minutes (green trace) and 2 minutes (orange trace). Eluent conditions: 30 mM phosphate buffer eluent (pH 3.0).

In a final attempt to achieve a rapid separation of nitrite, bromate, bromide, nitrate, iodide and thiocyanate the eluent concentration was increased from 30 to 50 mM phosphate buffer (pH 3.0). As the chromatogram in Fig. 5.22 demonstrated, a separation of the 6 anions was possible in less than 2 minutes using the 50 mM eluent (pH 3) and a flow rate of 4.9 mL/min. However, the van Deemter plot (see Fig. 5.26) indicates that the use of elevated flow rates again has a negative impact on efficiency values obtained for nitrite, which is the earliest eluting peak. Therefore, for the 50 mM eluent, two flow gradients were performed. Firstly the flow rate was increased from 1 to 4.9 mL/min over 5, 4, 3, and 2 minute periods and secondly the flow rate was increased from 2 to 4.9 mL/min, again over 5, 4, 3 and 2 minute periods. It is evident from Fig. 5.27 that the use of flow gradients not only reduced the run time but also caused an improvement in peak shape compared to the separation obtained at a constant flow rate of 1 mL/min. When the flow rate was increased from 1 to 4.9 mL/min over 2 minutes (3 sec intervals) the run times were under 3 minutes, while at the constant flow rate of 1 mL/min the run time was greater than 9 minutes.

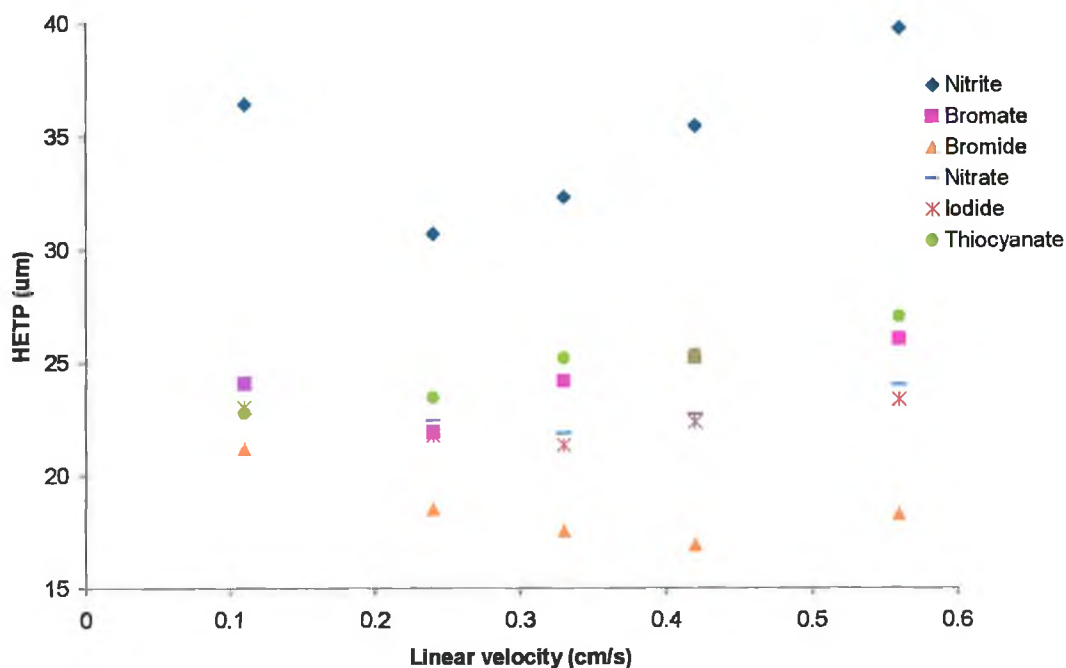


Figure 5.26: van Deemter curve obtained on the 10 cm L-lysine functionalised silica monolith. Eluent conditions: 50 mM phosphate buffer eluent, pH 3.0.

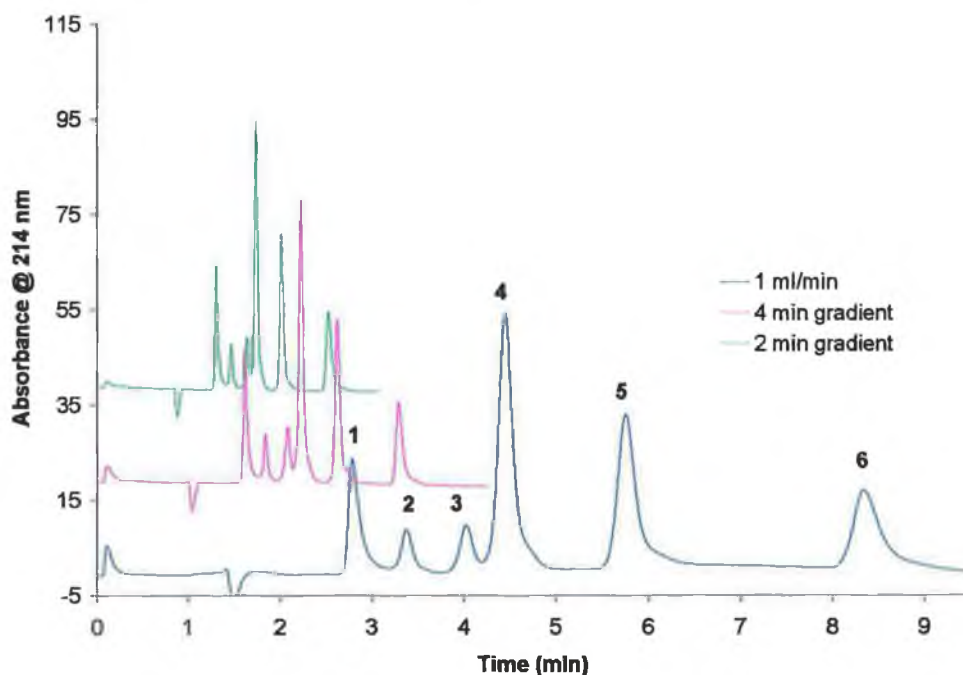


Figure 5.27: Overlays of 1-nitrite, 2-bromate, 3-bromide, 4-nitrate, 5-iodide and 6-thiocyanate separation on a 10 cm L-lysine functionalised silica monolith using a flow rate of 1 mL/min (blue trace), flow gradients: 1 - 4.9 mL/min over 4 minutes (pink trace) and 2 minutes (green trace). Eluent: 50 mM phosphate buffer eluent (pH 3.0).

A second flow gradient was applied to the separation using the 50 mM eluent. In this instance, the flow rate was increased from 2 to 4.9 mL/min again over the time periods of 5, 4, 3 and 2 minutes. The increase in flow rate from 2 to 4.9 mL/min over 2 minutes (flow rate increased by 0.1 mL/min every 4 sec) allowed the separation of the 6 anions in just over 2.5 minutes (see Fig. 5.28).

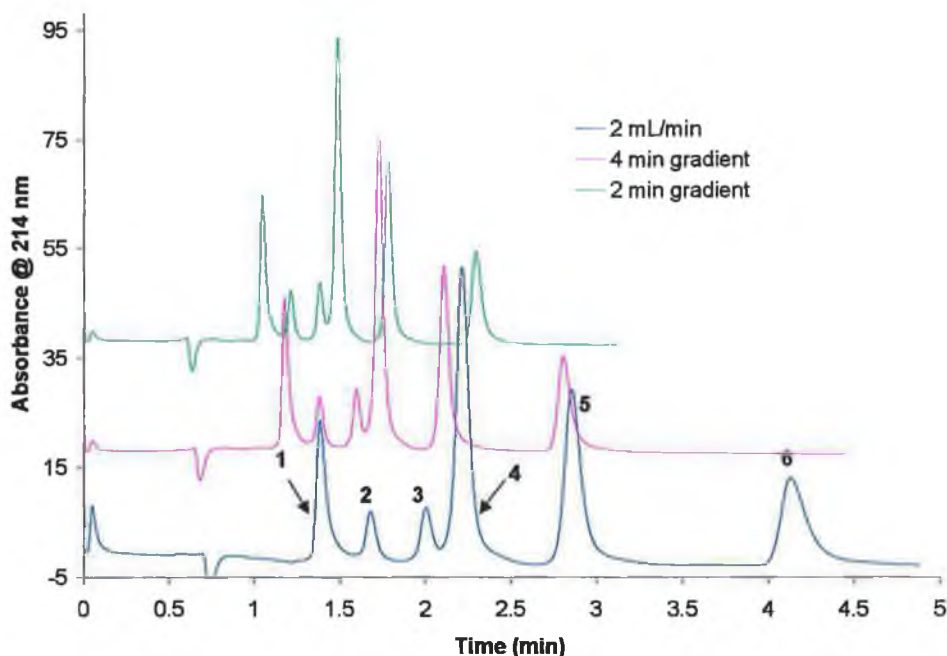


Figure 5.28: Overlays of 1-nitrite, 2-bromate, 3-bromide, 4-nitrate, 5-iodide and 6-thiocyanate separations on a 10 cm L-lysine functionalised silica monolith at 2 mL/min (blue trace) and using a flow gradient, i.e., the eluent flow rate was increased from 2 - 4.9 mL/min over 4 minutes (pink trace), 2 minutes (green trace) Eluent conditions: 50 mM phosphate buffer eluent (pH 3.0).

### 5.3.3.5: Analytical performance

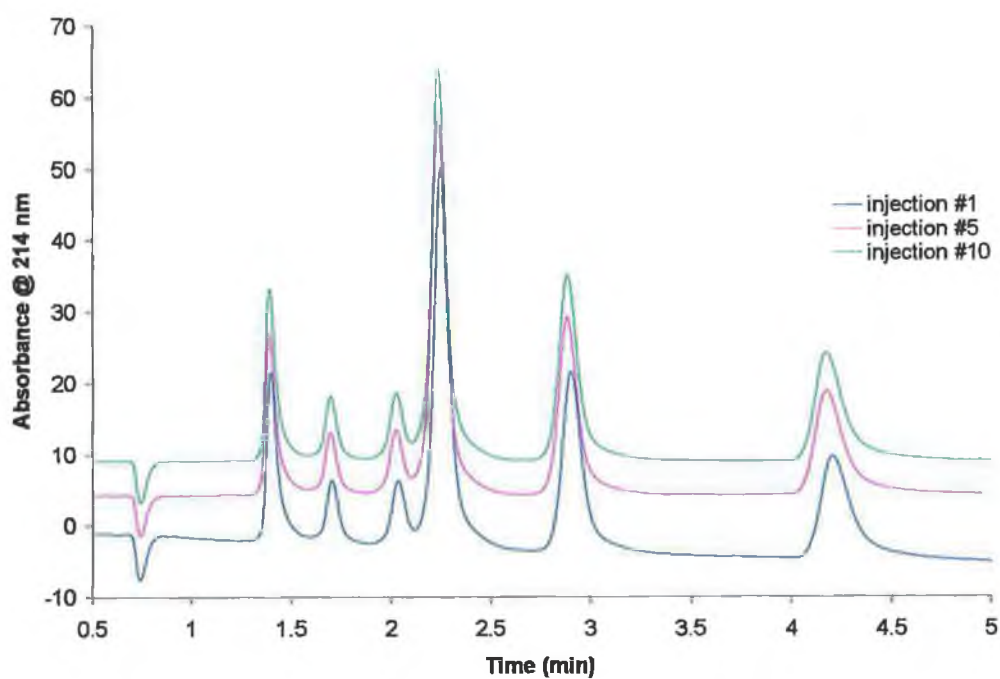
The effect of using elevated flow rates for rapid separation upon method precision was investigated. Using a 50 mM phosphate eluent, pH 3.0, a series of 10 injections of the 6-anion mixture was performed at 2 mL/min and 4 mL/min, and for each anion the % RSD for retention time and peak area was calculated. Overlays of the first, fifth, and tenth standard injections at 2 and 4 mL/min are shown in Fig. 5.29 (a) and (b).

Table 5.7: Summary of the results obtained for the precision study performed using a 10 cm L-lysine functionalised silica monolith. Eluent conditions: 50 mM phosphate buffer eluent (pH 3.0), flow rates 2 and 4 mL/min. A detection wavelength of 214 nm was employed.

	$\text{NO}_2^-$	$\text{BrO}_3^-$	$\text{Br}^-$	$\text{NO}_3^-$	$\text{I}^-$	$\text{SCN}^-$
<b>2 mL/min</b>						
$R_t$ %RSD	0.4	0.2	0.3	0.9	0.3	0.4
Peak Area	3.4	3.4	2.1	3.1	4.1	2.7
%RSD						
<b>4 mL/min</b>						
$R_t$ %RSD	0.2	0.2	0.2	0.2	0.3	0.3
Peak Area	5.4	4.9	5.0	4.0	2.0	4.5
%RSD						

Using the 50 mM phosphate eluent (pH 3.0), the run time for the separation of the six anions at 2 mL/min was just over 4 minutes, while when the flow rate was doubled to 4 mL/min, the run times was just over 2 minutes. As can be seen from the results in Table 5.7, in all but one case, the % RSD for the retention time was below 0.4 %, even at elevated flow rates, showing the stability of the phase under such conditions. The variation in retention time values at 4 mL/min was less than that observed for the analysis performed at 2 mL/min, except in the case of nitrate. The opposite trend was observed for the variation in peak area measurements, where apart from iodide peak, there was a greater variation in peak areas at the higher flow rate of 4 mL/min than was observed at 2 mL/min.

(a)



(b)

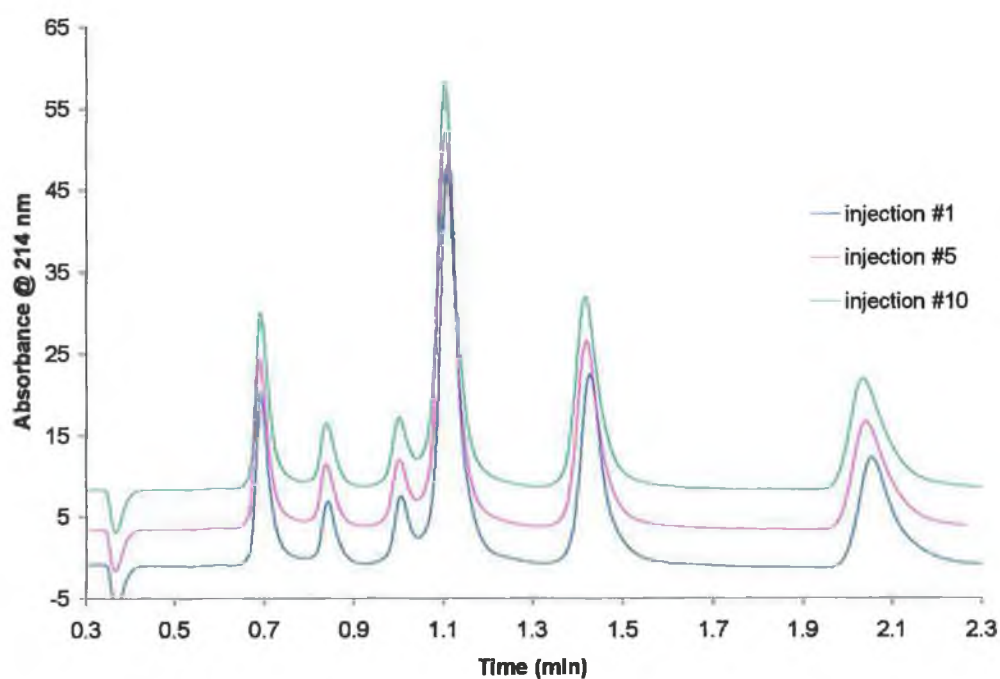


Figure 5.29: Overlays of injection number 1, 5, and 10 of the 10 ppm, 6-test anion mixture<sup>(c)</sup> on the 10 cm L-lysine functionalised silica monolithic column at flow rate (a) 2 mL/min and (b) 4 mL/min Eluent conditions: 50 mM phosphate buffer eluent, pH 3.0. Analytes were monitored using direct UV detection at 214 nm.

<sup>(c)</sup> Anion elution order as per Fig. 5.28

#### **5.4: Conclusion**

Previous studies performed using lysine bonded silica particle-packed columns have only described the retention of alkali and alkaline earth metal ions by cation-exchange. However in this study, the L-lysine functionalised silica monolith has been evaluated for both cation and anion selectivity. The L-lysine functionalised monolith column exhibited selectivity towards transition and heavy metal cations through complexation, whilst only limited retention of alkali and alkaline earth cations was observed. The behaviour of the Zn (II) analyte peak on the lysine functionalised monolith, i.e. the unusual broadening of the peak compared to the peak shapes of the other transition metals investigated, was similar to observations reported for the analysis of Zn (II) on the IDA silica monolith in Chapter 4. The cation-exchange capacity of the lysine functionalised monolith was found to be between 5 and 6  $\mu\text{moles Me}^{2+}$  per column. However, the anion-exchange capacity was much higher at 12-13  $\mu\text{moles A}^-$ , and was found to be dependent on column pH. Therefore, lysine functionalised silica monolithic column exhibited excellent selectivity and efficiency for inorganic anion separations. Using elevated flow rates of up to 5 mL/min the separation of nitrite, bromate, bromide, nitrate, iodide and thiocyanate was possible in approximately 100 seconds, with peak efficiency values between 20,000 and 50,000 N/m.

## **References**

1. K. Cabrera, *J. Sep. Sci.*, 27 (2004) 843.
2. F. Svec, *LCCG Europe*, 16 (2003) 24.
3. M. G. Kolapachnikova, N. A. Penner, P. N. Nesterenko, *J. Chromatogr. A*, 826 (1999) 15.
4. A. I. Elefterov, P. N. Nesterenko, O. A. Shpigun, *Anal. Chem.*, 51 (1996) 972.
5. P. N. Nesterenko, A. I. Elefterov, D. A. Tarasenko, O. A. Shpigun, *J. Chromatogr. A*, 706 (1995) 59.
6. P. N. Nesterenko, *J. Chromatogr.*, 605 (1992) 199.
7. P. N. Nesterenko, *J. High Res. Chromatogr.*, 14 (1991) 76.
8. G. V. Lisichkin, A.Y. Fadeev, A. A. Serdan, P. N. Nesterenko, P.G. Mingalyov, D. B. Furman, *Chemistry of Surface Grafted Compounds*, Fitzmatlit (Moscow) 2003.
9. O. Yamauchi, A. Odani, *Pure and Appl. Chem.* 68 (1996) 469.
10. P. Jones, M. Foulkes, B. Paull, *J. Chromatogr. A*, 673 (1994) 173.
11. E. Katz, R. Eksteen, P. Schoenmakers, N. Miler, *Handbook of HPLC, Chromatographic Science Series, Volume 78, Chromatographic Science Series*, Marcel Dekker (New York) 1998.
12. D. Connolly, B. Paull, *J. Chromatogr. A*, 917 (2001) 353.
13. A. Dudoit, S. Porgauts, *J. Anal. Atrom. Spec.*, 16 (2001) 575.
14. Z. Haung, *J. Anal. & Bioanal. Chem.*, 378 (2004) 1836.
15. B. Paull, C. Ó Ríordáin, P.N. Nesterenko, *Chem Comm.*, (2005) 215.
16. P. N. Nesterenko, M. A. Rybalko, *Mendeleev Comm.*, 14 (2004) 121.
17. C. Schafer, K. Cabrera, D. Lubda, K. Sinz D. Cunningham, *Am. Lab.*, 33 (2001) 25.

## **Chapter 6**

*Ligand-exchange chromatography of amino acids using a copper (II) modified L-lysine functionalised silica monolith*



There are five classes of amino acids, whose R groups are:

- Nonpolar and aliphatic (glycine, alanine, valine, leucine, isoleucine and proline).
- Aromatic, generally nonpolar (phenylalanine, tyrosine, tryptophan).
- Polar but uncharged (serine, threonine, cysteine, methionine, asparagine, glutamine).
- Negatively charged (aspartate, glutamate).
- Positively charged (lysine, arginine, histidine).

### ***6.1.2: Separation of amino acids***

Amino acids in their native form are generally weak chromophores and do not exhibit electrochemical activity, which means that for analytical purposes, they must first be chemically modified (derivatised) [4]. This derivatisation may take place either before or after the separation of the amino acids has been performed [5]. The separation of amino acids and their derivatives are readily achieved by using reversed-phase HPLC (pre-column derivatisation) and ion-exchange chromatography (post-column derivatisation) [6].

The reference method for amino acid analysis is cation-exchange chromatography with ninhydrin detection, because of its ability to resolve, in one analysis, all clinically important amino acids, and also because of its precision and minimal sample preparation [7]. The classic ion-exchange separation, followed by post-column derivatisation with ninhydrin has been improved considerably since its initial conception [8, 9], particularly with the availability of modern dedicated AA analysers [10]. A review by Fekkers [11] also described the popularity of *o*-phthalaldehyde (OAP) as a post-column derivatisation reagent used for the detection of amino acids separated by ion-exchange chromatography on commercial amino acids analysers. As discussed earlier, amino acids are amphoteric ions that can either gain protons to form cations, or lose protons to form anions. Cations are formed in the low pH region and to separate amino acids, a pH gradient is used, either continuous or in steps, starting at approximately pH 3.25, and moving upwards. The pH affects the charge and the proportion of the amino acid in the cationic form. The salt concentration also affects

the elution, because the cations of the salt compete with amino acid cations for ion-exchange sites on the stationary phase [12].

According to Fekkers [11], reversed-phase HPLC methods for derivatised amino acids [13-19] have replaced ion-exchange chromatography for the analysis of amino acids. Furst *et al.* [13] compared four pre-column derivatisation methods with *o*-phthaldialdehyde (OPA), 9-Fluorenylmethyl chloroformate (FMOC-Cl), phenylisothiocyanate (PITC) and dansyl-chloride, for the reversed-phase HPLC determination of free amino acids in biological materials. The methods permitted the measurement of 21-26 major amino acids in 13-40 minutes. In addition to ion-exchange chromatography and reversed-phase HPLC, another separation mechanism has been employed for the separation of standard amino acids, namely ligand-exchange chromatography.

Ligand-exchange chromatography (LEC) can be defined as a technique in which chelating ligands are added to the eluent and undergo sorption onto the stationary phase. These sorbed molecules can then act as chelating agents with certain solutes, e.g. copper salt can be added to the eluent for the chelation and separation of amino acids [20]. According to Walton [12], LEC depends on the exchange of electron donor ligands around a central metal ion. The metal ion chosen is usually Cu (II), because this ion forms the most stable complexes. To date, it is the technique of chiral ligand-exchange chromatography (CLEC) that has received a great deal of attention as a result of its ability to resolve a wide variety of racemic mixtures, including free and derivatised amino acids, hydroxy acids, amino alcohols and peptides [21-30]. Originally introduced by Rogozhin and Davakov, [31] CLEC involved the reversible formation of diastereomeric complexes between transition metal ions (Cu (II) is the most common), chiral ligands (generally amino acids) and enantiomers. For example, Remelli [21] demonstrated the separation of racemic mixtures of underivatised amino acids on a reversed-phase silica column dynamically coated with the chiral selector *N*-*n*-decyl-L-histidine, which was then loaded with Cu (II) ions, whereas Natalini *et al.* [22] employed a reversed-phase silica column dynamically coated with chiral reagent *N,N*-dimethyl-S-phenylalanine-Cu (II).

### 6.1.3: Detection of amino acids

Andersen [32] and Mant *et al.* [5] compared the relative merits of derivatisation before or after HPLC of amino acids. Although pre-column derivatisation is considered to be more sensitive than many of the post-column approaches [32,33], the disadvantages of this approach include the need to ensure complete reaction of the derivatisation reagent, the possibility of interference with the separation by excess reagent, the reaction medium, the formation of artefacts, and the production of several derivatives from one component [5]. Phenylisothiocyanate (PITC), also known as Edman's reagent, is by far the most commonly used pre-column derivatisation reagent [32]. Amino acids are determined as phenylthiocarbonyl (PTC) derivatives using reversed-phase HPLC and UV-Vis detection. Both primary and secondary amino acids (proline and hydroxyproline) produce PTC derivatives. However, this pre-column derivatisation method requires a high vacuum system and a long time for removing the excess reagent and by-products produced during derivatisation [34].

One of the main advantages of post-column derivatisation is that sample preparation is minimal compared to pre-column methods and there is no need for derivatisation to proceed to completion. However more complex instrumentation is required for post-column derivatisation, i.e. the addition of one or more pumps as well as the addition of a post-column reactor, which may lead to additional band broadening. In addition, the column eluate is continuously diluted by the post-column reagent, which results in a decrease in detection sensitivity [5,32,33]. The first automated system for amino acid analysis, described by Spackman, Stein and Moore [35] used ninhydrin as a post-column reagent. At high temperature ( $\geq 100^{\circ}\text{C}$ ), and under acidic conditions, all primary amino acids react with two molecules of ninhydrin to form a chromophore (Ruhemann's purple) with a maximum absorption at 570 nm, see Fig. 6.2. Proline and hydroxyproline, which are secondary amino acids, react with ninhydrin to form a product with an absorption spectrum distinctly different from that formed from primary amino acids. For this reason, amino acid separation and quantitation are monitored at two wavelengths, normally 440 nm and 570 nm [32,36].

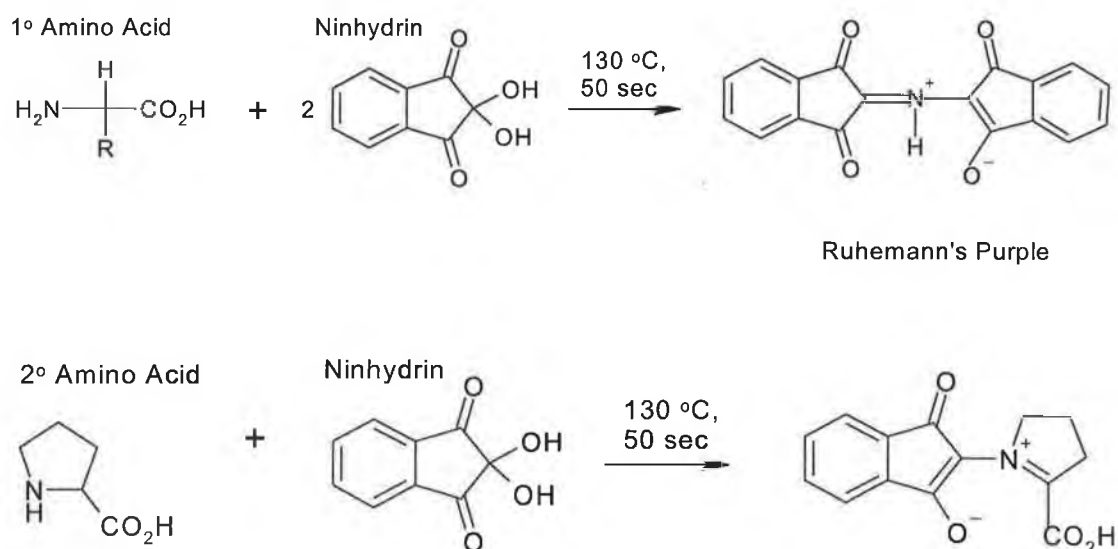


Figure 6.2: The reaction of primary and secondary amino acids with ninhydrin [39].

*o*-Phthaldialdehyde (OPA) was originally introduced as an alternative to ninhydrin in post-column derivatisation and provided a significant increase in sensitivity [37,38]. OPA reacts in alkaline medium with primary amines, and while OPA itself has no inherent fluorescence, its reaction products exhibit very high fluorescent yields. At high pH and in the presence of a thiol, the reaction proceeds almost instantaneously at room temperature to form an isoindole product (see Fig. 6.3), in which both the amino acid and the thiol are incorporated [39,40].

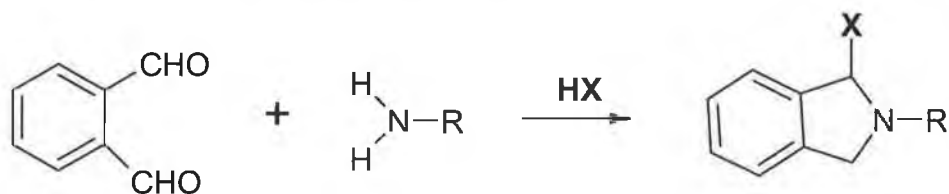


Figure 6.3: The reaction mechanism for the reaction of *o*-phthaldialdehyde with amino acids, where R is the amino acid residue, HX is the nucleophilic agent [41].

Some disadvantages of OPA are the instability of the OPA derivatives and the failure of OPA to react with secondary amines (i.e. proline and hydroxyproline), although this can be circumvented by their on-line oxidation with hypochlorite [39]. OPA is also widely used as a reagent for pre-column derivatisation, employed in conjunction with both reversed-phase and ion-exchange chromatography for the separation of amino acids. According to Mant *et al.* [5] the OPA method, and in particular the pre-column derivatisation methods, is frequently used for amino acid analysis because it is more sensitive and takes less time than other reversed-phase HPLC methods.

In addition to PITC, ninhydrin and OPA, there are a number of other derivatisation reagents. Fluorescamine was also introduced as a possible alternative to ninhydrin, and at high pH, fluorescamine reacts rapidly with primary amines to form fluorescent products [36,40]. 9-Fluorenylmethyl chloroformate (FMOC-Cl) reacts with all amino acids at alkaline pH and room temperature to produce highly stable amino acid derivatives, which have a fluorescent yield comparable to OPA derivatives [42]. Dansyl chloride (DNS-Cl) reacts with both primary and secondary amines to produce fluorescence derivatives, but this approach suffers from the presence of numerous side products and the formation of multiple derivatives of certain amino acids [36,40]. A reagent closely related to DNS-Cl, Dabsy chloride (DABS-Cl), also reacts with primary and secondary amino acids to produce derivatives that have a high absorbance in the visible range. However, a disadvantage of the DABS-Cl reagent is the limited tolerance to the presence of salts [5].

#### ***6.1.4: Objective***

In this Chapter, the separation of L-amino acids on a silica monolith, which has been functionalised with L-Lysine and then dynamically modified with Cu (II) ions, are presented. The effect of different eluent parameters on the amino acids' selectivity was investigated, and in addition, the detection of amino acids by fluorescence was described.

## ***6.2: Experimental***

### ***6.2.1: Column Preparation and modification.***

The on-column functionalisation of a 10 cm Chromolith Performance Si bare silica monolith with lysine groups has been previously described in Chapter 5 (Section 5.2.1). Following the experimental work performed on the lysine monolith in Chapter 5, the monolith was washed with a 10 mM dipicolinic acid solution for 30 minutes at 1 mL/min to remove any bound cations, then washed with 1 M KCl solution for 30 minutes to convert the column to the potassium form, and finally washed with DIW for 30 minutes. Following this wash procedure, the lysine monolith was converted to

the Cu (II) form by pumping a solution of 1 mM CuSO<sub>4</sub> at 1mL/min through the monolith for 90 minutes. The Cu (II) modified lysine monolith was then washed with DIW and equilibrated with the sodium acetate/acetic acid buffer eluent, containing 0.2 mM Cu (II) acetate, before use.

### **6.2.2: Instrumentation**

A Waters Model 600E Multisolvant Delivery System (Waters, Milford, MA, U.S.A.) was used to deliver the eluent. Samples were injected manually using a Rheodyne injector fitted with a 20 µl injection loop. A 1050 series, Hewlett Packard (Palo Alto, CA, U.S.A) UV-Vis spectrophotometric detector and a Waters Model 470 Scanning Fluorescence Detector (Waters, Milford, MA, U.S.A.) were used for the detection of amino acids. An Applied Biosystems 400 Solvent Delivery System (Foster City, CA, U.S.A.) was used for the introduction of the post-column reagent, which was mixed with the eluent using a 5 m PEEK reaction coil (0.25 mm i.d.). The PCR reaction coil was heated using a Mistral Model CL-1 column oven (Spark Holland, P.de Keyserstraat 8, 7825VE Emmen, Holland). An Upchurch Scientific Model P-470 Graduate Micro-splitter (619W Oak St., Oak Harbor, WA 98277, U.S.A) was employed for eluent flow rates > 3 mL/min. Data acquisition was at a rate of 10 Hz with processing of chromatograms performed using a PeakNet 6.0 chromatography workstation (Dionex). Fluorescence spectra were recorded using a Perkin Elmer LS 50B luminescence spectrometer (Perkin Elmer, Wellesley, MA, U.S.A).

### **6.2.3: Reagents**

Sodium acetate, copper (II) acetate (Aldrich chemicals Ltd., Gillingham, UK) and glacial acetic acid (Merck KGaA, Darmstadt, Germany) were used to prepare the required eluents. All eluents and standard solutions were prepared using DIW from a Millipore Milli-Q water purification system (Bedford, MA, U.S.A.), and were filtered through a 0.45 µm filter and degassed by sonication. The PCR reagent used for the detection of L-amino acids consisted of a mixture of 0.2 mM *o*-phthaldialdehyde (Alfa Aesar, GmbH and CoKG, Karlsruhe, Germany) and 10 mM Na<sub>2</sub>SO<sub>3</sub> (Sigma-

Aldrich, Tallaght, Dublin) or 10 mM N-acetyl-L-cysteine (Fluka Chimie, Buchs, Switzerland) prepared in borate buffer (0.1 M, pH 9.2). The kit containing the 20 standard L-amino acids and the D-form of valine, methionine, threonine and tryptophan were all obtained from Sigma-Aldrich, (Sigma-Aldrich Tallaght, Dublin).

### 6.3: Results and discussion

A number of chiral monolithic silica columns have been reported for enantiomeric separations of L- and D-form amino acids [42-44] and in 2004, a rapid pre-column HPLC method based on fluorescent detection for the measurement of a multiple amino acids from both *ex vivo* and *in vivo* biological samples using monolithic reversed-phase silica (C<sub>18</sub>) columns was reported by Dawson *et al.* [45]. In this Chapter, the selectivity of a ligand-exchange monolithic stationary phase for the separation of L-form amino acids will be investigated. As described in Section 6.2.1 the preparation of this monolithic ligand-exchange stationary phase involved the dynamic modification of a L-lysine functionalised silica monolith with Cu (II) ions. Copper (II) was chosen as it forms the most stable metal-ligand complexes.

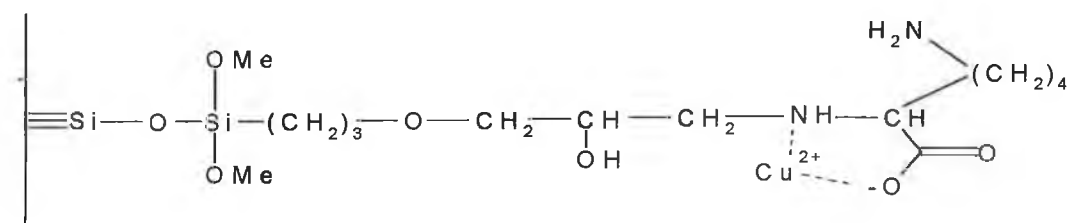


Figure 6.4: Schematic showing the structure of a Cu (II) modified L-lysine functionalised silica monolithic column.

The proposed structure of the Cu (II) modified L-lysine functionalised silica monolith is shown in Fig. 6.4. According to Yamouchi and Odani [46], lysine binds metal ions through the  $\alpha$ -amino and  $\alpha$ -carboxylate groups to form complexes of mono protonated lysine, M(HL)<sub>n</sub>, in acid-neutral solution. The  $\epsilon$ -ammonium group is not involved in metal binding in solution, because chelation through the two amino groups would result in an unstable eight-membered ring.

### 6.3.1: The effect of eluent concentration on amino acids retention

Using a simple sodium acetate buffer eluent (10 mM, pH 4.7), prepared from equimolar concentrations of sodium acetate/acetic acid, the retention of amino acids on the Cu (II)-L-lysine silica monolith was studied. Copper (II) acetate (0.2 mM) was also added to the eluent to minimise the problems of Cu (II) bleed from the L-lysine functionalised monolith. Initially a range of amino acid standards were injected and the retention of the amino acids was monitored using direct UV detection at 254 nm. Although there was little difference in selectivity between alanine, glycine, proline, valine, leucine, serine, methonine and threonine, the Cu (II)-lysine monolithic exhibited a higher degree of selectivity for phenylalanine, tyrosine and especially tryptophan.

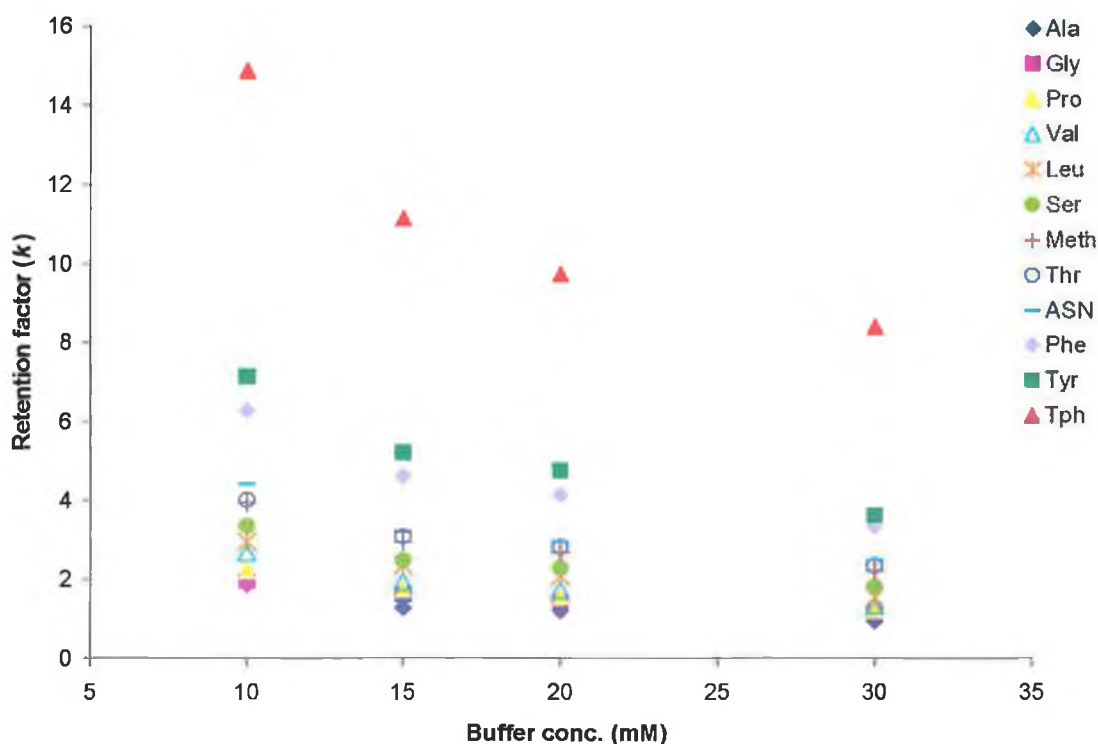


Figure 6.5: A plot of amino acid retention factor as a function of sodium acetate/acetic acid buffer concentration (mM), pH 4.7, flow rate 1 mL/min.

The concentration of the sodium acetate/acetic acid buffer was increased from 10 to 30 mM, and as Fig. 6.5 demonstrates, increasing the buffer concentration did not have a significant effect on the retention of amino acids, except in the case of the highly

retained tryptophan. Using the sodium acetate/ acetic acid buffer (pH 4.7) the elution order of amino acids studied was determined to be: alanine = glycine < proline < valine < leucine < serine < methonine = threoinine < asparagine < phenylalanine < tyrosine <<tryptophan. The selectivity exhibited for the amino acids was limited by the broadness of the amino acid analyte peaks, and with the peak shapes of the later eluting tyrosine and tryptophan being particularly poor.

The effect of varying the concentration of Cu (II) acetate added to the eluent was also studied, and the concentration of Cu (II) was decreased from 0.5 mM to 0.05 mM. The aim of this experiment was to investigate whether or not decreasing the Cu (II), would improve the amino acid peak shapes as well as decreasing the amino acid retention on the Cu (II)-L-lysine monolithic column. Although decreasing the Cu (II) concentration did result in a reduction in amino acid retention, with a significant decrease in the retention of tryptophan observed between 0.2 and 0.05 mM Cu (II) acetate, there was no improvement in amino acid peak shape.

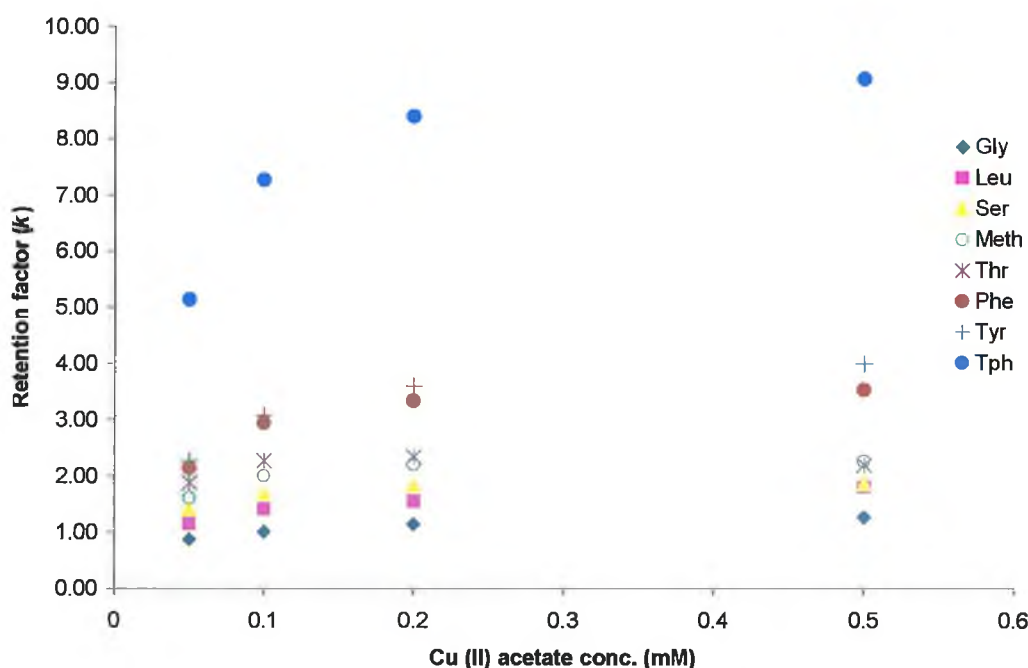


Figure 6.6: A plot of amino acid retention factor as a function of the Cu (II) acetate concentration present in the eluent (30 mM sodium acetate/acetic acid buffer, pH 4.7), flow rate 1 mL/min.

### 6.3.2: The effect of eluent pH on amino acids retention

Fig. 6.7 demonstrates that eluent pH is the most important parameter governing the retention of amino acids on the Cu (II)-L-lysine silica monolith. All the amino acids analysed are retained to a greater extent as the pH increases; the most significant changes concern the amino acids bearing an aromatic R group, i.e. phenylalanine, tyrosine and tryptophan, while for the remaining amino acids the effect seems less pronounced.

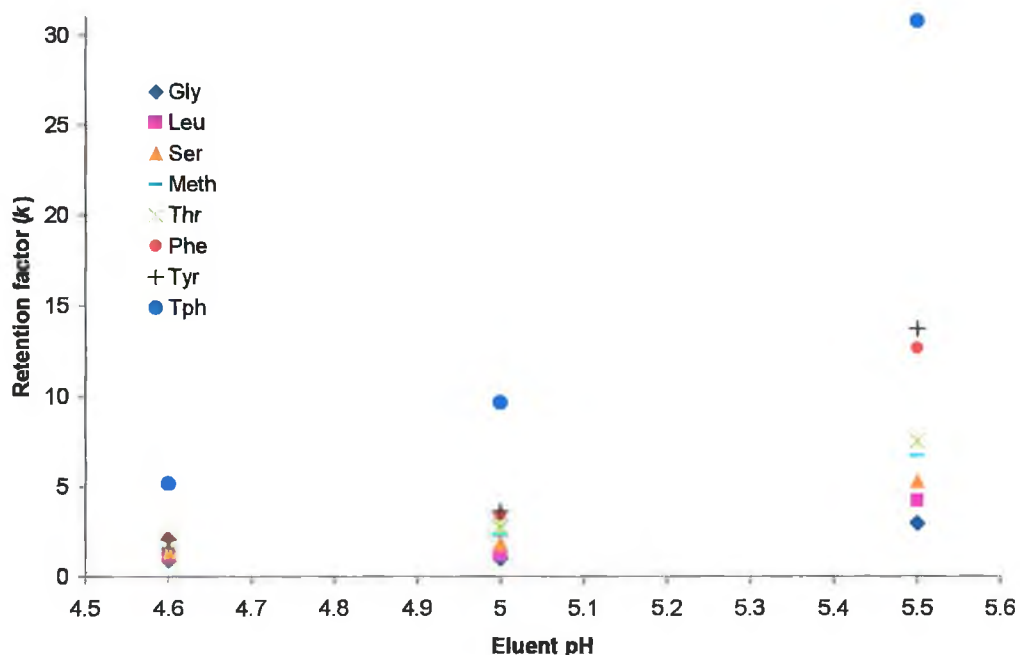


Figure 6.7: A plot of amino acid retention factor as a function of eluent pH (30 mM sodium acetate/acetic acid and 0.05 mM Cu (II) acetate), flow rate 1 mL/min.

In addition to investigating the effect of pH on the retention of the individual amino acid standards, mixtures of different amino acids were prepared, and the effect of eluent pH on the resolution of amino acid mixtures on the Cu (II)-L-lysine monolith was also studied. Two amino acid mixtures were prepared, the first containing 30 ppm glycine, serine, threonine, tyrosine and tryptophan and the second containing 30 ppm leucine, methonine and phenylalanine.

At pH 5.0, it is possible to achieve a separation of glycine, serine, threonine, tyrosine and tryptophan on the Cu (II)-L-lysine silica monolithic, using a 30 mM sodium acetate eluent, which also contained 0.05 mM Cu (II) acetate. Figure 6.8 demonstrates that it is necessary to increase the eluent pH to 5.2 before threonine and tyrosine can be fully resolved. However, increasing the eluent pH from pH 5.0 to 5.2 resulted in excessive retention of tryptophan, i.e. the retention time increased from 14 to 24 minutes, at a flow rate of 1 mL/min. The peak shape of tryptophan was also observed to broaden rapidly with increased retention. Fig. 6.8 also shows the separation of leucine, methionine and phenylalanine at pH 5.2. However, it is clear that the selectivity exhibited by the Cu (II)-L-lysine monolith would not be sufficient to achieve a separation of the 7 amino acid mixture, i.e. glycine, leucine, serine, methionine threonine, phenylalanine, tyrosine. Although the amino acid mixtures were prepared in the eluent used for the separations, there is evidence of a system peak that elutes just before the glycine peak.

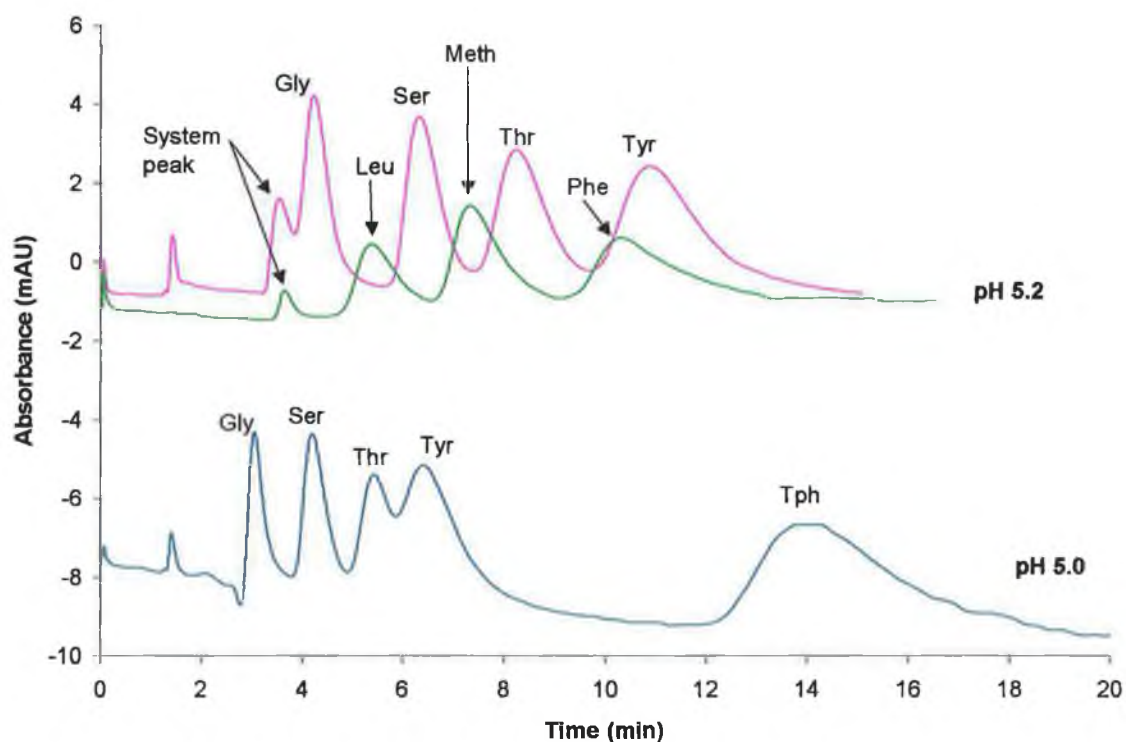


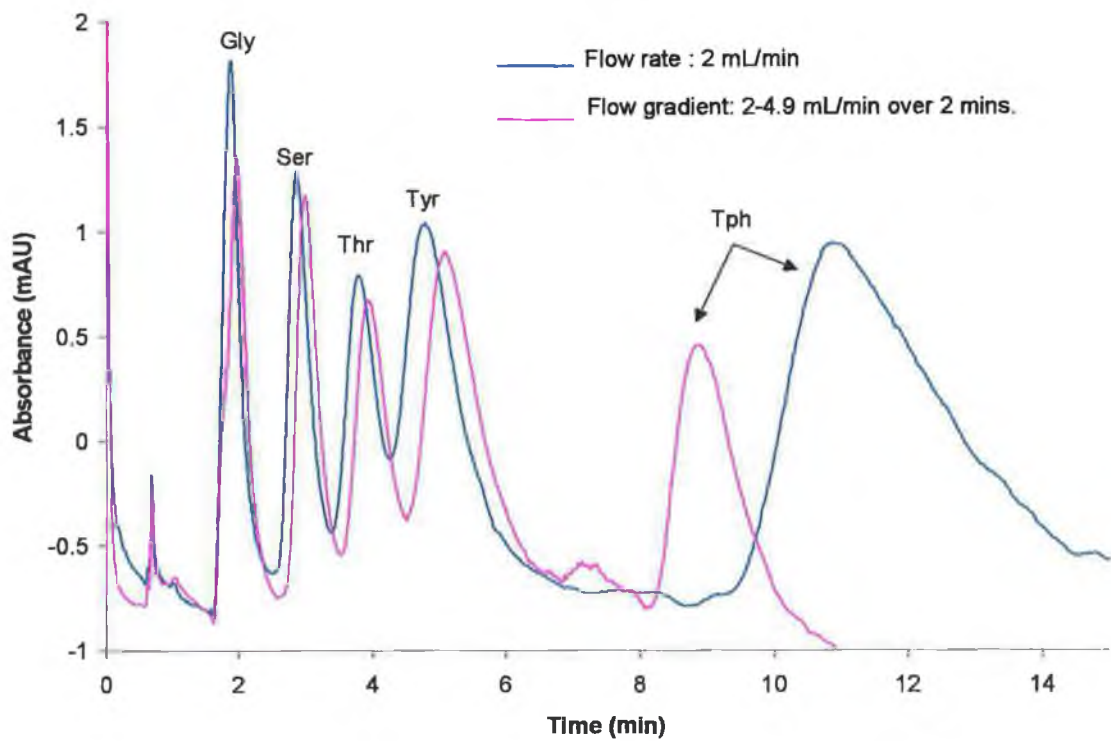
Figure 6.8: The separation of mixtures of amino acids on the 10 cm Cu (II)-L-lysine silica monolith, using a 30 mM sodium acetate/acetic acid buffer eluent containing 0.05 mM Cu (II) acetate, with the eluent pH adjusted to 5.0 and 5.2. Flow rate 1 mL/min and detection by UV detection @ 254 nm.

In order to reduce the excessive retention of tryptophan at pH 5.2, a flow gradient and elevated flow rates were applied to the separation of glycine, serine, threonine, tyrosine and tryptophan. For the flow gradient, the flow rate was maintained at 2 mL/min for 6 minutes to facilitate the separation of glycine, serine, threonine, and tyrosine after 6 minutes, the flow rate was increased from 2 to 4.9 mL/min over a 2-minute interval. It is clear from the separations overlaid in Fig. 6.9 (a) that the use of the flow gradient had a beneficial impact on the tryptophan peak shape, compared to the poor peak shape observed for tryptophan at 2 mL/min. When the mixture of glycine, serine, threonine, tyrosine and tryptophan was analysed at a constant flow rate of 4.9 mL/min, (see Fig. 6.9 (b)), the run time required for the separation of the 5 amino acids was less than 7 minutes. However, the system peak was now observed to interfere with the glycine peak, and the peak shape observed for tryptophan was still very broad in comparison with the other amino acid analyte peaks.

The pH of the 30 mM sodium acetate buffer was further increased to pH 5.7 in an attempt to facilitate the separation of glycine, leucine, serine, methionine, threonine, phenylalanine and tyrosine. Increasing the eluent pH from 5.2 to 5.7 improved the selectivity of the Cu (II)-L-lysine monolith for phenylalanine and tyrosine, while methionine was still observed to overlap with the serine and threonine peaks, see Fig. 6.10. However, despite the improvement in amino acid selectivity with increased eluent pH, the poor efficiency of the analyte peaks limited the resolution of leucine and serine and the phenylalanine, tyrosine resolution when a mixture of 6 amino acids, i.e. glycine, leucine, serine, threonine, phenylalanine and tyrosine, was injected. Once again, the increased eluent pH resulted in excessive retention of tryptophan and at a flow rate of 1 mL/min, the tryptophan peak only eluted after 47 minutes.

Clearly, a pH gradient needed to be employed to improve the peak efficiency observed for the amino acids on the Cu (II)-L-lysine functionalised silica monolith. However, the use of a pH gradient, i.e., using a citrate/citric acid buffer, would lead to a large increase in background absorbance over the gradient run. Therefore, to overcome this problem, fluorescence based detection was investigated.

(a)



(b)

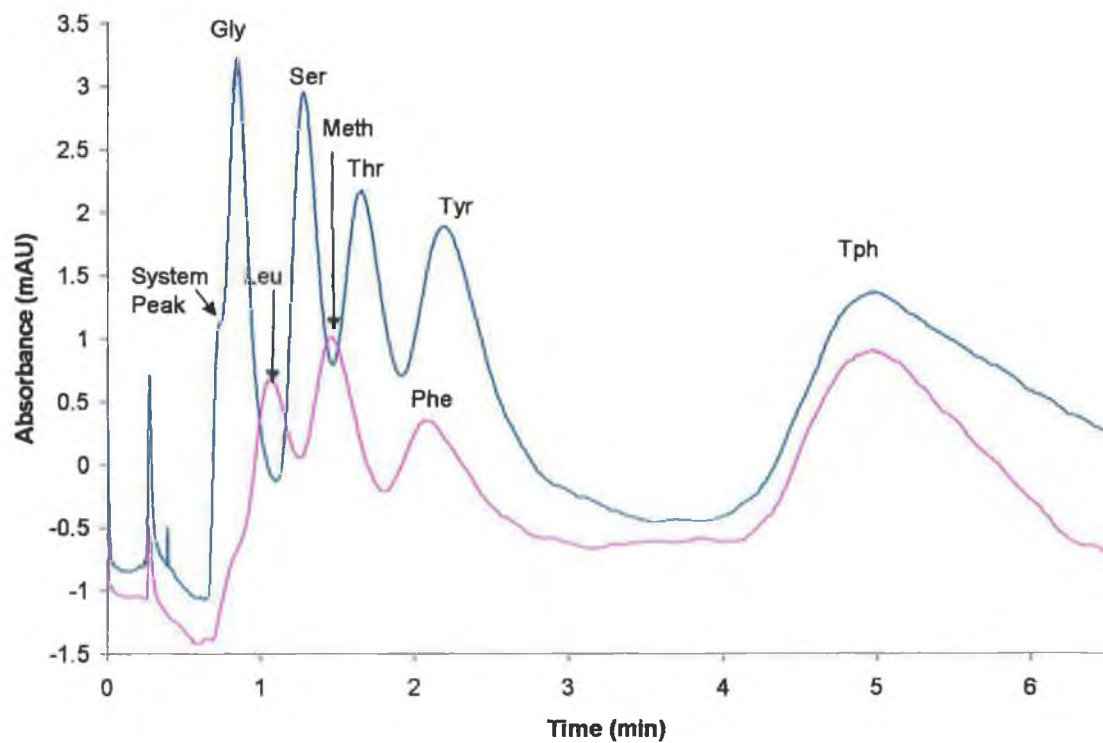


Figure 6.9: The separation of amino acid mixtures using (a) isofluent conditions and a flow gradient and (b) an elevated flow rate of 4.9 mL/min using a 30 mM sodium acetate/ acetic acid buffer (pH 5.2) eluent containing 0.05 mM Cu (II) acetate.

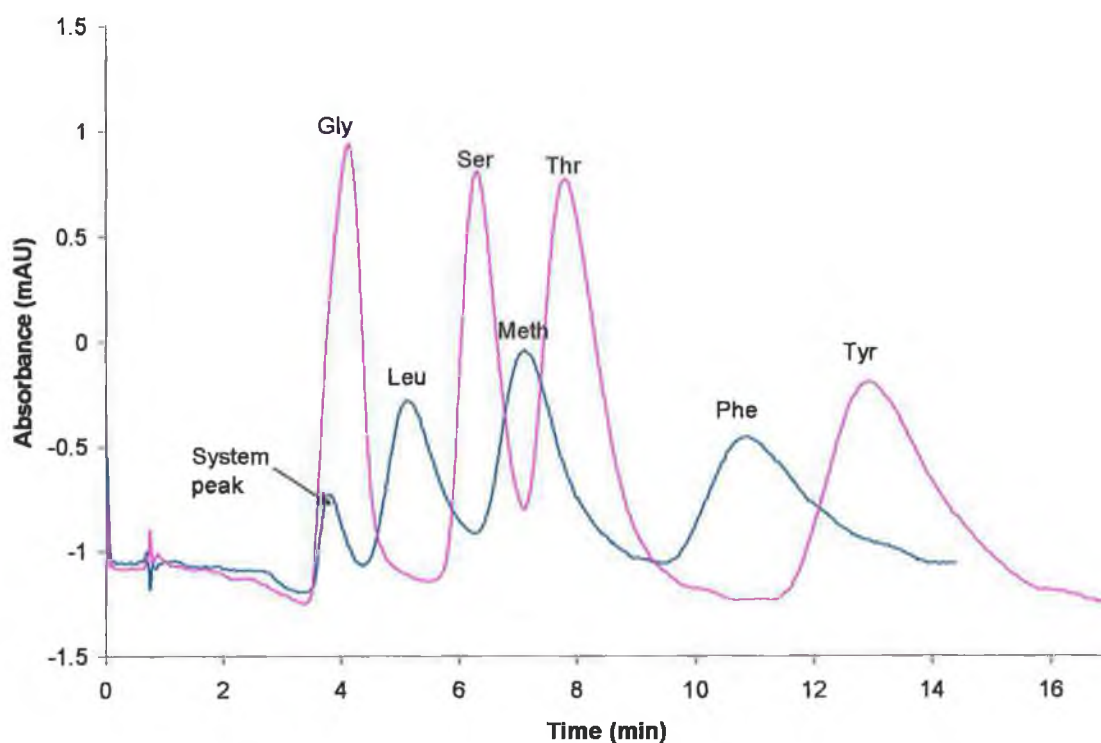


Figure 6.10: The separation of mixtures of amino acids on the 10 cm Cu (II)-L-lysine silica monolith, using a 30 mM sodium acetate/ acetic acid buffer eluent containing 0.05 mM Cu (II) acetate, eluent pH 5.7. Flow rate 2 mL/min and detection by UV detection @ 254 nm.

### 6.3.3: Fluorescence detection of amino acids

It was discussed in Section 6.1, that most amino acids have very low UV extinction coefficients (apart from tryptophan, tyrosine and to a lesser extent phenylalanine), and as a result, a number of reagents have been developed that will react with amino acids to give coloured or fluorescent compounds. Beketov *et al.* [40] investigated the analytical application of the reaction between amino acids and OPA using sulfite and cyanide ions as the nucleophilic agents. However, Beketov *et al.* [40] only investigated the reaction of OPA/Na<sub>2</sub>SO<sub>3</sub> with a single amino acid, i.e. glycine. Therefore, the applicability of the OPA/ Na<sub>2</sub>SO<sub>3</sub> post-column reagent for the sensitive detection of a range amino acids was investigated.

A post-column reagent composed of  $2 \times 10^{-4}$  M OPA,  $1 \times 10^{-2}$  M  $\text{Na}_2\text{SO}_3$  was used in conjunction with fluorescence detection ( $\lambda_{\text{ex}} = 328$  nm and  $\lambda_{\text{em}} = 400$  nm) for the detection of amino acids. As the optimum reaction time reported for fluorimetry is 60 minutes [14], a delay/reaction coil (delay time 0.3 minutes) was employed and this reaction coil was also heated to  $90^\circ\text{C}$ . Fig. 6.11 demonstrates that the fluorescent yield of individual amino acids varied, i.e. there was no response for the 50 ppm threonine standard, whereas the 50 ppm glycine standard exhibited a much greater fluorescence response than the 50 ppm alanine standard. The results suggest that sulphite was not a suitable nucleophilic agent for the rapid and sensitive determination of amino acids (apart from glycine) using OPA as a post-column reagent.

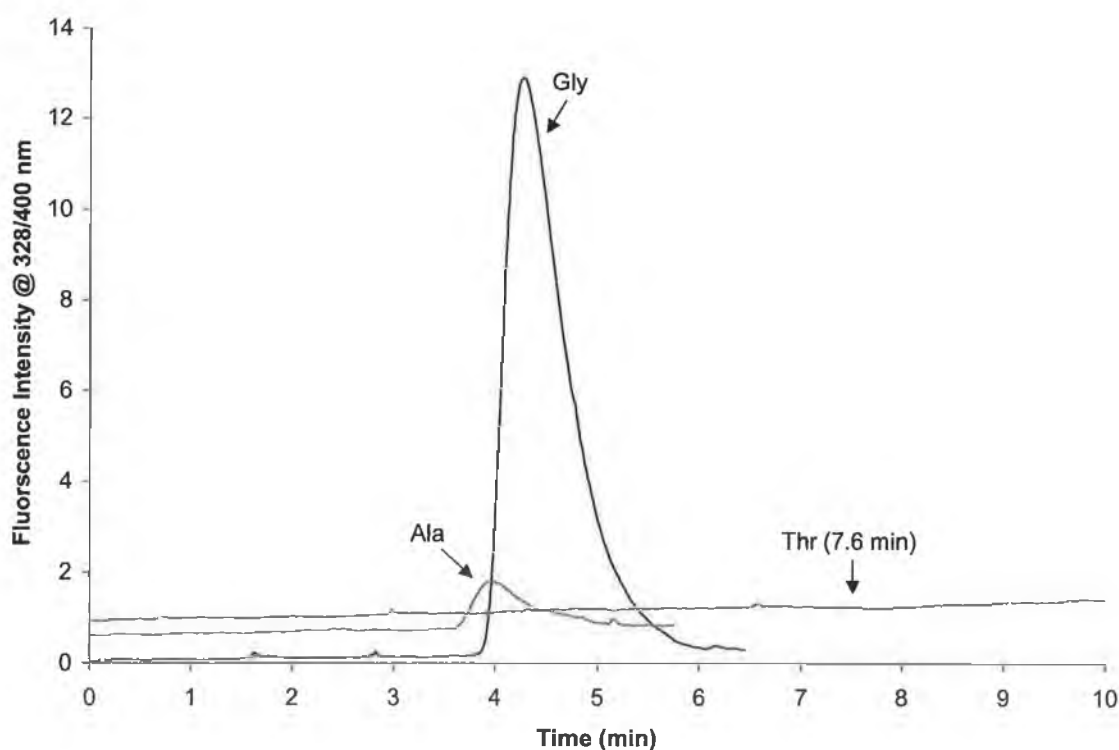


Figure 6.11: The detection of 50 ppm amino acids standards using PCR detection: a OPA/  $\text{Na}_2\text{SO}_3$  reagent, heated to  $90^\circ\text{C}$ , and fluorescence detection at 328/400 nm.

### 6.3.3.1: *Alternative nucleophilic agents.*

Fluorescent derivatives are also rapidly formed at room temperature when primary amino acids react with OPA/thiol based reagents [4] and hence, the thiol N-acetyl-L-

cysteine (NAC), shown in Fig. 6.12, was employed as an alternative nucleophile to sodium sulphite.

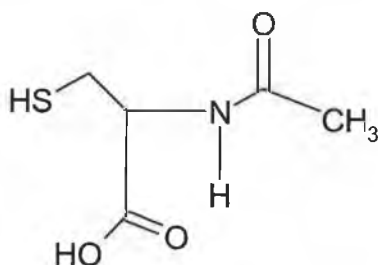


Figure 6.12: The structure of N-acetyl-L-cysteine (NAC).

Before the  $2 \times 10^{-4}$  M OPA/  $1 \times 10^{-2}$  M NAC reagent was used on-line with the HPLC system, the fluorescent yield obtained when this PCR reacts with a number of different amino acids was determined. Using a luminescence spectrometer, the absorption and fluorescence intensities of the amino acids (final concentration 1 ppm) were recorded immediately after the amino acid standard was added to a 1:1 mixture of the eluent (30 mM sodium acetate/ acetic acid buffer (pH 5.7) and 0.05 mM Cu (II) acetate) and the  $2 \times 10^{-4}$  M OPA/  $1 \times 10^{-2}$  M NAC post-column reagent. The resulting scans are shown in Fig. 6.13 (a). Following this experiment, each amino acid/eluent: PCR reagent mixture was allowed to react at room temperature for 30 minutes, and the absorption and fluorescence intensities were again recorded, see Fig. 6.13 (b).

There was a difference in the fluorescent yield obtained for the different amino acids, e.g. glycine, serine and leucine exhibited a much higher fluorescent signal than methionine, phenylalanine or tryptophan. But as Fig. 6.13 (b) demonstrates, when the amino acids were allowed to react with the OPA/NAC reagent for 30 minutes, there was a significant increase in the fluorescent yield observed for all the amino acids studied. Therefore, this suggests that once again a delay/reaction coil should be placed before the fluorescent detector and in addition, this reaction coil should be heated to speed up the amino-OPA/NAC reaction kinetics to facilitate sensitive detection. It is interesting to note that, as with the OPA/ $\text{Na}_2\text{SO}_3$  reagent, glycine behaves differently than the other amino acids studied, i.e. reacting with the OPA/NAC reagent to produce an intensely fluorescent derivative.

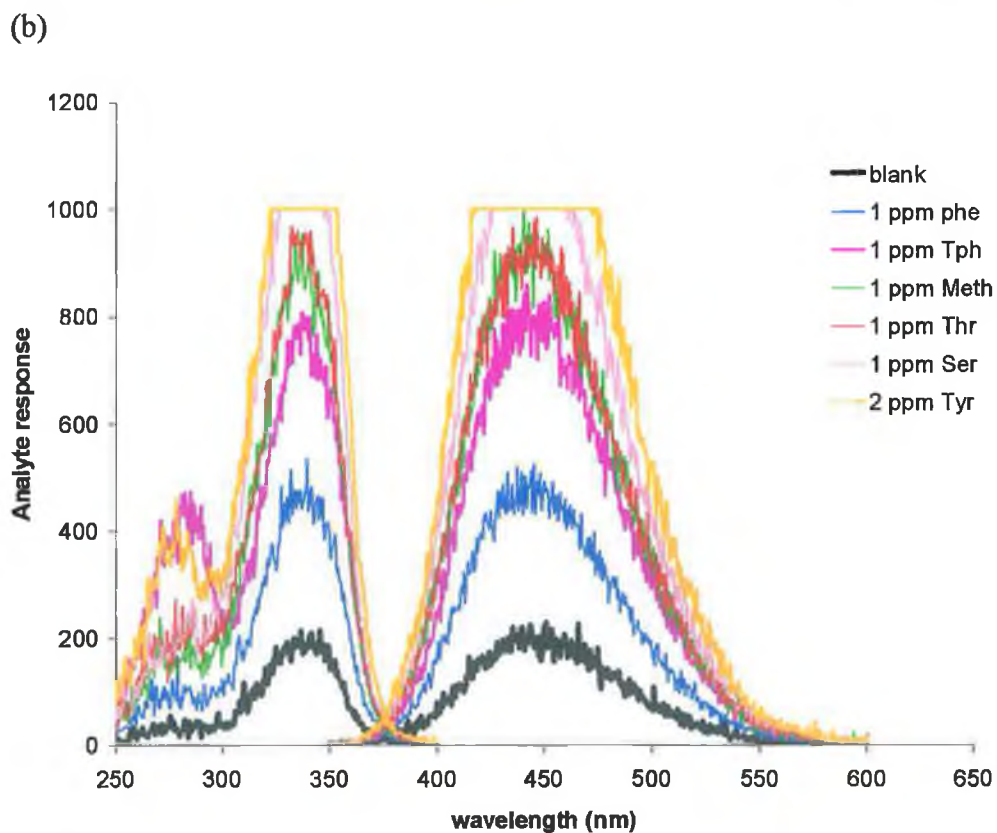
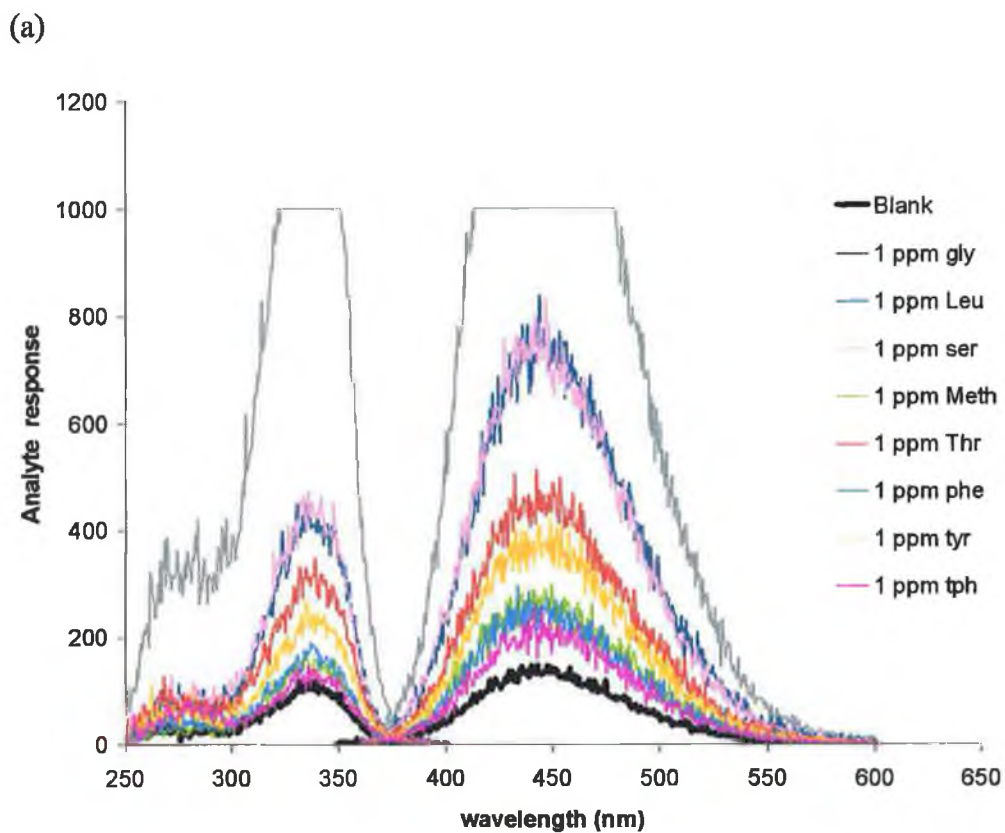


Figure 6.13: Absorption and fluorescence spectra for the amino acid-OPA/NAC reaction (a) reaction time = 0 minutes and (b) reaction time = 30 minutes reaction at room temperature.

Using the absorption and fluorescence spectra shown in Fig. 6.13, the optimum  $\lambda_{\text{excitation}}$  and  $\lambda_{\text{emission}}$ , for the analysis of amino acids with the OPA/NAC post column reagent, were determined to be 340 and 450 nm respectively. The post column reagent was composed of  $2 \times 10^{-4}$  M OPA and  $1 \times 10^{-2}$  M NAC, prepared in 0.1 M borate buffer (pH 9.2), and it was observed that increasing the temperature of the column oven that housed the reaction/delay coil had a significant affect on the sensitivity of the amino acid detection. In fact, increasing the temperature of the reaction coil from 30 to 90 °C resulted in the peak area of 10 ppm serine, threonine and tyrosine being increased by a factor of four (or a factor of 3 in the case of the 0.5 ppm glycine peak).

Beketov *et al.* [40] concluded that the use of nucleophiles such as KCN and  $\text{Na}_2\text{SO}_3$  did not compromise the analytical performance of the OPA-glycine reaction and subsequent detection by fluorescence, when compared with a thiol-based nucleophilic agent, such as 2-mercaptoethanol. However, for fluorescence detection of amino acids other than glycine it is clear that presence of a thiol, such as N-acetyl-L-cysteine, is required for the post-column derivatisation of amino acids with OPA.

Although fluorescence detection facilitated the analysis of a wide range of amino acids, which was not previously possible with direct UV detection, there are a number of limitations associated with the use of a detection method based on a post-column reaction. Signal-to-noise (S/N) ratios were calculated for a number of amino acid standards monitored by direct UV detection (254 nm) and PCR-fluorescence detection (340/450 nm). For early eluting amino acids such as glycine, leucine, serine, methionine and threonine, the S/N ratio calculated for the PCR-fluorescence based detection was approximately double that calculated for direct UV detection. However, for the later eluting tyrosine and tryptophan, the S/N ratio determined for PCR-fluorescence based detection was equal to that calculated for direct UV detection. Although fluorimetry is known to be more sensitive than colorimetry, the use of a second pump to deliver the post-column reagent obviously resulted in additional baseline noise, which adversely affected the sensitivity of the PCR-fluorescence detection method, particularly in the case of tyrosine and tryptophan.

Secondly, the addition of the second pump to deliver the PCR and the presence of the reaction coil (dead volume 0.25 ml) also contributed to band broadening, which adversely affected the efficiency of the amino acid separations. Increasing the acetate buffer pH did not improve the resolution between the amino acids because an increase in pH resulted in the excessive retention of the amino acids and associated peak broadening.

Therefore, to improve the efficiency of the amino acid separation, and hence, the resolution between the analytes, the use of a pH gradient was investigated. Using 10 mM sodium citrate/citric acid buffers (0.05 mM Cu (II) was also added to each buffer), a pH gradient from pH 7 to pH 4 was performed to try and focus the individual amino acids into narrow bands [47]. However, it was observed that the Cu (II) ions were removed from the surface of the modified L-lysine silica monolith as a result of complexation between the Cu (II) ions and the citrate in the eluent. The modification of the L-lysine silica monolith was repeated as described in Section 6.2.1, and the pH gradient experiment was repeated using a much lower concentration of sodium citrate/ citric acid buffer, i.e., 1 mM as opposed to 10 mM. The reduction of the buffer concentration did not prevent the Cu (II) ions being removed from the L-lysine silica monolith, and therefore, following a third re-modification of the L-lysine column with Cu (II) ions, all further experimental work was limited to the use of the sodium acetate/acetic acid buffer (pH 5.7).

#### ***6.3.4: Amino acid selectivity study***

Using the PCR-fluorescence detection method described in Section 6.3.3. it was now possible to determine the elution order of all but three of the twenty standard amino acids on the Cu (II) modified lysine monolith. OPA does not react with secondary amino acids, e.g. proline and, as discussed in Section 6.1.2, the reaction between OPA and cysteine results in a very poor fluorescent yield. Also, histidine was not analysed, as a free histidine amino salt was not available.

Table 6.1: Amino acid selectivity on the 10 cm Cu (II)-L-Lyisne functionalised monolith. Eluent: 30 mM sodium acetate/ acetic acid buffer (pH 5.7), 0.05 mM Cu (II) acetate; flow rate 2 mL/min. Fluorescence detection at 340/450 nm using PCR detection with OPA/NAC reagent.

<b>Amino acid</b>	<b>Properties of R group</b>	<b>pI</b>	<b>Retention factor, <i>k</i></b>
Glycine	Nonpolar and aliphatic	6.06	4.7
Alanine		6.11	4.0
Valine		6.00	5.3
Leucine		6.01	6.0
Isoleucine		6.05	5.8
Phenylalanine	Aromatic, generally nonpolar	5.49	12.2
Tyrosine		5.64	13.7
Tryptophan		5.89	29.9
Serine	Polar but uncharged	5.68	6.7
Threonine		5.60	7.9
Methionine		5.74	7.8
Asparagine		5.41	7.9
Glutamine		5.65	5.9
Lysine	Positively charged	9.6	1.1
Arginine		10.8	1.6
Aspartate	Negatively charged	2.85	43.9
Glutamate		3.15	32.8

The results presented in Table 6.1 demonstrate that there are a number of possible interactions possible with the Cu (II)- L-lysine functionalised silica monolith. As well as the formation of metal–ligand complexes, indicated by the strong pH dependence, additional interactions such as electrostatic interactions, hydrogen bonding and hydrophobic interactions between the amino acid side chain, R, and the hydrocarbon spacer may also affect amino acid retention [29].

The amino acid retention order on the Cu (II)-L-lysine functionalised monolith was observed to be as follows: amino acids with a net positive charge eluted first, followed by amino acids with a partial positive charge, while the amino acids whose

pI was ~ equal to the eluent pH were observed to elute before amino acids with a net negative charge, which exhibited excessive retention. The pI of arginine and lysine and Lys is > pH 9, so at pH 5.7, these amino acids will be positively charged and hence will experience electrostatic repulsion, and hence, as shown in Table 6.1, exhibit little retention. The next amino acids eluted are the nonpolar, aliphatic amino acids. These amino acids, i.e., alanine, glycine, valine, isoleucine and leucine, have a partial positive charge as their pI values are greater than the eluent pH. Therefore, they were observed to elute before the polar, uncharged amino acids, whose pI values are approximately equal to the eluent pH, and so these amino acids will exist predominately in their zwitterionic form. Therefore, the amino acids that exhibit no net charge, i.e. glutamine, serine, methionine and threonine, will exhibit increased retention due to the lack of repulsive electrostatic interactions

Even though the nonpolar, aromatic amino acids, i.e. phenylalanine, tyrosine and tryptophan, also exist predominantly in their zwitterionic form under the eluent conditions employed, they exhibited much stronger retention than the polar, uncharged amino acids. This could be due to the fact that the aromatic R groups could undergo some kind of secondary interactions, i.e. hydrophobic interactions between the aromatic amino acid side chains and the hydrocarbon spacer present in the lysine functionalised silica backbone. And as mentioned earlier, because aspartate and glutamate have a net negative charge, they will undergo both ligand exchange and attractive, electrostatic interactions with the Cu (II)-L-lysine functionalised column, which accounts for the excessive retention of these amino acids.

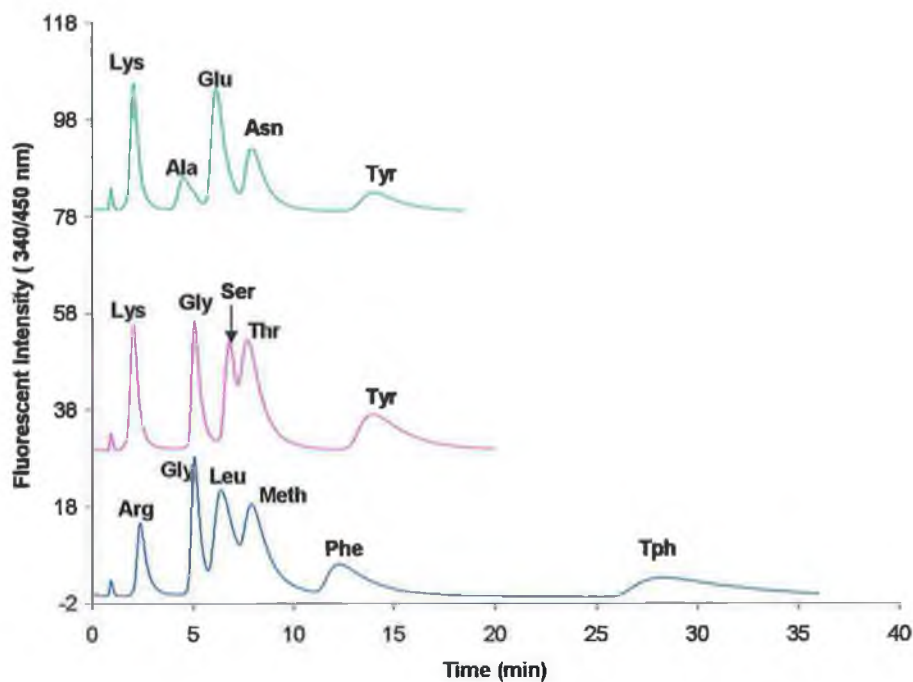
### ***6.3.5: Rapid amino acid separations***

It is clear that the use of high eluent pH has resulted in excessive retention of the amino acids. Therefore, elevated flow rates were employed to reduce the retention of the amino acids shown in Fig. 6.14 (a). A limitation to the use of elevated flow rates is the use of PCR detection, given that the PCR has to be delivered at a flow rate equal to that employed for the eluent, i.e., if an eluent flow rate of 7 mL/min is employed, the PCR pump must be also operated at 7 mL/min. This would cause a large reduction in sensitivity and a combined flow rate of 14 mL/min would not be suitable for the flow cell of the spectrofluorimeter.

Therefore, in order to achieve rapid separations using PCR detection, a flow splitter was placed just after the Cu (II)-lysine functionalised monolith and the eluent flow was split 1:6, so only an eluent flow of 1 mL/min entered the PCR reaction coil, and therefore, the PCR was delivered at 1 mL/min, giving a combined flow rate of 2 mL/min entering the flow cell. Figure 6.14 (b) shows the separation of 3 different amino acid mixtures at 7 mL/min (this was the upper limit of pump operation) and although there has been a reduction in analysis time, the peak shape for the majority of amino acids was still very poor, limiting the number of amino acids which it was possible to separate at flow rates > 4 mL/min.

Even at 7 mL/min, % RSD for the retention times of the amino acids analysed were between 0.1 and 0.6 % (see Table 6.2) however, as expected, the % RSD for amino acid peak area were very high for the majority of the amino acids analysed as a result of the poor peak shapes observed and low efficiency exhibited by the Cu (II)-modified lysine functionalised monolith.

(a)



(b)

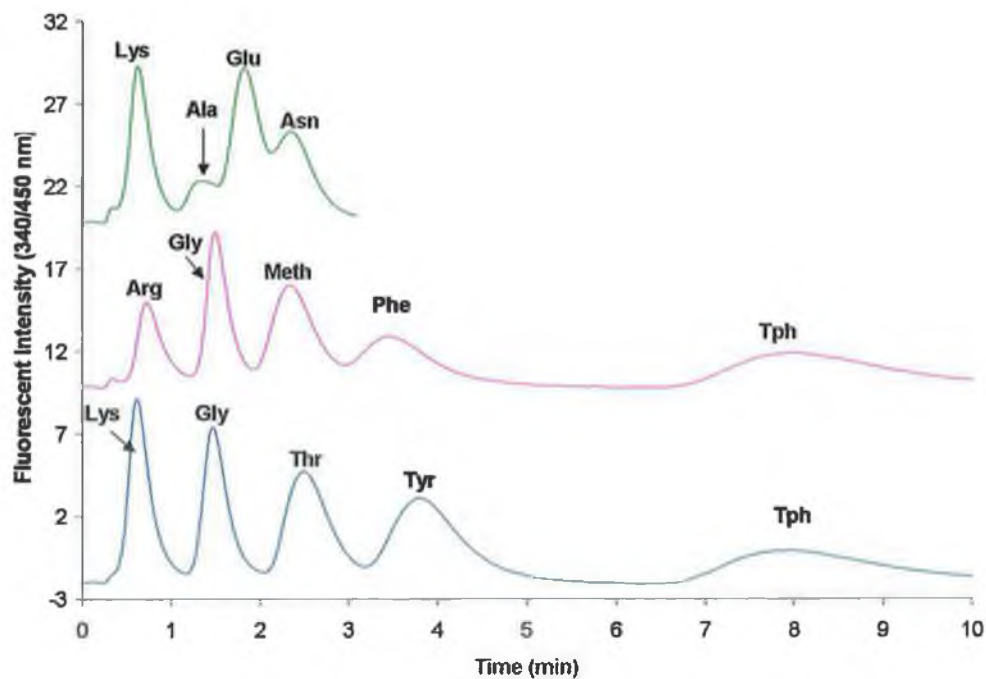


Figure 6.14: The separation of amino acids on the 10 cm Cu (II)-L-lysine functionalised silica monolith using a 30 mM sodium acetate/acetic acid buffer, pH 5.73, 0.05 mM Cu (II) acetate, at flow rates of (a) 2 mL/min and (b) 7 mL/min.

Table 6.2: Precision data for the analysis of amino acids on a 10 cm Cu (II) modified L-lysine functionalised silica monolith, using an eluent composed of 30 mM sodium acetate/acetic acid buffer and 0.05 mM Cu (II) acetate, pH 5.73, at a flow rate of 7 mL/min, (n = 6).

	<b>2 ppm Lys</b>	<b>10 ppm Arg</b>	<b>10 ppm Ala</b>	<b>1 ppm Gly</b>	<b>20 ppm Glu</b>	<b>20 ppm Meth</b>	<b>20 ppm Thr</b>	<b>20 ppm Asn</b>	<b>20 ppm Phe</b>	<b>20 ppm Tyr</b>	<b>30 ppm Tph</b>
<b>Retention Time (min)</b>											
Mean	0.61	0.71	1.28	1.49	1.81	2.31	2.33	2.35	3.39	3.91	7.94
St dev.	0.003	0.003	0.007	0.002	0.002	0.004	0.012	0.006	0.014	0.017	0.037
<b>% RSD</b>	<b>0.4</b>	<b>0.4</b>	<b>0.6</b>	<b>0.2</b>	<b>0.1</b>	<b>0.2</b>	<b>0.5</b>	<b>0.3</b>	<b>0.4</b>	<b>0.4</b>	<b>0.5</b>
<b>Peak Area</b>											
Mean	1.88	1.54	0.23	2.42	1.84	2.56	2.77	0.87	1.39	1.10	3.62
St dev.	0.087	0.039	0.016	0.029	0.096	0.039	0.334	0.036	0.146	0.096	0.238
<b>% RSD</b>	<b>4.7</b>	<b>2.5</b>	<b>6.9</b>	<b>1.2</b>	<b>5.2</b>	<b>1.5</b>	<b>12.1</b>	<b>4.2</b>	<b>10.5</b>	<b>8.8</b>	<b>6.6</b>

### 6.3.6: A study of the chiral ligand-exchange properties of Cu (II)-lysine functionalised silica.

For all standard amino acids (except glycine), the  $\alpha$  carbon is asymmetric, bonded to four different constituent groups: a carboxyl group, an amino group, an R group and a hydrogen atom. The  $\alpha$  carbon atom is thus a chiral centre. Because of the tetrahedral arrangement of the bonding around the  $\alpha$  carbon of amino acids, the four different substituent groups can occupy two different arrangements in space, which are non-superimposable mirror images of each other, and these two amino acid forms are called enantiomers or stereoisomers [3]. L-amino acids are those with the  $\alpha$ -amino group on the left and D-amino acids have the  $\alpha$ -amino group on the right; see Fig. 6.15.

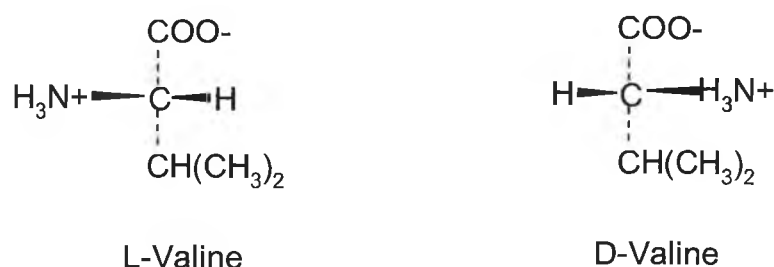


Figure 6.15: The two stereoisomers of valine.

CLEC is a well established method for resolving a wide variety of racemic mixtures, including free and derivatised amino acids. Chiral discrimination is achieved by interaction of each enantiomer with a chiral metal complex, usually Cu (II), leading to the formation of diastereomeric complexes of different stability and/or different affinity for the chiral stationary phase [20-22].

The ability of the Cu (II) modified L-lysine functionalised silica monolith to resolve D- and L-amino acids was investigated using an eluent composed of sodium acetate/acetic acid buffer and Cu (II) acetate. Unfortunately, the availability of D-amino acids was limited, and so, only the following four D-amino acids could be analysed: D-valine, D-methionine, D-threonine and D-tryptophan. The optimum separation of L-amino acids was achieved using an eluent composed of 30 mM

sodium acetate/acetic acid buffer (pH 5.7) and 0.05 mM Cu (II) acetate. However, it was observed that the poor efficiency observed for the L-amino acids on the Cu (II)-lysine monolith limited the number of amino acids that could be separated in a single run. As Fig. 6.16 demonstrates, the resolution of the D- and L- amino acids was also limited and there was little difference in selectivity observed for enantiomers of the amino acids studied. For valine, methionine and threonine, the D-amino acid standard was observed to elute before the L-amino acid standard in each case. However, for the later eluting tryptophan, the D-tryptophan standard was retained longer than the L-tryptophan standard.

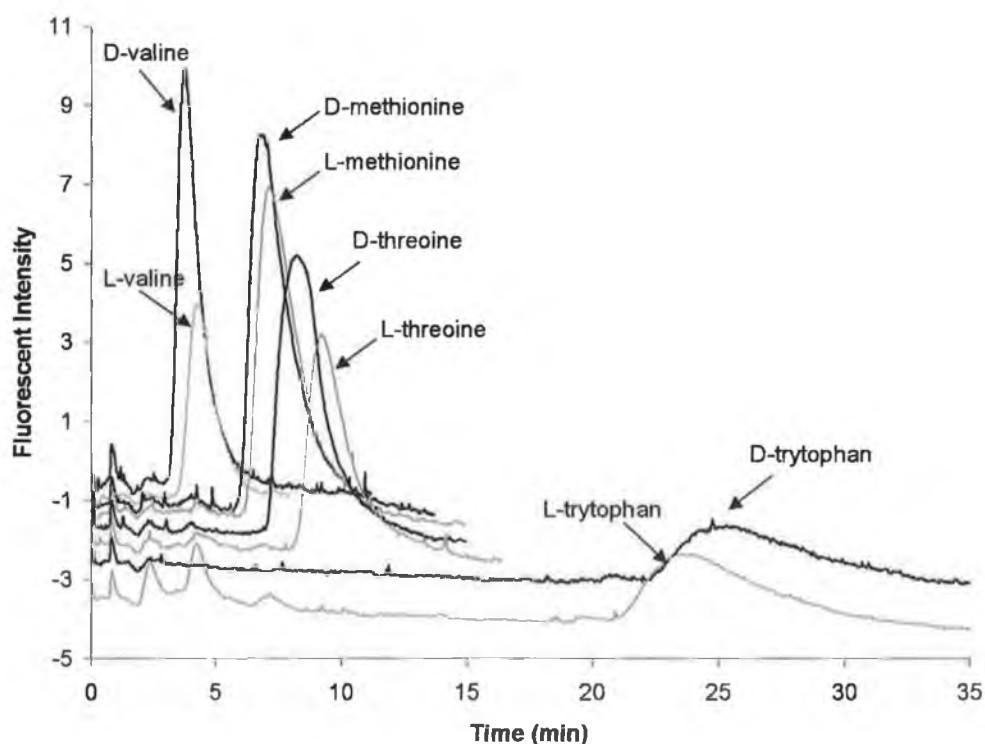


Figure 6.16: Overlays of L- and D-amino acid standards on the 10 cm Cu (II) modified-lysine monolith using a 30 mM sodium acetate buffer (pH 5.7) and 0.05 mM Cu (II) acetate eluent, flow rate 2 mL/min. Fluorescence detection at 340/450 nm using PCR detection with OPA/NAC reagent, 90°C.

## 6.4: Conclusion

Previously, the retention of both cations and anions was demonstrated on the L-lysine functionalised silica monolith. In addition, the separation of amino acids was possible on the L-lysine silica monolith following dynamic modification with Cu (II) ions. The selectivity of 17 standard L-amino acids on the Cu (II) modified-L-lysine silica monolith was investigated, and the effect of eluent parameters, such as ionic strength and pH, on the retention of the amino acids via ligand-exchange chromatography was studied. It was observed that eluent pH was the most important parameter governing amino acid retention and selectivity. Elevated flow rates, i.e. up to 7 mL/min, were employed to achieve rapid separations of different L-amino acid mixtures. The detection of amino acids was based on the reaction of amino acids with a PCR composed of *o*-phthaldialdehyde (OPA) and N-acetyl-L-cysteine (NAC), to produce fluorescent derivatives, which were detected at 340/450 nm. A disadvantage of using post column detection was the associated band broadening, which limited the number of L-amino acids that could be separated in a single run. Poor peak efficiencies were also observed for D-amino acids analysed on the Cu (II) modified-L-lysine monolith and therefore, this limited the resolution of the D- and L-amino acids achieved.

## References

1. Wikipedia, the free encyclopedia, Amino acid, data viewed 31/3/2005  
<[http://en.wikipedia.org/wiki/Amino\\_acid](http://en.wikipedia.org/wiki/Amino_acid)>
2. J. A. Dean, Analytical Chemistry Handbook, Mc Graw and Hill (New York) 1995.
3. M. Lehninger, L. Nelson and A. Cox , Principles of BioChemistry, 2nd Edition, Worth Publishers (New York) 1993.
4. Fluorescence detection of amino acid derivatised with OPA based reagents: Application Note; Dr. Jan Kenh, CMA/Microdialysis AB, Stockholm, Sweden, 2004.
5. C. T Mant, N.E Zhou, R.S Hodges, Chromatography 5<sup>th</sup> edition; Fundamentals and Applications of Chromatography and Related Differential Migration Methods Part B; Applications, edited by E. Heftmann, Elsevier (The Netherlands) 1992.
6. I.G. Casella, M. Contursi, Anal. Chim. Acta, 478 (2003) 179.
7. E. L. Schwarz, W.L. Roberts, M. Pasquali, Clin. Chim. Acta, 354 (2005) 83.
8. P.B. Hamilton, R.A. Anderson, Anal. Chem., 31 no.9 (1959) 1504.
9. J. LeBoucher, C.Charret, C. Coudry-Lucas, J. Giboudeau, L. Cynober, Clin. Chem, 43:8 (1997) 1421.
10. D. Fekkes, J. Chromatogr. B, Biomed. Appl., 682 (1996) 3.
11. H.F. Walton, Chromatography 5<sup>th</sup> Edition; Fundamentals and Applications of Chromatography and Related Differential Migration Methods Part A; Fundamentals and Techniques, edited by E. Heftmann, Elsevier (The Netherlands) 1992.
12. P. Furst, L.Pollack, T.A. Graser, H. Godel, P. Stehle, J. Chromatogr. A, 499 (1990) 557.
13. T. Teerlink, P.A.M. van Leeuwen, A. Houdjik, Clin Chem, 40:2 (1994) 254.
14. D. Fekkes, A van Dalen, M. Edelman, A. Voskuilen, J. Chromatogr. B, Biomed. Appl, 669 (1995) 177.
15. Q. Yong, R.H. Slocum, J.Fu, W.E. Rassmussen, H.D. Rector, J.B. Miller, J.G. Coldwell, Clin. Chimica Acta, 312 (2001) 153.
16. V. Fierabracci, P.Masiello, M. Novelli, E. Bergamini, J. Chromatogr. B: Biomed. Appl., 570 (1991) 285.

17. A.M. Uhe, G.R. Collier, E.A. McLennan, D.J. Tucker, K. O'Dea, J. Chromatogr. B: Biomed. Appl., 564 (1991) 81.
18. H. Liu, H.G. Worthen, J. Chromatogr. B: Biomed. Appl., 579 (1992) 215.
19. R.E. Majors and P.W. Carr, LCGC Editor Advisory board, Glossary of Liquid Phase Separation Terms, date viewed 19/8/2005, <<http://www.lcsupport.com/glossary.htm>>
20. M. Remelli, P. Fornasari, F. Pulidori, J. Chromatogr. A, 761 (1997) 79.
21. B. Natalini, M. Marinozzi, R. Sardella, A. Macchiarulo, R. Pellicciari, J. Chromatogr. A, 1033 (2004) 363.
22. G. Galaverna, R. Corradini, A. Dossena, E. Chiavaro, R. Marchelli, F. Dallavalle, G. Folesani, J. Chromatogr. A, 829 (1998) 101.
23. V. Cucinotta, A. Giuffrida, D. La Mendola, G. Maccarrone, A. Puglisi, E. Rizzarelli, G. Vecchio, J. Chromatogr. B, 800 (2004) 127.
24. G. Gubitz, W. Jellenz, W. Santi, J. Chromatogr., 203 (1981) 337.
25. M. Doury-Bethod, C. Poitrenaud, B. Tremillon, J. Chromatogr., 179 (1979) 37.
26. N. Watanabe, J. Chromatogr., 260 (1983) 75.
27. M. Caude, A. Foucault, Chromatog. Rev., 6 no.1 (1980) 4.
28. M. Schlauch, F-J. Volk, K.P. Fondekar, J. Wede, A.W. Frahm, J. Chromatogr. A, 897 (2000) 145.
29. V. Carunchio, A. Messina, M. Sinibaldi, S. Fanali, J. High Res. Chrom., 11 (1988) 401.
30. D.A. Davakov, S. V. Rogozhin, J. Chromatogr., 60, 1971, 280.
31. T.T Anderson, Albany Medical College, New York, Practical amino acid analysis; date viewed 30/5/2005 <<http://www.abrf.org/ABRFNews/1994/September1994/94practicalaaa.html>>
32. A. Waston and P.R. Brown, HPLC and CE; Principles and Practices, Academic Press (New York) 1997.
33. K-L Woo, Q-C Hwang, H-S Kim, J. Chromatogr. A, 740 (1996) 31.
34. D.H. Spackman, W.H. Stein, S. Moore, Anal. Chem., 30 no.7 (1958) 1190.
35. D.J Holm and H. Peck, Analytical Biochemistry, 3<sup>rd</sup> Edition, Logan (UK) 1998.
36. M. Roth, Anal. Chem., 43 no. 7 (1971) 880.

37. R.C. Dorresteyn, L.G. Berwald, G. Zoomer, C.D. Gooijer, G. Wieten, E.C. Beuvery, J. Chromatogr. A, 724 (1996) 159.
38. Reagents and Conditions-Thomas Instrument Company, Oceanside, California, Trione for UV/Vis Detection and OPA for Fluorescence Detection, date viewed 30/5/2005 <<http://www.hplc1.com/Pickering/PPG49.htm>>
39. Molecular Probes- Invitrogen Detection Technologies, Paisley, UK, Reagents for the analysis of low molecular weight amines, date viewed 11/5/2005 <<http://probes.invitrogen.com/handbook/sections/0108.html>>
40. V.I Beketov, R.D. Voronia, D.G. Filatova, N.B. Zorov, Russ. J. Anal. Chem., 55 no. 12 (2000) 1148.
41. A. R. Bank, E. J. Janse, B. Beekman, J. M teKoppele, Anal. Biochem. 240, (1996) 167.
42. Z. Chen, K. Uchiyama, T. Hobo, J. Chromatogr. A, 942 (2002) 83.
43. Z. Chen, M. Niitsuma, K. Uchiyama, T. Hobo, J. Chromatogr. A, 990 (2003) 75.
44. D. Lubda, W. Lindner, J. Chromatogr. A, 1036 (2004) 135.
45. L. A. Dawson, A. J. Organ, P. Winter, L. P. Lacroix, C. S. Shilliam, C. Heidbreder, A.J. Shah, J. Chromatogr. B; Biomed. Appl., 807 (2004) 235.
46. O. Yamauchi, A. Odani, Pure Appl. Chem, 68 no.2 (1996) 469.
47. T. Anderson, M. Pepaj, R. Trones, E. Lundanes, T. Greibrokk, J. Chromatogr. A., 1025 (2004) 217.

## **Chapter 7**

### ***Solvent enhanced ion chromatography on a bare silica monolith***

## 7.1: Introduction

Silica is the base material for most commonly used packings in HPLC. The silica used for HPLC column packings is essentially porous and non crystalline with the general formula  $\text{SiO}_2 \cdot x\text{H}_2\text{O}$ . There are three types of silanol groups (Si-OH) found on the surface of most forms of silica [1]:

1. When two hydroxyl groups are situated on vicinal silicon atoms, these groups are called vicinal silanols.
2. If the hydroxyl groups are borne by the same silicon atom, the two groups are termed germinal silanols
3. The third type of silanol group is termed isolated or free silanol groups.

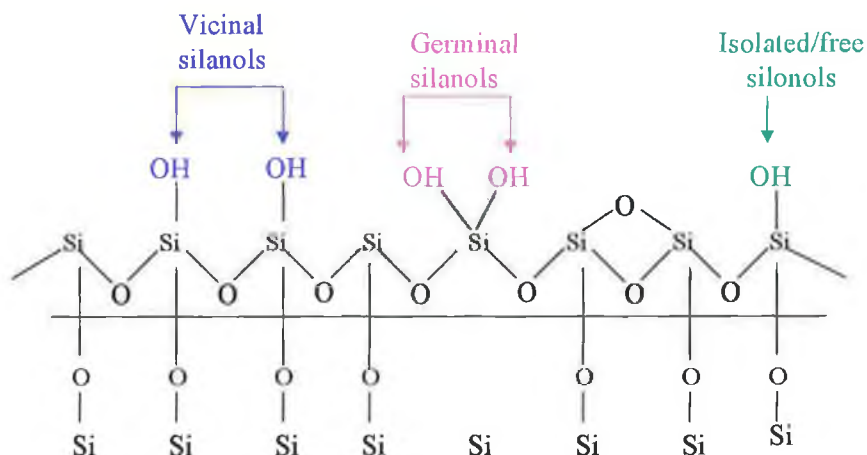


Figure 7.1: The types of silanols groups present on the surface of silica.

These silanol groups are used to graft various organic moieties onto the silica surface, which results in the wide variety of bonded silica essential for HPLC stationary phases. Most of the chemical properties of silica are due to the presence of surface silanols. The hydroxyl acidity is responsible for the acid/base properties of silica and the silanol group is known to behave as a weak acid with a  $pK_a = 7.1$ .

According to a review by G. B. Cox [2], studies performed on unmodified silica columns concluded that the principle mechanism of retention was ion-exchange chromatography on the acidic silanol groups. Berthod [1] also concluded that the

acidic character of surface silanols confers some ion-exchange properties on the porous silica. In buffer or electrolyte solutions, the hydronium ions (protons) of the silanol groups are exchangeable by cations of the solution. The ion-exchange properties of silica are dependent on the pH of the solution, the surface area and the silanol concentration.

Many applications of unmodified silica gels as cation-exchange stationary phases for the separation of alkali, alkaline earth and transition metals have been described. Early reports describing the separation of mono- and divalent cations on unmodified silica gel columns usually employed weakly acidic to neutral eluents with Li as the eluent counter ion [3,4]. However, this resulted in low detection sensitivity (i.e. for conductimetric detection) and short life times of the silica gel column. Therefore, the use of strongly acidic eluents was investigated. Ohta *et al.* [5] achieved the separation of Na, NH<sub>4</sub>, Mg (II) and Ca (II) on a Develosil 30-5 (150 x 4.6 mm i.d.) unmodified silica gel column, using 1.5 mM nitric acid and 0.5 mM pyridine-2,6-dicarboxylic acid as an eluent. The separation was successfully applied to the simultaneous determination of the five cations in rain and river water samples. The simultaneous separation of Na, NH<sub>4</sub>, Mg (II) and Ca (II) in various natural water samples was also demonstrated on an unmodified silica gel column (Super Micro Beads Silica Gel B-5) with an eluent composed of 1 mM oxalic acid/3 mM 18-crown-6 [6]. Using the Develosil 30-5 (150 x 4.6 mm i.d.) unmodified silica gel column, Ohta *et al.* [7] also attempted simultaneous separations of alkali, alkaline earth and transition metal cations under acidic conditions. Using a 1.5 mM oxalic acid eluent it was possible to separate Li, Na, K, Rb, Cs, NH<sub>4</sub>, Mg (II), Ca (II) and Ba (II), as well as achieving a simultaneous separation of the following alkaline earth and transition metal cations: Mg (II), Ca (II), Ba (II), Pb (II), Ni (II), Zn (II), Co (II), Fe (II) and Mn (II) on the unmodified silica gel column.

However, the separations of the alkali, alkaline earth and transition metal cations described above required run times of between 15 and 20 minutes. Therefore, the transition from silica gel to silica monolithic columns is an obvious choice when trying to develop a high-throughput ion chromatography method. As explained previously, the structure of monolithic silica columns consist of both macropores and mesopores that form a network of interconnected flow paths. Due to the high surface

area within the monolithic column, and a reduction in both diffusion path length and flow resistance, faster, higher efficiency separations are now possible [8]. In Chapter 2, the retention of alkali and alkaline earth metal ions on a 10 cm bare silica monolith (Chromolith Si) was demonstrated. Under non-acidic conditions, i.e. using a LiCl eluent, pH 6, limited retention of  $\text{Na} < \text{NH}_4 < \text{K} < \text{Cs}$  was observed. With a 5 mM KCl eluent, retention of alkaline earth metals over pH 4.5 to 6.5 was investigated. The bare monolith showed significant retention of the alkaline earth metal ions over the latter half of this pH range, although selectivity was limited. In 2005, Pack and Risley [8] reported a new approach for the separation of cations on silica monoliths. As opposed to coating a silica monolith with ionic surfactants or bonding ion-exchange functionalities to the silica surface, Pack and Risely used a bare silica monolith for the separation of alkali metals, namely Li, Na and K, in conjunction with an evaporative light scattering detector. Using an eluent of 80 % acetonitrile and 20 % ammonium acetate (50 mM, pH 3.75), and a flow rate of 5 mL/min, the baseline separation of Li, Na and K was possible in less than 2.5 minutes. The optimised method was applied to the rapid determination of Na concentration in several pharmaceutically relevant salts, e.g. naproxen and warfarin.

As mentioned earlier in this introduction, the retention of alkali and alkaline earth metal ions on bare silica supports has been shown in many previous studies [3-7, 9-11] and in each case, weak ion-exchange interactions were deemed responsible for observed ion retention. However, under conditions of high concentrations of organic solvent within the eluent such interactions will become stronger due to a reduced number of waters of hydration associated with the ion. Reduced hydration results in enhanced analyte ion interaction with the stationary phase exchange sites and thus increased retention; hence the separation mode is termed solvent enhanced ion chromatography (SEIC). In addition, selectivity will also be affected by the extent of hydrogen bonding of the solvent molecules with the surface silanol groups. In cation-exchange increasing the organic solvent content of the eluent has been observed to cause significant changes, but the exact effect depends on the dielectric constant of the organic solvent and its ability to form hydrogen bonds. Solvents that exhibit strong hydrogen bonding properties should result in a relatively smaller retention increase, or even decrease, compared to solvents that do not exhibit such properties [9,10,12].

### **7.1.1: Objective**

The aim of this study was the characterisation of alkaline earth and transition metal selectivity on a bare silica monolith using organic based eluents. In addition, the effect of using different organic solvents and alternative acetate buffers on the cation selectivity was also investigated.

## **7.2: Experimental**

### **7.2.1: Instrumentation**

A Dionex Model GPM2 Gradient Pump Module (Sunnyvale, CA, USA) was used to deliver the eluent (1.0 – 4.0 mL/min). An automated injection valve, fitted with a 20- $\mu$ l injection loop was used for the introduction of standards. A PEEK lined bare silica monolithic column (Performance Si) of 10 cm in length and 4.6 mm i.d. was purchased from Merck KGaA (Damstadt, Germany). According to the manufacturer the silica monolith had a surface area of 300 m<sup>2</sup>g<sup>-1</sup>, with a 2  $\mu$ m macroporous and 13 nm mesoporous structure. A pressure driven Dionex Reagent Delivery Module was used for the introduction of the PCR, which was mixed at room temperature with the eluent using a 0.5 m PEEK reaction coil (0.25 mm i.d.). An Applied Biosystems 400 Solvent Delivery System (Foster City, CA, U.S.A.) was used to deliver the PCR when eluent flow rates greater than 3 mL/min were employed. A 1050 series, Hewlett Packard UV-Vis detector (Paloalto, CA, U.S.A) was used to monitor the resultant chromatograms. When working with eluent flow rates between 1 and 5 mL/min, a Waters Model 600E Multisolvent Delivery System (Waters, Milford, MA, U.S.A.) was used as the eluent delivery system, the applied Biosystems 400 Solvent Delivery System (Foster City, CA, U.S.A.), was required to deliver the PCR, and a Shimadzu model SPD-6AV UV-Vis detector (Kyoto, Japan) was used to monitor the resultant chromatograms. Data acquisition was at a rate of 10 Hz with processing of chromatograms performed using a PeakNet 6.0 chromatography workstation (Dionex).

### 7.2.2: Reagents

Acetonitrile, methanol (HPLC grade, LabScan Ltd., Stillorgan Ind. Park, Dublin), ammonium acetate (Aldrich chemicals Ltd., Gillingham, UK) and glacial acetic acid (Merck KGaA, Damstadt, Germany) were used to prepare the required eluents\*. All eluents and standard solutions were prepared using DIW from a Millipore Milli-Q water purification system (Bedford, MA, U.S.A.), and were filtered through a 0.45  $\mu\text{m}$  filter and degassed by sonication. The PCR reagent used for the detection of transition metals consisted of a mixture of 0.4 mM 4-(2-pyridylazo) resorcinol (PAR, purchased from Sigma-Aldrich, Gillingham, UK) and 0.5 M ammonia (BDH Laboratory Supplies, Poole, England), adjusted to pH 10.5 (monitored at 510 nm). For the detection of alkaline earth metals the PCR reagent used was 0.4 mM *o*-cresolphthalein complexone (*o*-CPC, Sigma-Aldrich, Gillingham, UK), 0.25 M boric acid (Sigma-Aldrich, Tallaght, Dublin, Ireland) adjusted to pH 10.5 with 1 M NaOH (monitored at 570 nm). Low-level standard solutions of metal cations were generally made up freshly each day from stock solutions (1000 ppm). Mg (II), Ca (II), Sr (II), Ba (II), Mn (II), Co (II), Ni (II), Cd (II), Zn (II) and Pb (II) standards were prepared from their chloride salts (Sigma-Aldrich, Tallaght, Dublin) and Fe (II) and Cu (II) standards were prepared from their sulphate salts (Sigma-Aldrich, Tallaght, Dublin).

\* To calculate the actual buffer concentration present in the each eluent the volume change upon mixing of acetonitrile and the aqueous phase had to be calculated for the 60:40, 70:30 and 80:20 mixtures and using this factor, the diluted buffer concentration in acetonitrile/aqueous eluent could be determined. For example, the % volume loss due to contraction was determined to be 5 %, 4 % and 3 % for the 60, 70 and 80 % acetonitrile/aqueous eluents respectively, and therefore, when 50 mM ammonium acetate/acetic acid buffer was added to acetonitrile to give a final volume of 500 mls, the actual buffer concentrations present in the eluent were as follows:

- At 60 % acetonitrile, the buffer concentration = (200 mls) (50 mM) / (475mls), which is equal to 21.1 mM
- At 70 % acetonitrile, the buffer concentration = (150 mls) (50 mM) / (480mls), which is equal to 15.6 mM
- At 80 % acetonitrile, the buffer concentration = (100 mls) (50 mM) / (485mls), which is equal to 10.3 mM

### 7.3: Results and discussion

#### 7.3.1: Alkaline earth metal ion selectivity on a bare silica monolith

##### 7.3.1.1: The effect of % organic solvent on alkaline earth retention

Following on from the work of Pack and Risely [8], the retention of alkaline earth metal cations on a 10 cm Chromolith Si bare silica monolith was investigated. Using an ammonium acetate/acetic acid buffer, the effect of varying the % acetonitrile in the eluent was investigated. As the results in Table 7.1 demonstrate, increasing the % acetonitrile from 60 to 80% (with the final buffer concentration kept constant at 30 mM) resulted in a significant increase in alkaline earth metal ion retention. Numerous studies have concluded that the degree of hydration of the analyte and eluent ions have a major influence upon selectivity, and that by including organic solvents within the eluent, both ions in solution and fixed ion-exchange sites within the stationary phase will lose waters of hydration, and in most cases, reduced hydration results in enhanced analyte ion interaction with the stationary phase exchange sites [9,10,12].

Table 7.1: Effect of increasing % acetonitrile on the retention of Mg (II), Ca (II), Sr (II) and Ba (II) on a 10 cm bare silica monolithic column. Eluent conditions: acetonitrile and 30 mM ammonium acetate/acetic acid buffer, pH 4.6, flow rate 1 mL/min.

% Acetonitrile	Retention factor ( <i>k</i> )			
	Mg (II)	Ca (II)	Sr (II)	Ba (II)
60	0.8	0.9	1.0	1.3
70	1.4	1.7	1.9	2.6
80	3.9	3.8	Not detected	Not detected

The retention order shown with the acetonitrile based eluents was typical of that seen with ion-exchange, namely Mg (II) < Ca (II) < Sr (II) < Ba (II), although at 80 % acetonitrile, it was observed that Mg (II) was retained slightly longer than Ca (II).

The post-column reagent employed for the detection of the alkaline earth metal cations consisted of 0.4 mM *o*-CPC and 0.25 M boric acid, pH 10.5, ( $\lambda = 570$  nm). However, as the % of acetonitrile was increased in the eluent, the solubility of boric acid decreased and precipitated out of solution when the eluent was mixed with the post-column reagent. Therefore, when the 80 % acetonitrile, ammonium acetate buffer eluent was employed, the *o*-CPC, boric acid solution was replaced with 0.4 mM PAR in 0.5 M ammonia, pH 10.5, as the post-column reagent. Although PAR is the post-column reagent of choice for transition ions, it was still possible to detect Mg (II)- and Ca (II)- PAR complexes at 510 nm even though the detector response was very weak, but it was not possible to detect Sr (II) or Ba (II).

### ***7.3.1.2: The effect of buffer concentration on alkaline earth ion retention.***

The effect of varying the eluent buffer concentration upon cation selectivity was investigated. The ammonium acetate/acetic acid buffer concentration was increased from 25 to 100 mM ( $n = 4$ ). However, this buffer concentration refers to the undiluted buffer concentration prior to mixing with the acetonitrile. The calculation of the actual buffer concentration present in the each eluent is shown in Section 7.2.2.

At each % acetonitrile, it was observed that as the ammonium acetate/acetic acid buffer concentration increased there was a corresponding decrease in alkaline earth metal retention, due to fewer opportunities for the analyte ions to interact with the active silanol sites on the silica surface<sup>1</sup>. At 60 % acetonitrile, the concentration of the ammonium acetate/acetic acid buffer was increased from 10.5 mM to 42.1 mM. Over the range of buffer concentrations investigated, the Mg (II), Ca (II) and Sr (II) peaks were observed to co-elute but it was possible separate Ba (II) from the other three alkaline earth metal ions. Using eluents composed of 70 % acetonitrile, (buffer concentrations: 7.8-31.3 mM), it was possible to separate Sr (II) and Ba (II). However, Mg (II) and Ca (II) were still observed to co-elute over the range of buffer concentrations studied. The close selectivity exhibited for Mg (II) and Ca (II) was unexpected, particularly when compared to previous studies on silica gel columns, but it should be noted that in most previous studies complexing agents have been used,

---

<sup>1</sup> (See Table 3.1A, Appendix III for the alkaline earth metal cation retention data at each % acetonitrile and buffer concentration (M))

which obviously affected the observed selectivity. Fig. 7.2 shows an overlay of injections of the four alkaline earth metals and it is clear that both the Sr (II) peak and to a lesser extent the Ca (II) peak appear to be split. This peak splitting was also observed for the Sr (II) peak using the 60 % acetonitrile and ammonium acetate/acetic acid buffer eluents. Section 7.3.1.6 will deal with the efforts that were undertaken to try and eliminate this problem of peak splitting.

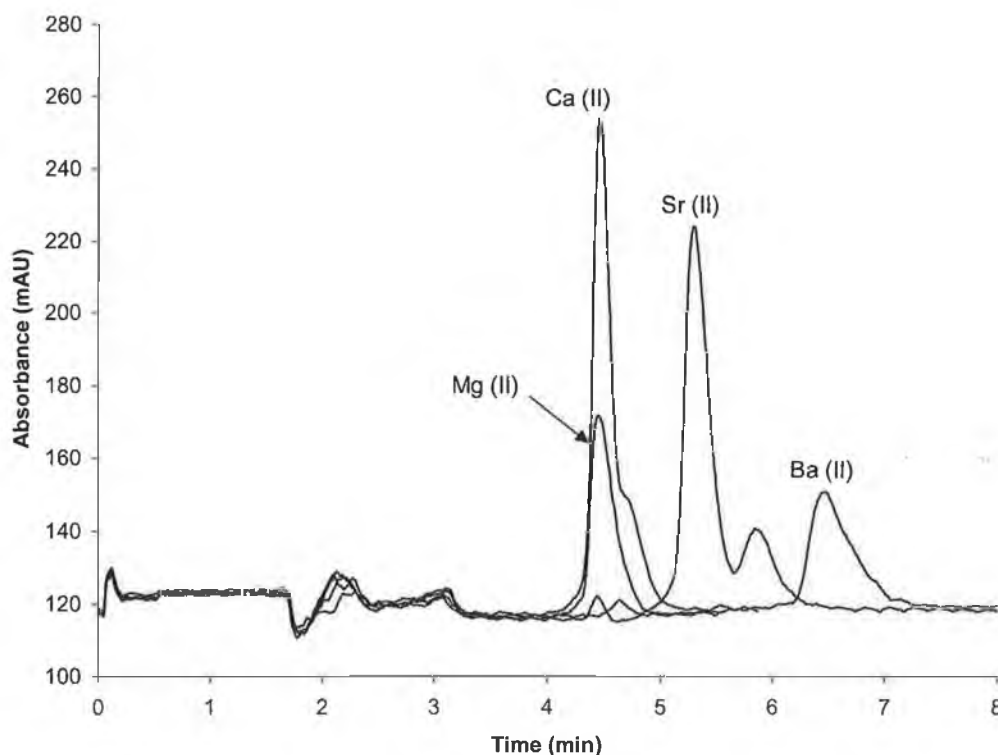


Figure 7.2: Overlays of 20 ppm Mg (II), 20 ppm Ca (II), 40 ppm Sr (II) and 60 ppm Ba (II) standards on a 10 cm bare silica monolith. Eluent conditions: 70 % acetonitrile and 31.3 mM ammonium acetate buffer, pH 4.6, flow rate 1 mL/min. Detection conditions: post-column reaction with *o*-CPC monitored at 570 nm.

In an effort to resolve the Mg (II) and Ca (II) peaks, the eluent acetonitrile content was increased to 80 % and the effect of varying the concentration of the ammonium acetate/acetic acid buffer (5.2 – 41.2 mM) was again investigated. Even though a slight improvement in the Mg (II) and Ca (II) selectivity was observed using an eluent composed of 80 % acetonitrile and acetate buffer, the excessive retention of Mg (II) and Ca (II) resulted in very broad peak shapes, and so again, a separation of Mg (II) and Ca (II) was not achieved. It should also be noted that between 20.6 and 41.2 mM

buffer, the peak for the 20 ppm Ca (II) standard was observed to elute just before the 20 ppm Mg (II) peak. The effect of buffer concentration on peak symmetry is shown in Fig. 7.3. At each set of eluents investigated, i.e. 60, 70, 80 %, the peak symmetry was observed to improve with increasing buffer concentration, whereas at very low buffer concentrations, the analyte peaks were observed to exhibit fronting.

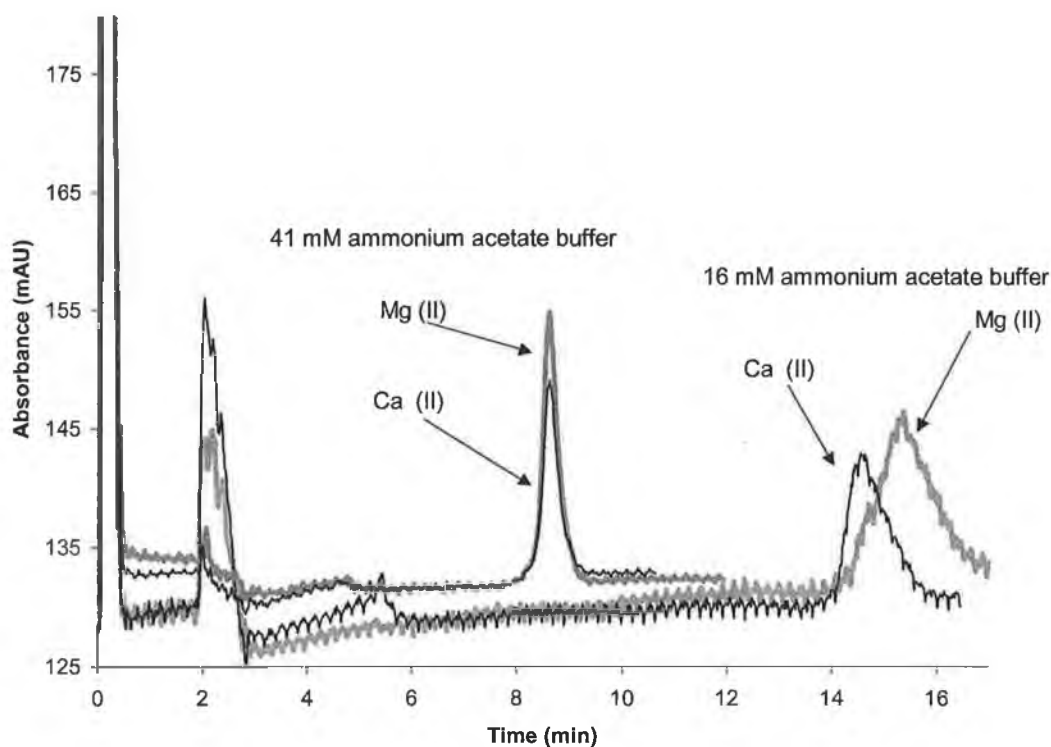


Figure 7.3: Overlays of 20 ppm Mg and 20 ppm Ca injections on a 10 cm bare silica monolith. Eluent conditions: 80 % acetonitrile and ammonium acetate buffer, pH 4.6, flow rate 1 mL/min. Detection conditions: post-column reaction with PAR monitored at 510 nm.

A linear relationship was observed between  $\text{Log } k$  and  $\text{Log } [E^+]$  with eluents containing 70 and 80 % MeCN. For all cations except Ba (II), a slight reduction in slope with increasing % acetonitrile was observed, and in general, the slopes for all four alkaline earth metals did not vary significantly, see Table 7.2.

Table 7.2: Slope and linear correlation coefficient data determined from plots of  $\log k$  versus  $\log [E^+]$  for each alkaline earth metal cation, flow rate 1 mL/min.

% Acetonitrile	Mg (II)		Ca (II)		Sr (II)		Ba (II)	
	Slope	R <sup>2</sup>						
60	-0.884	0.932	-0.853	0.913	-0.790	0.903	-0.930	0.842
70	-0.884	0.989	-0.937	0.997	-0.920	0.981	-0.862	0.979
80	-1.211	0.975	-1.186	0.979	-		-	

### 7.3.1.3: Effect of buffer pH

Varying the % acetonitrile and the concentration of ammonium acetate/acetic acid buffer in the eluent did not improve the selectivity of the bare silica monolith for Mg (II) and Ca (II). Therefore, the next parameter to be investigated, with a view to achieving a separation of the four alkaline earth metal ions, was the pH of the buffer. Since the silanol groups on the silica surface have a  $pK_a$  7.1, the cation-exchange capacity of the bare silica monolith should increase with increasing buffer pH because as the pH increases there are more deprotonated silanols, and this results in the observed increase in analyte retention.

The effect of increasing buffer pH on the retention time of all four alkaline earth metal ions was investigated using an eluent composed of 70 % acetonitrile and 23.4 mM ammonium acetate/acetic acid buffer. The *o*-CPC post-column reagent could be employed with these eluent conditions. The pH of the ammonium acetate/acetic acid buffer was increased by 0.5 pH units from pH 4.6 to pH 5.55, and the retention factors for Mg (II), Ca (II), Sr (II) and Ba (II) were determined at each pH, see Table 7.3. As expected, the increase in buffer pH resulted in an increase in alkaline earth metal retention; however, interestingly, there was a greater increase in Mg (II) retention relative to Ca (II), see Fig. 7.4. Unfortunately, the increase in pH also had a negative impact on the Mg (II) peak shape, which inhibited the separation of Ca (II) and Mg (II) at pH 5.55. The effect of increasing pH on the efficiency of the Mg (II) peak will be discussed in Section 7.3.1.4.

Table 7.3: The effect of ammonium acetate buffer pH on the retention of alkaline earth metal cations on a 10 cm bare silica monolith using an eluent composed of 70 % acetonitrile and 23.4 mM ammonium acetate/acetic acid buffer, flow rate 1 mL/min.

	Retention factor ( <i>k</i> )		
	pH 4.6	pH 5.01	pH 5.55
<b>Mg (II)</b>	1.6	2.0	3.0
<b>Ca (II)</b>	1.7	1.9	2.3
<b>Sr (II)</b>	1.9	2.5	3.2
<b>Ba (II)</b>	2.6	3.7	4.2

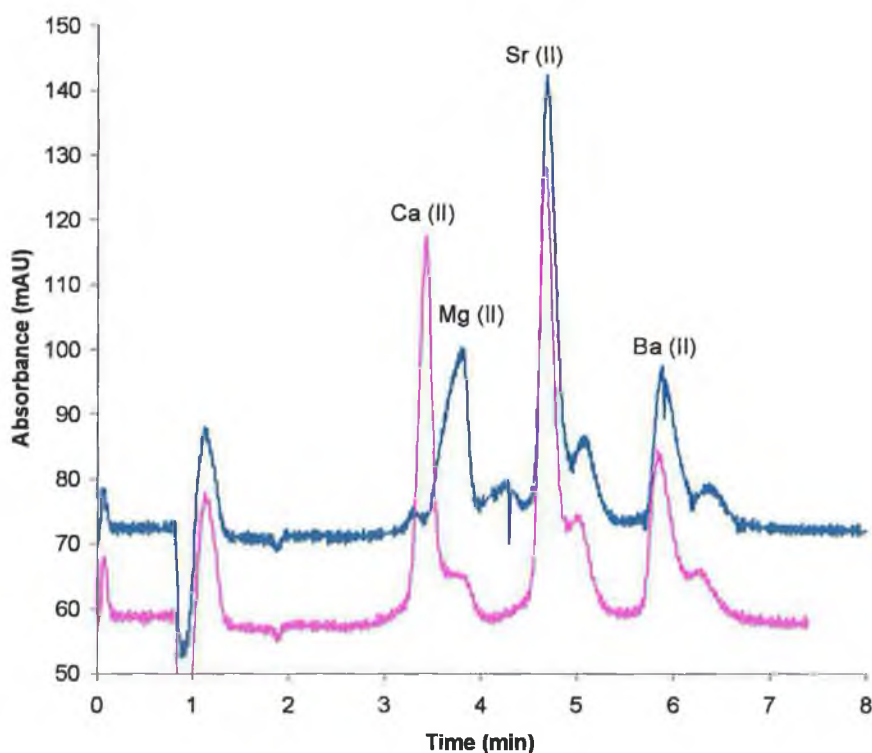


Figure 7.4: Overlays of the separations obtained for the following mixtures: 20 ppm Ca (II), 40 ppm Sr (II) and 60 ppm Ba (II) and 20 ppm Mg (II), 40 ppm Sr (II) and 60 ppm Ba (II). Eluent conditions: 70 % acetonitrile and ammonium acetate buffer (23.4 mM, pH 5.55) eluent, flow rate 2 mL/min. Detection by post-column reaction with *o*-CPC monitored at 570 nm.

As Fig. 7.4 demonstrates, a small degree of peak splitting was now noted for all four peaks. Therefore, a further pH study was then undertaken using an eluent composed of 80 % acetonitrile and 41.2 mM ammonium acetate/acetic acid buffer. It was reported in Section 7.3.1.2 that a concentration of 41.2 mM resulted in the optimum analyte peak shapes. When the pH of the 41.2 mM buffer was increased > pH 5.0 there was some improvement in the Mg (II), Ca (II) selectivity. However, the resultant peaks for both Mg (II) and Ca (II) were very broad at pH values 5.4 and 5.9, and as Fig. 7.5 demonstrates, it was not possible to resolve a mixture of Mg (II) and Ca (II).

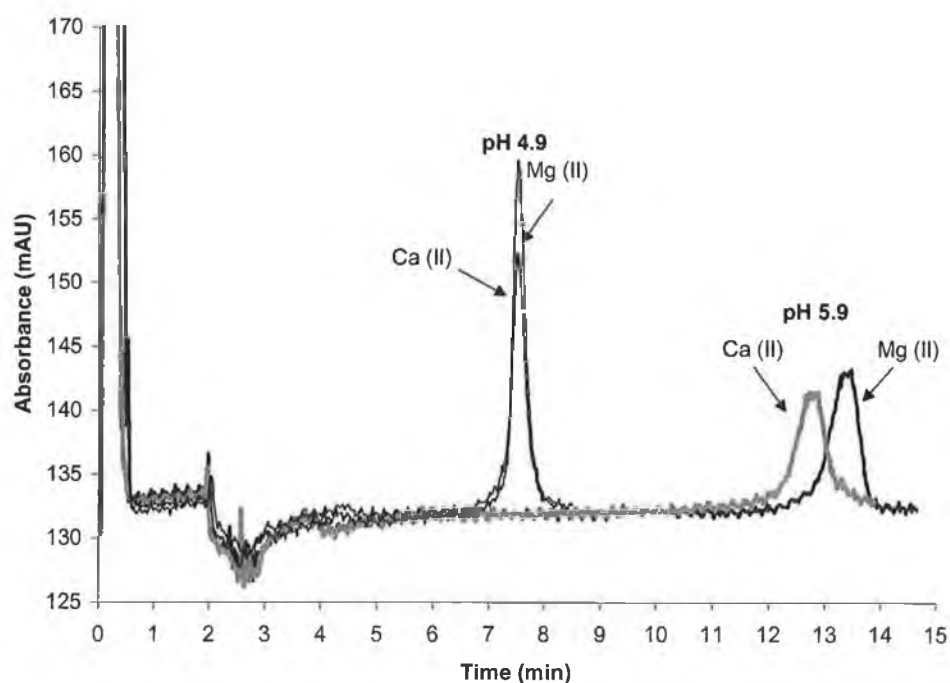


Figure 7.5: Overlays of 20 ppm Mg (II) and 20 ppm Ca (II) standards on a bare silica monolith. Eluent conditions: 80 % acetonitrile and 41.2 mM ammonium acetate/acetic acid buffer with pH increased from 4.9–5.9. Flow rate 1 mL/min and detection by post-column reaction detection using PAR monitored at 510 nm.

#### 7.3.1.4: Flow rate study

As it was not possible to separate all four alkaline earth metal ions, the application of elevated flow rates could only be applied to mixtures of (a) Ca (II), Sr (II) and Ba (II) or (b) Mg (II), Sr (II) and Ba (II). At 4 mL/min the run time for the separation of Mg (II), Sr (II) and Ba (II) or Ca (II), Sr (II) and Ba (II) was less than 2.5 minutes.

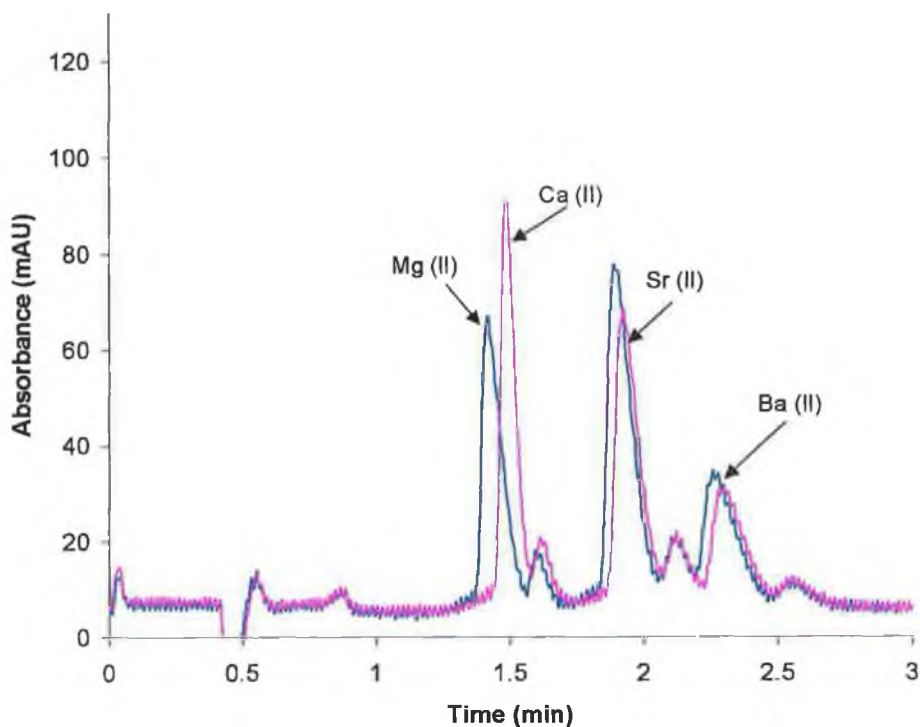


Figure 7.6: Separations of mixtures of 20 ppm Ca (II), 40 ppm Sr (II) and 60 ppm Ba (II) and 40 ppm Mg (II), 40 ppm Sr (II) and 60 ppm Ba (II). Eluent conditions: 70 % acetonitrile and ammonium acetate/acetic acid buffer (23.4 mM, pH 4.6), flow rate 4 mL/min. Detection by post-column reaction with *o*-CPC monitored at 570 nm.

The separations shown in Fig. 7.6 were monitored between 1 and 4 mL/min, and at each flow rate the peak efficiency for each analyte was calculated and a van Deemter plot, as shown in Fig. 7.7, was constructed. It is clear that the use of elevated flow rates had a positive impact on the peak efficiencies of the alkaline earth metal ions, as the plate height (HETP) values initially decrease and appear to level off between 2 and 4 mL/min. In Section 7.3.1.3, the effect of increasing the pH of the ammonium acetate/acetic acid buffer to 5.55 on the Mg (II) peak shape was discussed. Therefore, to explore this effect in more detail, once again mixtures of (a) 20 ppm Ca (II), 40 ppm Sr (II) and 60 ppm Ba (II), and (b) 20 ppm Mg (II), 40 ppm Sr (II) and 60 ppm Ba (II) were prepared and separations were performed at eluent flow rates between 1 and 4 mL/min. It is clear from the van Deemter plot shown in Fig. 7.8 that the major effect of increasing buffer pH was a negative one in terms of the shape and efficiency of the Mg (II) peak.

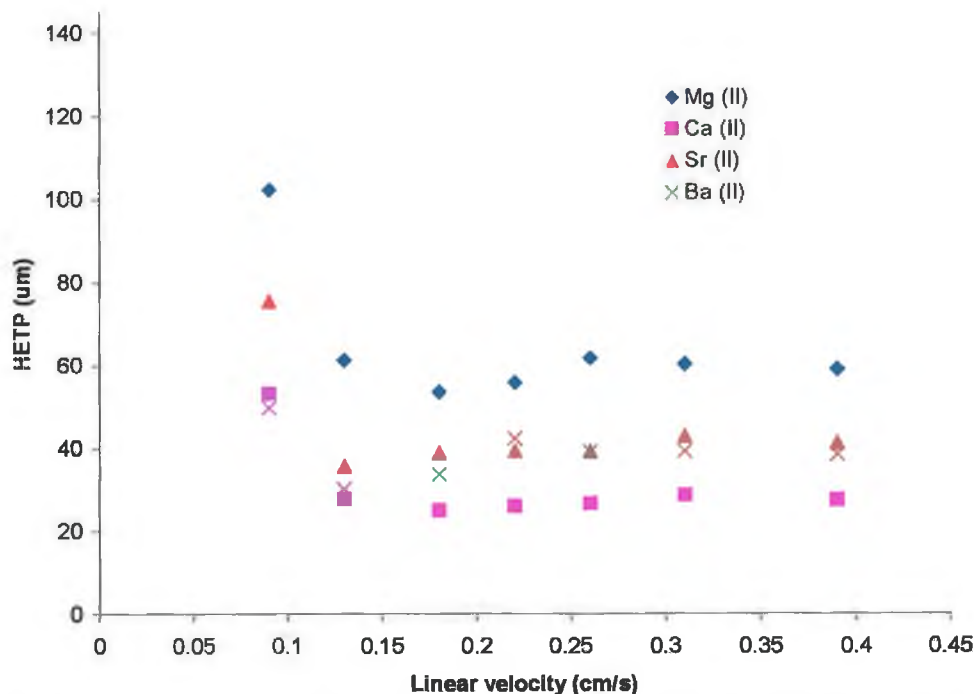


Figure 7.7: van Deemter plot for alkaline earth metal cations, obtained using 70 % acetonitrile and ammonium acetate/acetic acid buffer, (23.4 mM, pH 4.6), on a 10 cm bare silica monolith.

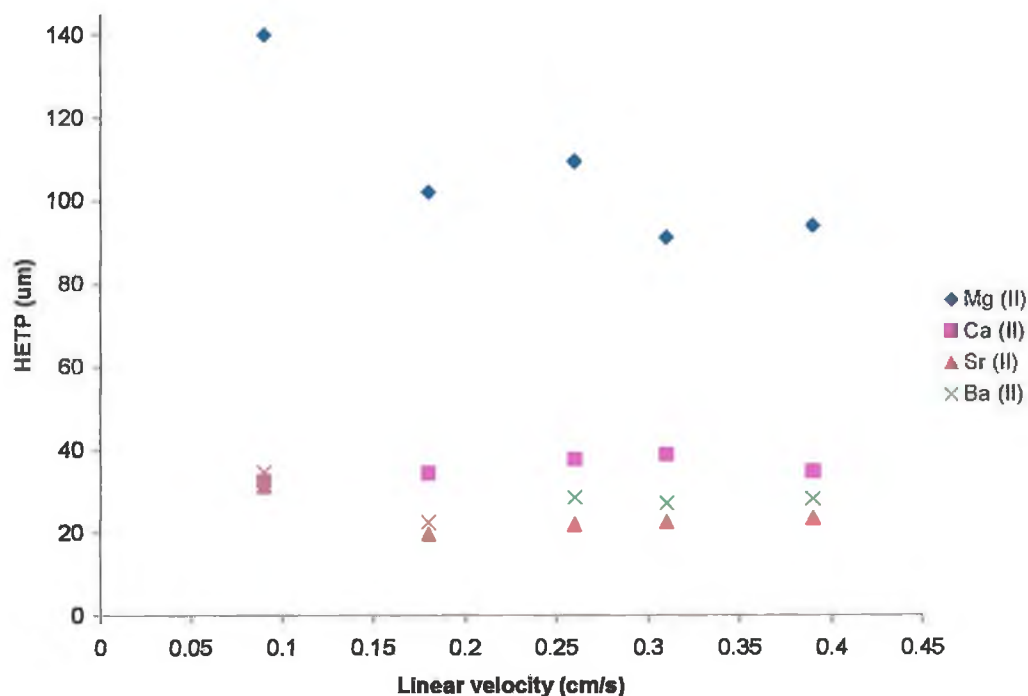


Figure 7.8: van Deemter Plot for alkaline earth metal cations at pH 5.5 obtained using 70 % acetonitrile and ammonium acetate/acetic acid buffer (23.4 mM, pH 5.5), on a 10 cm bare silica monolith.

### 7.3.1.5: The use an alternative acetate buffer

In an effort to eliminate the problem of split peaks observed for the alkaline earth metals, the ammonium acetate/acetic acid buffer was replaced with sodium acetate/acetic acid buffer (pH 4.6). At 70 % acetonitrile, the concentration of the sodium acetate/acetic acid buffer in the eluent was increased from 7.8 to 62.5 mM, and the effect on alkaline earth metal ion peak shape was investigated. The presence of the sodium acetate did not improve the problem of peak splitting observed for the Ca (II) and Sr (II) peaks, except at high buffer concentrations. In addition, the analytes were prepared in a 70:30 acetonitrile: deionised water diluent. However, this did not impact the observed peak shape, and so the experiment was also performed on a second, new 10 cm Chromolith Performance Si column, but again, the pattern of peak splitting was also evident on the new column.

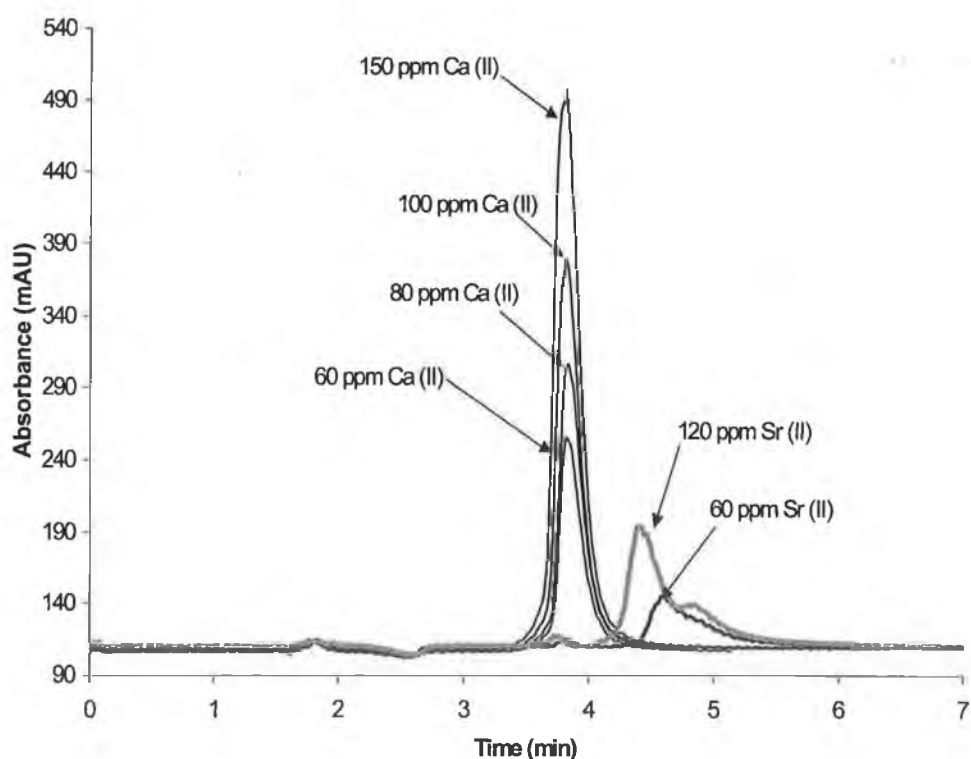


Figure 7.9: Ca (II) and Sr (II) standards on the 10 cm bare silica monolith using an eluent composed of 70 % acetonitrile containing 31.25 mM sodium acetate/acetic acid buffer (pH 4.6), flow rate 1 mL/min. Detection by post-column reaction with *o*-CPC monitored at 570 nm.

To ascertain whether or not the peak splitting had actually been eliminated at higher buffer concentrations, i.e. 31.3 mM, a series of Ca (II) and Sr (II) standards were injected. Fig. 7.9 demonstrates that, although the Ca (II) peaks did not exhibit any sign of splitting up to 150 ppm, the Sr (II) peak was found to exhibit peak splitting when a 120 ppm standard was injected. Therefore, only the Ca (II) peak splitting was eliminated as a result of increasing the buffer concentration. To improve the Sr (II) peak shape, the concentration of the buffer present in the 70 % acetonitrile eluent was further increased to 62.5 mM. As Fig. 7.10 demonstrates, peak splitting was not evident for Sr (II) peak up to a concentration of 200 ppm.

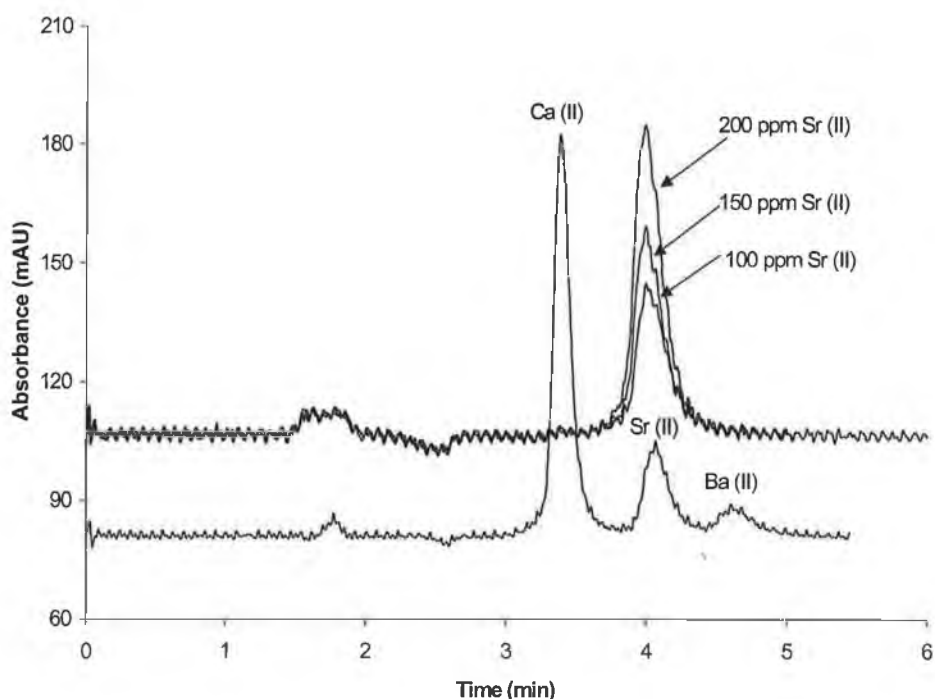


Figure 7.10: Sr (II) standards on the 10 cm bare silica monolith using a mobile phase composed of 70 % acetonitrile containing 62.5 mM sodium acetate/acetic acid buffer (pH 4.6), flow rate 1 mL/min. Detection by post-column reaction with *o*-CPC monitored at 570 nm.

At each sodium acetate/acetic acid buffer concentration, i.e. 7.8–31.3 mM, a plot of  $\log k$  versus  $\log [E^+]$  was constructed. Similar slope and linear correlation coefficient values were obtained for the alkaline earth metal ions using both the sodium acetate and ammonium acetate/ acetic acid buffers<sup>2</sup>.

<sup>2</sup> (See Table 3.2A, Appendix III for retention data for the alkaline earth metal cations using both ammonium acetate and sodium acetate/ acetic acid buffers and 70 % acetonitrile.)

### 7.3.2: Transition and heavy metal ion selectivity on a bare silica monolith

#### 7.3.2.1: The effect of organic solvent concentration on cation retention

The selectivity of the silica monolith for Cu (II), Fe (II), Cd (II), Ni (II), Co (II), Mn (II), Zn (II) and Pb (II) was investigated using acetonitrile based eluents, ranging again from 60-80 % acetonitrile, buffered once more with varying concentrations of ammonium acetate/acetic acid buffer (pH 4.6). To avoid potential column contamination from Fe (III), 1 mM ascorbic acid was also added to all eluents, to reduce Fe (III) to Fe (II). Significant retention of the metal cations listed above was observed. However, the analyte signal observed for Fe (II) was very poor, eluting only as a small peak between Cu (II) and Cd (II). As the data in Table 7.4 demonstrates, an increase in the amount of acetonitrile in the eluent resulted in significant increases in transition and heavy metal ion retention due to the enhanced ion-exchange interactions of the metal cations with the surface silanol groups.

Table 7.4: The retention factors of transition metal cations on a bare silica monolith using eluents composed of acetonitrile and 20 mM ammonium acetate/acetic acid buffer, pH 4.6, eluent flow rate of 1 mL/min.

% MeCN	Retention factor ( <i>k</i> )					
	Cu (II)	Cd (II)	Ni (II)	Co (II)	Mn (II)	Pb (II)
60	0.3	0.6	0.8	0.9	1.0	1.8
70	0.4	0.8	1.4	1.6	1.6	3.8
80	0.6	1.7	3.2	4.2	4.6	10.5

In contrast to Cd (II), Ni (II), Co (II) and Mn (II), the Cu (II) peak exhibited only a slight increase in retention with increasing % acetonitrile. This unusual behaviour of Cu (II) could be attributed to the formation of Cu (II)-MeCN complexes [13], leading to a reduction in retention of Cu (II) relative to the other analyte cations.

At 60 and 70 % acetonitrile, Ni (II), Co (II) and Mn (II) were not resolved. However, a separation of Cu (II), Cd (II), Ni (II), Co (II) and Mn (II) was possible when the % acetonitrile was increased up to 80 %. Unfortunately, an eluent containing 80 %

acetonitrile resulted in excessive retention of Pb (II) and complete retention of Zn (II). In fact Zn (II) was strongly retained under all conditions, only eluting under conditions of low acetonitrile (60 %) and high buffer concentrations, and even under such conditions, Zn (II) elutes as an excessively broad and tailed peak. This unusual selectivity and poor peak shapes for Zn (II), on similar silica monolithic columns (Merck Performance-Si) has been specifically noted in two previous Chapters, one where the silica monolith was modified with IDA (Chapter 4), and the second where the silica monolith was modified with lysine (Chapter 5). This would seem to indicate that the effects reported in these Chapters originated from the monolith backbone itself, rather than the attached functionalities.

It is interesting to note that the retention order observed on the bare silica monolith, i.e. Cu (II) < Fe (II) < Cd (II) < Ni (II) < Co (II) < Mn (II) < Pb (II) << Zn (II) is quite different from those observed by others on bare silica gel columns. Iler [14] postulated that the adsorption of transition metal ions on silica is due to interaction with active sites at the silica surface, which act like ligands, and the specificity of adsorption is therefore related to the tendency of the metal atom to form covalent bonds. This theory was supported by Schindler *et al.* [15], who found that the ligand properties of surface silanol groups for transition metal ions (Fe (III), Cu (II), Cd (II) and Pb (II)) strongly correlates with known stability constants for corresponding metal-hydrocomplexes. This stability data is in good agreement with the selectivity reported [16], where the following order of specificity of formation of covalent bonds with silica surface was observed to be: Cd (II) < Ni (II) < Zn (II) < Co (II) < Cu (II) < Pb (II).

Janos *et al.* [17] reported the separation of Cu (II), Cd (II), Pb (II) and Tl (I) on bare silica particle-packed columns using sodium acetate, sodium tartrate and sodium hydroxybutyrate aqueous solutions of different pH and concentration. It was reported by Janos *et al.* that the separation selectivity depends on secondary complexation equilibria with organic acids from the eluents. Here, with the monolithic silica column, the eluent contained ammonium acetate, so both ammonium and acetate could affect the observed selectivity through complexation.

### 7.3.2.2: Effect of buffer concentration on cation retention.

As in the case of the alkaline earth metal cations, an increase in ammonium acetate/acetic acid buffer concentration resulted in a corresponding decrease in transition metal cation retention factors<sup>3</sup>. Table 7.5 shows the slope and linear correlation coefficients obtained for a plot of  $\log k$  versus  $\log [E^+]$  at each % acetonitrile, and the results indicate that ion-exchange was the dominant retention mechanism.

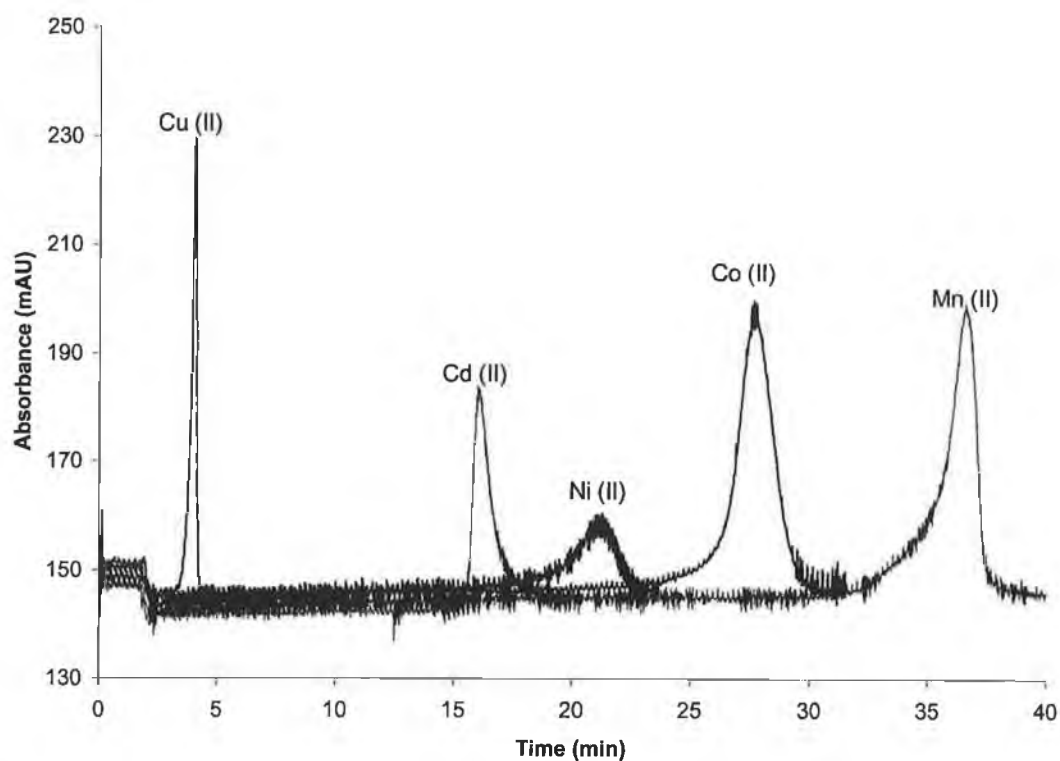
Table 7.5: Slope and linear correlation coefficient data determined from plots of  $\log k$  versus  $\log [E^+]$  constructed for each transition metal cation.

	<b>Cu (II)</b>	<b>Cd (II)</b>	<b>Ni (II)</b>	<b>Co (II)</b>	<b>Mn (II)</b>	<b>Pb (II)</b>
<b>60 % MeCN, (4.2 –31.5 mM)</b>						
<b>Slope</b>	-0.551	-1.188	-0.988	-0.964	-1.00	-0.967
<b>R<sup>2</sup></b>	0.999	0.999	0.999	0.999	0.999	0.971
<b>70 % MeCN, (3.1– 23.4 mM)</b>						
<b>Slope</b>	-0.650	-1.162	-0.904	-0.852	-0.906	-1.213
<b>R<sup>2</sup></b>	0.987	0.998	0.995	0.986	0.985	0.986
<b>80 % MeCN, (2.1-20.6 mM)</b>						
<b>Slope</b>	-0.443	-1.057	-0.849	-0.786	-0.912	-1.087
<b>R<sup>2</sup></b>	0.990	0.995	0.982	0.992	0.990	0.967

In addition, the buffer concentration was also observed to impact cation peak shape, i.e. at low buffer concentrations the analyte peaks exhibited fronting. This problem was more pronounced using eluents, which contained 80 % acetonitrile, as a result of the excessive analyte retention. Fig. 7.11 (a) and (b) demonstrates the difference in analyte peak shapes using 5.2 mM and 20.6 mM buffer concentrations.

<sup>3</sup> (See Table 3.3A, Appendix III for the complete set of transition metal cation retention data at 60, 70 and 80 % acetonitrile and a range of ammonium acetate/acetic acid buffer concentrations (M))

(a)



(b)

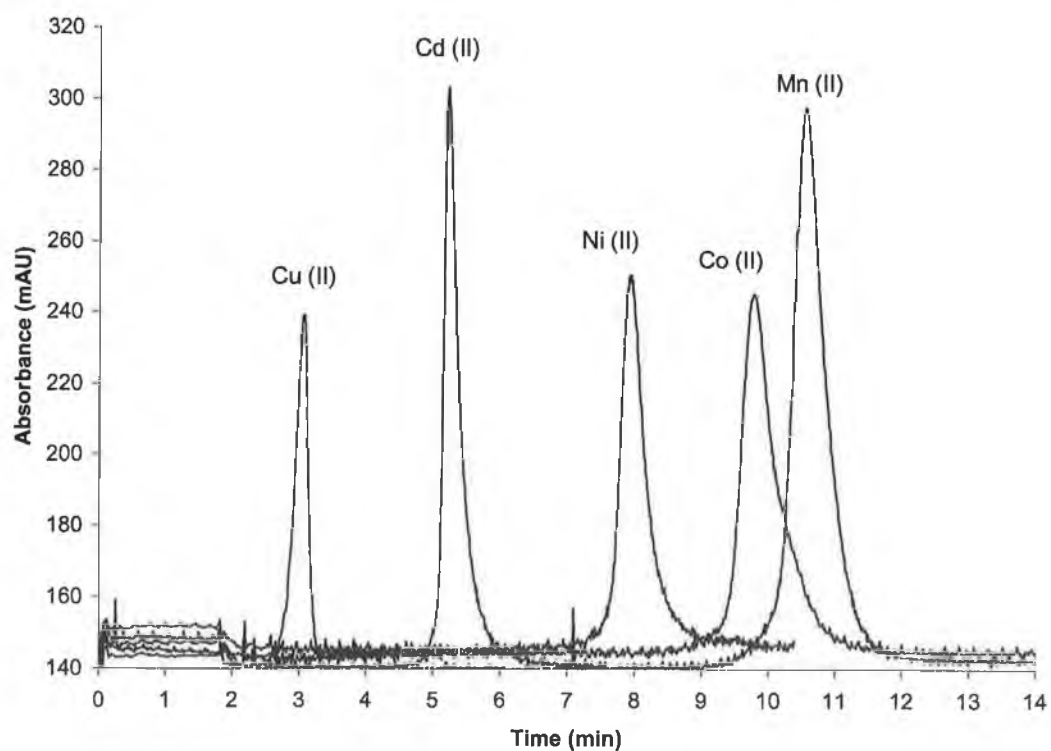


Figure 7.11: The effect of eluent buffer concentration on cation peak shape using 80 % acetonitrile and (a) 5.2 mM and (b) 20.6 mM ammonium acetate buffer, (pH 4.6).

### 7.3.2.3: The combined effect of varying % acetonitrile and buffer concentration.

It is clear from the results presented in Section 7.3.1.1 and 7.3.1.2, that the retention of selected transition and heavy metal ions on a bare silica monolith is affected by: (1) the % acetonitrile in the eluent, as the retention of cations is enhanced by increasing the acetonitrile %, and (2) increasing the buffer concentration, which results in a decrease in cation retention. The combined effects of % acetonitrile and buffer concentration on cation retention are presented in Fig. 7.12.

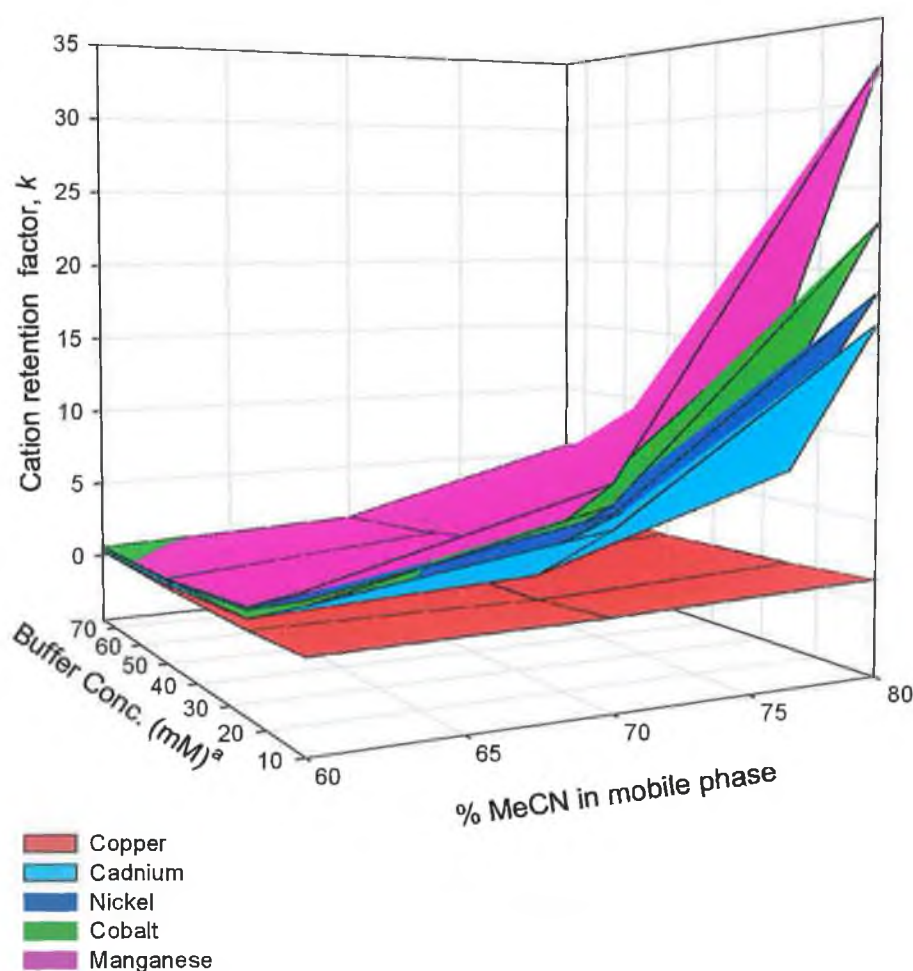


Figure 7.12: Plots for Cu (II), Cd (II), Ni (II), Co (II) and Mn (II) showing the variation of cation retention factors as the % acetonitrile and ammonium acetate/acetic acid buffer concentration (pH 4.6) in the eluent increased.

<sup>a</sup> refers to the undiluted buffer concentration.

Up until this point, only individual standards of each cation had been injected onto the 10 cm bare silica monolith. Even though the chromatogram shown in Fig. 7.13 demonstrates some evidence of either peak fronting or tailing, it was still possible to achieve a baseline separation of Cu (II), Cd (II), Ni (II), Co (II) and Mn (II) using an eluent composed of 80 % acetonitrile and the optimum buffer concentration, which taking into account the dilution factor, i.e. (100 mLs) \*(50 mM)/ 485 mLs, was determined be 10.3 mM, (pH 4.6).

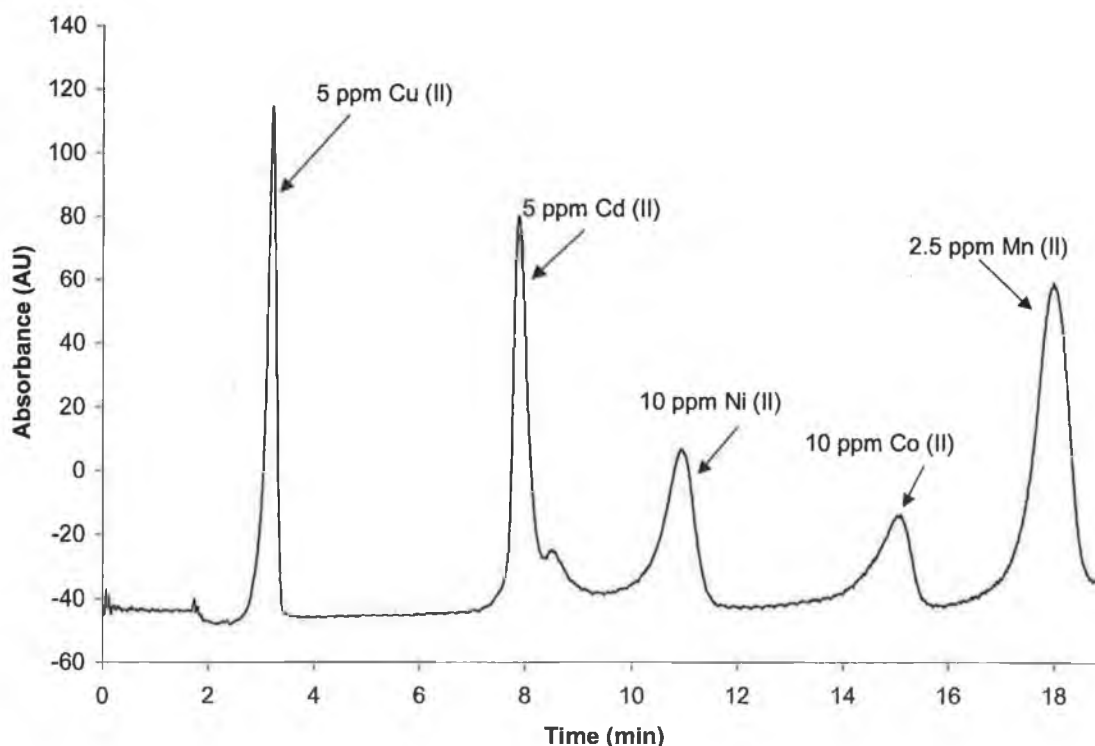


Figure 7.13: Baseline separation of selected transition and heavy metal cations on a bare silica monolith. Eluent conditions: 80 % acetonitrile and 10.3 mM ammonium acetate buffer, pH 4.6, flow rate 1 mL/min. Detection by post-column reaction with PAR monitored at 510 nm.

#### 7.3.2.4: Effect of pH on cation retention

The effect of buffer pH on the retention of the transition metal cations is shown in Table 7.6. Below pH 4.6, the resolution between Cd (II), Ni (II), Co (II), Mn (II) was lost completely. The pH of the ammonium acetate buffer was further increased to 5.1 and 5.6, and the retention of all cations, apart from Cu (II) dramatically increased. At

pH 5.61 only the Cu (II), Cd (II) and Ni (II) peaks eluted after 60 minutes, while Co (II) and Mn (II) were still retained after 120 minutes. Pack and Risely [8] also observed a similar effect when the effect of increasing buffer pH on the retention of alkali metals (Li, Na and K) was investigated. Using an eluent composed of 90% acetonitrile, the retention times of Li, Na and K were 10.0, 15.0 and 18.5 minutes respectively, at pH 3.55 and when the pH was adjusted to 6.65, the retention times increased to 16.7, 23.6 and 28.6 minutes respectively

Table 7.6: Retention data showing the effect of varying the ammonium acetate/acetic acid buffer pH on the retention of transition and heavy metal ions on a 10 cm bare silica monolith. Eluent conditions: 80 % acetonitrile and 10 mM buffer, flow rate 1 mL/min.

	<b>Retention factor (<i>k</i>)</b>				
<b>Buffer pH</b>	<b>Cu (II)</b>	<b>Cd (II)</b>	<b>Ni (II)</b>	<b>Co (II)</b>	<b>Mn (II)</b>
3.51	0.3	0.9	0.8	1.0	1.0
3.98	0.3	1.5	1.8	1.8	1.9
4.62	0.8	2.9	3.9	5.6	6.8
5.10	0.8	5.3	6.8	14.2	16.1
5.61	0.8	9.9	31.8	No signal after 130 minutes	

### **7.3.2.5: Flow Rate Study**

Fig. 7.13 demonstrates the separation of Cu (II), Cd (II), Ni (II), Co (II) and Mn (II) on the bare silica monolith using SEIC. However, at 1 mL/min the run time was approximately 20 minutes. Therefore, because monoliths can be operated at elevated flow rates without excessive backpressures or loss of peak efficiency, the eluent flow rate was increased up to 5 mL/min, in an effort to reduce separation time for the 5 cations. Two flow rate studies were carried out using: (1) Dionex system and pressure driven reagent delivery system, and (2) a Waters system with an external pump for PCR delivery.

Using the Dionex HPLC system the flow rate was increased from 1 mL/min, in 0.5 mL/min increments up to 3.5 mL/min, and at each flow rate the efficiency of the analyte peaks in the mixture of Cu (II), Cd (II), Ni (II), Co (II) and Mn (II) was calculated<sup>4</sup>. However, at flow rates greater than 3.5 mL/min, the reagent delivery system did not allow sufficient mixing of the eluent, and so, PCR detection of the analytes was not possible. Even at a modest flow of 3.5 mL/min it was possible to reduce the run time necessary to separate Cu (II), Cd (II), Ni (II), Co (II) and Mn (II) to approximately 5 minutes.

Using the Waters system and an external pump to deliver the PCR, it was possible to run the separation of the 5-cation mixture at flow rates as high as 5 mL/min. One problem encountered when the Dionex system was replaced by the Waters system was that with the Shimadzu UV-Vis detector attached to the Waters system, the Ni (II) and Co (II) peaks could not be accurately integrated due to differences in detector sensitivity, and hence only a mixture of 5ppm Mn (II), Cd (II) and Cu (II) could be analysed, and retention times and peak efficiency values accurately determined, see Fig. 7.14.

At 5 mL/min Cu (II) eluted after 0.6 minutes, followed by Cd (II) at 1.7 minutes, and Mn (II) at 3.9 minutes. The HETP values for all the analytes increased between 1-3 mL/min. However, between 3-5 mL/min, there was only a gradual increase in HETP values for Cu (II) and Cd (II), whereas the HETP values for later eluting Mn (II) appeared to level off at flow rates greater than 3.5 mL/min, see Fig 7.15.

---

<sup>4</sup> (See Fig. 3.1A, Appendix III for the van Deemter plot constructed from the efficiency data obtained between 1 and 3.5 mL/min on the Dionex HPLC system)

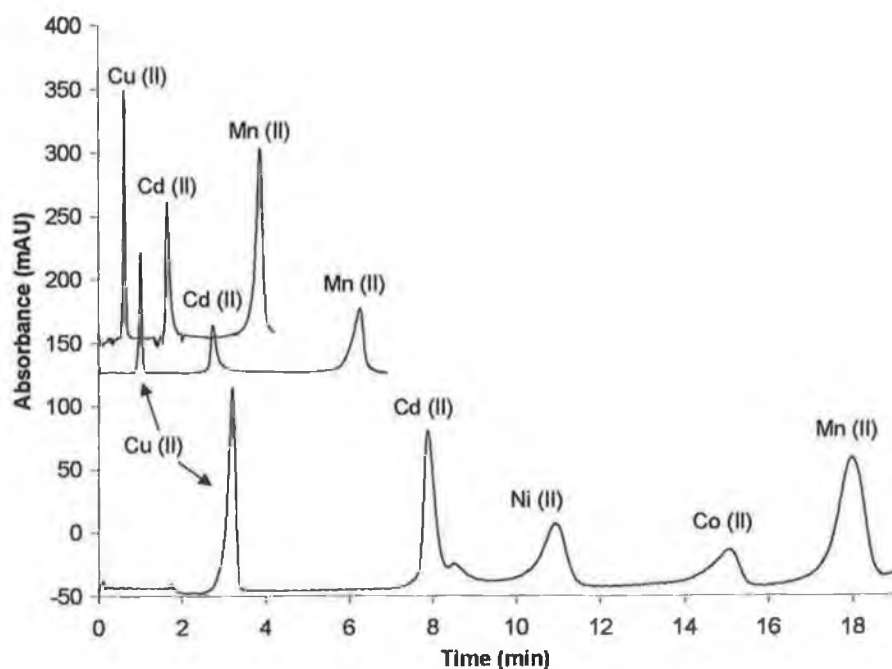


Figure 7.14: Separation of a mixture of the transition metal cations on a bare silica monolith using an eluent composed of 80 % acetonitrile and 10.3 mM ammonium acetate buffer (pH 4.62), at flow rates 1, 3 and 5 mL/min. Detection by post-column reaction with PAR monitored at 510 nm.

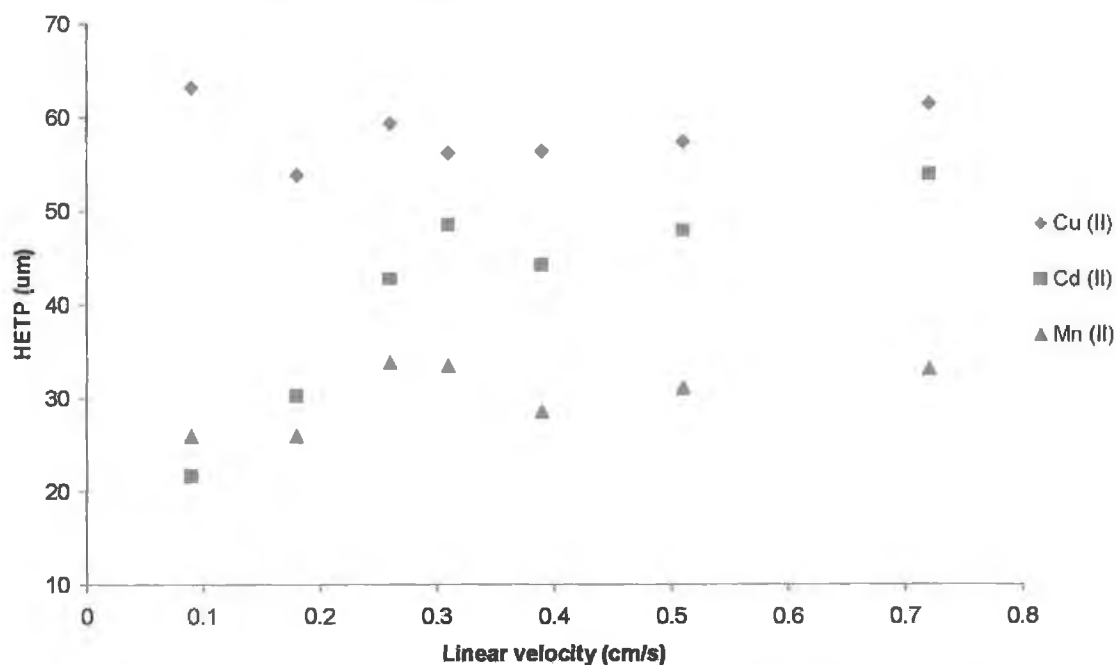


Figure 7.15: van Deemter plots for Cu (II), Cd (II) and Mn (II) on the 10 cm bare silica monolith. Eluent conditions as per Fig. 7.14.

### 7.3.2.6: The use of an alternative acetate buffer.

The elution order observed for the acetonitrile, ammonium acetate/acetic acid buffer eluent on the bare silica monolith was Cu (II) < Cd (II) < Ni (II) < Co (II) < Mn (II) <<< Pb (II). However, when a sodium acetate/acetic acid buffer was employed, a change in the elution order was observed, i.e. Cu (II) no longer eluted first, in fact as the data in Table 7.7 demonstrates, Cu (II) eluted after Mn (II). In addition, the retention factors observed for all the analytes were observed to increase when using a sodium acetate/acetic acid buffer. It is possible that this difference in retention could be as a result of complex formation with ammonium, and hence, when the ammonium acetate was replaced with sodium acetate, an increase in retention times at each % acetonitrile was observed.

Table 7.7: The effect of increasing acetonitrile content on cation retention on a bare silica monolith, using a mobile phase composed of acetonitrile containing 16 mM sodium acetate buffer/ acetic acid, pH 4.6, 1 mL/min.

% MeCN	Retention factor ( <i>k</i> )					
	Cd (II)	Ni (II)	Co (II)	Mn (II)	Cu (II)	Pb (II)
60	0.9	1.3	1.5	1.6	2.8	4.3
70	1.4	1.9	2.6	2.8	4.9	9.8
80	2.6	4.5	7.1	8.1	10.2	21.4

Using an ammonium acetate/acetic acid buffer, the retention of Cu (II) was only marginally affected by changes in the buffer concentration. In contrast, with the sodium acetate/acetic acid buffer, the retention of Cu (II) is significantly affected by increasing the buffer concentration, i.e. an increase in the sodium acetate/acetic acid buffer concentration from 15.5 to 41.2 mM resulted in a change in retention order from Cd (II) < Ni (II) < Co (II) < Mn (II) < Cu (II) << Pb (II) to Cd (II) < Ni (II) < Cu (II) < Co (II) < Mn (II) < Pb (II), see Fig. 7.16. Therefore, it was clear from this study that the retention of Cu (II) was affected by both the formation of Cu (II)-MeCN complexes and complexation with ammonium in the eluent<sup>5</sup>.

<sup>5</sup> (See Table 3.4A, Appendix III for the transition metal cation retention data over the range of sodium acetate/acetic acid buffer concentrations studied)

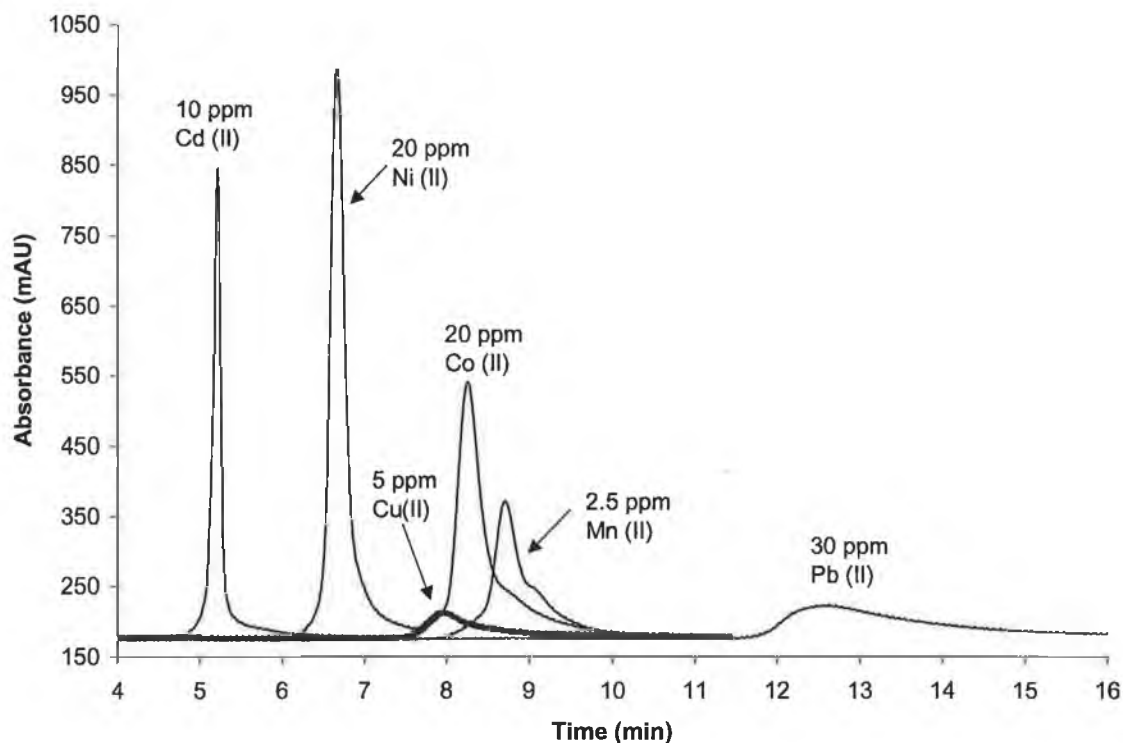


Figure 7.16: Separation of transition metal cations on a 10 cm bare silica monolith using an eluent composed of 80 % acetonitrile and 41.2 mM sodium acetate/acetic acid buffer (pH 4.6), flow rate of 1 mL/min. Detection by post-column reaction with PAR monitored at 510 nm.

The optimum eluent conditions for the separation of the Cd (II), Ni (II), Co (II) and Mn (II) was 80 % acetonitrile containing 10.3 mM sodium acetate/acetic acid buffer (pH 4.6). However, the run time required for the separation of these four analytes, using an eluent composed of 80 % acetonitrile containing 10.3 mM sodium acetate buffer (pH 4.6) was ~ 35 minutes, (compared to ~ 20 minutes when 10.3 mM ammonium acetate/acetic acid buffer was employed), and as a result, excessive retention of Cu (II) and, especially Pb (II), was observed.

### 7.3.3: The effect of solvent polarity on cation retention and selectivity.

The chromatographic behaviour of cations observed for solvent enhanced ion-exchange is based on a reduction in the degree of hydration of both ions in solution and fixed ion-exchange sites within the stationary phase as a result of including

organic solvent within the eluent. In most cases reduced hydration results in enhanced analyte ion interaction with the stationary phase exchange sites and thus increased retention. However, the exact nature of this effect would depend upon the relative solvation of the analyte and eluent ions and on the nature of the organic solvent, namely its dielectric constant. Solvents that exhibit strong hydrogen bonding properties, i.e., hydrogen bonding of the solvent molecules with surface silanol groups, should result in a relatively smaller retention increase or even decrease compared to solvents that do not exhibit such properties.

Solvents can be classified into three categories according to their polarity, i.e. polar protic, dipolar protic and non-polar. Protic refers to a hydrogen atom attached to electronegative atom and that electronegative atom is almost exclusively oxygen, and hence, polar protic solvents can be represented by the general formula ROH. The polarity of the polar protic solvent stems from the dipole of the O-H bond. Aprotic describes a molecule that does not contain an O-H bond. Solvents in this case all contain a bond that has a large bond dipole. Typically this bond is a multiple bond between carbon and either oxygen or nitrogen [18].

Table 7.8: Dielectric constant data for acetonitrile and methanol.

Solvent Name	Structure	Dielectric constant
acetonitrile	CH <sub>3</sub> CN	36.6
methanol	CH <sub>3</sub> OH	33

To investigate whether the nature of the organic solvent may have been an important factor in the observed cation selectivity, a brief study was undertaken using methanol in place of acetonitrile. Methanol is known to form strong hydrogen bonds with the surface silanol groups and so it was expected that the relative retention should be less in this case. In addition, the solvation of metal ions with methanol molecules is different when compared to acetonitrile, and so this should also alter the observed selectivity.

### ***7.3.3.1: The effect of % methanol on transition and heavy metal selectivity***

To assess the effect of solvent polarity on the retention of cations, a series of eluents containing 50-90 % methanol and ammonium acetate/acetic acid buffer were prepared, and initially, the retention of Cu (II), Cd (II) and Mn (II) on the 10 cm bare silica monolith was investigated. When the acetonitrile in the eluent was replaced by methanol, a change in the elution order of the three cations was observed, such that at 70, 80 and 90% methanol, there was a dramatic increase in Cu (II) retention relative to Cd (II) and Mn (II), see Fig. 7.17. This observation supports the assumption made in Section 7.3.2.1 that selective Cu (II)-MeCN interactions are primarily responsible for the relatively low retention of Cu (II) with acetonitrile based eluents.

For each methanol-based eluent studied, Cd (II) was still observed to elute before Mn (II), as in the case of the acetonitrile study. However, between 50 and 70 % methanol, Cd (II), Mn (II) and Cu (II) were observed to co-elute, which was not the case with acetonitrile. A separation of Cd (II), Mn (II) and Cu (II) was possible only when the methanol content was increased to greater than 80 %. As well as investigating the effect of % methanol on Cd (II), Mn (II) and Cu (II) retention, a number of other cations were also studied<sup>6</sup>.

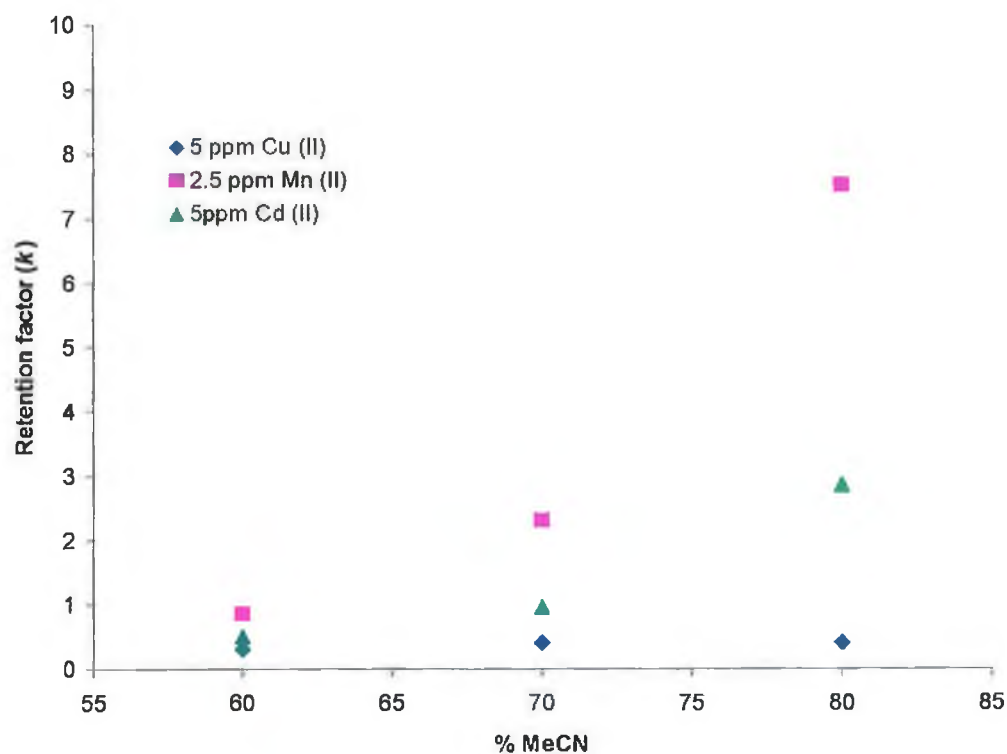
The bare silica monolith operated in the SEIC mode, with a methanol based eluent, also exhibited very high Zn (II) selectivity. Even at 60 % methanol, the peak shape for Zn (II) was extremely broad, even though the retention time for Zn (II) was only ~ 8 minutes, see Fig. 7.18 (a). Pb (II) was again selectively retained on the bare silica monolith using the methanol/ammonium acetate/acetic acid buffer eluent. Fig. 7.18 (b) shows very pronounced broadening of the Pb (II) peak at high % methanol.

An increase in the methanol content to 90 % (5.1 mM ammonium acetate/acetic acid buffer) facilitated the separation of Cd (II), Co (II) and Mn (II) in ~ 6 minutes at a flow rate of 1 mL/min. However, under these conditions, Ni (II) and Co (II) were still observed to co-elute and excessive retention of Cu (II) and, in particular, Pb (II) was observed.

---

<sup>6</sup> (See Table 3.5A, Appendix III for the retention data for all transition metals studied between 50-90% MeOH)

(a)



(b)

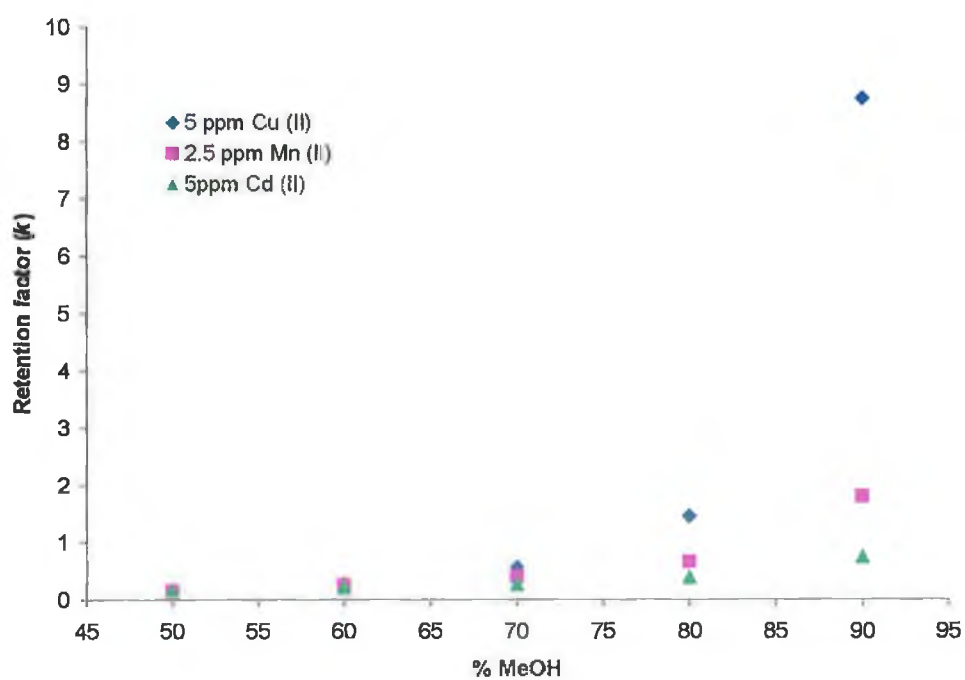


Figure 7.17: The effect of increasing (a) % acetonitrile (MeCN) and (b) % methanol (MeOH) on the retention of Cu (II), Cd (II) and Mn (II). Eluent conditions: organic solvent and 50 mM ammonium acetate/acetic acid buffer (undiluted concentration), pH 4.6. Flow rate: 1 mL/min.

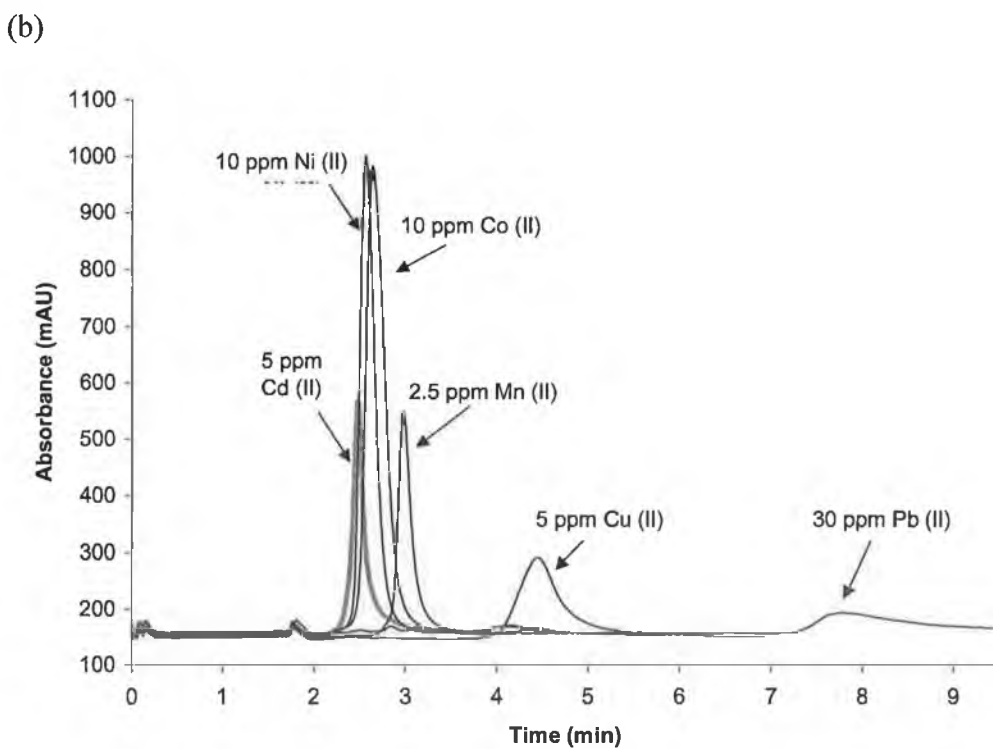
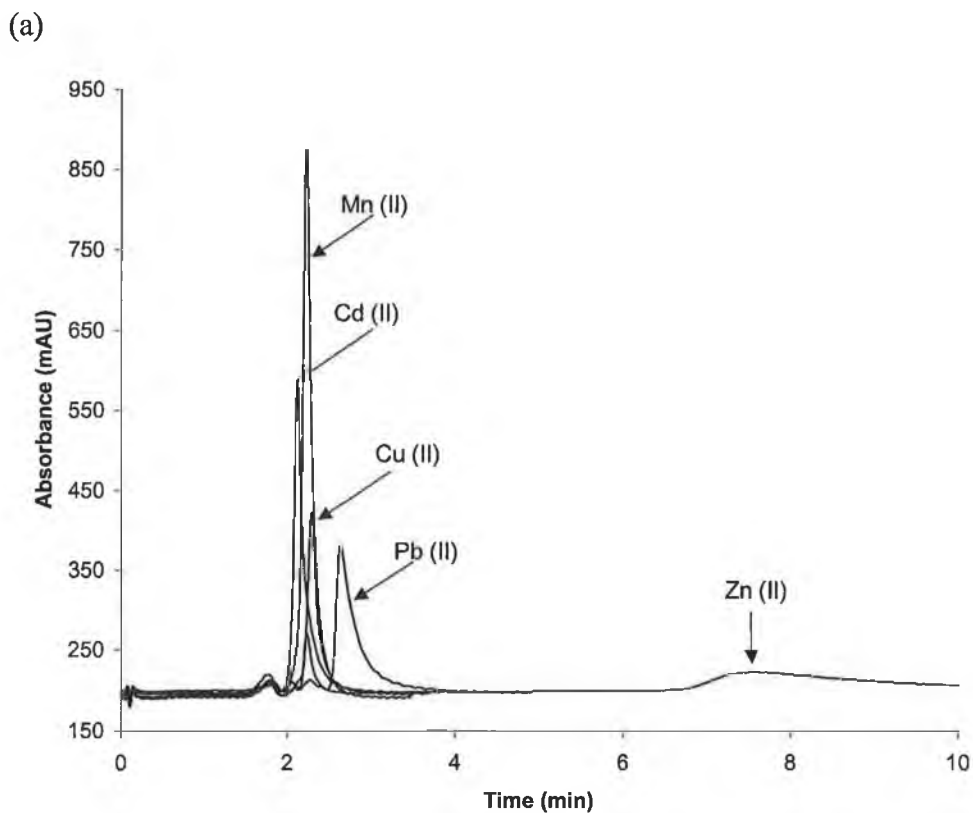


Figure 7.18: Overlays of selected transition and heavy metal ion standard injections using (a) 60% methanol containing 21.1 mM ammonium acetate buffer and (b) 80% methanol containing 10.3 mM ammonium acetate buffer (pH 4.6), flow rate 1 mL/min. Detection by post-column reaction with PAR monitored at 510 nm.

## **7.4: Conclusion**

The results of this study show that bare silica monoliths can be used for fast separations of alkaline earth and transition metal cations, without surface modification, through the use of organic based eluents, in what can be best described as solvent enhanced ion chromatography (SEIC). The organic nature of the eluents enhances the electrostatic interaction of the analyte ions and the fixed ion-exchange sites, which in this case were the dissociated silanol groups, through reducing the associated number of waters of hydration. However, it was demonstrated that this effect is dependent upon the nature of the organic solvent, and that significant selectivity changes can be obtained through the correct choice of solvent. The assumption that the observed retention is simply enhanced ion-exchange has been verified by the observation that cation retention increases with decreasing ammonium acetate/ acetic acid buffer concentration, but increases with increasing buffer pH. This is the expected retention behaviour for a simple ion-exchange system.

Finally, the bare silica monolithic column has been observed to exhibit unique Zn (II) selectivity, but also very broad peak shapes for Zn (II), which suggests that the behaviour of Zn (II) in the IDA and lysine studies (Chapters 4 and 5) originate from the monolithic backbone itself, rather than the attached functionalities.

## **References:**

1. A. Berthod, *J. Chromatogr. A*, 549 (1991) 1.
2. G. B. Cox, *J. Chromatogr. A*, 656 (1993) 2.
3. R. L. Smith, D. J. Pietrzyk, *Anal Chem*, 56 (1984) 611.
4. D. M. Brown and D. J. Pietrzyk, *J. Chromatogr. A*, 466 (1989) 291.
5. K. Ohta, M. Sando, K. Tanaka K, P. R. Haddad, *J Chromatogr. A*, 752 (1996) 167.
6. K. Ohta, K. Tanaka, *Anal. Chim. Acta*, 381 (1999) 265.
7. K. Ohta, K. Tanaka, B. Paull, P.R. Haddad, *J. Chromatogr. A*, 770 (1997) 219.
8. B. W. Pack and D. S. Risely, *J. Chromatogr. A*, 1073 (2005) 269.
9. E. Munaf, Rahmiana Zein, T. Takeuchi, T. Miwa, *Anal. Chim. Acta*, 334 (1996) 39.
10. E. Munaf, R. Zein, T. Takeuchi, T. Miwa, *Anal. Chim. Acta*, 341 (1997) 225.
11. Y. Takeda, K. Ishida, T. Hasegawa, A. Katoh, *J.Chromatogr. A*, 1094 (2004) 233.
12. G. J. Moody, J. D. R. Thomas, *Analyst*, 93 (1968) 557.
13. V. N. Vandyshev, *Russ. J. Glen. Chem.* 73 (2003) 855.
14. R. K. Iler, *The Chemistry of Silica, Solubility, Polymerisation, Colloid and Surface Properties and Biochemistry*, J. Wiley and Sons (New York) 1979.
15. P.W. Schindler, B. Furst, R. Dick, P.U. Wolf, *J. Colloid Interface Sci.* 55 (1976) 469.
16. H. H. Tran, F.A. Roddick, J.A. O'Donnell, *Water Res.*, 33 (1999) 2992.
17. P. Janos, K. Stulik, V. Packova, *Talanta*, 38 (1991) 1445.
18. O=Chem Directory, Dept. of Chemistry, University of Southern Maine, Portland, Maine, Solvents, date viewed: 9/5/2005  
<[http://www.usm.maine.edu/~newton/Chy251\\_253/Lectures/Solvents/Solvents.html](http://www.usm.maine.edu/~newton/Chy251_253/Lectures/Solvents/Solvents.html)>

## *Overall Summary and Future Work*

The aim of this project was the development and characterisation of novel monolithic stationary phases for the rapid separation of inorganic and organic ions. The results presented in Chapters 2-7 have shown:

- Rapid separations of inorganic cations on both a bare silica monolith and an IDA functionalised silica monolith, while a highly efficient separation of inorganic anions was achieved, in less than 100 seconds, using the lysine functionalised silica monolith.
- A comparison of the chromatographic performance of the 10 cm functionalised silica monoliths and commercially available 25 cm IDA silica gel and lysine silica gel columns, in order to identify possible differences in selectivity, and other specific properties, between stationary phases consisting of the same chemistry of the attached functional groups, but differing in the nature of the porous silica substrate.
- In addition, the ability of a Cu (II) modified-lysine functionalised monolithic column to separate mixtures of L-amino acids, via ligand-exchange chromatography, was also reported.

A 10 cm silica monolith has been modified on-column with IDA groups and characterised for its selectivity toward alkali, alkaline earth and selected transition and heavy metal cations (Chapters 2-4). Significant retention of alkaline earth and transition/heavy metal ions was observed over a range of eluent pH and ionic strength conditions. For alkaline earth and transition/heavy metal ions, the selectivity of the 10 cm IDA silica monolith was found to closely match the selectivity observed for a 25 cm IDA modified silica gel particle-packed column, although the separation of alkali metal ions was noticeably poorer on the monolithic column. Under eluent conditions of high eluent ionic strength and pH, the IDA silica monolith operates as a high performance monolithic chelating-exchange column, which can be applied to the rapid determination of trace amounts of alkaline earth metal ions in complex matrices. The determination of Mg (II) and Ca (II) in 1 and 2 M NaCl and KCl brines was achieved in less than 40 seconds. The separation of Mg (II), Sr (II) and Ba (II) in the

presence of excess Ca (II) (up to 1000 ppm), was also demonstrated on the IDA silica monolithic column.

A second 10 cm silica monolith was functionalised with lysine (2,6-diaminohexanoic acid) groups and was observed to exhibit both cation- and anion-exchange capacity (Chapter 5). In contrast to lysine functionalised silica gel particulate columns, the lysine monolith exhibited limited cation-exchange capacity, and as a result, limited retention ion of both alkali and alkaline earth metal ions was observed. The lysine monolithic column did show selectivity towards transition and heavy metal ions through complexation. However, the lysine monolith exhibited a higher anion-exchange capacity, which facilitated selective and efficient separations of inorganic anions. The effect of eluent concentration, pH and flow rate on anion selectivity was investigated and it was observed that the use of elevated flow rates facilitated the separation of nitrite, bromate, bromide, nitrate, iodide and thiocyanate in under 100 seconds with peak efficiencies of between 20,000 and 50,000 N/m.

By dynamically modifying the surface of the lysine functionalised silica monolith with Cu (II) ions, it was possible to separate amino acids through ligand-exchange chromatography (Chapter 6). The pH of the sodium acetate buffer eluent was found to be the most important factor affecting the selectivity of the L-amino acids on the Cu (II)-modified lysine monolith. However, the retention of amino acid, and hence, the effect of peak broadening increased rapidly with increased eluent pH. A selectivity study involving 17 of the 20 standard amino acids showed that the elution order on the Cu (II)-modified lysine monolith was as follows: amino acids with positively charged R groups eluted first, followed by amino acids with nonpolar, aliphatic R groups, then amino acids with polar but uncharged R groups, followed by amino acids with aromatic R groups and finally amino acids with negatively charged R groups elute. Using elevated flow rates, the separation of different mixtures of amino acids was reduced from > 40 minutes to less than 10 minutes. It was necessary to employ a post-column reaction for the detection for amino acids and in this case, the detection of the amino acids was achieved by fluorescence (340/450 nm) following post-column reaction of the analytes with a mixture of *o*-phthaldialdehyde/ N-acetyl-cysteine.

Finally, the ion-exchange properties of a bare silica monolith were evaluated. Under non-acidic eluent conditions, limited retention of both alkali and alkaline earth metal ions was observed on a 10 cm Performance Si monolithic column (Chapter 7). However, under conditions of high concentrations of organic solvent within the eluent, the weak ion-exchange ion interactions exhibited by silica increase due to both ions in solution and fixed ion exchange sites within the stationary phase losing waters of hydration. Therefore, the high-performance separation of alkaline and transition metal ions on a 10 cm bare silica monolith was possible using acetonitrile or methanol based ammonium and sodium acetate buffered eluents. The effect of eluent ionic strength, organic content and pH on cation retention were evaluated, and it was found that increasing the eluent acetonitrile content from 60-80 % resulted in a 10-15 fold increase in cation retention due to enhanced ion-exchange interactions with the surface silanol groups. The nature of the organic solvent employed was found to be an important factor in the observed selectivity. The optimum separation of Cu (II), Cd (II), Ni (II), Co (II) and Mn (II) was achieved using an eluent composed of 80 % acetonitrile with 10.3 mM ammonium acetate buffer (pH 4.6), and using elevated flow rates, the run time required for the separation reduced to under 4 minutes.

### *Future Work*

The column modification procedure employed for the preparation of the IDA and lysine functionalised silica monoliths needs to be refined in an effort to obtain homogenous IDA or lysine surface coverage throughout the entire length of the silica monolith. Some of the possible approaches that could be applied include an increase in reaction time, reversing the direction of reagent flow through the monolith during the modification process, increasing the concentration of the ion-exchange groups in the reagent mixture, and also, the isolation of the IDA- or lysine-silane species prior to the modification procedure. In addition, the reproducibility of the modification procedure needs to be investigated, i.e., a number of silica monoliths should be modified on-column. Both the selectivity and ion-exchange capacity of each functionalised monolith should be investigated and results compared to achieve a quantitative measure of the reproducibility of the modification procedure.

Although both the IDA silica monolith and lysine silica monolith demonstrated a number of potential applications, i.e. the rapid determination of Mg (II) and Ca (II) impurities in the chloro-alkali industry and  $\text{NO}_2^-$  and  $\text{NO}_3^-$  in water samples, a number of other potential applications of the IDA and lysine functionalised silica monoliths exist. For example, the ability to determine Hg (II) in the presence of Cd (II) and Pb (II) on the IDA silica monolith could be significant, and in addition, the potential of the lysine functionalised silica monolith to separate  $\text{NO}_2^-$  and  $\text{NO}_3^-$  and  $\text{PO}_4^{3-}$  in a single run needs to be investigated. Therefore, when future monoliths are functionalised and characterised to determine the reproducibility of the on-column modification procedure, the selectivity of the IDA silica monolith for Hg (II) and the selectivity of the lysine silica monolith for  $\text{PO}_4^{3-}$  should be determined.

It was discussed in Chapter 1 that the motivation for the development of faster HPLC separations was the desire to achieve higher sample through-put in the laboratory, which would mean increased operating efficiency, lower costs and ultimately higher profits. The unique properties of monolithic columns were exploited in this project to achieve separations of cations and anions in seconds rather than minutes using elevated eluent flow rates ( $> 4 \text{ mL/min}$ ), while maintaining excellent peak efficiency and acceptable column backpressure. However, a disadvantage of using elevated eluent flow rates is the generation of large volumes of reagent waste, and this problem is exacerbated when post-column detection is also employed. Another potential limitation of the HPLC system described in this project is the long equilibrium time ( $> 30$  minutes) necessary before any sample analysis can be performed. Therefore, although the potential exists for the 10 cm functionalised monolith columns to be successfully employed by environmental laboratories for high throughput analysis of ions in a wide variety of matrices, the prospect of achieving real-time analysis at sampling sites in the field will require significant modifications of the HPLC system set up.

Some approaches, which could be employed, include reducing the dimensions of the functionalised monolithic column from 100 to 10 mm. As a result the HPLC reagent delivery pumps could be replaced by micro-peristaltic pumps (flow rate  $5\text{-}50 \mu\text{L/min}$ ), which would still provide an acceptable analysis time while generating

minimum reagent waste. Hence, the first area that would need to be investigated is the functionalisation of a 1 cm bare silica monolith with ion-exchange groups to ascertain whether there was significant ion-exchange capacity to facilitate the desired separation of anions and cations. At present, bare silica monolithic columns are only manufactured in 10 cm dimensions, therefore, the in-house preparation of bare silica monoliths would be required. Another area that must be considered is the detection of the target analytes in a particular matrix. In terms of producing a HPLC system suitable for real-time analysis, the detection of UV absorbing anions would require a less complex detection system than necessary for the post-column detection of cations. For example, a simple LED detector could be employed for the detection of anions in water samples following separation on a 1 cm lysine functionalised silica monolith. Another approach towards system miniaturisation could involve the synthesis of the IDA or lysine-silica monolithic stationary phase within the confines of a capillary column (15 x 0.1 cm i.d.), using the sol-gel process, for use in conjunction with a capillary-LC system. At present, the technology is currently available to achieve this goal, i.e. this capillary-LC system could incorporate a nano-pump (flow rate 0.1–10  $\mu\text{L}/\text{min}$ ), a nano-injector (injection volume 10-20 nL) and also a contactless conductivity detector, for on column detection. Both of these approaches could dramatically reduce reagent consumption, which still facilitating efficient separation of target analytes in a reasonable time frame.

In addition to the future work described in the previous paragraphs, a number of difficulties were encountered while trying to rapidly separate and detect amino acids, and it is envisaged that significant improvements in the future chromatographic performance could be achieved if the following areas could be addressed.

- Although separations of L-amino acids were achieved using the Cu (II) modified-lysine functionalised silica monolith, the application of a pH gradient would greatly enhance the separation efficiency. However, as discussed in Chapter 6, the use of a citrate/ citric acid pH gradient resulted in Cu (II) being stripped of the lysine silica monolith. Therefore a non-complexing buffer needs to be found, with a large working pH range, to successfully apply the pH gradient to the separation of the L-amino acids.

- In addition, the detection method employed, i.e. fluorescence based post-column detection, also contributed to the poor efficiency of the amino acid peaks due to the detrimental effects of band broadening. Therefore, the reaction conditions for the post-column reaction of amino acids with the OPA/NAC reagent needs to be fully optimised (i.e. reagent concentration, buffer pH and reaction temperature) in order to reduce the requirement of an excessively long post-column reaction coil. Also, the use of alternative thiol reagents could be examined to determine the suitability of the N-acetyl-L-cysteine as the optimum nucleophilic agent for use in the reaction of OPA with amino acids to produce fluorescent derivatives.

# **Appendix I**

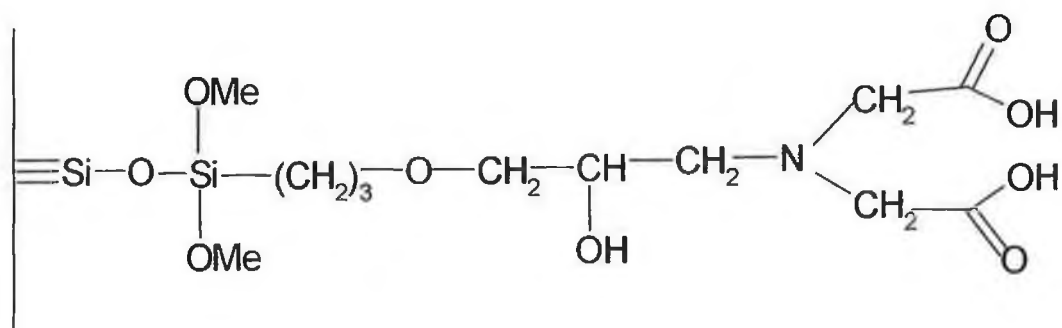


Figure 1.1A: The proposed structure of the IDA functionalised silica monolithic column.

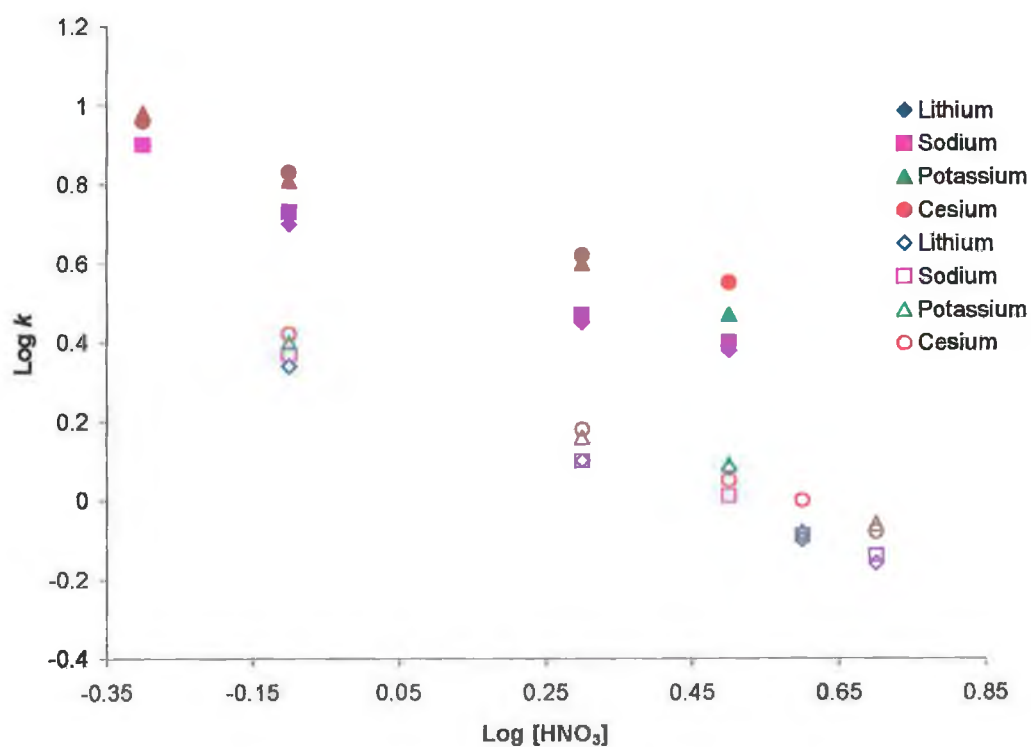


Figure 1.2A: The effect of HNO<sub>3</sub> eluent concentration on the retention of alkali metals on the 25 cm IDA silica gel column (solid symbols) and the 10 cm IDA silica monolith (open symbols).

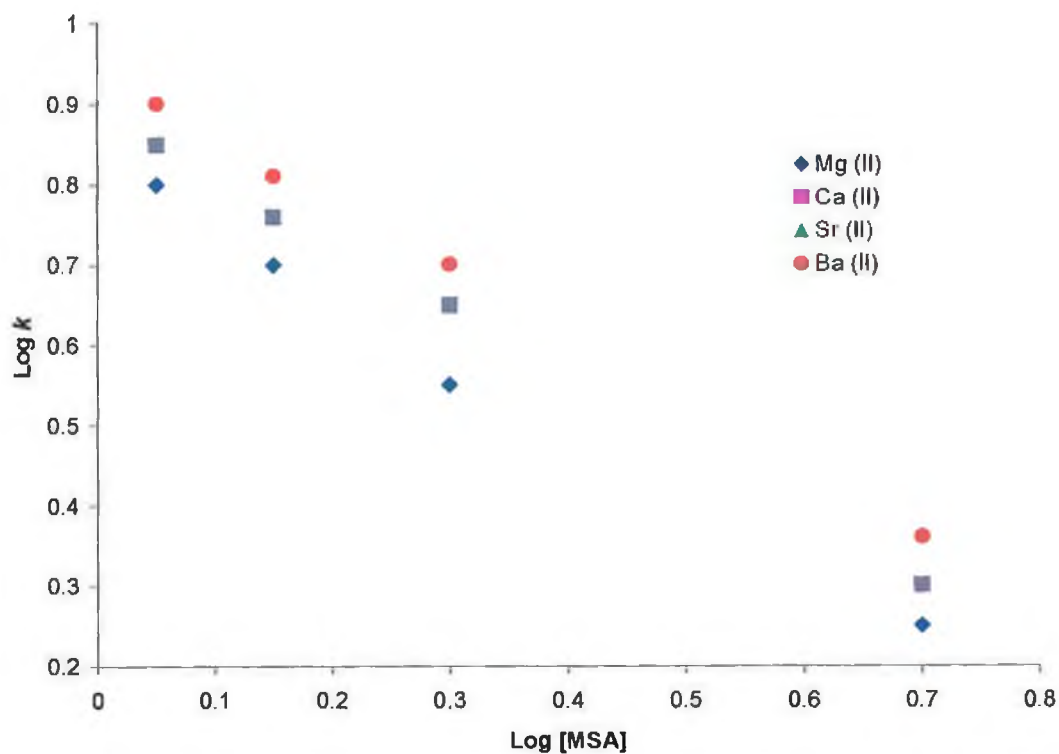


Figure 1.3A: The effect of eluent concentration on the retention of alkaline earth metal cations on a 10 cm IDA functionalised monolithic silica column.

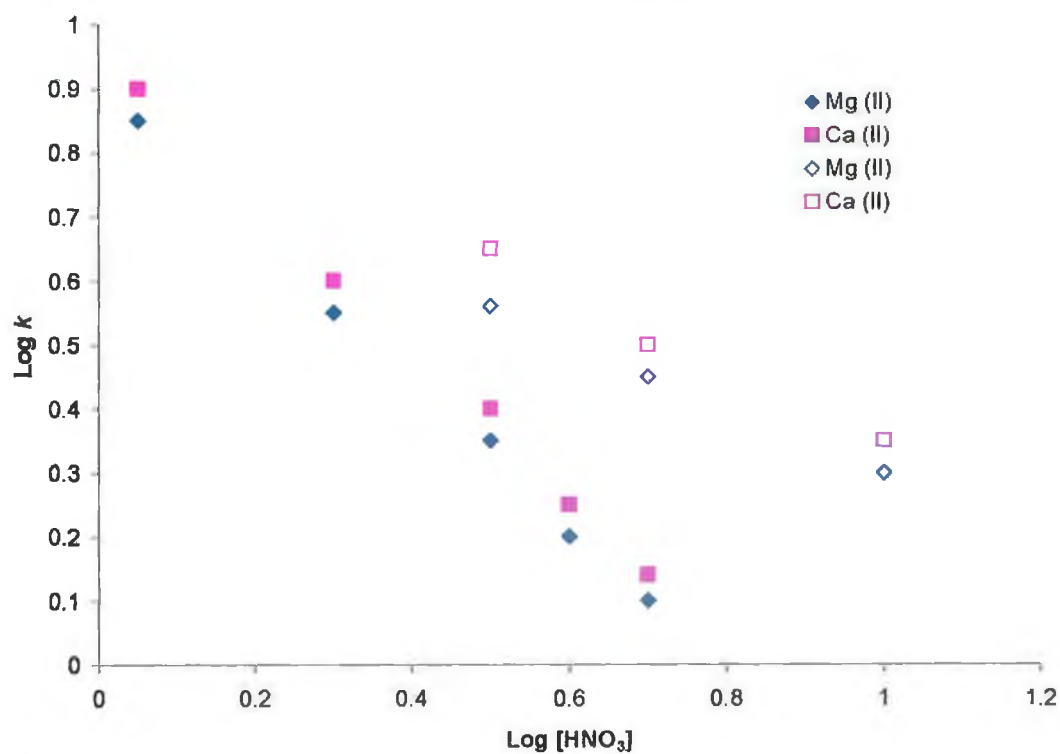


Figure 1.4A: The effect of  $\text{HNO}_3$  eluent concentration on the retention of Mg (II) and Ca (II) on a 10 cm IDA functionalised silica monolith (solid symbols) and a 25 cm IDA functionalised silica gel column (open symbols).

# **Appendix II**

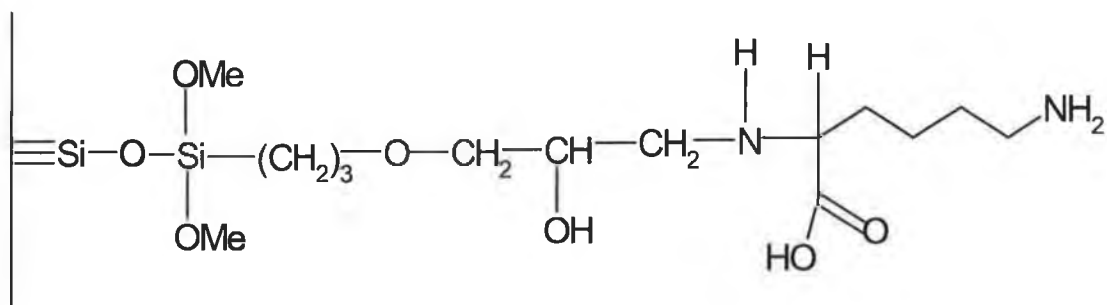


Figure 2.1A: The proposed structure of the lysine functionalised silica monolithic column.

Table 2.1A: The structure and chemical properties of the 20 standard amino acids

Amino Acid	Structure	pK <sub>1</sub> (COOH)	pK <sub>2</sub> (NH <sub>3</sub> <sup>+</sup> )	pK <sub>r</sub> (R)	pI
Glycine	$\begin{array}{c} \text{H} \\   \\ \text{H}_3\text{N}^+ - \text{C} - \text{COO}^- \\   \\ \text{H} \end{array}$	2.35	9.78		6.06
Alanine	$\begin{array}{c} \text{CH}_3 \\   \\ \text{H}_3\text{N}^+ - \text{C} - \text{COO}^- \\   \\ \text{H} \end{array}$	2.35	9.87		6.11
Valine	$\begin{array}{c} \text{CH}(\text{CH}_3)_2 \\   \\ \text{H}_3\text{N}^+ - \text{C} - \text{COO}^- \\   \\ \text{H} \end{array}$	2.39	9.74		6.00
Leucine	$\begin{array}{c} \text{CH}_2\text{CH}(\text{CH}_3)_2 \\   \\ \text{H}_3\text{N}^+ - \text{C} - \text{COO}^- \\   \\ \text{H} \end{array}$	2.33	9.74		6.01

Isoleucine	$  \begin{array}{c}  \text{CH}_3 \\    \\  \text{CH}_2 \\    \\  \text{H} - \text{C} - \text{CH}_3 \\    \\  \text{H}_3\text{N}^+ - \text{C} - \text{COO}^- \\    \\  \text{H}  \end{array}  $	2.32	9.76		6.05
Proline	$  \begin{array}{c}  \text{COO}^- \\    \\  \text{H} \\  / \quad \backslash \\  \text{H}_2\text{N}^+ \quad \text{CH}_2 \\    \quad \quad   \\  \text{C} \quad \quad \text{CH}_2 \\    \\  \text{H}_2  \end{array}  $	1.95	10.64		6.30
Phenylalanine	$  \begin{array}{c}  \text{C}_6\text{H}_5 \\    \\  \text{CH}_2 \\    \\  \text{H}_3\text{N}^+ - \text{C} - \text{COO}^- \\    \\  \text{H}  \end{array}  $	2.20	9.31		5.49
Tyrosine	$  \begin{array}{c}  \text{OH} \\    \\  \text{C}_6\text{H}_4 \\    \\  \text{CH}_2 \\    \\  \text{H}_3\text{N}^+ - \text{C} - \text{COO}^- \\    \\  \text{H}  \end{array}  $	2.20	9.21	10.46	5.64

Tryptophan	$  \begin{array}{c}  \text{C}_6\text{H}_5 \\    \\  \text{HN} \\    \\  \text{C} \\    \\  \text{H} \\    \\  \text{CH}_2 \\    \\  \text{H}_3\text{N}^+ - \text{C} - \text{COO}^- \\    \\  \text{H}  \end{array}  $	2.46	9.41		5.89
Serine	$  \begin{array}{c}  \text{CH}_2\text{OH} \\    \\  \text{H}_3\text{N}^+ - \text{C} - \text{COO}^- \\    \\  \text{H}  \end{array}  $	2.19	9.21		5.68
Threonine	$  \begin{array}{c}  \text{CH}_3 \\    \\  \text{H} - \text{C} - \text{OH} \\    \\  \text{H}_3\text{N}^+ - \text{C} - \text{COO}^- \\    \\  \text{H}  \end{array}  $	2.09	9.10		5.60
Cysteine	$  \begin{array}{c}  \text{CH}_2\text{SH} \\    \\  \text{H}_3\text{N}^+ - \text{C} - \text{COO}^- \\    \\  \text{H}  \end{array}  $	1.92	10.7	8.37	5.05
Methionine	$  \begin{array}{c}  \text{CH}_2\text{CH}_2\text{SCH}_3 \\    \\  \text{H}_3\text{N}^+ - \text{C} - \text{COO}^- \\    \\  \text{H}  \end{array}  $	2.13	9.28		5.74
Asparagine	$  \begin{array}{c}  \text{O} \\     \\  \text{NH}_2 \\    \\  \text{CH}_2 \\    \\  \text{H}_3\text{N}^+ - \text{C} - \text{COO}^- \\    \\  \text{H}  \end{array}  $	2.14	8.72		5.41

Glutamine	$  \begin{array}{c}  \text{O} \quad \text{NH}_2 \\  \parallel \\  \text{C} \\    \\  \text{CH}_2 \\    \\  \text{CH}_2 \\    \\  \text{H}_3\text{N}^+ - \text{C} - \text{COO}^- \\    \\  \text{H}  \end{array}  $	2.17	9.13		<b>5.65</b>
Lysine	$  \begin{array}{c}  \text{CH}_2\text{CH}_2\text{CH}_2\text{CH}_2\text{NH}_3^+ \\    \\  \text{H}_3\text{N}^+ - \text{C} - \text{COO}^- \\    \\  \text{H}  \end{array}  $	2.16	9.06	10.54	<b>9.6</b>
Arginine	$  \begin{array}{c}  \text{NH}_2^+ \\     \\  \text{CH}_2\text{CH}_2\text{CH}_2\text{CH}_2\text{NH} - \text{C} - \text{NH}_2 \\    \\  \text{H}_3\text{N}^+ - \text{C} - \text{COO}^- \\    \\  \text{H}  \end{array}  $	1.82	8.99	12.48	<b>10.8</b>
Histidine	$  \begin{array}{c}  \text{H} \\    \\  \text{N} - \text{C} \\  // \quad   \\  \text{HC} \quad \text{H} \\  \backslash \quad / \\  \text{N} - \text{H} \\    \\  \text{CH}_2 \\    \\  \text{H}_3\text{N}^+ - \text{C} - \text{COO}^- \\    \\  \text{H}  \end{array}  $	1.80	9.33	6.04	<b>7.60</b>
Aspartate	$  \begin{array}{c}  \text{CH}_2\text{COO}^- \\    \\  \text{H}_3\text{N}^+ - \text{C} - \text{COO}^- \\    \\  \text{H}  \end{array}  $	1.99	9.90	3.90	<b>2.85</b>
Glutamate	$  \begin{array}{c}  \text{CH}_2\text{CH}_2\text{COO}^- \\    \\  \text{H}_3\text{N}^+ - \text{C} - \text{COO}^- \\    \\  \text{H}  \end{array}  $	2.10	9.47	4.07	<b>3.15</b>

# **Appendix III**

Table 3.1A: Retention data for alkaline earth metal ions on a 10 cm bare silica monolithic column using an eluent composed of acetonitrile and ammonium acetate buffer (pH 4.6), flow rate 1 mL/min.

Log [E <sup>+</sup> ]	Log <i>k</i>			
	Ca (II)	Mg (II)	Sr (II)	Ba (II)
		<b>60 % MeCN</b>		
-1.98	0.324	0.283	0.324	0.436
-1.68	0.057	0.053	0.068	0.182
-1.50	0.000	-0.013	0.049	0.161
-1.38	-0.260	-0.284	-0.210	-0.208
Slope	-0.853	-0.884	-0.790	-0.930
R <sup>2</sup>	0.913	0.932	0.903	0.842
		<b>70 % MeCN</b>		
-2.11	0.728	0.683	0.821	0.914
-1.81	0.430	0.418	0.509	0.635
-1.63	0.260	0.223	0.328	0.449
-1.51	0.170	0.170	0.289	0.418
Slope	-0.937	-0.884	-0.920	-0.862
R <sup>2</sup>	0.997	0.989	0.981	0.979
		<b>80 % MeCN</b>		
-2.28	1.417	1.450		
-1.99	0.969	0.985		
-1.81	0.849	0.879		
-1.67	0.694	0.704		
Slope	-1.1856	-1.2114		
R <sup>2</sup>	0.979	0.975		

Table 3.2A: A comparison of retention data obtained for alkaline earth metals on a 10 cm bare silica monolith using 70 % acetonitrile containing sodium acetate and ammonium acetate/ acetic acid buffers (pH 4.6), flow rate 1 mL/min.

<b>Sodium Acetate buffer</b>		<b>Log <i>k</i></b>			
<b>Conc (mM)</b>	<b>Log [E<sup>+</sup>]</b>	<b>Mg (II)</b>	<b>Ca (II)</b>	<b>Sr (II)</b>	<b>Ba (II)</b>
7.8	-2.11	0.68	0.68	0.83	0.96
15.6	-1.81	0.41	0.40	0.54	0.65
23.4	-1.63	0.16	0.16	0.29	0.39
31.3	-1.51	0.12	0.12	0.27	0.36
Slope		-0.988	-0.986	-0.985	-1.046
R <sup>2</sup>		0.979	0.980	0.969	0.973
<b>Ammonium Acetate buffer</b>		<b>Log <i>k</i></b>			
<b>Conc (mM)</b>	<b>Log [E<sup>+</sup>]</b>	<b>Mg (II)</b>	<b>Ca (II)</b>	<b>Sr (II)</b>	<b>Ba (II)</b>
7.8	-2.11	0.68	0.73	0.82	0.91
15.6	-1.81	0.42	0.43	0.51	0.64
23.4	-1.63	0.22	0.26	0.33	0.45
31.3	-1.51	0.17	0.17	0.29	0.42
Slope		-0.884	-0.937	-0.92	-0.862
R <sup>2</sup>		0.989	0.997	0.981	0.979

Table 3.3A: Retention data for transition and heavy metal ions on a 10 cm bare silica monolith with an eluent composed of acetonitrile and ammonium acetate buffer (pH 4.6), flow rate 1 mL/min.

<b>Log [E<sup>+</sup>]</b>			<b>Log k</b>			
	<b>Cu (II)</b>	<b>Cd (II)</b>	<b>Ni (II)</b>	<b>Co (II)</b>	<b>Mn (II)</b>	<b>Pb (II)</b>
			<b>60 % MeCN</b>			
-2.38	-0.12	0.53	0.56	0.58	0.62	0.84
-1.98	-0.35	0.04	0.19	0.22	0.24	0.59
-1.68	-0.52	-0.30	-0.13	-0.10	-0.07	0.22
-1.50	-0.60	-0.53	-0.30	-0.26	-0.26	0.00
Slope	-0.551	-1.188	-0.988	-0.964	-1.00	-0.967
R <sup>2</sup>	0.999	0.999	0.999	0.999	0.999	0.971
			<b>70 % MeCN</b>			
-2.51	0.06	0.78	0.83	0.86	0.93	
-2.11	-0.26	0.28	0.48	0.55	0.59	1.09
-1.81	-0.40	-0.02	0.24	0.33	0.37	0.78
-1.63	-0.52	-0.26	0.02	0.09	0.11	0.50
Slope	-0.650	-1.162	-0.904	-0.852	-0.906	-1.213
R <sup>2</sup>	0.987	0.998	0.995	0.986	0.985	0.986
			<b>80 % MeCN</b>			
-2.68	0.16	1.23	-	1.36	1.51	-
-2.28	0.02	0.85	0.98	1.11	1.24	-
-1.99	-0.16	0.46	0.67	0.81	0.88	1.33
-1.80	-0.22	0.31	0.57	0.71	0.74	1.19
-1.69	-0.25	0.20	0.47	0.59	0.63	1.10
Slope	-0.443	-1.057	-0.849	-0.786	-0.912	-1.087
R <sup>2</sup>	0.990	0.995	0.982	0.992	0.990	0.967

Table 3.4A: Retention data for transition and heavy metal ions on a bare silica monolith using an eluent of 80 % acetonitrile containing sodium acetate/ acetic acid buffer (pH 4.6), flow rate 1 mL/min.

Conc (mM)	Log [E <sup>+</sup> ]	Log <i>k</i>					
		Cd (II)	Ni (II)	Co (II)	Mn (II)	Cu (II)	Pb (II)
10.3	-1.99	0.56	0.80	1.07	1.20	-	-
15.5	-1.80	0.38	0.62	0.82	0.88	0.98	1.31
20.6	-1.69	0.27	0.52	0.71	0.76	0.82	1.11
41.2	-1.39	0.16	0.37	0.50	0.53	0.47	0.72
Slope		-0.691	-0.701	-0.937	-1.080	-1.211	-1.392
R <sup>2</sup>		0.915	0.969	0.971	0.960	0.996	0.994

Table 3.5A: A comparison of the retention of transition metal ions on a 10 cm bare silica monolith, with eluents composed of MeCN or MeOH: and ammonium acetate/ acetic acid buffer (50 mM undiluted conc., pH 4.6), flow rate 1 mL/min.

Buffer Conc. (mM)	Retention factor ( <i>k</i> )						
	Cu (II)	Cd (II)	Ni (II)	Co (II)	Mn (II)	Pb (II)	Zn (II)
20 mM							
60 % MeCN	0.30	0.50	0.75	0.80	0.85	1.65	> 14
60 % MeOH	0.20	0.10	-	-	0.15	0.3	2.8
15.6 mM							
70 % MeCN	0.40	1.15	2.0	2.45	2.65	6.65	-
70 % MeOH	0.50	0.15	-	-	0.25	0.9	-
10.3 mM							
80 % MeCN	0.70	2.85	4.65	6.40	7.5	21.5	
80 % MeOH	1.20	0.25	0.30	0.35	0.5	2.9	-
5.1 mM							
90 % MeOH	8.25	0.65	0.75	1.0	1.65	-	-

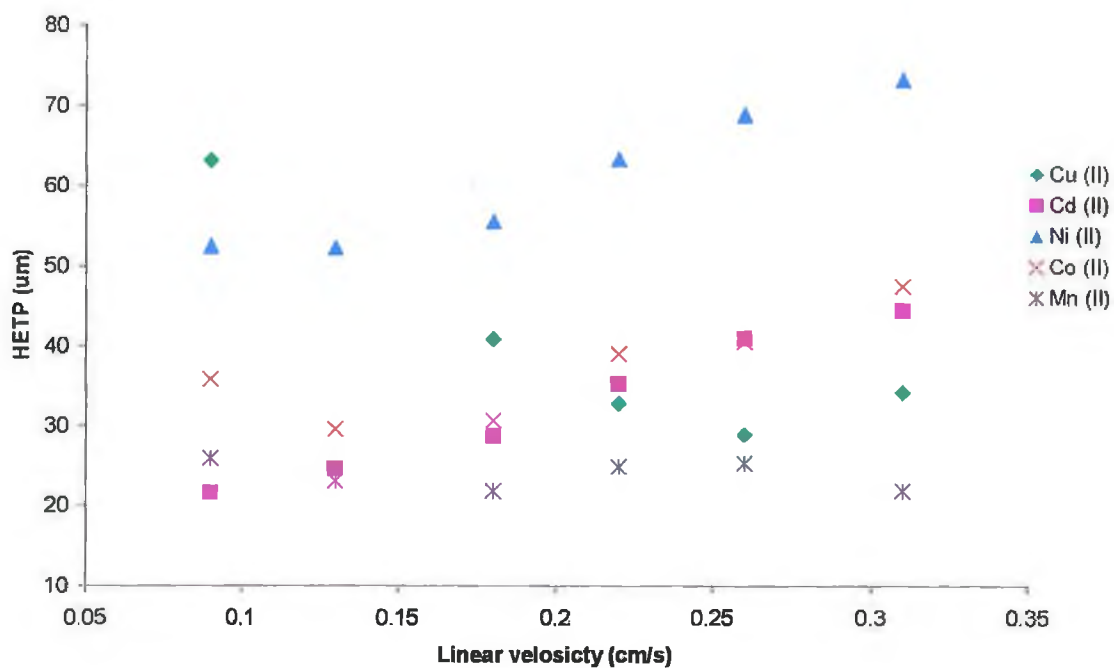


Figure 3.1A: van Deemter curves for transition metal cations on 10 cm bare silica monolith using a Dionex HPLC system.

